NASA CR-66946

CONTINUATION OF NASA ROCKET MOTOR DEFECTS INVESTIGATION

Prepared Under Contract Number NAS 1-9293
by
HERCULES INCORPORATED
CHEMICAL PROPULSION DIVISION
ALLEGANY BALLISTICS LABORATORY
CUMBERLAND, MARYLAND

for

NATIONAL AERONAUTICS and SPACE ADMINISTRATION

ABSTRACT

The objective of this NASA program was to continue the investigation of methods by which damaged fiberglass rocket motors can be successfully repaired. The following areas were investigated: (1) resin shear capabilities, (2) shear distribution improvements in the patch, (3) repair of cylindrical defects in an X259 chamber and (4) effect of aging on resin shear strength. The investigation of the repair system provided the following conclusions:

(1) A stress analysis indicated that use of a rubber filler ply in the bond line between the parent case and the first ply can help to reduce peak shear stresses at the defect edge and make the loading in the patch plies more uniform.

(2) The present four-ply fiberglass cloth patch design has inadequate strength to repair a 5.0-in. longitudinal defect completely through the wall of an X259 motor case cylindrical section.

(3) Bottle hydroburst tests indicate that the shear strength of the Epon 946 resin bonded patch is significantly greater than previously indicated by double-lap shear tests.

(4) Double-lap shear tests data indicated no significant loss in shear strength for the repair system after nine months of aging.

(5) For the best void-free application of a repair patch, individual plies must be applied separately. Except for the anti-fraying border, the resin must not be applied to any ply before positioning and rolling down the ply.

NASA CR-66946

CONTINUATION OF NASA ROCKET MOTOR DEFECTS INVESTIGATION

JUNE 1969 THROUGH MAY 1970

By

R. B. Enie

Prepared Under Contract No. NAS 1-9293 by
Hercules Incorporated
Chemical Propulsion Division
Allegany Ballistics Laboratory
Cumberland, Maryland

for

NATIONAL AERONAUTICS AND SPACE ADMINISTRATION

TABLE OF CONTENTS

TABLE OF CONTENTS (CONT.)

LIST OF TABLES

LIST OF FIGURES

LIST OF FIGURES (Continued)

LIST OF FIGURES (Continued)

LIST OF FIGURES (Continued)

LIST OF FIGURES (Continued)

SUMMARY

OBJECTIVE AND PROGRAM PLAN

This program was concerned with the investigation of the following areas: (1) resin shear capabilities, (2) shear distribution improvements in the patch, (3) repair of cylindrical defects in an X259 chamber, and (4) effect of aging on resin shear strength. The loading capabilities of the patch system were investigated in a series of tests on small bottles with circumferential defects completely through and around the bottles. These bottles were repaired and then hydroburst to determine the maximum load that could be carried by the patch system. The shear improvement analysis consisted of the use of mathematical models to determine the shear stress distribution in the bond line of the repair. This bond line was modified to determine if the maximum shearing stresses could be decreased. The X259 hydroburst served as a demonstration of the capabilities of the fiberglass cloth - Epon 946 repair system on defects five inches long and completely through the chamber wall. The effects of aging on the shear strength of the resin were determined at intervals up to nine months.

RESULTS AND CONCLUSIONS

This program has provided a critical evaluation of the repair system with the following conclusions being demonstrated during the program:

(1) A stress analysis indicated that use of a rubber filler ply in the bond line between the parent case and the first ply can help to reduce peak shear stresses at the defect edge and make the loading in the patch plies more uniform.

(2) The present four-ply fiberglass cloth patch design has inadequate strength to repair a 5.0-in. longitudinal defect completely through the wall of an X259 motor case cylindrical section.

(3) Bottle hydroburst tests indicate that the shear strength of the Epon 946 resin bonded patch is significantly greater than previously indicated by double-lap shear tests.

(4) Double-lap shear test data indicated no significant loss in shear strength for the repair system after nine months of aging.

(5) For the best void-free application of a repair patch, individual plies must be applied separately. Except for the anti-fraying border the resin must not be applied to any ply before positioning of and rolling down the ply.

SECTION I

INTRODUCTION

A. OBJECTIVES

Under Contract NAS-1-9293, Hercules Incorporated, Allegany Ballistics Laboratory (HI/ABL) was authorized to conduct a program to continue the investigation of methods by which damaged fiberglass rocket motors can be successfully repaired.

The objectives of this program were:

(1) To establish shear loading capabilities of the repair system previously demonstrated under Contract NAS 1-6367.

(2) To investigate possibilities of significantly increasing shear load capacity by modification of repair design.

(3) To investigate the application of the repair system to a modern flight-type motor case and demonstrate such applications under hydrotest conditions.

(4) To establish the effect of aging on the repair system.

B. BACKGROUND

Many high-performance solid rocket motor designs have incorporated filament-wound fiberglass cases to achieve a higher strength-to-weight ratio. During the past several years, a number of such motors have been rejected for flight use because of damaged fiberglass windings. These rejections resulted in schedule slippage and increased program costs.

Under Contract NAS-1-6367, Hercules Incorporated demonstrated a laminated patch repair system on a number of X248 motor firings conducted at chamber pressure well above normal for those motors.(1-3) That program provided a critical evaluation of the size, location, orientation, and repair of gouge-type defects in the fiberglass chamber of the X248 rocket motor. Major achievements and conclusions resulting from that program were:

(1) Certain partial defects can be sustained in the domes and cylindrical sections of the X248 motor without affecting motor performance.

(2) A field repair technique was developed for the repair of defects completely through the wall of the cylindrical section of the X248 rocket motor. This technique includes

a laminated fiberglass cloth patch bonded to the chamber by a room temperature cure elastomeric adhesive. The technique has been used to successfully repair defects with little regard to size or orientation of the defect. Repair by this system requires no major tooling or equipment.

(3) Although the stress analyses were vital to the interpretation of empirical results, the analytical methods used are inadequate to evaluate chamber damage and repairs. This is due largely to the geometrical limitations of the method; that is, it cannot account for the finite lengths of defects.

Treating all defects as having infinite length tends to produce highly conservative solutions for the stress-strain distributions in the models. However, the analyses can still be used to indicate trends in patch parameters which might affect the stress-strain distributions. Test results on the X248 motors indicated that even the maximum-length (15 inch) defect repaired and tested did not load the patch to the degree that the infinite length analysis predicted. See Figure 88. As shown in Figure 89 the analyses did indicate that action was necessary to assure a thickened bond line close to the defect lip.

(4) The feasibility of repairing fiberglass defects in a rocket motor dome was demonstrated in a 6-in.-diameter bottle program.

(5) Although complete penetration defects and their repairs can be evaluated, further effort remains to be completed before valid accept/reject criteria can be established for defects and repairs in general.

From static firings of defected and repaired X248 motors, it was concluded that gouge-type defects can be repaired regardless of X248 model. However, it may be necessary to optimize the patch technique for situations where patch weight and size must be restricted and where higher pressure loads than those for the X248 are to be transferred by the bond layer.

It is believed that the basic assumptions used to design the patch for the X248 can be applied to other motors as well. The patch itself can be decreased in size based on the X248 test results. Use of these test results would tend to reduce the conservatism of the patch design for smaller defects. However, because of the possibility of patch irregularities, it may be best to continue using the conservative assumptions until the patch application technique has been perfected. The parameters that must be considered in designing a repair patch are (1) motor pressure, (2) motor case radius, (3) winding geometry, (4) defect size and depth, and (5) patch material properties.

C. SUMMARY OF PROGRAM PLAN AND SCOPE

This program was concerned with the investigation of the following areas: (1) resin shear capabilities, (2) improvements in shear distribution through the patch, (3) repair of cylindrical defects in an X259 chamber, and (4) effect of aging on resin shear strength.

The loading capabilities of the patch system were investigated in a series of tests on small bottles. Circumferential defects completely through and around the bottles were used to establish defects of infinite length. These defected bottles were repaired using S/81-904 finish fiberglass cloth and an Epon 946. The epoxy resin system incorporated a heavier bond line at the defect lip than was previously used. After repair, the bottles were hydroburst to determine the maximum load that could be carried by the patch system. This load could then be compared with the values obtained from double-lap shear tests.

The shear improvement analysis consisted of the use of mathematical models to determine the shear stress distribution in the bond line of the repair. The bond line adjacent to the parent case was then modified to determine if the shear stress distribution could be significantly altered. A reduction of the peak shear stress at the edge of the defect was highly desirable.

An X259 hydroburst test served to demonstrate the capabilities of the present patching technique. Longitudinal and circumferential defects in the cylindrical section were repaired with the Epon 946 and S/81-904 finish fiberglass cloth. The chamber was hydrotested to determine the success of the repair of such defects.

The effects of aging on shear strength of the patch system were also investigated. Three-plate shear specimens were withdrawn from storage (65-85°F) and tested at intervals up to nine months to determine if the shear strength degraded over this time span.

SECTION II

CONCLUSIONS AND RECOMMENDATIONS

A. CONCLUSIONS

The present work that has been completed under the follow-on NASA Defects Program (Contract NAS1-9293) has provided a critical evaluation of the repair system that was initially developed under NASA Contract NAS1-6367. Each of the four tasks provided additional data which can be used in conjunction with previous data to better evaluate the repair of defects. The following conclusions were drawn:

(1) The series of theoretical stress analyses investigating modifications of the patch system indicated that shear stresses at the bond line and load distribution per ply can both be altered. The peak shear stresses at the defect edge can be reduced significantly and the load distribution per ply can be made more uniform by introducing a thin filler ply of rubber into the bond line adjacent to the parent case.

(2) The X259 hydrotest indicated that a four-ply patch of the tensile strength determined in this study was not capable of successfully repairing a 5.0-in. longitudinal defect completely through the cylindrical section of an X259 motor case. However, the repair of circumferential defects can be accomplished with the present repair technique.

(3) Bottle hydroburst tests indicate that the shear strength of the Epon 946 resin-bonded patch is significantly greater than previously indicated by double-lap shear tests. The new strength value varies from approximately 2000 lb/in. to 2600 lb/in.

(4) The double-lap shear test data have indicated that no significant loss in shear strength has resulted from room-temperature aging of the repair patch materials for storage periods up to nine months.

(5) The technique of applying individual dry patch plies to a surface coated with the bonding compound is required to minimize the probability of void development. This technique was used successfully on the repairs of the X259 motor case defects to eliminate voids in the repair patch.

B. RECOMMENDATIONS

To improve the present system, an investigation of other glass cloths and resins should be conducted to determine their applicability to the repair of the fiberglass defects. The use of new patch design features, particularly the use of a rubber filler ply materials in the bond lines of the repair, should be investigated in subscale tests. The resulting new technology should then be applied to repair defects in full-scale chambers. The X259 chamber would be a likely candidate for such an evaluation. Also, a combined analytical-effort to develop and validate a computer analysis technique capable of recognizing the effect of defect length on patch loading and on unrepaired strength must be completed.

SECTION III

DISCUSSION OF TESTS AND RESULTS

A. INTRODUCTION

This program was a continuation of the investigation of methods by which damaged fiberglass rocket motors can be successfully repaired. The program was comprised of four tasks.

Task I consisted of the testing of repaired circumferential defects that extended completely around 6-inch-diameter bottles. The purpose of these tests was to establish the shear loading capabilities of the Epon 946 resin system.

Task II was concerned with analytical investigations of repair patch configurations. The purpose of this task was to investigate the possibilities of attaining significant increases in shear load capacity by modifying the patch design.

Task III of the program consisted of a hydroburst test of a defected and repaired X259 chamber. The objective of this program task was to investigate the application of the patch system to an X259 chamber and to demonstrate the capability of the patch system under hydrotest conditions.

Task IV in the program was concerned with aging of the Epon 946 resin system. The purpose of the task was to establish the effect of aging (up to nine months) on the shear strength of this resin system.

B. TASK I - SUBSCALE BOTTLE PROGRAM

1. Technical Approach

Double-lap shear tests in the original program indicated that the Epon 946 resin had a shear strength of 1600 lb/in. However, it was believed that this value was lower than the strengths that were actually exhibited by the repair technique used in the repair of X248 motors. A more exact value for this shear strength would be required for the application of the repair technique to situations where loads to be transferred are higher than the X248 loads. Therefore, the objective of the first task in the program was to determine the shear strength of the Epon 946 resin system used in the repair of fiberglass defects in rocket motor chambers. The investigation of the shear strength was conducted with 6-in.-diameter bottles. The physical dimensions and winding data for the fabrication of the ten bottles in this task are shown in Figure 1.

The bottles were wound over Styrofoam mandrels covered by two layers of thin rubber, using single-end S-994 glass with an Epon 826/CL resin system. The winding geometry and sequence consisted of four hoop layers followed by four 9° helical layers and four additional hoop layers. The fourth helical layer in this winding geometry was used to increase the burst pressure capabilities of the bottles from 2100 psi to approximately 2800 psi. This pressure permits a maximum axial load of approximately 4500 lb/in. which is sufficient to give a critical evaluation of the shear capabilities of the patch system.

The defects were 0.10-in. wide and were machined completely through the bottle wall; care was taken not to cut the rubber insulator inside the fiberglass bottles. The defects extended 360° circumferentially around the bottles and were located at the mid-point of the cylindrical section. This infinite length defect causes all of the axial load to be transferred through the patch.

A preliminary finite element analysis of a three-ply repair of this defect indicated that a fourth ply should be added. This additional ply was needed because the desired location for failure in the hydroburst test was in shear in the bond layer between the patch and the bottle. The stress distribution among the plies directly above the defect for the three-ply repair at a 1000 psi internal pressure was predicted to be

	Axial Stress, psi
Ply 1	58,000
Ply 2	32,000
Ply 3	20,000

Tensile test data from the original program, as listed in Table I, indicate that the tensile strength of a single ply of glass cloth is 5600 psi. Thus, based on an allowable tensile strength of 56,000 psi, a fourth ply was needed to ensure shear failures as opposed to tensile failures in the patch. A plot of the stress distribution per ply for a three-ply patch is shown in Figure 2. By assuming the same type of differences for three- and four-ply distributions of load per ply as shown in Reference (2), Figure 115, an extrapolation of this analysis data was performed. An extrapolation of the outermost ply strains from three-ply repairs to four-ply repairs indicates a 1.39% strain for an internal pressure of 1000 psi in the bottles with a four-ply repair. This value will be used for comparison with the strains measured during actual bottle hydroburst tests.

The assumed bond line thickness in the analysis was 0.010 in. Figure 3 shows the shear stress distribution in the bond line as a function of distance from the defect center. A maximum value of 5700 psi occurs at the defect lip for an internal pressure of 1000 psi. Previous analyses of three- and four-ply repairs indicates that the variation in the number of plies should reduce the peak shear stress at the defect lip to about 5000 psi.

2. Bottle Repair and Test Procedures

After the bottles were wound and cured, they were defected. The bottles were placed on a lathe and a sharp cutting tool was used to machine the defects through the bottle walls. After defecting, the bottles were repaired. The general repair procedure is outlined below; deviations for each particular bottle test are also described.

The repair area was marked off and then sanded until the bottle gloss had been removed. The sanded area was then cleaned and degreased with methylene chloride. A minimum 0.010-in.-thick coat of Epon 946 was applied to the repair area within 1.0 in. of the defect. This coat was then allowed to B-stage for a minimum of six hours, and care was taken to prevent resin accumulation at any one location. This precoating was done to assure an adequate bond line thickness in the high shear stress areas adjacent to the defect. A fresh coat of resin was then applied to the entire sanded area. The first ply of fiberglass cloth was placed over the defect, and the resin was worked up through the ply. More resin was then added. The next ply was placed over the first ply, and the resin was again worked up through the ply. This step was repeated for the two subsequent plies. Upon the completion of patching, the repaired bottle was allowed to cure for a minimum of seven days at room temperature (75 $\pm$ 5°F).

The materials used for the repair patch were Owens-Corning S/81-904 finish glass cloth and Epon 946 resin. The repair patch consisted of four plies of overlapping cloth. The dimensions of the four plies including a 1/4-in. fringe were as follows:

Ply 1 - 22.5 in. long and 3.0 in. wide

Ply 2 - 23.0 in. long and 4.0 in. wide

Ply 3 - 23.5 in. long and 5.0 in. wide

Ply 4 - 24.5 in. long and 6.0 in. wide

Each of these plies extended completely around the bottle and had a minimum of a one-inch overlap at the ends.

When the repair patch had been completely cured, the Styrofoam mandrels were dissolved by using acetone. The dissolving process did not completely dissolve the Styrofoam. A thin coating of residue remained on the interior wall of the bottles.

After repair the bottles were hydrotested to burst using the Data-Trak programmed closed-loop servo system controlling the Miller Ram Pressurization System. All the bottles were instrumented with strain grids as shown in Figure 4. Pressurization of the bottles at a rate of 50 psi/sec was controlled by a Data-Trak program which provided the pressure profile shown in Figure 5. A schematic diagram of the test setup is shown in Figure 6.

3. Test Results

The first two bottles in the program were repaired using a four-ply repair and the repair procedure outlined previously. These bottles were hydrotested, and both bottles developed a leak in the bond layer between the repair patch and the bottle wall. This leaking was attributed to a failure in the rubber insulator. As the bottles were pressurized, the resin in the defect cracked, permitting the thin rubber insulator to be extruded into the cracks and resulting in a failure of the rubber. Apparently, the water then placed the bond line in radial tension because the repair patch has a much lower modulus than the bottle. As a result, the bond line failed and the water was able to force its way out of the bottle, causing the resulting water leakage.

Both bottles developed leaks between the patches and the bottles. The maximum pressures achieved were 925 psi on Bottle No. 1 and 850 psi on Bottle No. 2. Axial strains measured on the outer patch ply are shown in Figures 7 and 8. A picture of Bottle No. 1 in the hydrotest setup is shown in Figure 9. Bottle No. 1 was sectioned to permit internal examination. It was noted that the residue from the Styrofoam dissolving process had crazed during the tests. Also, a failure path was found in the bond line which permitted escape of the water. A method of sealing the chamber interior would be required in future tests.

Bottle No. 2 was hydrotested again after the entire inside cylindrical section had been sealed with Prestite. This was done to ensure that leakage would not result from the crazing of the residue or from resin failure in the defect. The bottle failed in shear at 965 psi in the bond line of the repair. The origin of the shear failure appeared to be in the leakage path developed during the previous test. This pressure corresponded to an axial load of approximately 1545 lb/in. of applied defect length. As a result of this test, it was concluded that Prestite should be used in future tests to cover the internal cylindrical section to prevent the development of leaks.

The next test sequence consisted of hydrotests of two bottles. The patching of these bottles varied from that used in the first two tests to make the application of the repair patches easier. The first bottle (No. 3) contained a three-ply repair patch. The second bottle (No. 4) contained an inverted four-ply repair ("inverted" referring to reversal of the order of ply application to the bottle; i.e., beginning with the largest ply and ending with the smallest). The inverted patch was selected because its tendency to conform to the bottle surface was superior to that of the normal patch. In addition, analyses indicated that the characteristics of the inverted patch would be similar to those of the normal patch.

Another change in the repair procedure was needed. Because of difficulty encountered in holding individual plies in fixed positions, the patches for Bottle No. 4 and all subsequent bottles were applied integrally to the bottles. This technique is shown in Figures 16, 17 and 18. Post-test inspections of sheared bond lines showed later that this technique of application was undesirable. See Figures 31 through 38. Air bubbles were trapped instead of being permitted to vent through successive plies as when the plies were applied dry to a freshly precoated surface in accordance with previous practice. Integral assembly, in addition, resulted in an unduly stiff patch, and as a consequence resistance to conforming to the bottle surface remained a problem.

The results of the hydroburst tests for these two bottles indicate that the three-ply patch failed in tension at a pressure of 1143 psig and that the four-ply patch failed in shear at a pressure of 1606 psig. These two different types of failures were clearly apparent upon examination of the bottles. The patch of Bottle No. 3 failed in tension directly above the defect. The patch of Bottle No. 4 pulled away from the bottle at one end of the bottle. The post-test pictures of these two bottles are shown in Figures 10 and 11, respectively.

Plots of axial strain versus pressure for Bottles Nos. 3 and 4 are shown in Figures 12 and 13. These values at 1000 psi are lower than indicated by the analysis. The higher strains for the three-ply repair are noted by comparing these two figures.

The next four bottles to be tested were repaired with four-ply, inverted fiberglass cloth patches. This patch configuration and technique had been used previously on Bottle No. 4. The inverted patching procedure is different from the procedure outlined for a normal four-ply repair. After the surface had been defected and sanded, a minimum 0.010-in.-thick coat of Epon 946 was applied to the repair area within 1.0 in. of the defect (Figure 14). After B-staging for at least six hours, the remaining repair areas was coated with a fresh layer of Epon 946 (Figure 15). The four-ply inverted patch was applied by the integral assembly technique (Figures 16, 17 and 18). As illustrated in Figure 16, the patch was assembled by bonding one end of each ply to the previous ply in a staggered manner. This was done for ease of application and provided assurance that the plies were and would remain in proper position during application. After the patch had been wrapped around the bottle, the roller was used to force out air and to help smooth the patch. The repaired bottle is shown in Figure 19.

Before testing one of the two ballon bladders was removed from the inside of each of the four bottles during the dissolving of the Styrofoam mandrels. This was done to remove the residue deposited in the bottle during the dissolving process. Next, two coats of Lagz were applied to the interior surfaces of the four bottles in an attempt to prevent water weeping or leaks during hydrotest. This method was used as a substitute for the time-consuming application of a Prestite coating.

The initial bottle tested in this series (No. 8) developed a leak in the defect area at ~ 1150 psig; this leakage was similar to those occurring in Bottle Nos. 1 and 2. In view of this problem, it was decided to coat Bottle No. 8 and the remaining three bottles with a Prestite layer and to retest No. 8. Bottle No. 8 was retested at a higher pressurization rate, 2750 psig/sec, because of some detected leakage. The bottle failed in shear at a pressure of 1622 psig (2600 lb/in. of defect length) in the area where the leakage had occurred. Plots of axial strain versus pressure for the two tests of Bottle No. 8 are shown in Figures 20 and 21. A comparison of the two graphs indicates a small difference in strain readings at similar pressures for the two tests. The resulting difference was primarily due to the higher pressurization rate used in the retest. The failure pressure, equivalent to a 2600 lb/in. axial load carried by the bond system is much higher than the double-lap shear value of 1600 lb/in.

Bottle No. 5 was tested next. It failed in shear at a pressure of 1477 psig (2365 lb/in. of defect length) at the 270° location. A plot of the axial strain versus pressure is shown in Figure 22. This plot does indicate a more rapid increase in strain at the 270° location.

The final two bottles (Nos. 6 and 7) were tested on December 3, 1969. The results of these tests indicate shear failure at pressures of 1270 psig (2035 lb/in. of defect length) at 1350 psig (2160 lb/in. of defect length), respectively. In Bottle No. 6, voids were present in the bond line at the failure location. These voids were the probable cause of failure at the lower pressure. Plots of the pressure versus axial strain are shown in Figures 23 and 24 for these two bottles.

Examination of the five bottles using the inverted repair technique has indicated that numerous voids occurred in the bond lines. This was due primarily to the difficulty encountered in making the glass cloth patches conform to the bottle surface. In areas where the patches did not adhere, air pockets remained. These voided areas caused disruption of the stress distribution in the bond line, resulting in shear stress buildups which caused a premature failure of the patch. In all cases, the motion picture films indicated that failure was in shear.

The post-burst pictures of Bottle Nos. 5, 6, 7 and 8 are shown in Figures 25 through 28. The bottle halves were separated after the tests, and the areas of resin void were outlined with a white marker. Pictures of these areas for Bottle Nos. 4 through 8 are shown in Figures 29 through 33. The voids in Bottle Nos. 5 through 8 were deeper than those in Bottle No. 4 because they contained more resin in the bond line. Also, the bond line thicknesses in the areas near the defect edge varied from 0.035 in. to 0.045 in. These values, which are well above the 0.010 in. minimum required in the test plan, were due to the technique employed which provided more thickness than was anticipated.

Photomicrographs of some of the different types of voids found in Bottle No. 6 are shown in Figures 34 through 38. Figures 35 and 36 show different views of one void, approximately 0.75 in. wide x 0.55 in. long, found in Bottle No. 6. In all cases these voids appear to be of such magnitude or location as to seriously alter the shear stress distribution of the bond line

The strain gage measurements for the bottles with the four-ply inverted patches show an average of 0.85% axial strain at 1000 psi. This value is considerably lower than the analytically extrapolated value of 1.39%. The lower strains are probably due to the numerous voids in the bond line which resulted in lower loads being transferred out to the outer plies, and the added stiffening of the patch because of the overlapping of the joints in eacl ply. The same factors were probably also the cause of the considerable variation in the strain measurements, even within the same test.

The results of this task have indicated that shear strength of the Epon 946 is at least 27% higher than the 1600 lb/in. indicated by the testing of the double-lap shear specimens. This value could be possibly as much as 60% higher if the large voids in the bond lines of the repair patch could be avoided. The minimum axial load to be transferred was 2035 lb/in. for Bottle No. 6. The maximum axial load to be transferred under normal test conditions was 2570 lb/in. in Bottle No. 4. It is believed that values as high as those measured for Bottle No. 4 can be consistently achieved if the void problem can be eliminated.

The bottle test results are summarized in Table II. An average failure pressure for Bottle Nos. 4, 5 and 7 was 1477 psig (2365 lb/in. of defect length). Bottle No. 8 was not counted because of higher loading rate, and Bottle No. 6 was not counted because of the numerous voids that were detected in its bond line. Based on these results a bond line strength of 2400 lb/in. of defect length should be considered conservative in repairs which have no voids.

The comparison of the strain measurements with analytically predicted values possibly indicates that the repair patch may have been closer to a five-ply repair. This was due to the overlaps in the integral repair technique that was utilized.

The remaining two bottles in the program were not tested because (a) the results of the first eight tests have indicated a substantial increase in shear strength and (b) the problem of voids in the bond line encountered with the patching technique had to be overcome.

C. TASK II - SHEAR IMPROVEMENT ANALYSIS

1. Technical Approach

The objective of this task was to find, by analyses, a design modification of the laminated patch repair system which would significantly reduce the peak shear stresses present in normal patch loading. This would help to increase the potential load-carrying capacity of the repair system.

The analyses were performed by utilizing the Hercules Finite Element Computer Program. This digital computer program is based upon a finite-element direct stiffness method for obtaining elastic stress-strain solutions for bodies of revolution; the program can be used to analyze two-dimensional geometric approximations of the actual three-dimensional configuration. A major feature of the program is its capability to consider the anisotropic material properties for all elements. Temperature dependence of the anisotropic properties is also automated through the use of material property input to the computer program.

The Hercules finite element computer program comprises four functionally separate subprograms which perform the following operations:

(1) generate nodal locations of interior grid elements,

(2) generate individual stiffness matrices and loads for the various quadrilateral elements in the grid and store them in an intermediate magnetic tape,

(3) assemble individual stiffness matrices generated by subprogram (2) and obtain the composite stiffness matrix for the total structure, then solve for the equilibrium displacement field, and

(4) solve for strains and stresses in the finite elements through elasticity relationships between the strains and displacements and stresses and strains.

In using these analytical techniques, the body under consideration is approximated by an assemblage of quadrilateral elements. The corners of each element are described as nodal points. Within each element, the displacement field is assumed to have a known linear form and is, therefore, given in terms of the unknown nodal displacements. Based upon the linear theory of elasticity, stresses are then expressed in terms of nodal displacements associated with each element under consideration together with the applied forces. The procedure is repeated for each element of the system. The solution is obtained when minimization associated with the principle of virtual work is accomplished with respect to each of the independent unknown nodal displacements. This results in a system of linear algebraic equations which describe the equilibrium state for the body. Solution of the system of linear algebraic equations yields displacements from which strains and stresses can be obtained. Use of this technique permits a detailed study of overall structural deformations and detailed analyses of movements of individual fibers or structural elements within quadrilateral elements.

2. Results

a. Four-Ply Repair

(1) Normal Patch Repair

The first analysis was of a four-ply repair of an infinite circumferential defect. The analysis was performed for a chamber with geometry similar to that of the X259 chamber. The defect was assumed to be infinite because of the geometrical limitations of the computer program. The repaired chamber was analyzed at an internal pressure of 1000 psi for convenience. This pressure is equivalent to an axial load of 7500 lb/in. Figure 39 shows the cross-section of the repaired area and the breakdown of the structure into elements and their respective dimensions.

Plots of the axial strain distribution, axial stress distribution per ply and shear stress distribution in the bond line are shown in Figures 40, 41 and 42, respectively. In all three figures the patterns are similar to those already observed in earlier analyses.(1) The stress magnitudes are above the allowables of the cloth and resin because of the more severe loading condition than had previously been imposed. However, they can still be used for valid comparisons to determine improvements in shea distributions.

(2) Inverted Patch Repair

The second analysis was of a four-ply inverted patch used to repair a circumferential defect in a chamber with geometry similar to that of the X259 chamber. Again the chamber was analyzed for 1000 psi internal pressure. Figure 43 shows the cross-section of the repaired area and the breakdown of the structure into elements and their respective dimensions.

Plots of the axial strain distribution, axial stress distribution per ply and shear stress distribution in the bond line are shown in Figures 44, 45 and 46, respectively. In all three figures the patterns and magnitudes are similar to those observed in the four-ply repair analysis. The axial strain and axial stress distribution are slightly different in magnitudes, but the shear stress distributions in the bond layers are almost exactly the same.

(3) Comparison of Normal and Inverted Patch Repair

A comparison of the stress distribution per ply is shown in Table III for these two types of repair. Although the magnitudes vary, the total load carried by the patches is the same. The comparison of these two analyses indicates that the repairs are almost equivalent, but that the normal four-ply orientation is slightly better because of lower maximum stresses in the first ply.

b. Bond Line Filler Plies

The next analyses were concerned with the addition of a filler ply in the bond between the chamber and the first ply of the normal four-ply patch to help lower the peak shear stresses at the defect edge. The location of a filler ply in the bond line can be found in Figure 48. Again, for convenience, the loading consisted of a 1000 psi internal pressure. Initially, two types of fillers were considered. First, a filler ply of S/81-904 glass cloth with the weave oriented at 45° to the defect axis was considered. This material is the same as used in all repair patches in this program with only the orientation varied. Plots of the axial strain distribution, axial stress distribution per ply, and the bond line shear stress distribution are shown in Figures 47, 48 and 49. The axial strain and stress distributions indicate lower values when compared to the basic four-ply analysis. However, comparison of the shear peaks of Figures 42 and 49 indicates that the shear stress levels were not lowered. Therefore, this analysis indicates an unsuccessful redistribution of bond line shear stresses when a fiberglass cloth filler ply is used.

The second type of filler ply consisted of a 0.0067-in.-thick rubber material with a low modulus (i.e., 1000 psi). Plots of the axial strain distribution, axial stress distribution per ply, and the shear stress distribution for a rubber filler are shown in Figures 50, 51 and 52. The stress and strain plots indicate that the load to be carried has been more uniformly distributed across the plies. This condition would permit the addition of outer plies of cloth to help reduce the maximum stresses in the first ply. The shear stress distribution plot indicates a significant decrease at the defect edge. The maximum shear stress has been shifted to the edge of the rubber and is about 70% of the maximum for a normal four-ply repair. This analysis has indicated that the use of a rubber filler material in the bond line can both significantly reduce peak shear stresses and can provide a more uniform distribution in the patch plies. This can be readily evaluated by comparing Figure 52, which shows the shear stress distribution in a bond line with a rubber filler, with Figure 42.

To gain additional information concerning the effects of adding a rubber filler, a parametric study of rubber filler configurations was performed. This series of computer analyses attempted to determine the effects of rubber variations on the shear stress distribution. Figures 53 through 59 show the shear stress distributions resulting from changes in shape, thickness, length, and location. Comparisons of these figures indicate that a 0.003-in.-thick filler located above the bond line midsection would reduce the stresses most significantly. However, in absolute numbers there is less than a 10% difference in maximum bond line shear stresses for the various rubber configurations considered.

D. TASK III - X259 MOTOR CASE HYDROTEST

1. Introduction

The results obtained in the original program(1) clearly demonstrated that certain defects will not affect motor performance and that extensive fiberglass defects can be successfully repaired. However, these results were obtained from one specific type of rocket motor. The question remained as to whether or not results obtained from the X248 chambers were applicable to other fiberglass rocket motors. Thus, the objective of Task III was to demonstrate that the present patching technique could be successfully applied to a modern design motor case such as the X259 rocket motor.

2. X259 Stress Analysis

The first step of this task was to perform a brief stress analysis of the X259 chamber cylindrical section to determine the stress-strain distribution in this section. These data would then be used to determine defect location and size and to establish the patch design. A picture of a loaded X259 chamber is shown in Figure 60.

The stress analysis of the X259 cylindrical section utilized the Hercules Finite Element Program (62105). The following winding geometry is found in the cylindrical section:

Fiberglass/Resin Layers	Fiber Orientation
1	90°
1	30°
1	90°
2	30°
1½	90°
3	25°
1	90°
2	25°

The analysis indicated that for an internal pressure of 1000 psi, used for convenience in computation, the strains were uniform along almost the entire cylindrical section. These values start to vary in the area of the junction of the skirt, dome and cylindrical section. The magnitudes of the strains were:

Hoop = 2.8%
Axial = 0.58%

Data taken from the results of earlier hydrotests of X259 chambers(4) indicate the following measured strains at 250 psi:

Hoop = 0.63%
Axial = 0.13%

When extrapolated to 1000 psi:

Hoop = 2.5%
Axial = 0.52%

Comparison of these values to the analytical data indicates agreement between the two sets of values.

Since the strain distribution in the cylindrical section was uniform along almost the entire length, the selection of defect locations was not restricted.

3. X259 Motor Case: Defects, Repair, and Test

a. Defect Selection and Description

These defects and their respective locations are shown in Figure 61

The following four defects were machined into the cylindrical section of the X259 chamber:

Defect No. 1 - A circumferential defect 5.0 in. long x 0.10 in. wide x 100% deep (completely through fiberglass) and located 18.5 in. aft of the face of the forward skirt ring and centered at 310°.

Defect No. 2 - A circumferential defect 5.0 in. long x 0.10 in. wide x 100% deep (completely through fiberglass) and located 41.5 in. aft of the face of the forward skirt ring and centered at 50°.

Defect No. 3 - A longitudinal defect 5.0 in. long x 0.10 in. wide x 100% deep (completely through fiberglass) and located at 310° between 39.0 in. and 44.0 in. aft of the face of the forward skirt ring.

Defect No. 4 - A longitudinal defect 5.0 in. long x 0.10 in. wide x 100% deep (completely through fiberglass) and located at 50° between 16.0 in. and 21.0 in. aft of the face of the forward skirt ring.

The X259 was judged to be sufficiently large to permit testing two longitudinal and two circumferential defects without impairing test validity. The use of two sets of similar defects would help to confirm test data to be developed. Also, data as comparable to X248 (1,2) data as possible were sought.

The 0.10-in. width of the defects was chosen in order to maintain consistency with the X248 defects. The lengths of the defects were determined from an extrapolation of X248 test and analyses data to the X259 test requirements.

Under Task I of this program the small bottle tests indicated that (1) the Epon 946 bond system was capable of transmitting a load of 2400 lb/in. of defect length for an infinite defect and (2) the strength of a four-ply patch was sufficient to produce a bond shear failure before a tensile failure. From X248 data for a 7.5-in.-long defect with a four-ply repair the observed strain on the outermost ply was 1.3%. The predicted strain from the theoretical stress analyses for an infinite defect was 3.9%. It was recognized that at least two factors might be involved in this discrepancy. These are the chamber winding geometry and the repair patch characteristics. No determination could be made as to the degree of effect from either. In the selection of a defect length, it was assumed that the 1.3/3.9 actual to theoretical strain ratio was valid for a four-ply repair of an X259 defect.

The test plan included a dwell period of 520 psi followed by a pressure increase to failure. The 520 psi was used as the basis of a minimum failure. At 520 psi, the X259 chamber has a theoretical hoop load of 7800 lb/in. of defect length to be transferred over a defect. However, based on the 0.33 actual to theeretical correction factor, this load would only be 2580 lb/in. for a four-ply repair. In order to reduce this load to below the 2400 lb/in. resin strength, the defect length was reduced to 5.0 inches. This, in turn, would reduce the load to be transferred to 2220 lb/in.

b. Repair Materials

The resin system, Epon 946, used in the repair of the applied defects was the same as used on the bottle repairs in Task I and on earlier repairs of X248 motors.(1-3) The fiberglass repair cloth, Owens-Corning S/81-904, is the same as used to repair the Task I bottles; however, it differs slightly from the S/81-901 used in the X248 repairs. The difference is in the finish of the cloth. The S/81-904 cloth was selected for use throughout the present program because (a) comparative specimen tests (1-3) indicated the substitution would not affect the patch strength and (b) the 904 finish cloth has superior shelf life characteristics and can be stored at room temperature while 901 requires storage under refrigeration.

c. Repair Procedure

The procedure used to repair the X259 motor case defects was basically the same as that used to repair the X248 motors in the earlier program. However, two modifications to the repair procedure were implemented. First, the bond line under the first ply of the patch was thickened close to the defect by precoating an area of the case within 1.0 inch of the defect with Epon 946 and then allowing it to B-stage. The B-stage precoat had been used to successfully produce much thicker bond lines in Task I than had been previously achieved in X248 repair. Theoretical analyses had indicated a drop in peak shear stresses at the defect edge for thicker bond lines. It was therefore expected that bond line strengths would show a considerable improvement over the strength that was previously demonstrated in the original program. The second modification consisted of reducing the size of the patch plies. This was done because the patch strains beyond the defect area are quite low (see Figure 40).

After the defects had been machined into the chamber, the chamber was repaired. The size of the repair plies and repair procedure are found in the X259 Test Plan in Appendix A. The repair procedure is repeated below, and reference is made to these figures which illustrate the technique:

(1) The repair area was marked off and then sanded until the surface gloss on the chamber had been removed (Figure 62).

(2) The sanded area was then cleaned with methylene chloride.

(3) A thick layer (minimum of 0.020 in.) of Epon 946 resin, which had been B-staged for ½ hour, was applied to the area within one inch of the defect (Figure 63).

(4) After the applied resin had been allowed to B-stage for a minimum of four hours, the edges of the resin were tapered to avoid air pockets during patch application (Figure 64).

(5) A thick layer of Epon 946 resin, B-staged for 15 minutes, was then applied to the chamber.

(6) The first ply of fiberglass cloth was placed over the defect, and the resin was worked up through the ply (Figure 65).

(7) Another layer of resin was then added. The next ply was placed over the resin-coated first ply, and the resin was worked up through the second ply. This step was repeated for all the subsequent plies (Figures 66 through 68).

(8) Upon the completion of patching, the repaired chamber was allowed to cure for a minimum of seven days at room temperature.

(9) The two defects at the 310° location were repaired first. A minimum of 36 hours elapsed before the unit was rotated so that the two defects at 50° could be repaired.

The repair procedure established for fiberglass defects in the cylindrical section of any motor is presented in detail in Appendix B.

d. Hydrotest Arrangement

Upon completion of patch cure, the X259 chamber was instrumented in accordance with Table I of the Appendix A. These strain gage locations are shown in Figure 69. A schematic diagram of the X259 hydrostatic test arrangement is shown in Figure 70. The pretest pictures of the hydrotest setup are shown in Figures 71 and 72. The plot of the pressure versus time program is shown in Figure 73. A constant pressure of 200 psig was used to measure increase in strain because this pressure was considered a safe level at which the strain gage readings could be analyzed. The 520-psig hydrotest pressure was chosen because it was used to evaluate damaged chamber S/N HPC-162 in an earlier investigation of fiberglass defects and the data could be compared. Also, on the basis of the favorable result of that test, another motor with similar damage was accepted for flight and was used successfully.

4. Test Results

The X259 chamber was hydrotested on February 23, 1970. At a pressure of 312 psig, a patch failure occurred in the aft longitudinal defect (Defect No. 3). This pressure is only 48% of the original burst capability of approximately 660 psig. This low pressure failure, especially in tension, had not been expected. Post-test pictures (Figures 74 and 75) and an examination of the patch which indicated that it was still fully bonded to the chamber eliminate the possibility of a shear failure.

A review of motion picture films showed the mode and progression of the patch failure. Figures 76A through 76F are motion picture frames from the films of the failure sequence. These pictures, taken at intervals of 1/1000 of a second, illustrate the tension failure in the patch. The escape of water in the defected area shows the progression of the failure along the defect. Subsequent examination of the case showed the rip to be directly over the defect.

For the post-test examination of the unit, the two longitudinal defects were sectioned in one-inch increments. An examination of each section indicated that the patches had good bond thicknesses and contained no voids. The good bond line thickness (0.020 in. minimum in defected areas) and the absence of voids are quite apparent from these photos. The resin in Defect No. 4 was cracked as shown in photomicrographs of several sections (Figures 77 through 80). This cracking was probably due to the high strain in this particular area. Cracks of this type had developed in the bottle tests of Task I at load levels as low as 1350 lb/in. of defect length. The presence of such cracks is not considered to indicate patch failure. However, such cracks must be sealed to prevent leakage of water and possible premature patch failure during hydroburst. In this test, Prestite was used to prevent leakage in the defected areas.

As indicated in the previous text, the strain data were recorded by gages on the chamber wall and on the patches. Table IV lists the hoop and axial strains versus pressure for the gages on the chamber wall. These values were 1.29 to 1.38 times higher than had been expected on the basis of results from previous hydrotests and stress analyses. This was probably due to the defects being near the areas of strain reading. These data indicate an increase of load around the defects and into the undefected portions of the chamber.

Plots of the strain versus pressure for strain gages located on the patches are shown in Figures 81 through 84. The plot of hoop strain versus pressure for Defect No. 3 indicates a considerable increase in strain at pressures above 290 psig. It is believed that this was due to the initiation of a failure in the first ply of the patch which would have caused the load to be transferred to the three other plies, resulting in the abrupt increase in strain measurements on the outer ply. The strain data for Defect No. 4 does not reflect this sharp increase. However, the strain data recorded one inch forward of the defect center are higher than those for the center of the patch. This is due partly to a 6° error in the orientation of the center gage. Therefore, an indication of higher loading occurring away from the patch center should not be derived from this plot. The strains over the circumferential defects are considerably lower and are in good agreement with each other. Plots of the strain versus time for all gages are located in Appendix C.

The recorded strains from an X248 test and those for this X259 hydrotest were compared. The X248 (NPP-242) test was of a four-ply repair for a 7.5-in.-long defect. These strain data were compared with strain data from Defect No. 3 in the X259 chamber (NPP-98). The comparisons will not account for the variation between the lengths of the defects. First, strain values were compared at the same pressure, 290 psig (Figure 85). This graph shows that the higher strain values were located in the outer ply of the X259 repair. The maximum strains at the center of the patch are only approximately 1.38 times higher in the X259 repair than in the X248 because of the higher loading at this pressure. This result was expected because of the smaller defect in the X259 chamber and the variations in both wall thickness and winding geometry. Strains were then compared at supposedly equivalent loading conditions in Figure 86. Because the X259 radius is 1.67 times larger than that of the X248, the X248 pressure was 375 psig and the X259 pressure was 224 psig. This dissimilarity resulted in a considerable difference between the strain values. The lower X259 values were probably due to the use of a smaller defect and the first ply bearing much more load than the subsequent plies. The difference in the shape of the curves in Figure 86 seems to indicate a more uniform loading in the X259 repair patch. This could possibly be due to the differences that exist between the two types of chambers (i.e., winding geometry, radius and thickness), as well as the better patches obtained in the X259 tests.

In conclusion, it is believed that excellent repair patches were obtained in the X259 tests. However, failure in the glass cloth patch under the high loading conditions indicates that the patch must be modified. The Task II analyses indicated one modification which might produce better load and shear distributions. The use of stronger cloth or the addition of more plies may also be necessary. These possibilities should be investigated in the future.

E. TASK IV - EPON 946 AGING STUDY

1. Objective

The objective of Task IV was to determine to what extent, if any, the most critical physical properties of the repair materials, primarily the Epon 946 resin, change with age.

2. Surveillance Test Plan

For this resin-aging study, 35 specimens (of the configuration shown in Figure 87) were fabricated, cured for different time periods at ambient temperature and tested to determine shear stress levels, failure modes and failure locations. The three-plate shear specimens are 1.0-in.-wide and the bonding area is 1.0-in.-long. The specimens consist of glass cloth bonded to Spiralloy mat with the Epon 946 resin system. This was, in turn, bonded to Side A and Side B of the three-plate shear specimens. The following five groups of specimens were tested at a cross-head speed of 3 in./in./min:

Group	No. Specimens	Aging Time
1 (control)	10	One week
2	5	One month
3	5	Three months
4	5	Six months
5	5	Nine months

The five remaining specimens will be retained for possible testing at a later date.

3. Test Results

a. Group 1 (One-Week Aging)

Results for the control group (ten specimens), aged one week at room temperature, are given below:

Sample No.	Shear Stress (psi)	Modes of Failure: Side A	Modes of Failure: Side B
1	1745	100% - Epon 946 to Spiralloy	50% - Delamination in Spiralloy 50% - Failure of C7 bond to Spiralloy
2	1675	100% - Epon 946 to Spiralloy	Same as above
3	1550	100% - Epon 946 to Spiralloy	100% - Failure at C7 bond to Spiralloy
4	1280	50% - Epon 946 to Spiralloy 50% - Split between 2 plies of S904 cloth	100% - Failure at C7 bond to Spiralloy
5	1525	100% - Epon 946 to Spiralloy	100% - Failure at C7 bond to Spiralloy
26	1600	100% - Epon 946 to Spiralloy	100% - Epon 946 to Spiralloy
27	1375	100% - Epon 946 to Spiralloy	100% - C7 to Spiralloy
28	1635	100% - Epon 946 to Spiralloy	50% - C7 to Spiralloy 50% - Delamination of Spiralloy
29	1697	100% - Epon 946 to Spiralloy	100% - C7 to Spiralloy
30	1388	100% - Epon 946 to Spiralloy	100% - C7 to Spiralloy
Average	1547		

The failure modes were very nearly identical in every case; however, the reasons for the comparatively high variation are not obvious. The specimens may have differed in bond line thickness, and the aluminum plates may have been misaligned.

b. Group 2 (Aged One Month)

The next five specimens were tested one month after the initial 7-day cure period. Results are given below:

Sample No.	Shear Stress (psi)	Modes of Failure	
		Side A	Side B
6	1455	Epon 946 to Spiralloy	C7 to Spiralloy
7	1367	Epon 946 to Spiralloy	C7 to Spiralloy
8	1720	Epon 946 to Spiralloy	75% C7 to Spiralloy 25% delamination in Spiralloy
9	1825	Epon 946 to Spiralloy	75% C7 to Spiralloy 25% delamination
10	1697	Epon 946 to Spiralloy	25% C7 to Spiralloy 75% delamination
Average	1613		

This average is 66 psi higher than the average for the controls. Some of the individual shear values were higher in this set than in the controls, probably reflecting continued curing of the specimens at room temperature. Delaminations in the Spiralloy did not appear to be detrimental to the shear values.

c. Group 3 (Aged Three Months)

The next five specimens were tested three months after the 7-day cure period. Results are given below:

Specimen No.	Shear (psi)	Modes of Failure	
		Side A	Side B
11	905	Epon 946 to Spiralloy	Glass mat delaminated
12	1662	Epon 946 to Spiralloy	C7 to Spiralloy
13	1537	Epon 946 to Spiralloy	C7 to Spiralloy
14	1450	Epon 946 to Spiralloy	C7 to Spiralloy
15	1325	Epon 946 to Spiralloy	50% C7 to Spiralloy and 50% glass mat delaminated.
Average	1376		

The very low value of Specimen No. 11 was attributed to delamination on one side. The average of the five specimens is 1376 psi or 11% lower than the average of the control specimens. At this time, the difference does not appear to be of major significance because of the very low value obtained for Specimen No. 11.

d. Group 4 (Aged Six Months)

The next five specimens were tested six months after the 7-day cure period. Results are given below:

Specimen No.	Shear (psi)	Modes of Failure	
		Side A	Side B
16	1410	Epon 946 to Spiralloy	50% C7 to Spiralloy 50% Spiralloy delaminated
17	1565	75% Epon 946 to Metal 25% Epon 946 to glass mat	25% C7 to Spiralloy 75% Spiralloy delaminated
18	1712	Epon 946 to Spiralloy	C7 to Spiralloy
19	1165	Epon 946 to Spiralloy	100% Spiralloy delaminated
20	1735	Epon 946 to Metal	C7 to Spiralloy
Average	1517		

Where the Spiralloy had delaminated, shear values were lower, as expected. The average shear for these five specimens is 1517 psi, a loss of 2.0% from the control average.

e. Group 5 (Aged Nine Months)

The final five specimens were tested nine months after the 7-day cure period. Results are listed below:

Specimen No.	Shear (psi)	Modes of Failure	
		Side A	Side B
21	1100	Epon 946 to Spiralloy	C7 to Spiralloy
22	1440	Epon 946 to Metal	C7 to Spiralloy
23	1487	Epon 946 to Spiralloy	50% C7 to Spiralloy 50% Spiralloy Delamination
24	1790	Epon 946 to Spiralloy	C7 to Spiralloy
25	1500	Epon 946 to Spiralloy	C7 to Spiralloy
Average	1463		

The 1463 psi average represents a 5.0% decrease in shear strength. However, this decrease is due primarily to the low value obtained for Specimen No. 21.

The data obtained for the intervals up to the nine-month room temperature aging indicates no significant loss in shear strength for the S81-904 glass cloth and Epon 946 resin combination. Any variations are due primarily to one specimen in each group exhibiting a low failure level. In most cases this is due to glass delaminations.

f. Evaluation of Testing Method

The three-plate shear specimen method for determining shear strength has provided consistent results. Variations are due primarily to the complexity of the construction of the specimen (see Figure 87). Considering the complexities, the feasibility of fabricating uniform specimens appears to be quite doubtful. However, the results obtained indicated that of all the specimens fabricated, only a few were of substandard quality.

REFERENCES

(1) Enie, R. B. and Hitt, C. R., Jr., "Comprehensive Report on NASA Rocket Motor Defects Investigation - From August 1966 to June 1968," Hercules Incorporated/Allegany Ballistics Laboratory, National Aeronautics and Space Administration Contract NAS 1-6367, Volume I - Technical Investigation, NASA CR-66813.

(2) Ibid., Volume II - Tables and Figures, NASA CR-66814.

(3) Ibid., Volume III - Appendices, NASA CR-66815.

(4) Morash, Richard T. and Driscoll, Richard F., "Pressure Growth of X259 A2 Spiralloy Chambers," Hercules Incorporated/Allegany Ballistics Laboratory, ABL/X-101, July 1963.

TABLE I

TENSILE STRENGTH S/81/901 GLASS CLOTH/EPON 946 PATCHES - 3 IN./IN./MIN

Gage Length = 1.7 in. CHS = 5.0 in./min

Approximate Thickness of 1 Ply of Cloth = 0.014 in.

No. of Plies	Direction of Load	Specimen Number	Specimen Load (lb)	Stress (psi)	Deflection (in.)	Strain (in/in)	Modulus $\times 10^5$ (psi)
1	Warp	2	287	54,700	.136	.080	6.83
		3	312	59,400	.147	.087	6.86
		4	258	49,100	.132	.078	6.34
		5	303	57,700	.146	.086	6.72
1	Fill	1	255	48,600	.134	.079	6.17
		2	244	46,500	.128	.075	6.18
		3	228	43,400	.125	.074	5.92
		4	257	49,000	.142	.084	5.87
		5	243	46,300	.128	.075	6.16
2	Warp	1	552	52,600	.147	.087	6.07
		2	492	46,900	.138	.081	5.77
		3	502	47,800	.128	.075	6.35
		4	449	42,800	.139	.082	5.23
		5	570	54,300	.159	.094	5.81
3	Warp	1	830	52,700	.177	.104	5.07
		2	865	54,900	.182	.107	5.13
		3	900	57,100	.186	.109	5.22
		4	970	61,600	.189	.111	5.53
		5	830	52,700	.165	.097	5.43
4	Warp	1	1190	56,700	.191	.112	5.04
		2	1340	63,800	.195	.115	5.57
		3	1275	60,700	.193	.113	5.35
		4	1415	67,400	.215	.126	5.33
		5	1515	72,100	.232	.136	5.29

TABLE II

SIX-INCH BOTTLE TEST RESULTS

Bottle No.	Type of Repair	Test Results
1	Four Ply	Developed a leak at 925 psig.
2	Four Ply	Developed a leak at 850 psig. Leak was sealed. Retest yielded a shear failure at 965 psig.
3	Three Ply	Failed in tension at 1143 psig.
4*	Four Ply Inverted	Failed in shear at 1606 psig. Large voids in bond line.
8	Four Ply Inverted	Developed leak at 1150 psig. Leak sealed. Retest. Failure in shear at 1622 psig. Large voids in bond line.
5*	Four Ply Inverted	Failed in shear at 1477 psig. Large voids in bond line.
6	Four Ply Inverted	Failed in shear at 1270 psig. Numerous large voids in bond line.
7*	Four Ply Inverted	Failed in shear at 1350 psig. Large voids in bond line.

* Based on these tests the average failure pressure was 1477 psig (2365 lb/in. of defect length)

TABLE III

STRESS DISTRIBUTION FOR FOUR-PLY AND FOUR-PLY INVERTED REPAIRS

	STRESS, PER PLY, psi	
	STANDARD FOUR PLY	FOUR PLY INVERTED
PLY 4		
Element 1	51043	40265
Element 2	59620	50261
Element 3	68304	61104
Element 4	71736	66606
Element 5	70528	66910
Element 6	66928	60669
PLY 3		
Element 1	83516	80298
Element 2	84005	78300
Element 3	81398	73353
Element 4	76004	67551
Element 5	69894	57800
Element 6	63892	45816
PLY 2		
Element 1	122050	123660
Element 2	114660	11595
Element 3	99268	100140
Element 4	82760	82962
Element 5	69766	69475
Element 6	60057	53589
PLY 1		
Element 1	210260	220030
Element 2	157410	164270
Element 3	107740	111770
Element 4	77649	79729
Element 5	60328	61275
Element 6	49550	43670

NOTE: Element No. 1 is adjacent to the centerline of the defect. Each subsequent element is further from the defect centerline. All elements are 0.05 in. wide. These elements can be found in Figure 39 for the standard four-ply and Figure 43 for the four-ply inverted.

TABLE IV

STRAINS MEASURED FROM GAGES LOCATED ON X259 CHAMBER SURFACE

Axial Gages Nos.	Time (sec) / Pressure (psig)	Strain (%) 13.475 / 201	14.958 / 251	16.142 / 290	16.408 / 300	16.767 / 312
1		.19	.25	.28	.30	.30
3		.17	.22	.25	.26	.27
4		.18	.23	.26	.27	.27
7		.17	.21	.25	.26	.27
Hoop Gages Nos.						
2		.64	.80	.92	.94	.97
5		.68	.83	.97	1.00	1.03
8		.63	.80	.91	.94	.98
9		.62	.79	.91	.94	.99

NOTE: Gage locations are shown in Figure 69.

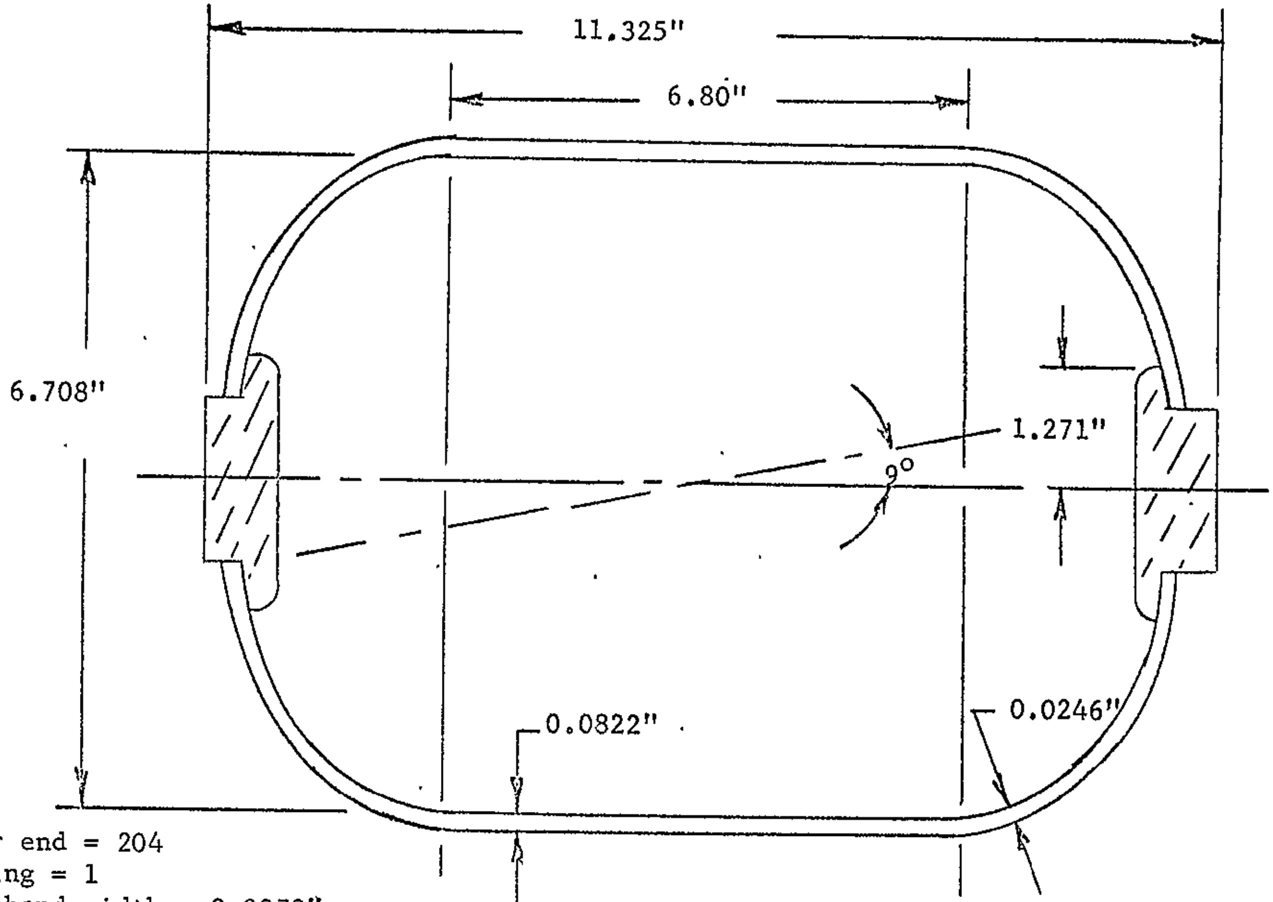

Filaments per end = 204
Ends per roving = 1
Longitudinal band width = 0.0078"
Hoop band width = 0.0072"
Band density = 256 ends/inch/layer
Geometry for dome failure: 4 longitudinal + 8 hoop
t_α/layer = 0.0082 t_{90} /layer = 0.0072

Figure 1. Dimensions and Winding Data for Fabrication of 6-In.-Diameter Bottles

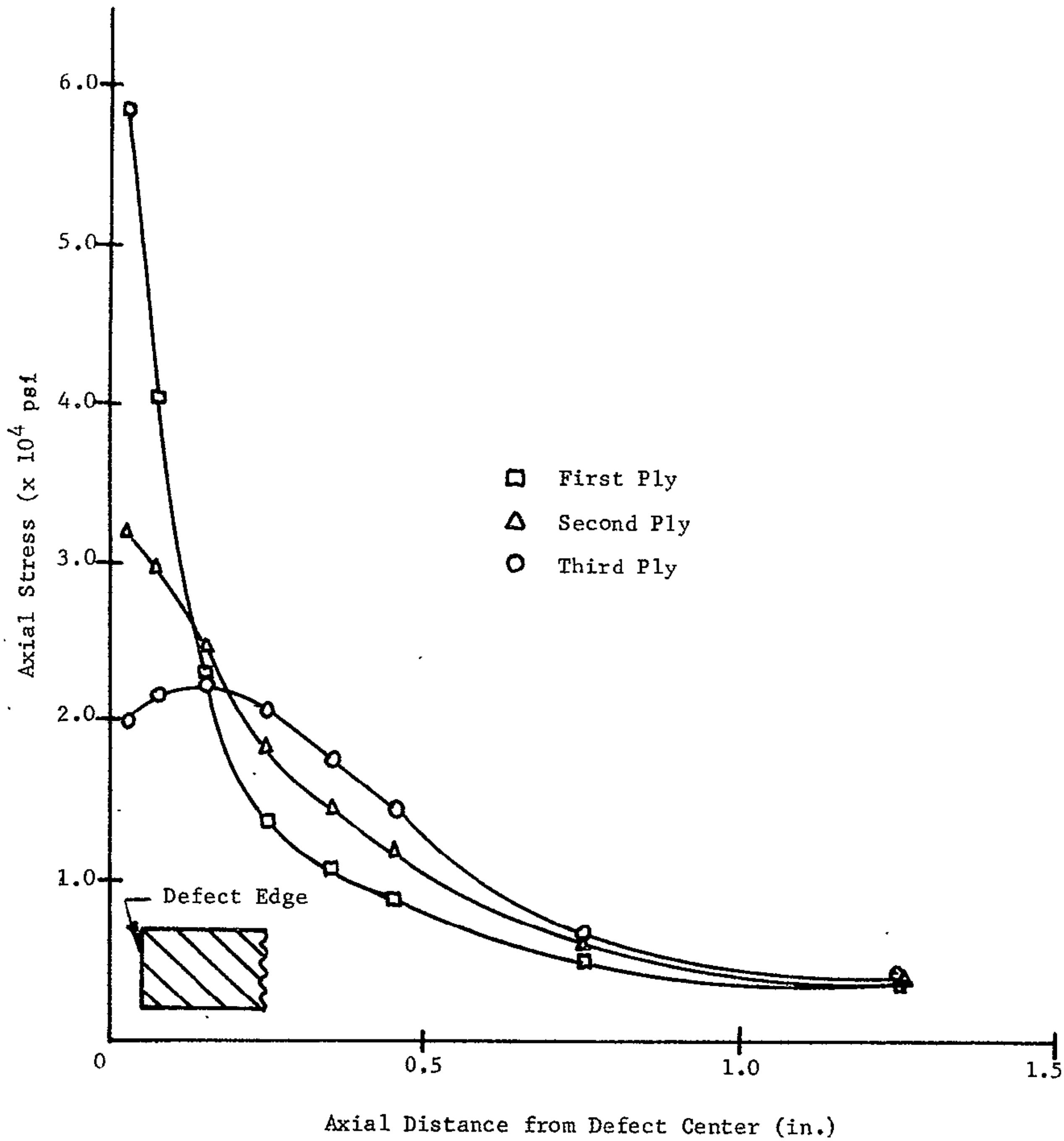

Figure 2. Axial Stress in Three-Ply Patch for 1000 psi Internal Pressure (Axial load = 1600 lb/in.) - Small Bottle Repair

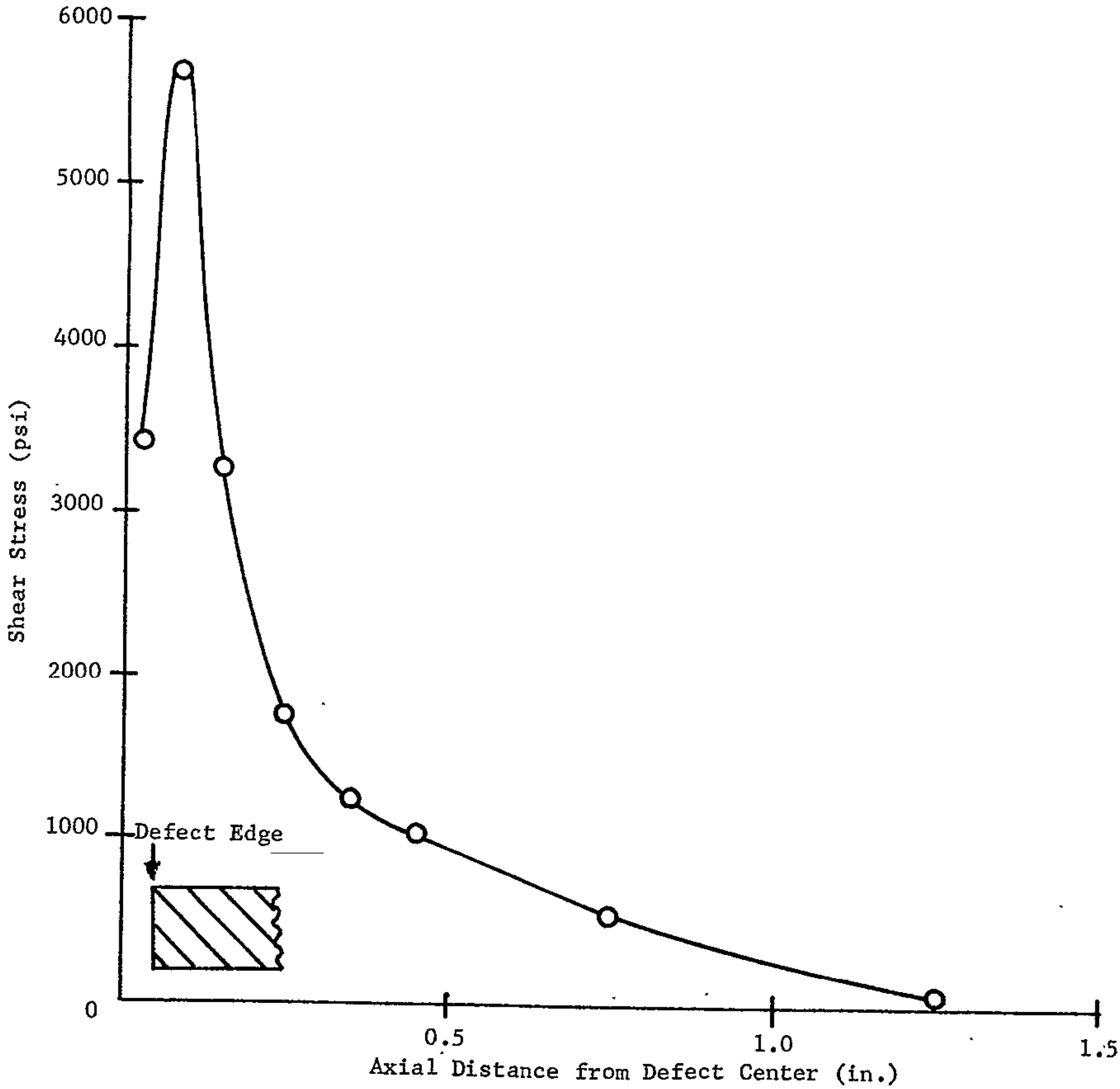

Figure 3. Shear Stress Distribution in Bond Layer for 1000-psi Internal Pressure (Axial load = 1600 lb/in.) - Small Bottle Repair

S1 @ 0° - Axial
S2 @ 90° - Axial
S3 @ 180° - Axial
S4 @ 270° - Axial
S5 @ 0° - Hoop
S6 @ 90° - Hoop

NOTE: Use BLH PA-7 Strain Gages, or equivalent

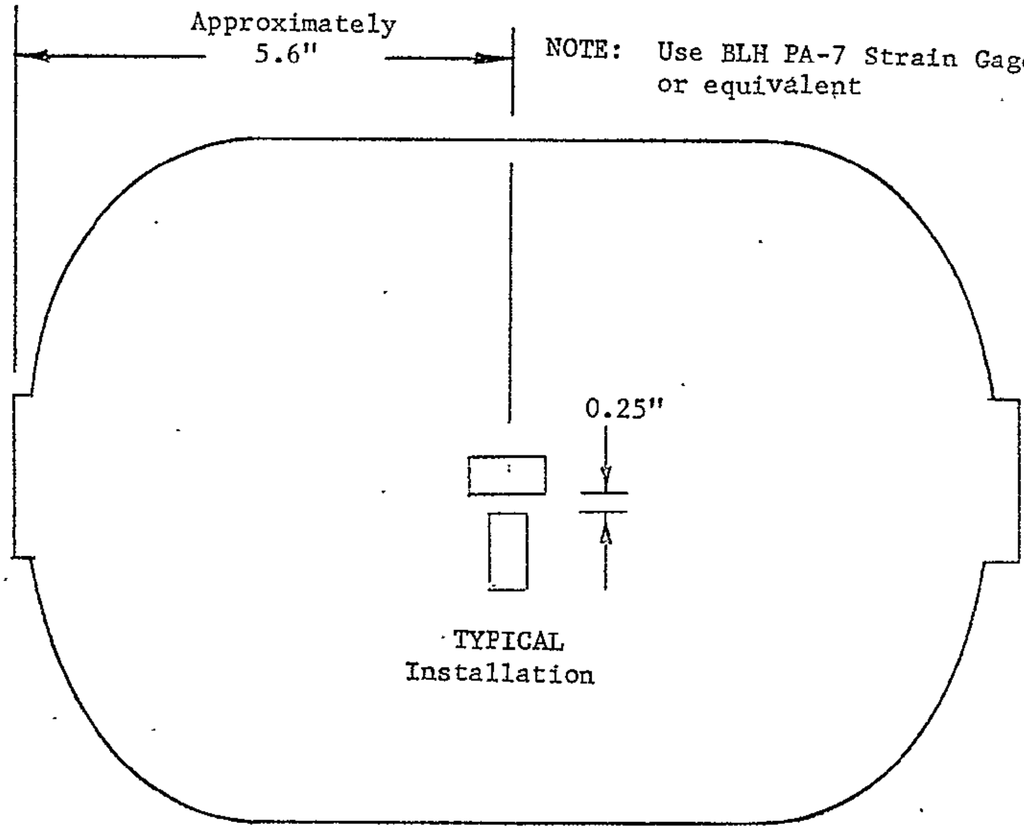

NOTE: Strain gage axial dimension is only approximate. Use dimension noted on each bottle as exact location (center of defect).

Figure 4. Strain Gage Locations

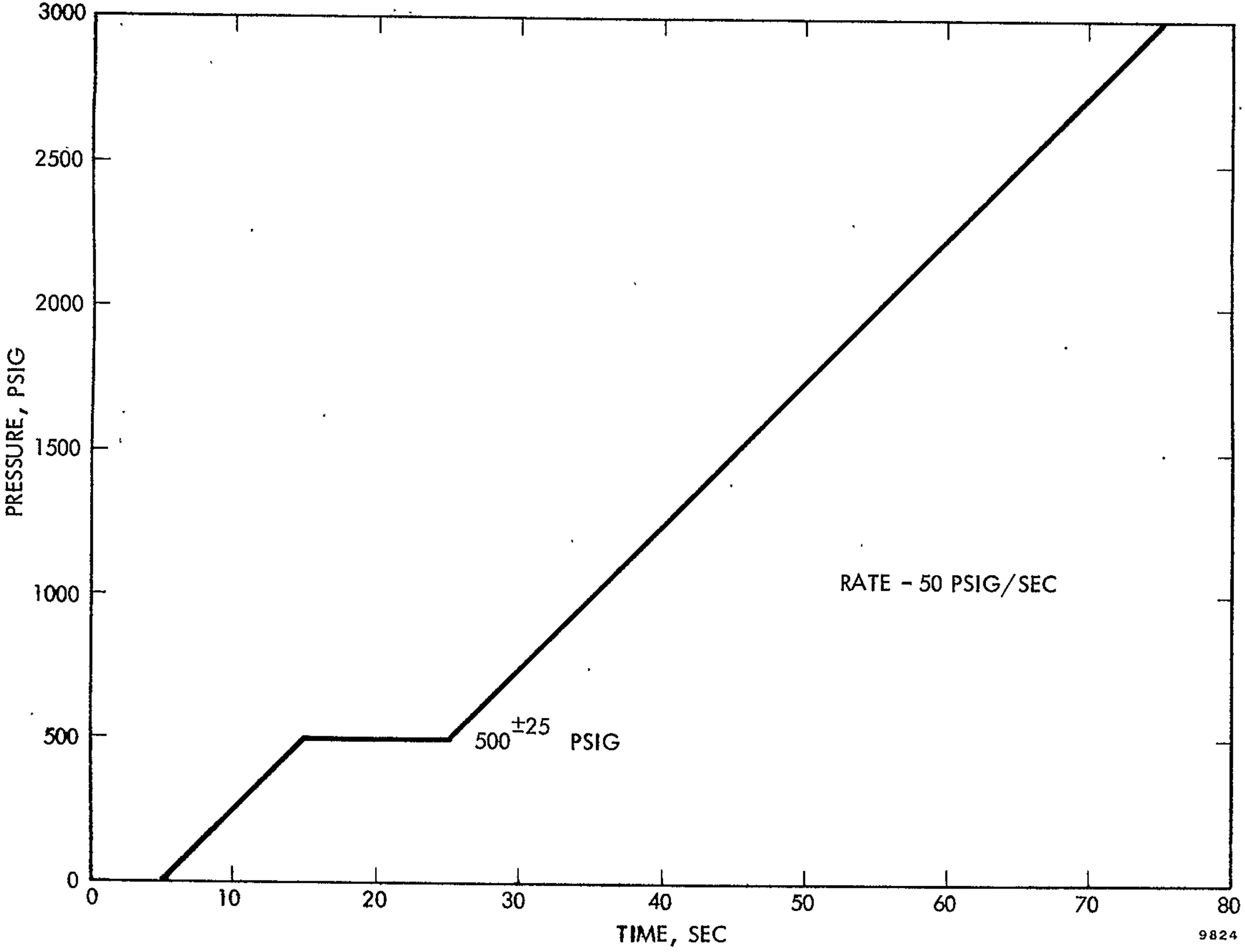

Figure 5. Pressure vs Time Profile --- Data-Trak Program

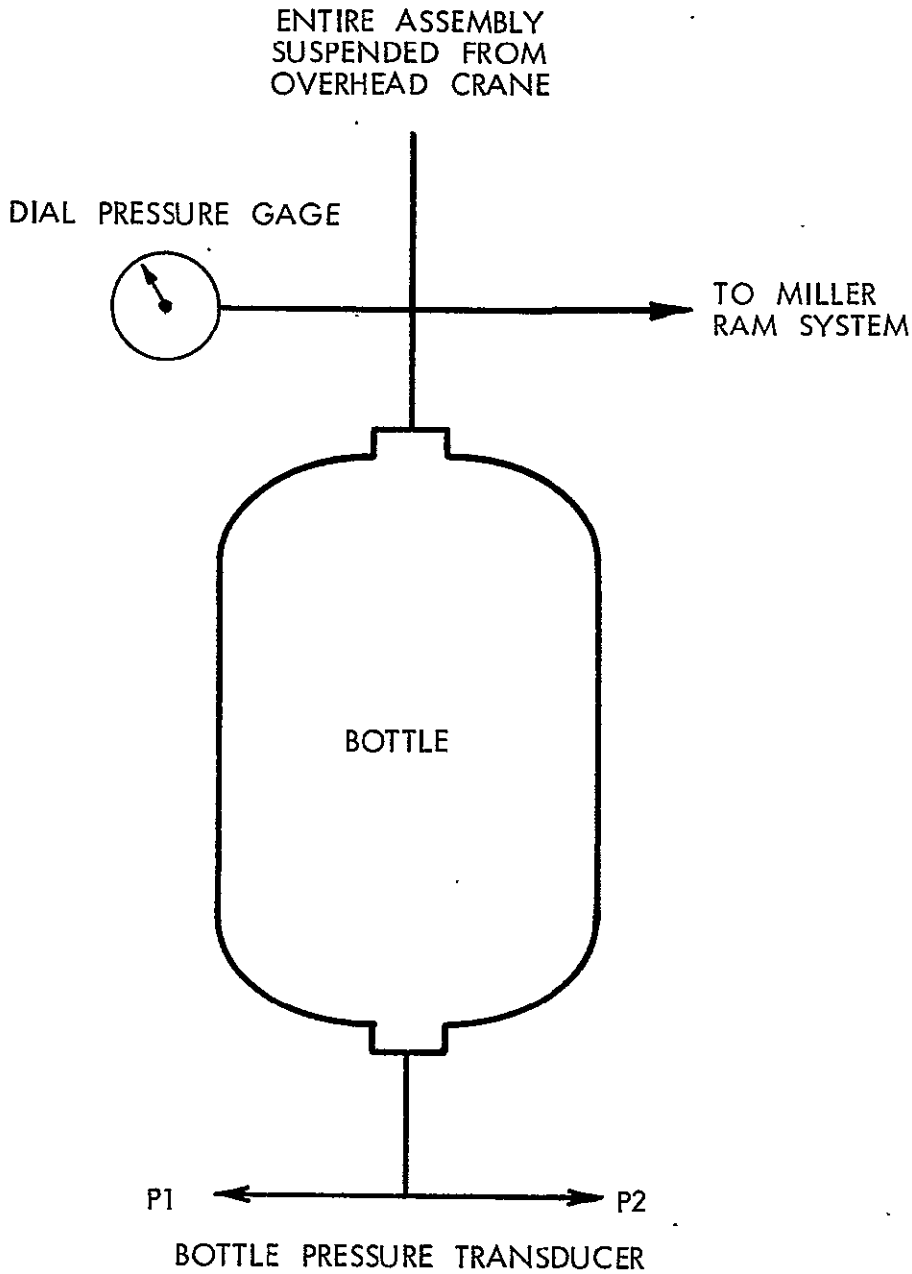

NOTE: P3 (Pressure Transducer) located on the Miller Ram System provides the feedback for the servo system.

9832

Figure 6. Diagram of Bottle Test Arrangement

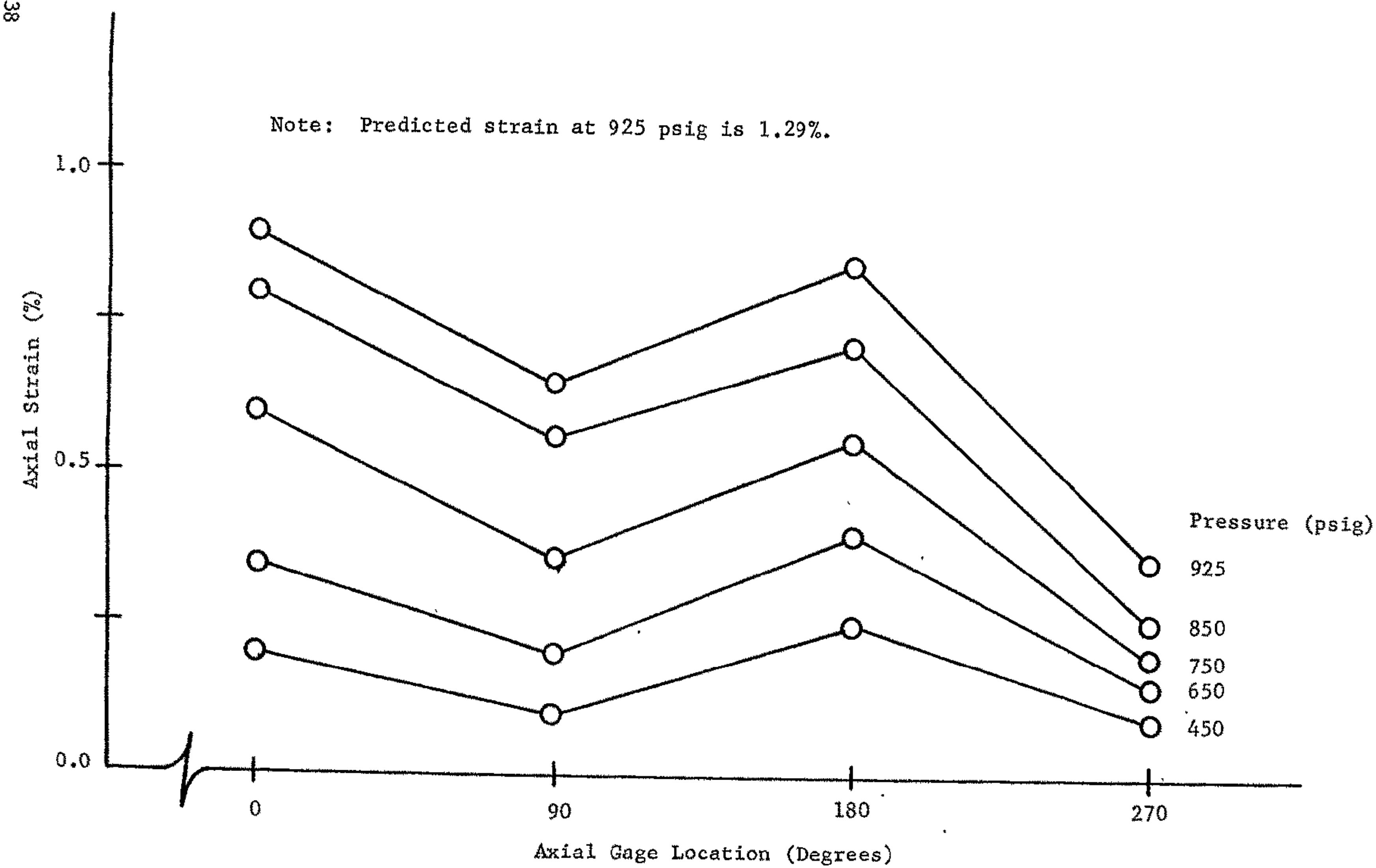

Figure 7. Bottle Test No. 1 - Axial Strain Versus Pressure (Failure at 270°)
(Maximum Axial Load = 1550 lb/in.)

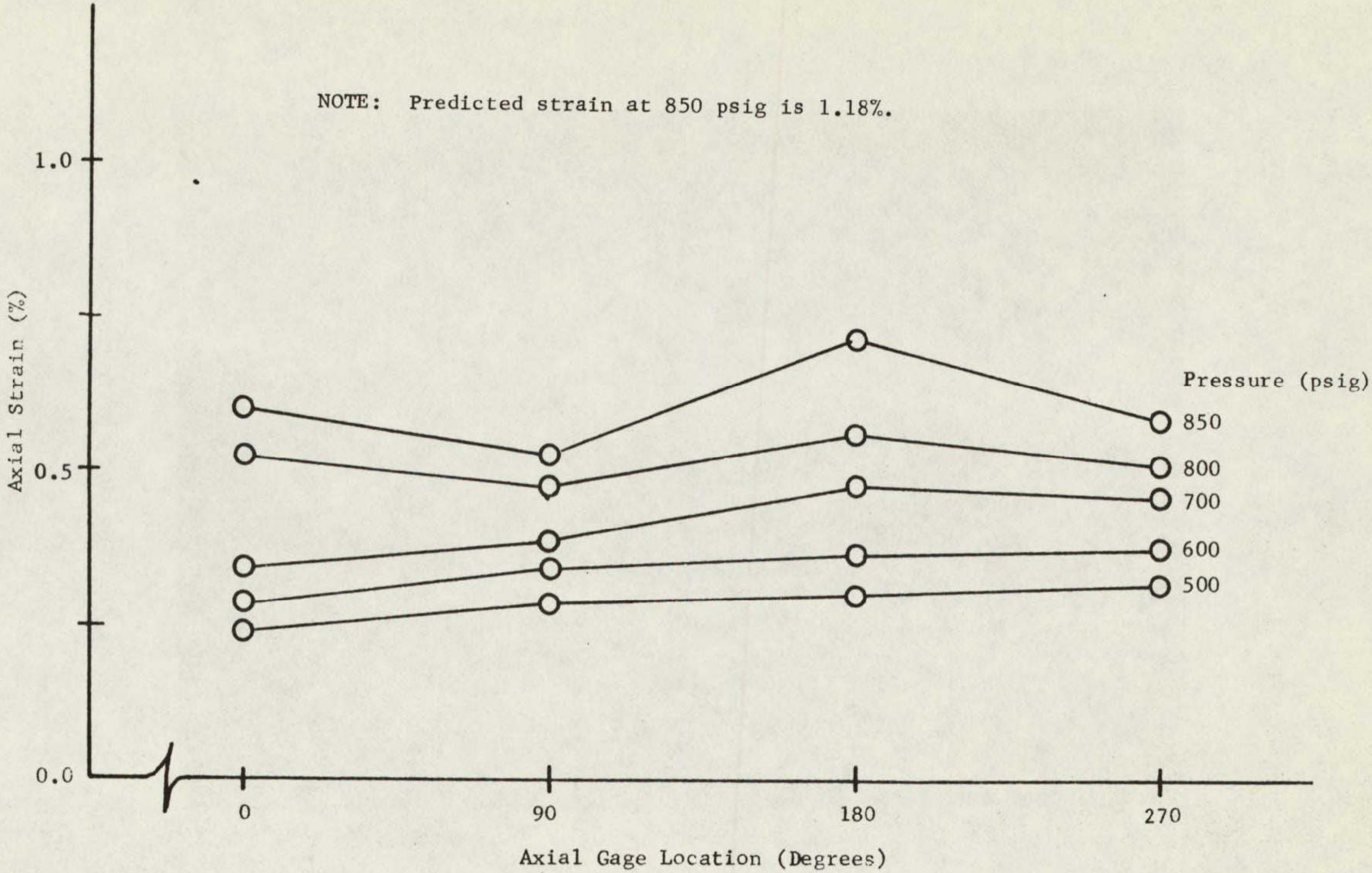

Figure 8. Bottle Test No. 2 - Axial Strain Versus Pressure (Failure at 120°)
(Maximum Axial Load = 1425 lb/in.)

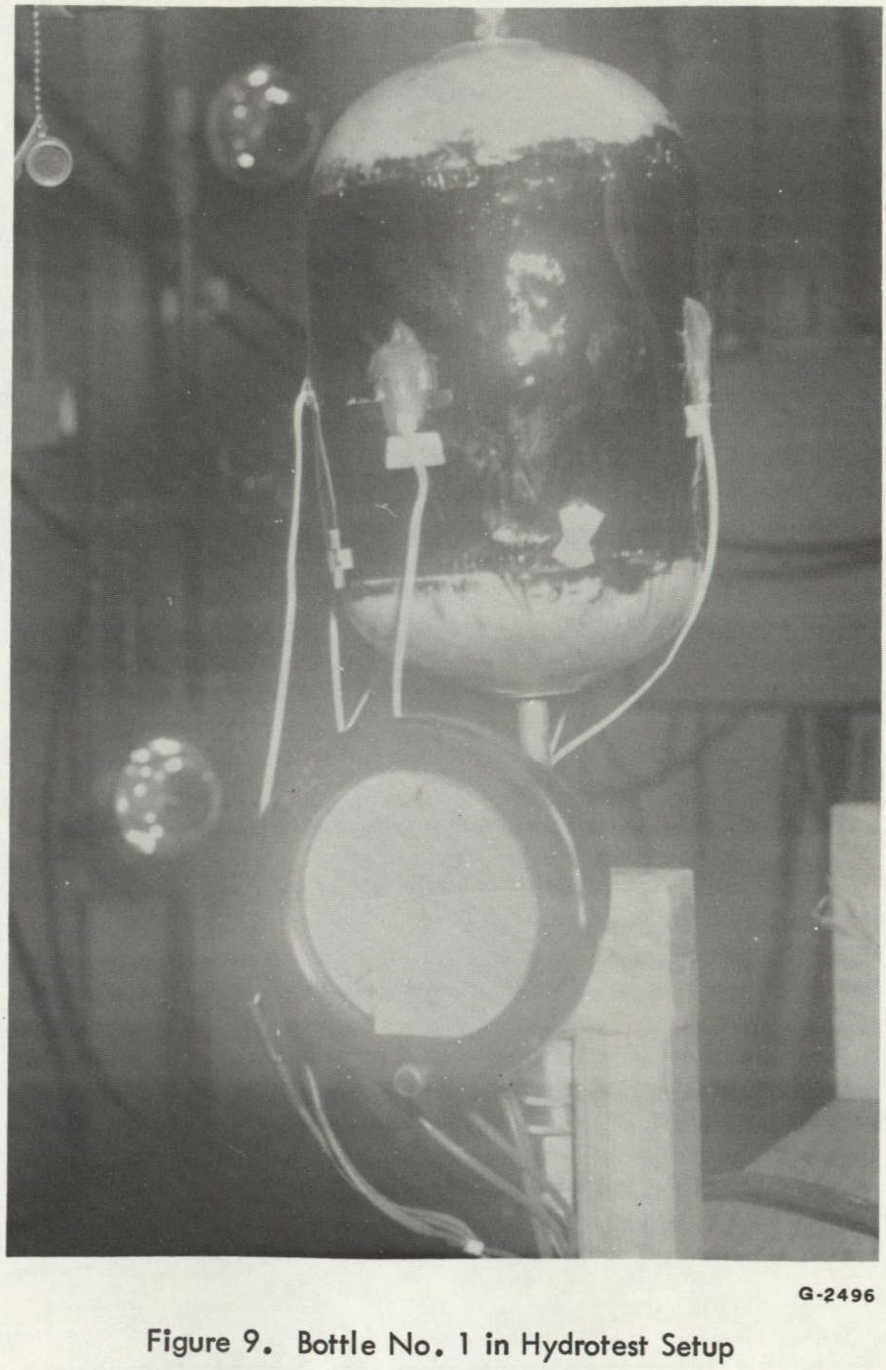

G-2496

Figure 9. Bottle No. 1 in Hydrotest Setup

Figure 10. Bottle No. 3 - Post Test View of Three-Ply Tension Failure

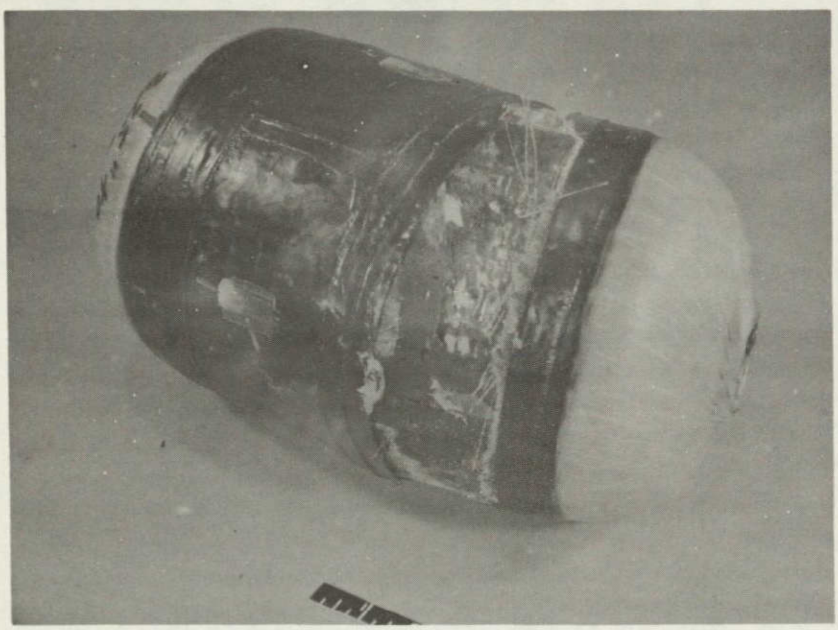

G-2490

Figure 11. Bottle No. 4 - Post Test View of Four-Ply Shear Failure

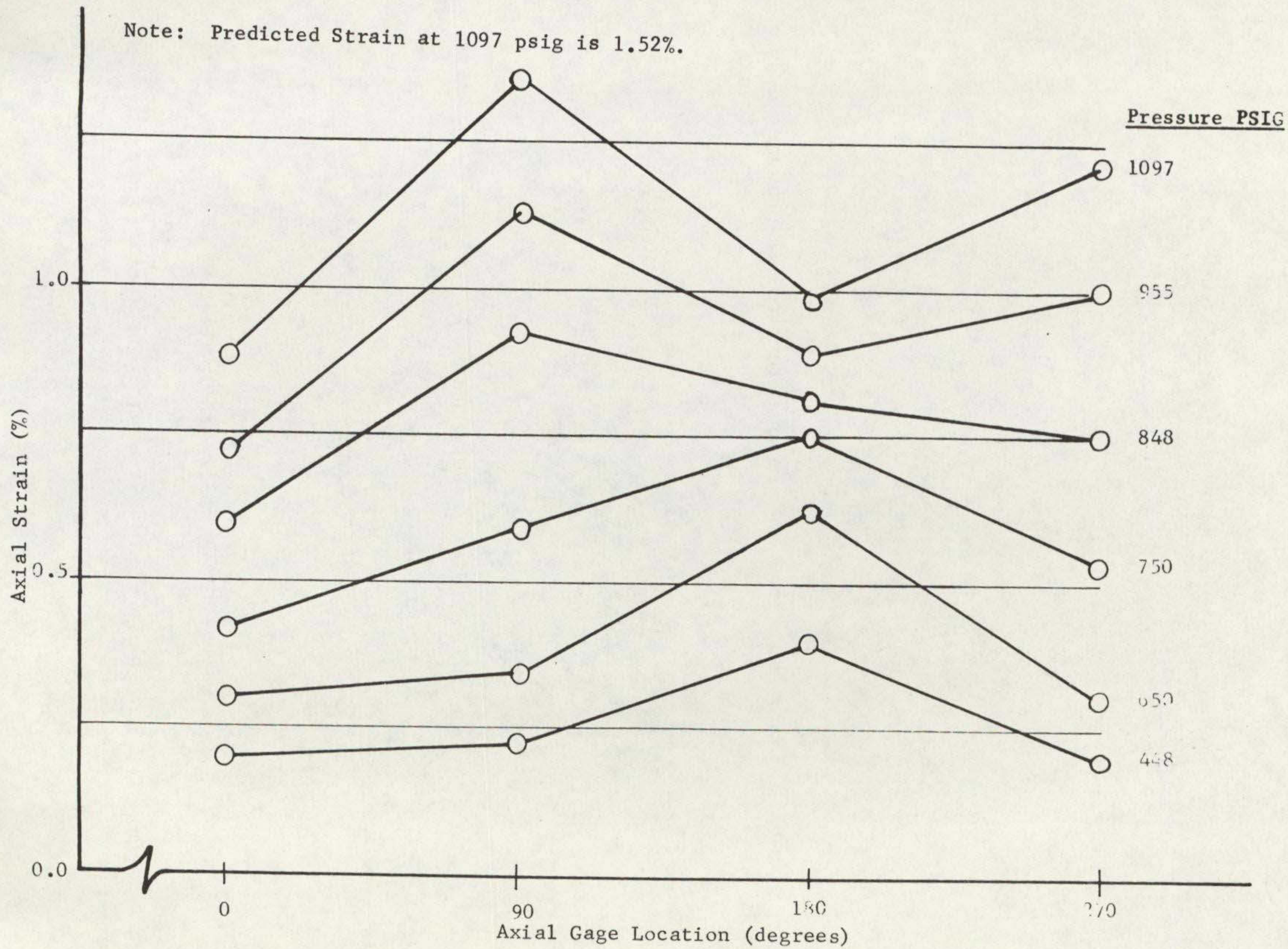

Figure 12. Bottle No. 3 - Axial Strain Versus Pressure (Maximum Axial Load = 1830 lb/in.) (Failure at 0°)

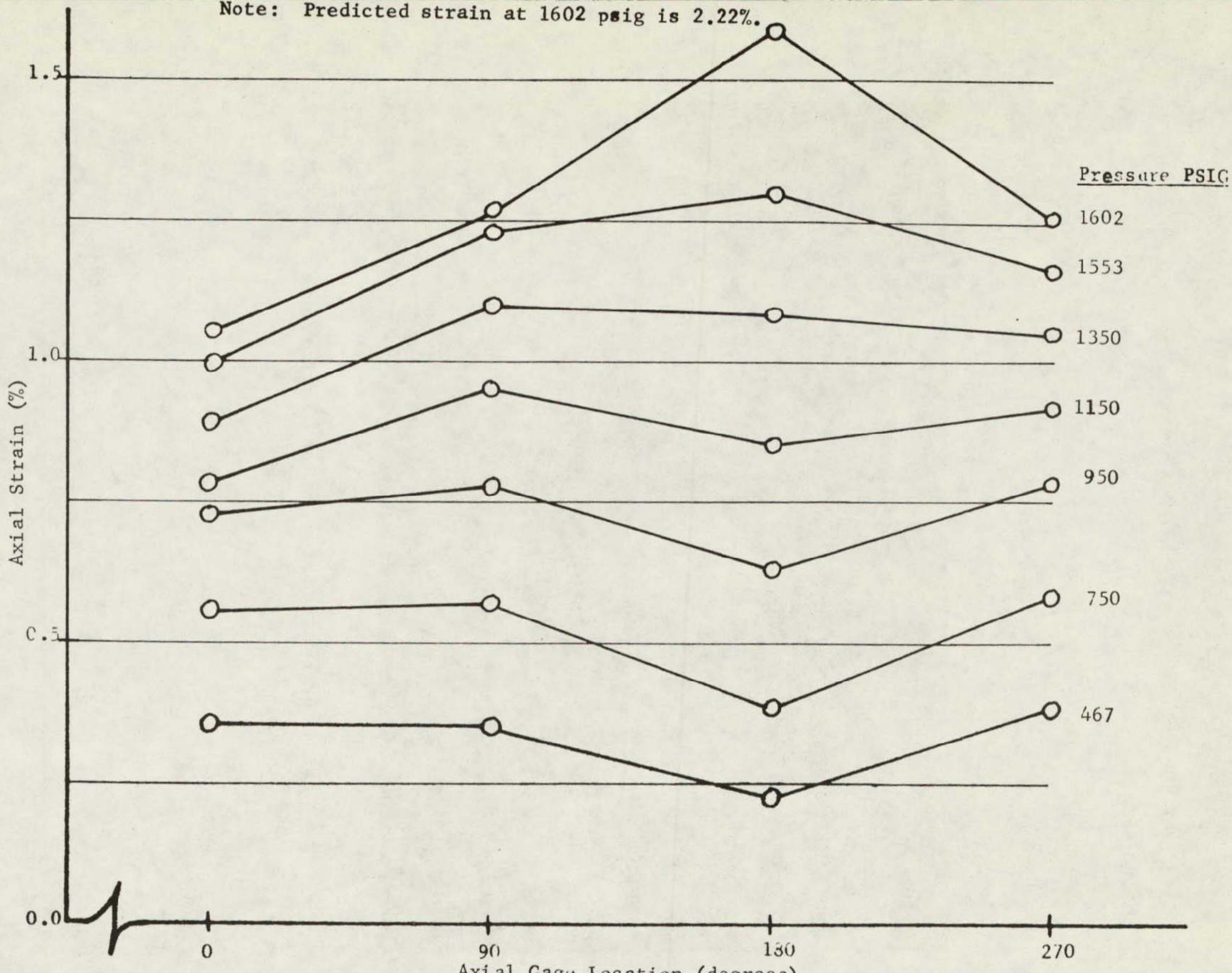

Figure 13. Bottle No. 4 - Axial Strain Versus Pressure (Maximum Axial Load = 2570 lb/in.) (Failure at 180°)

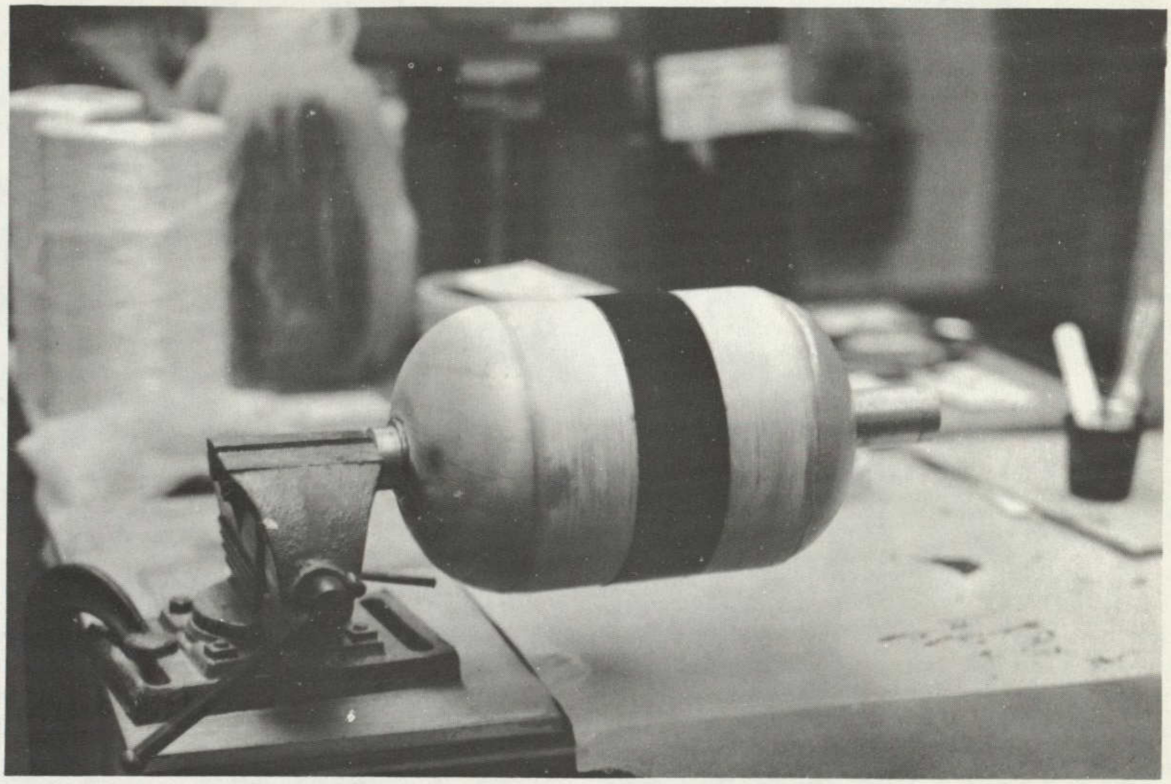

G-2495

Figure 14. Precoat of Epon 946 on Defected Bottle

G-2497

Figure 15. Adding Epon 946 Resin Coat to Repair Area

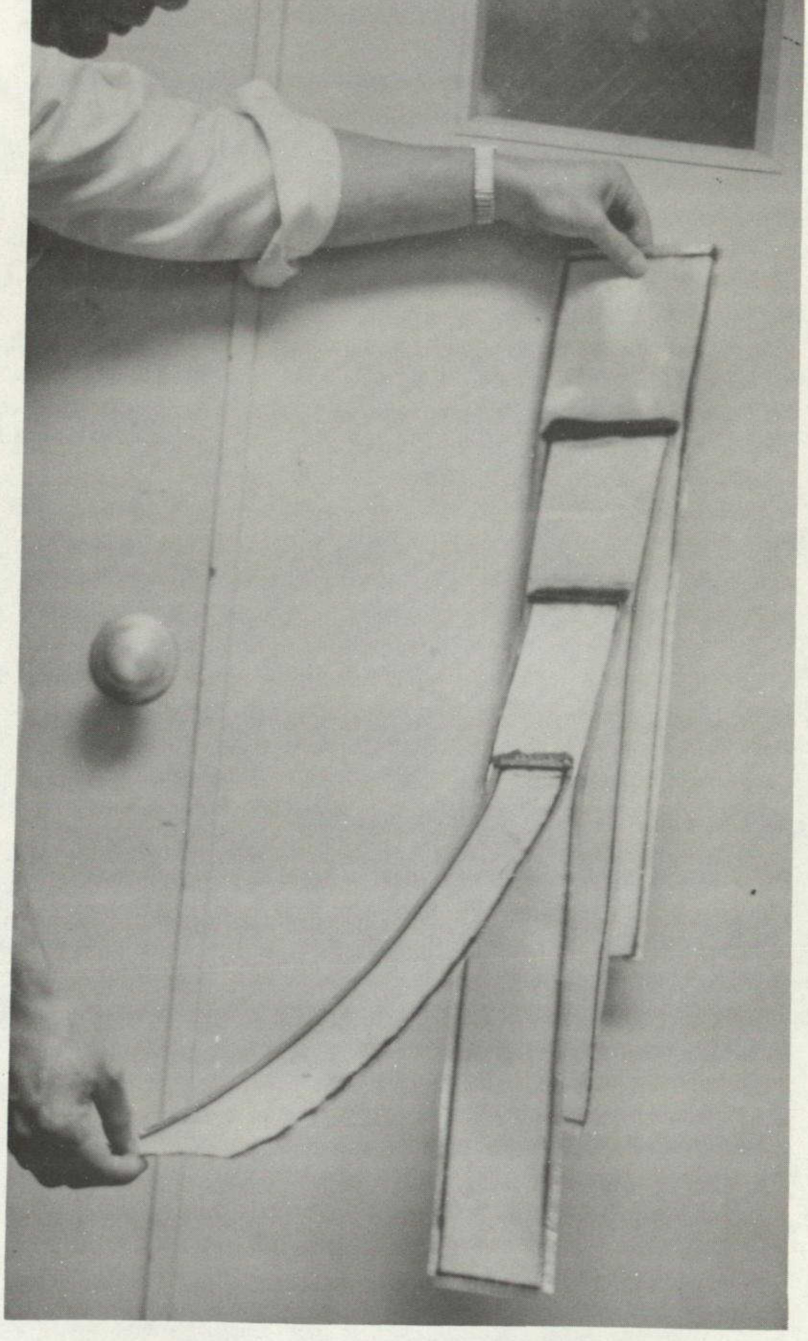

G-2501

Figure 16. Interconnected Four-Ply Patch

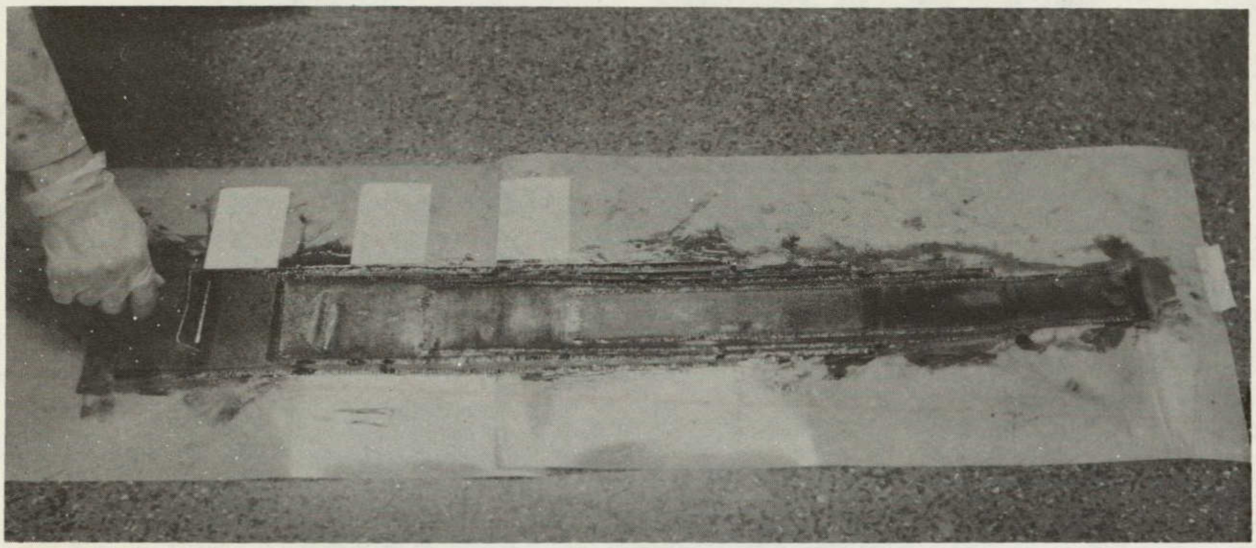

G-2499

Figure 17. Saturation of Cloth with Epon 946 Resin Using Roller

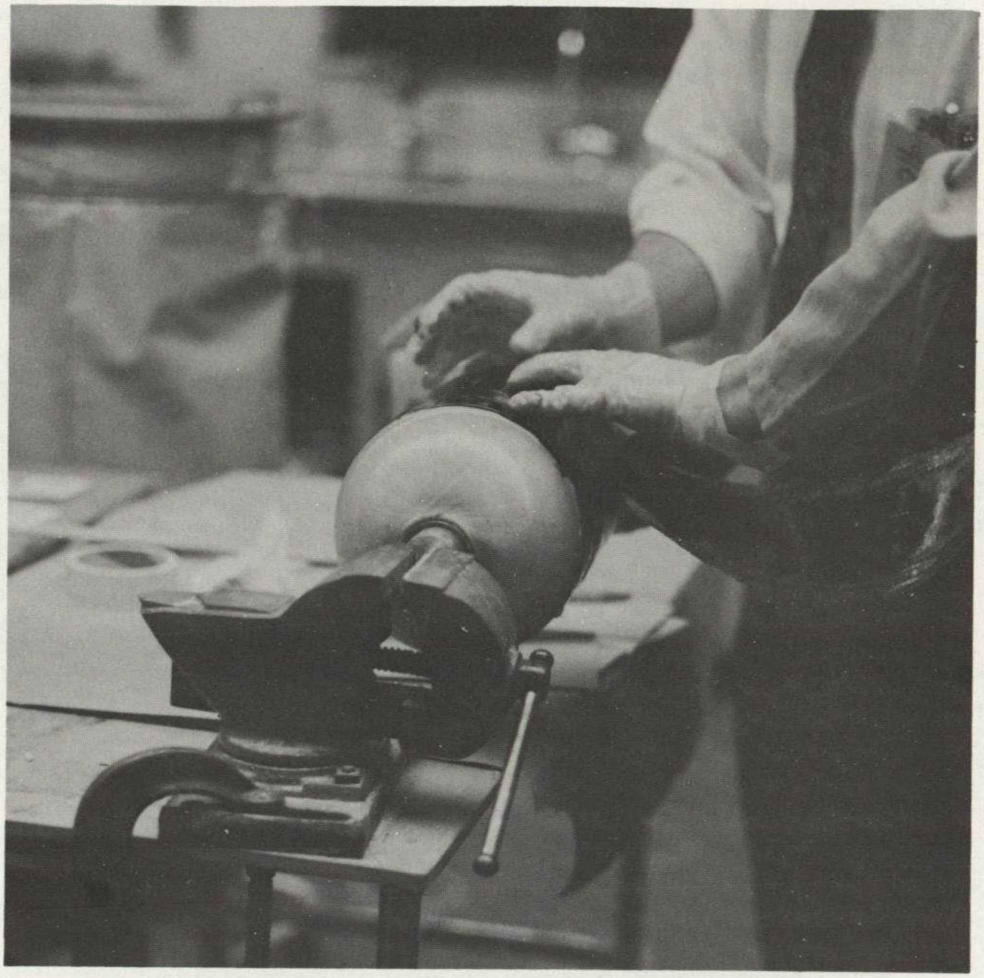

C-2500

Figure 18. Application of Patch to Bottle

2

G-2498

Figure 19. Bottle Repaired with Inverted Patch

Note: Predicted strain at 1126 psig is 1.57%.

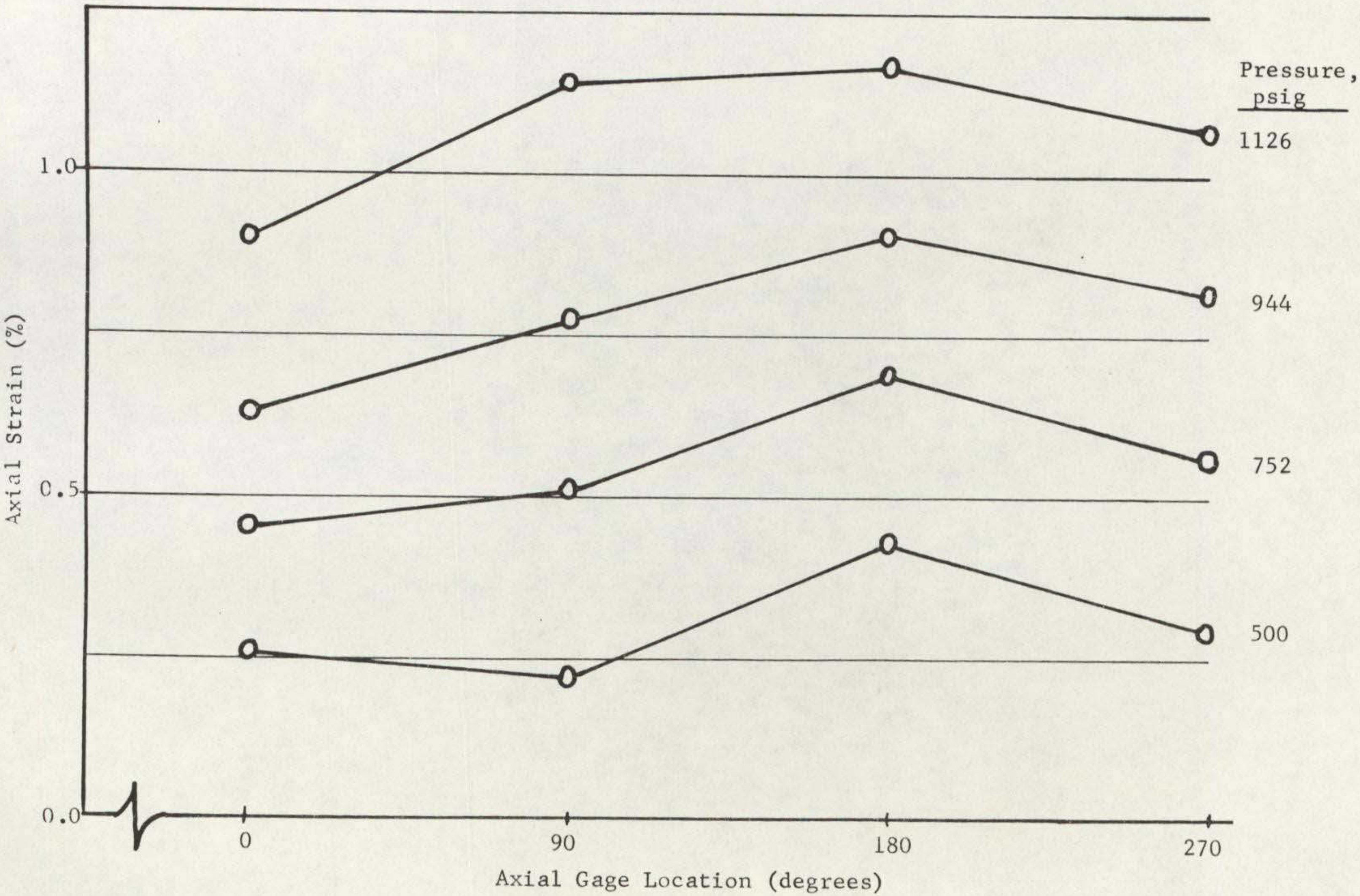

Figure 20. Bottle No. 8 - Axial Strain Versus Pressure (Maximum Axial Load = 1840 lb/in.) (Leak occurred at 180°)

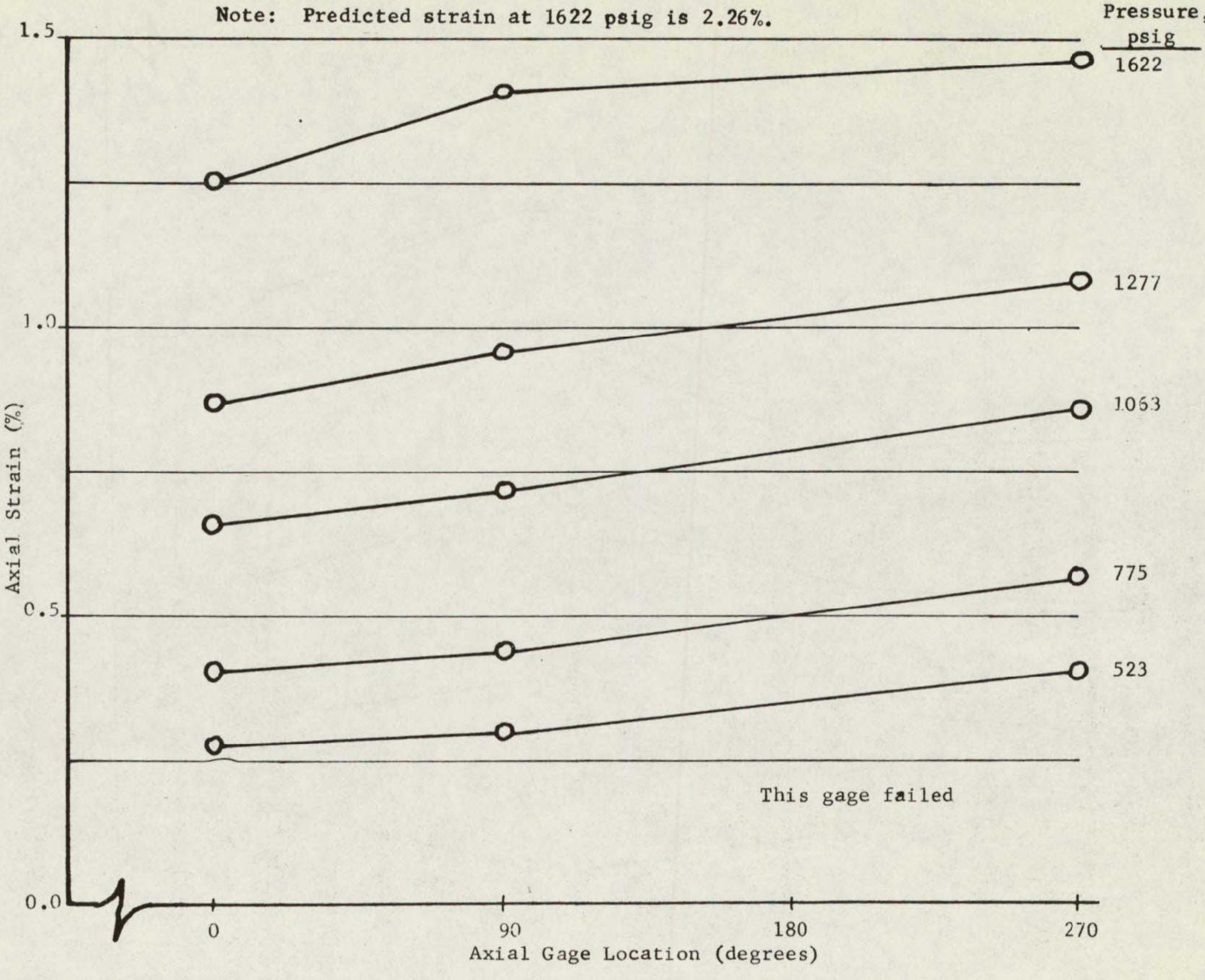

Figure 21. Bottle No. 8 Retest - Axial Strain Versus Pressure for Pressurization Rate of 2750 psi/sec (Maximum Axial load = 2600 lb/in.) (Failure occurred at 180°)

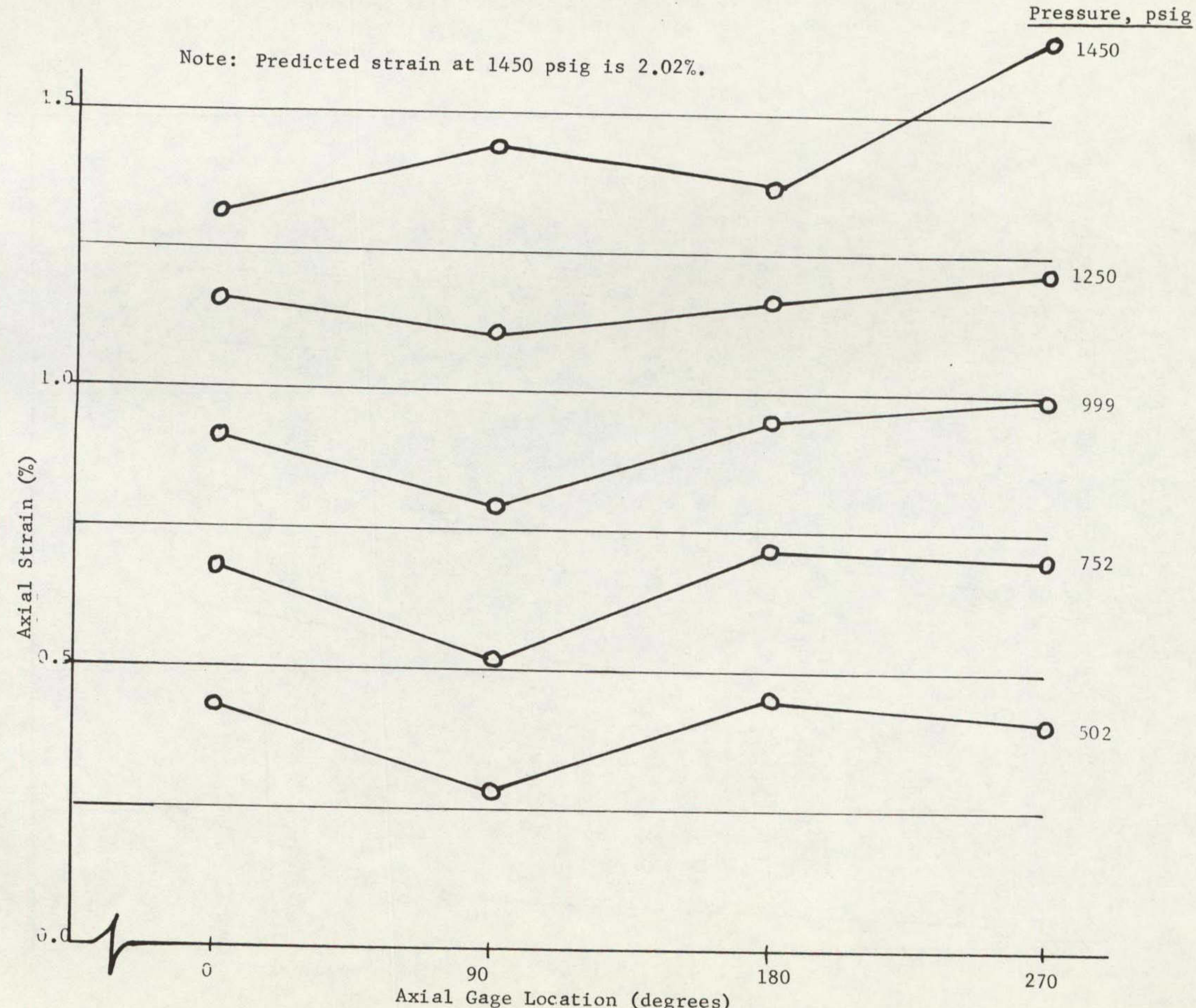

Figure 22. Bottle No. 5 - Axial Strain Versus Pressure (Maximum Axial Load = 2365 lb/in.) (Failure occurred at 270°)

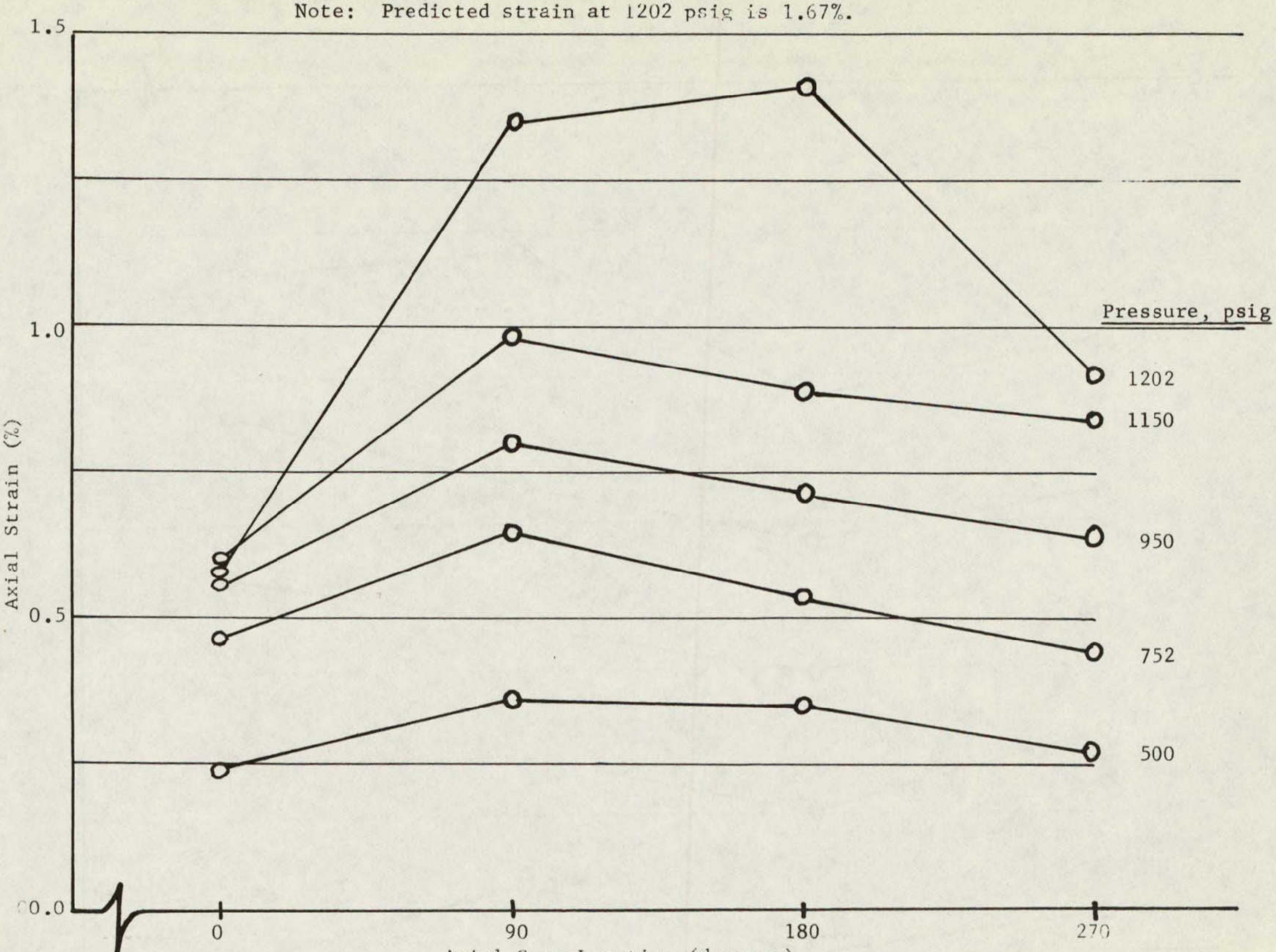

Figure 23. Bottle No. 6 - Axial Strain Versus Pressure
(Maximum Axial Load = 2035 lb/in.)
(Failure at 90°)

Note: Predicted strain at 1364 psig is 1.9%.

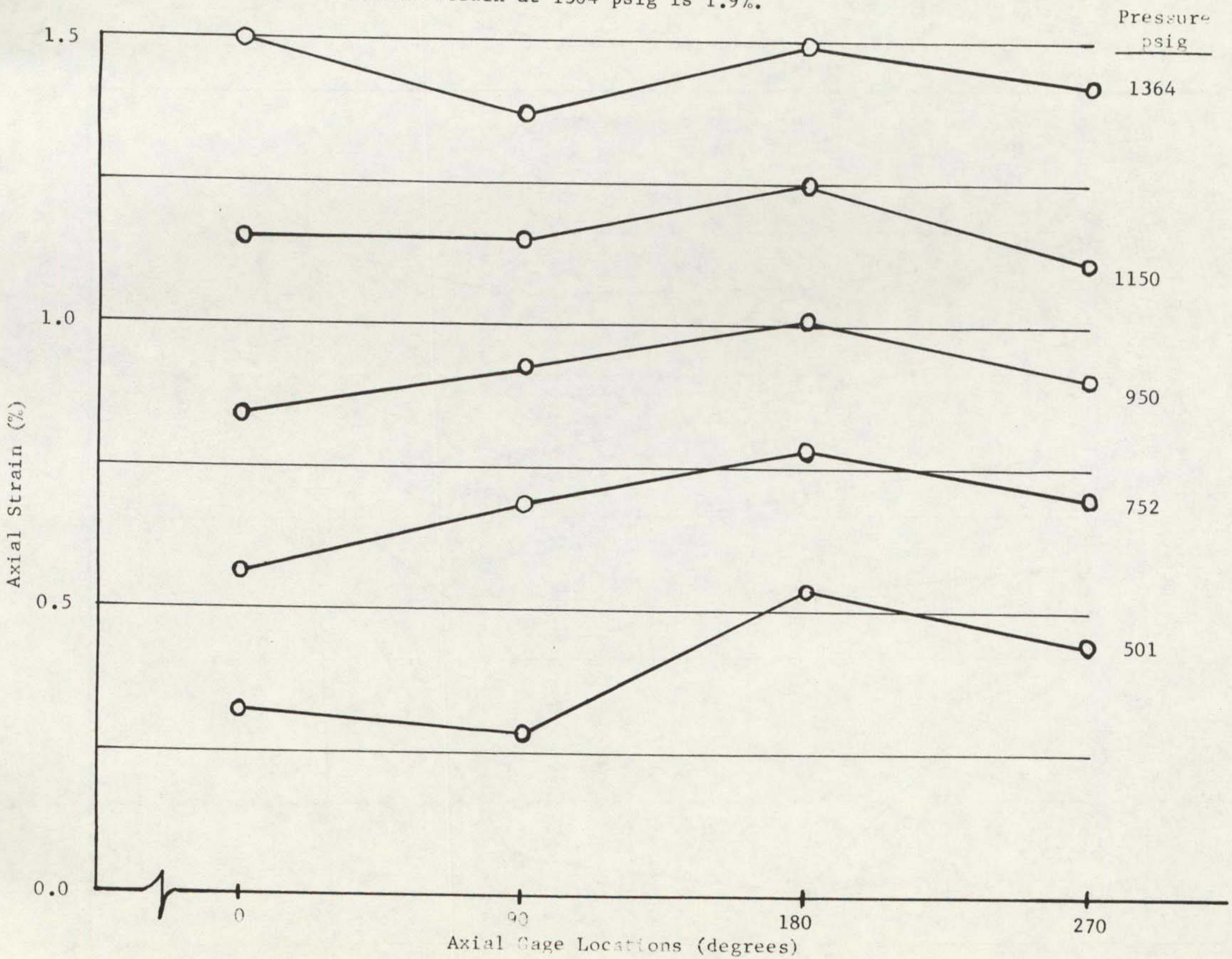

Figure 24. Bottle No. 7 - Axial Strain Versus Pressure
(Maximum Axial Load = 2160 lb/in.) (Failure at 120°)

Figure 25. Post-burst View of Bottle No. 5 with Four-Ply Inverted Repair

G-2492

Figure 26. Post-burst View of Bottle No. 6 with Four-Ply Inverted Repair

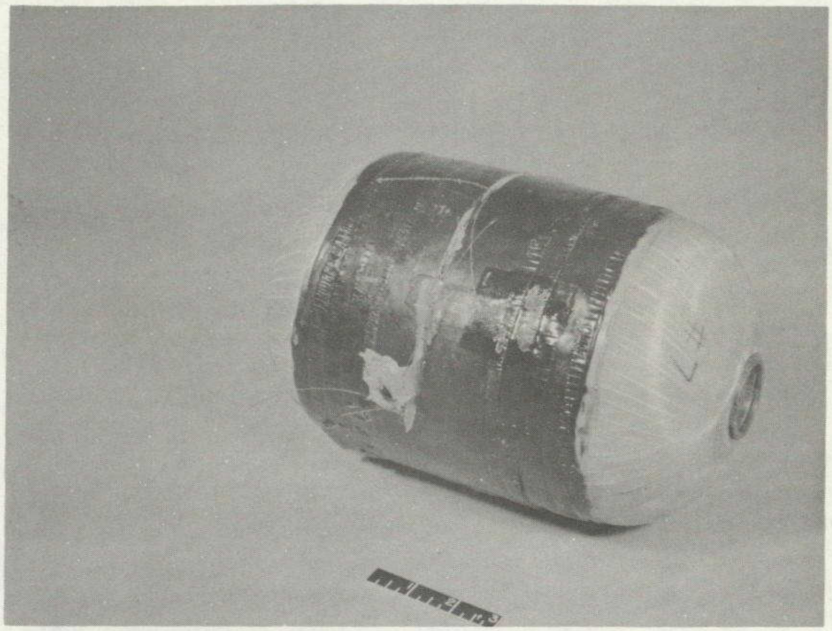

Figure 27. Post-burst View of Bottle No. 7 with Four-Ply Inverted Repair

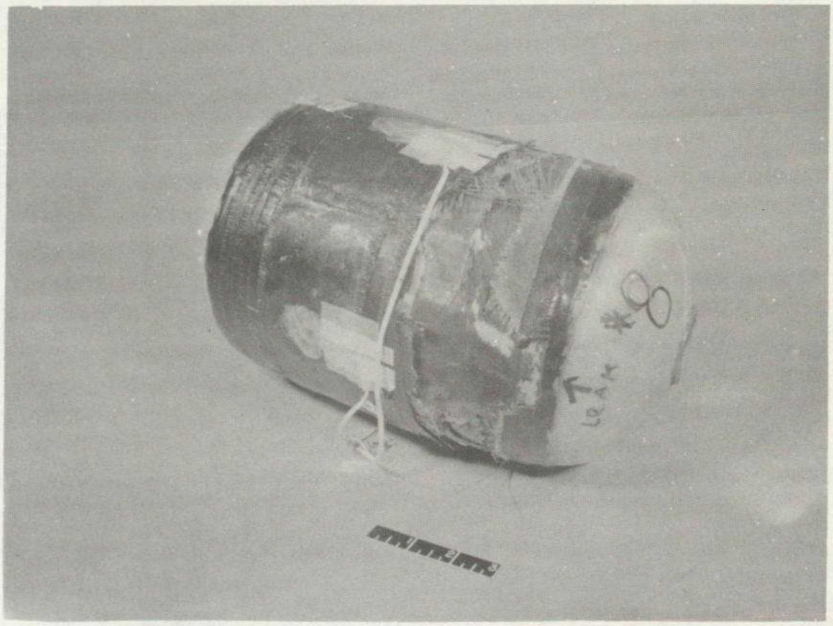

G-2491

Figure 28. Post-burst View of Bottle No. 8 with Four-Ply Inverted Repair

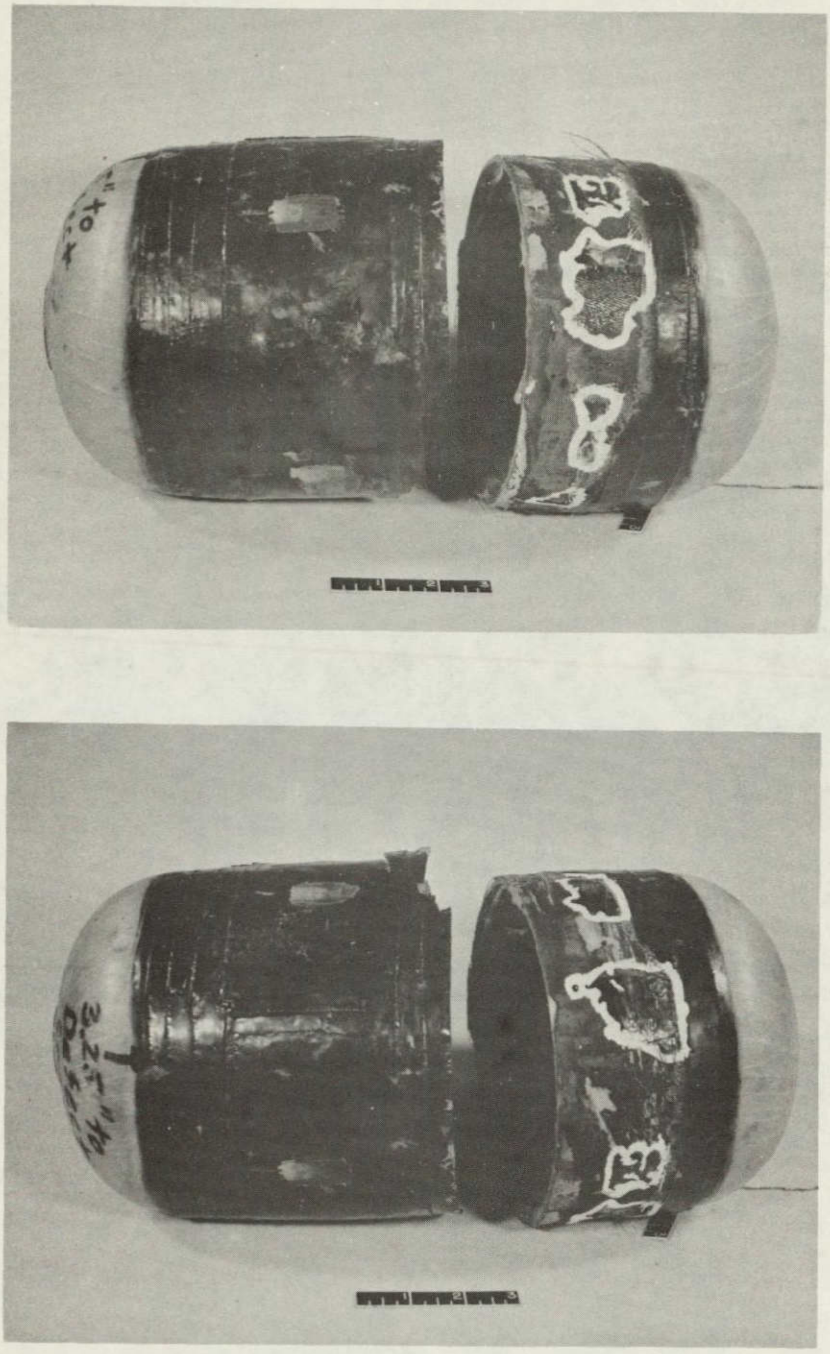

G-2488

Figure 29. Void Areas in Bottle No. 4
(Located inside white boundaries)

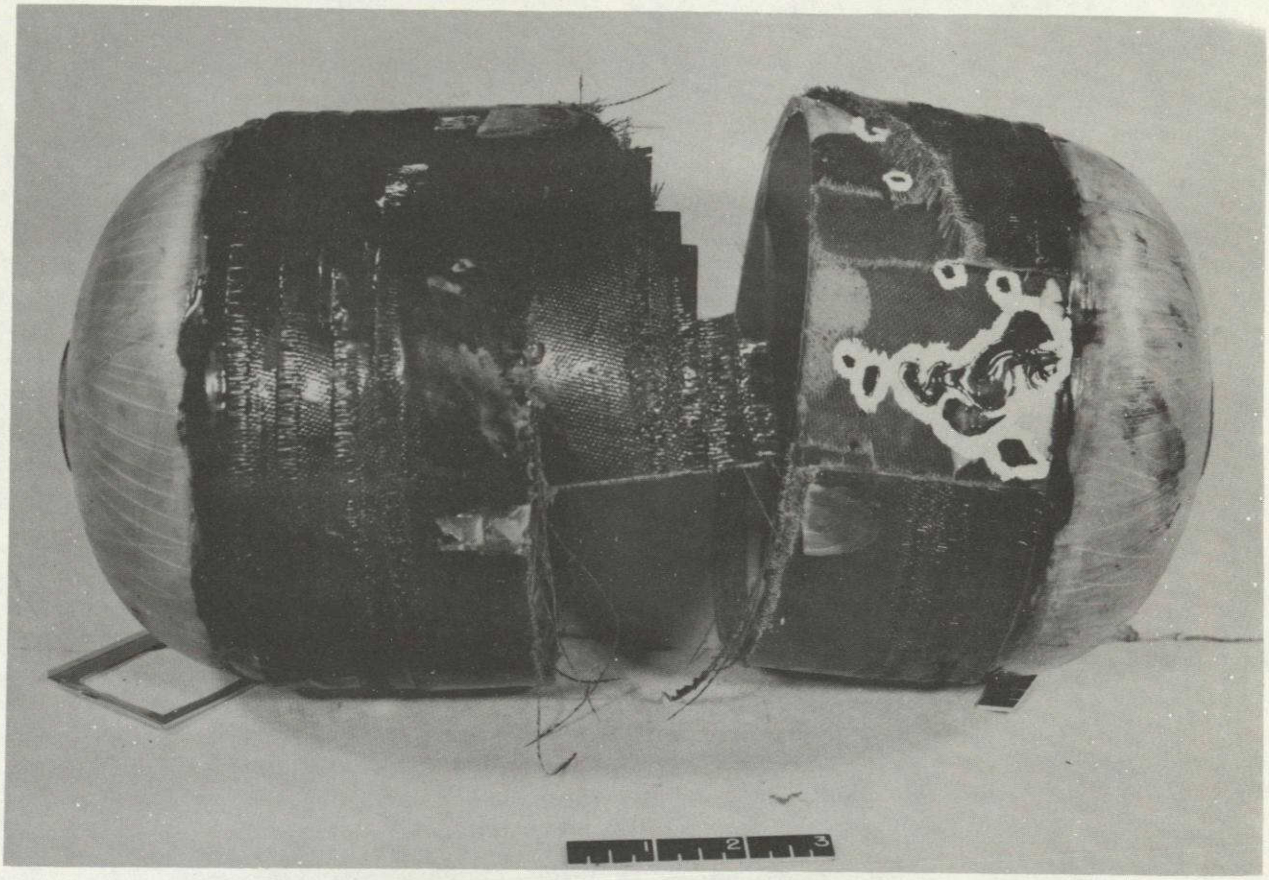

G-2493

Figure 30. Void Areas in Bottle No. 5 (failure area located inside white boundaries at the 270° location)

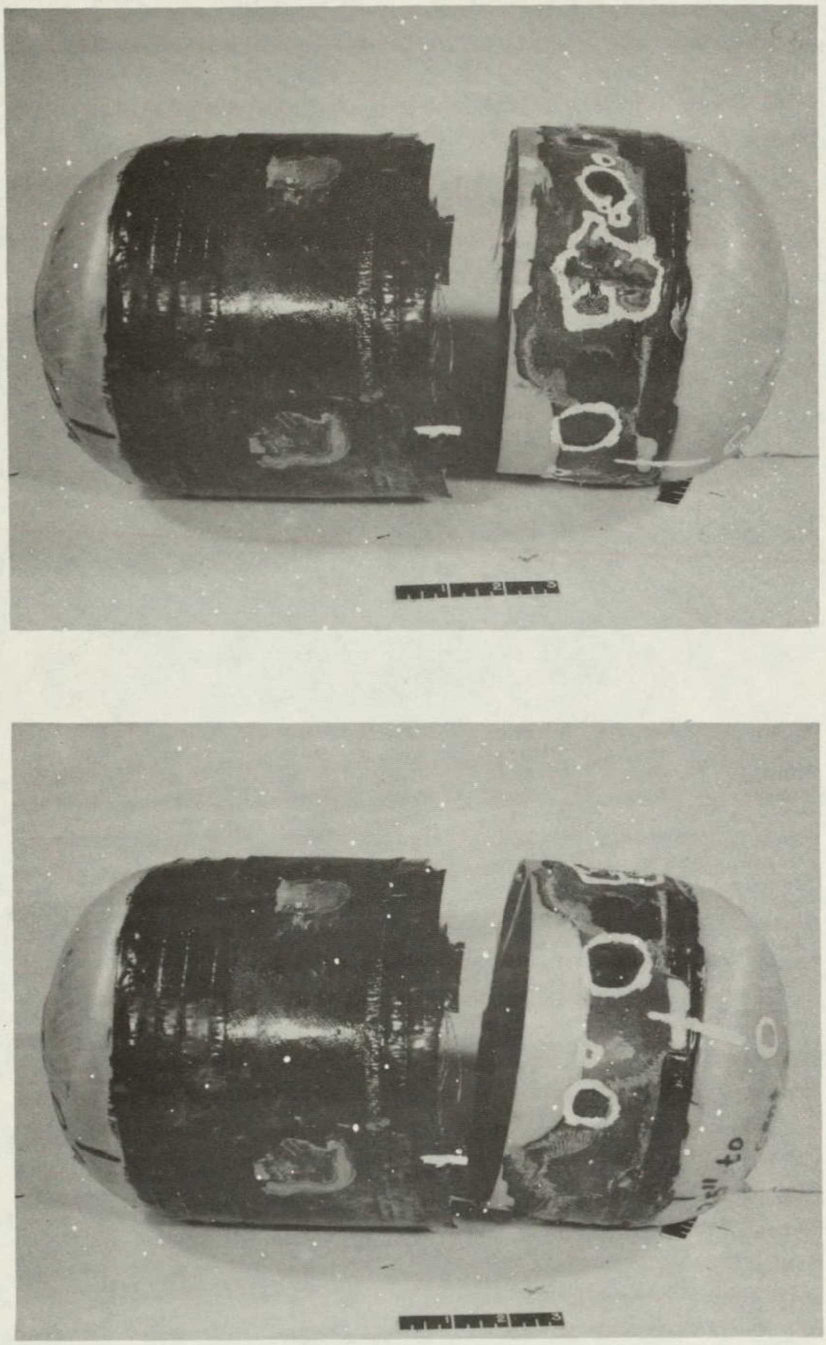

G-2487

Figure 31. Void Areas in Bottle No. 6
(located inside white boundaries)

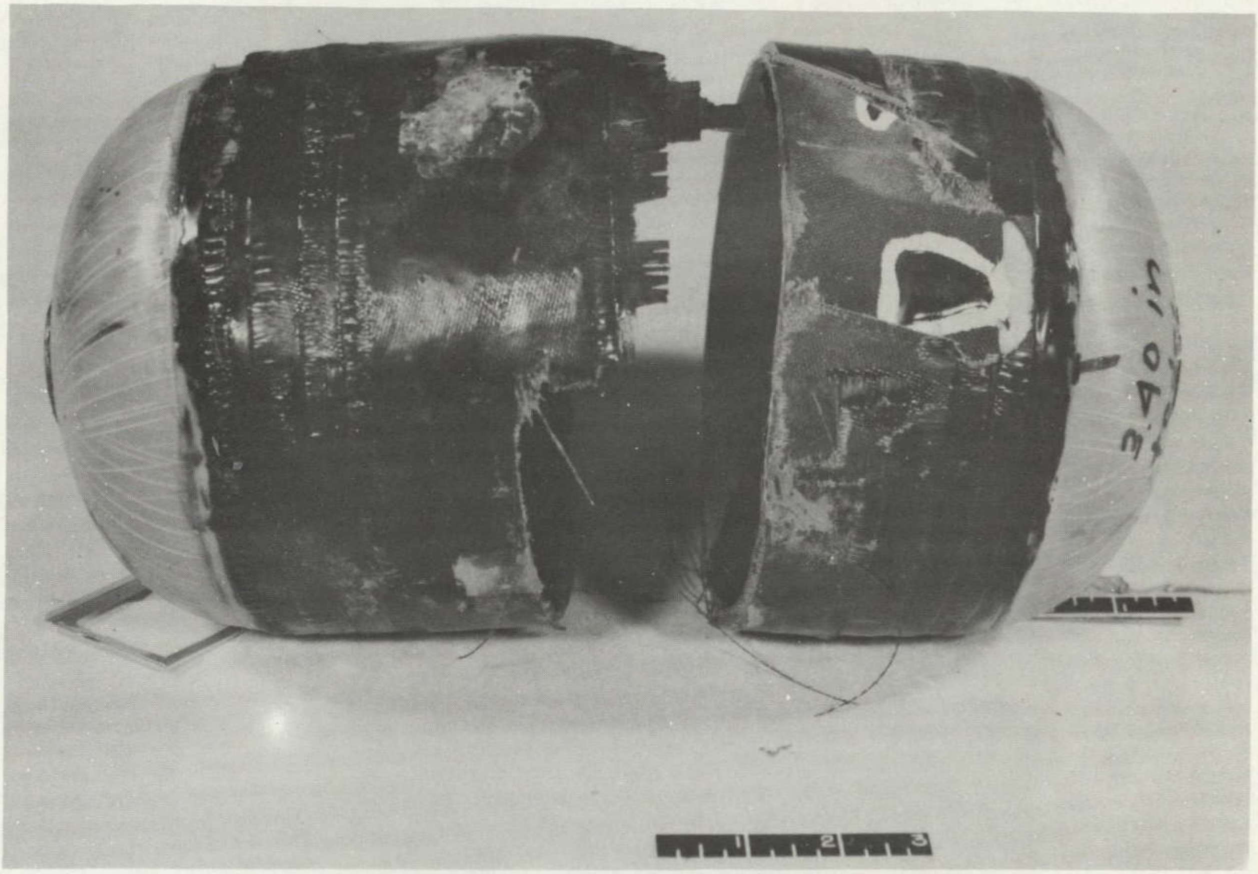

G-2494

Figure 32. Void Areas in Bottle No. 7 (located inside white boundaries)

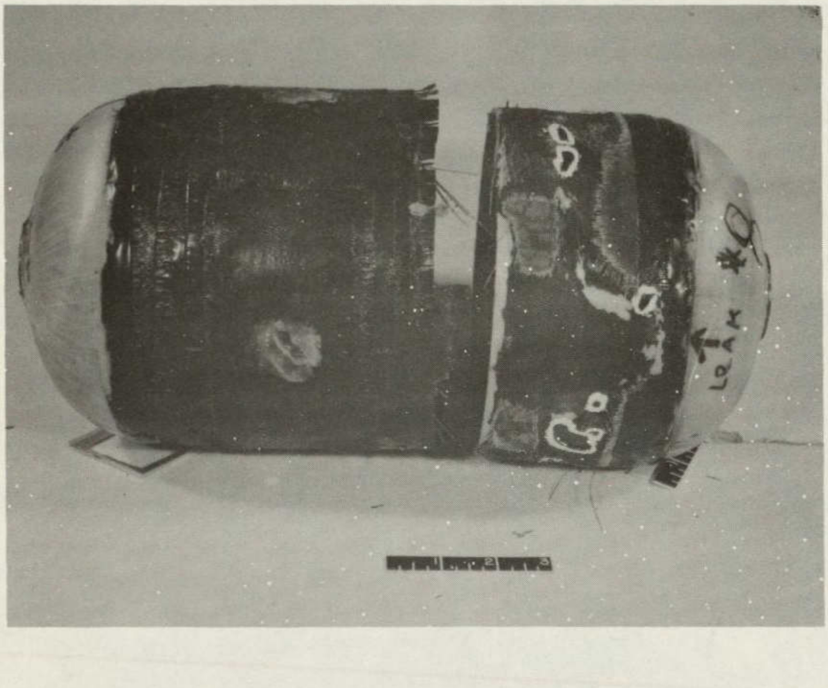

G-2489

Figure 33. Void Areas in Bottle No. 8
(located inside white boundaries)

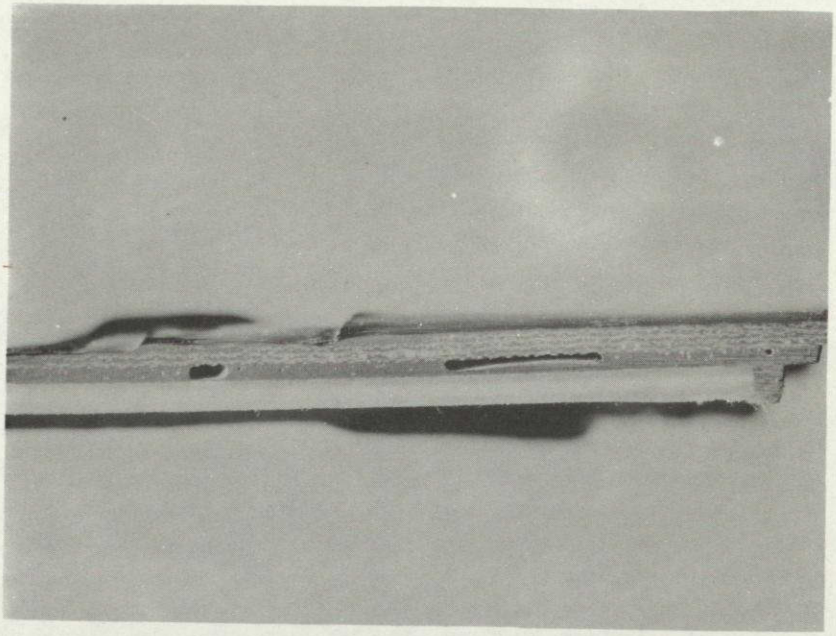

Mag. 2X

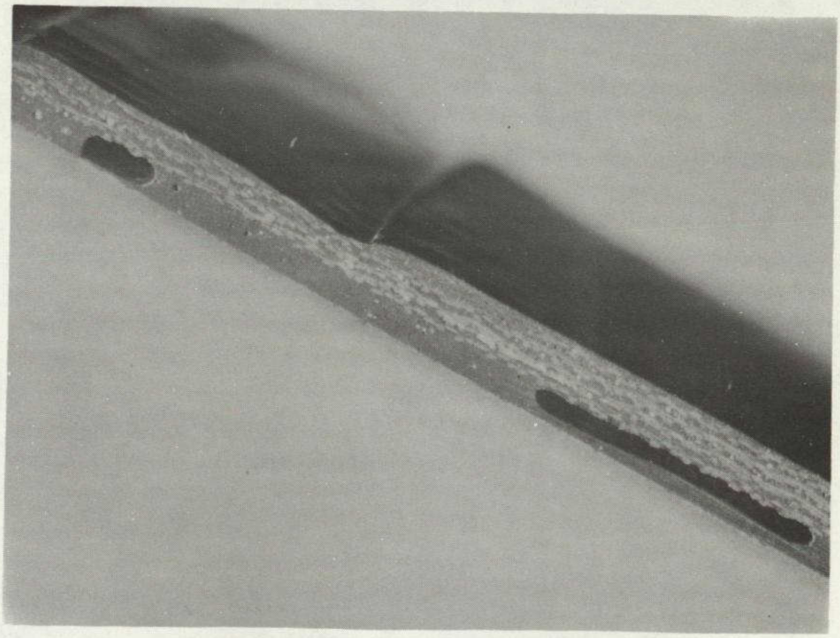

G-2483

Mag. 4X

Figure 34. Voids in Bond Line of Bottle No. 6

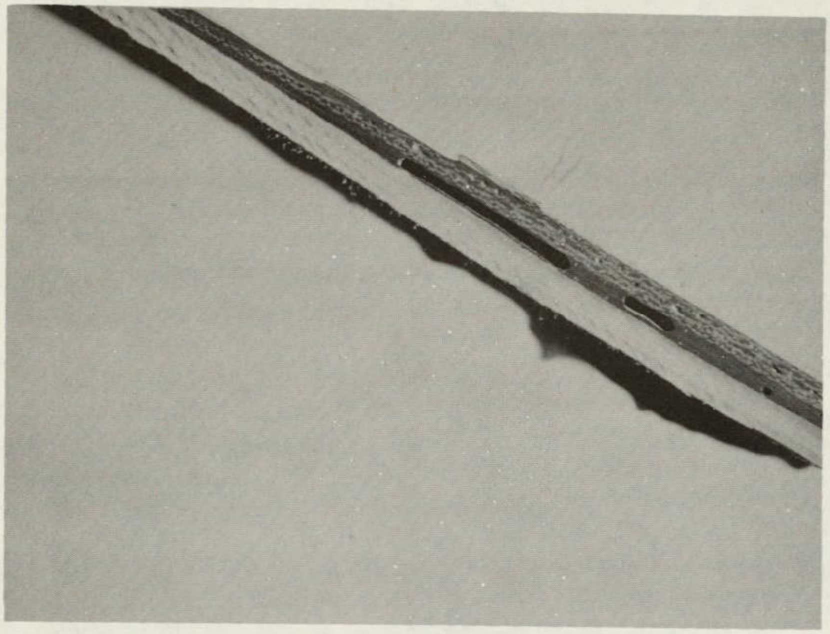

Mag. 2X

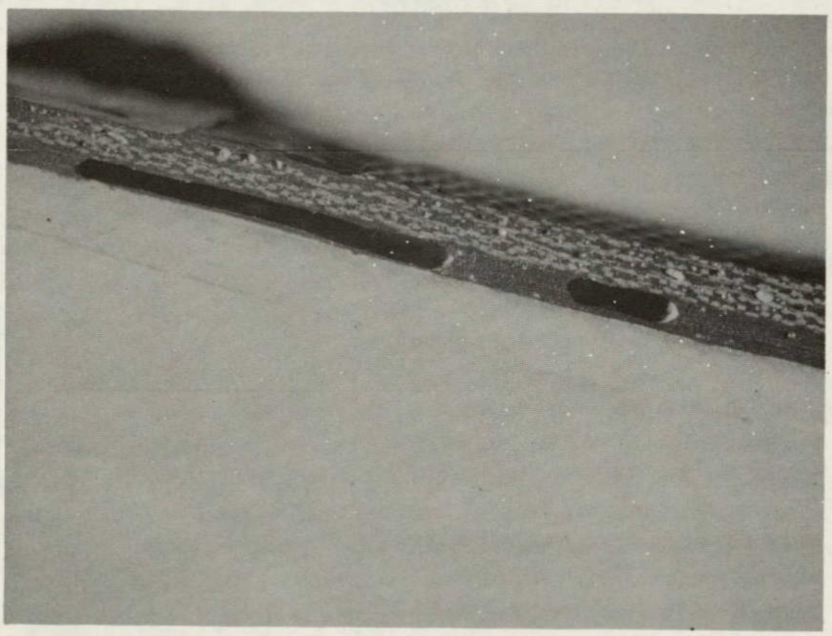

G-2484

Mag. 4X

Figure 35. Voids in Bond Line of Bottle No. 6

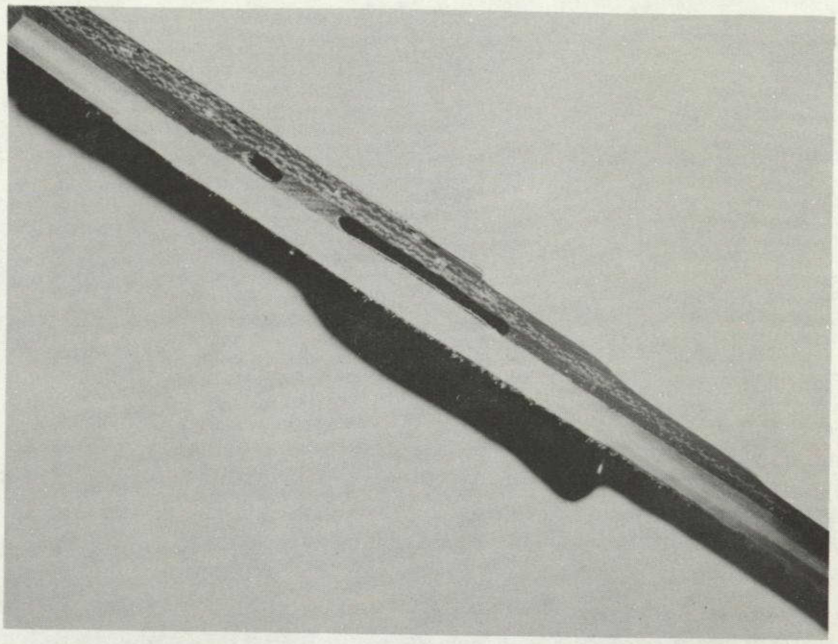

Mag. 2X

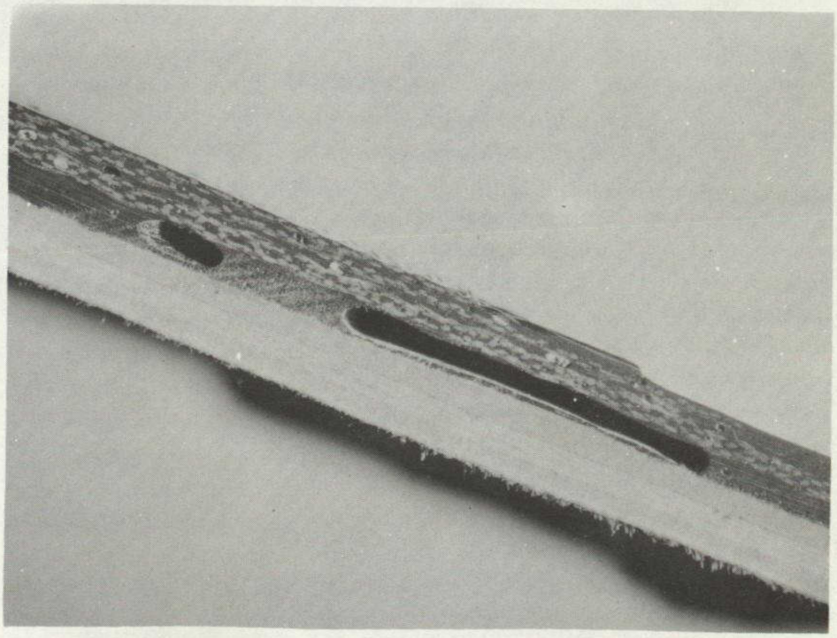

G-2482

Mag. 4X

Figure 36. Voids in Bond Line of Bottle No. 6

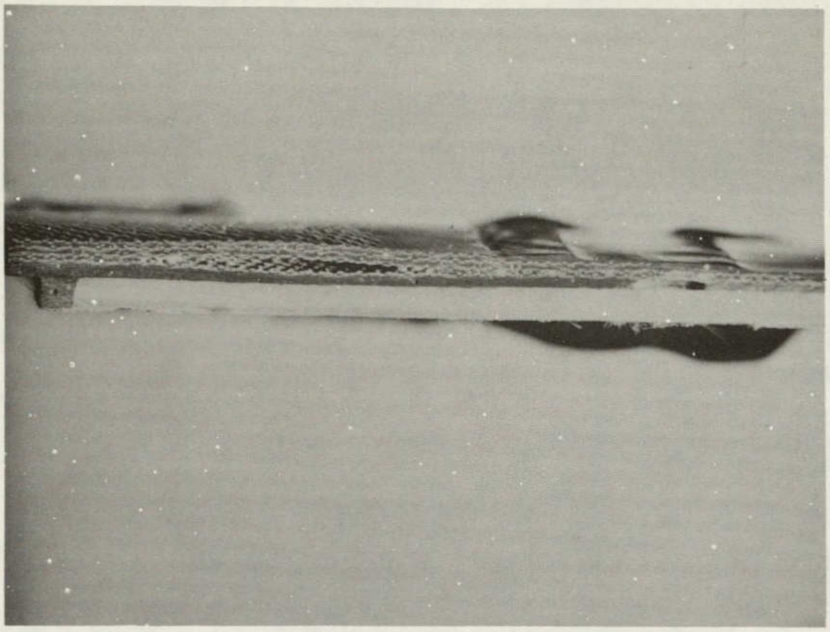

Mag. 2X

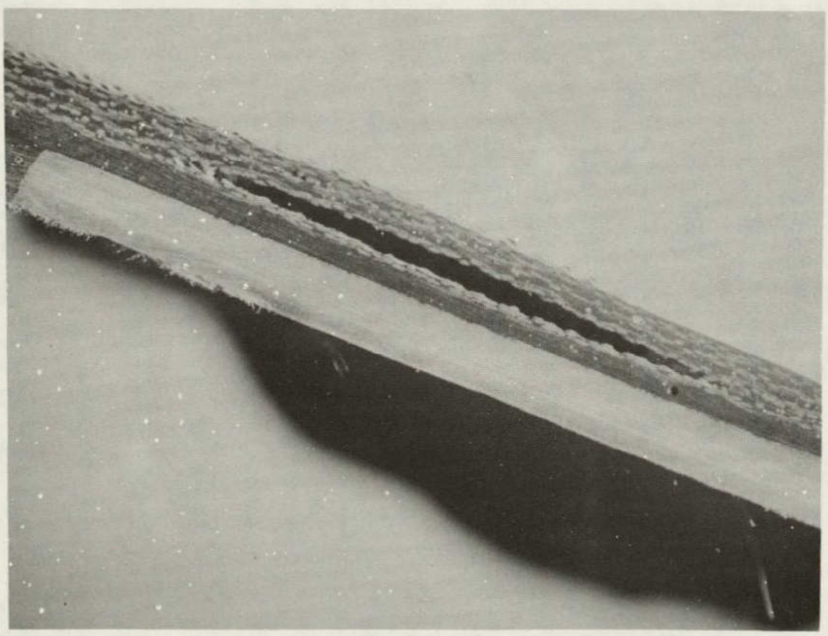

G-2485

Mag. 4X

Figure 37. Voids Between Plies of Bottle No. 6

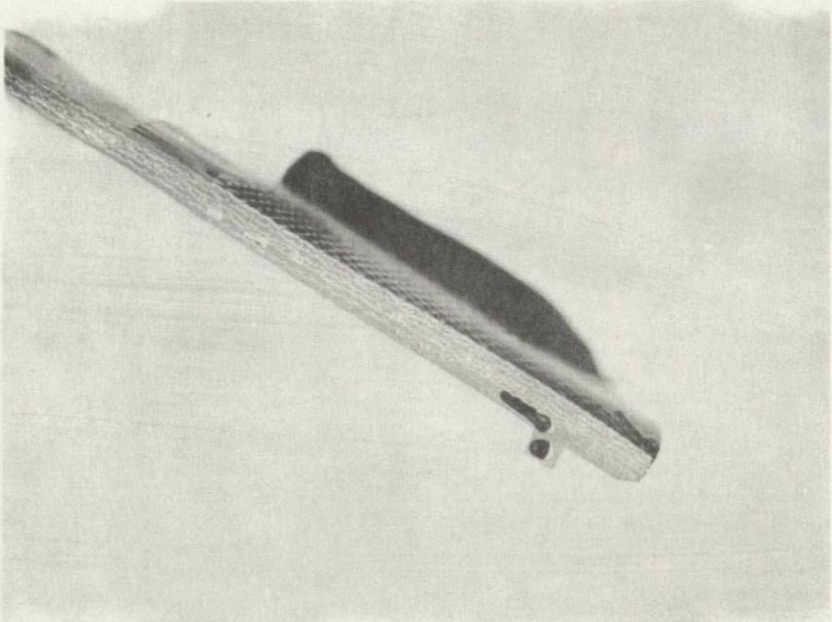

Mag. 2X

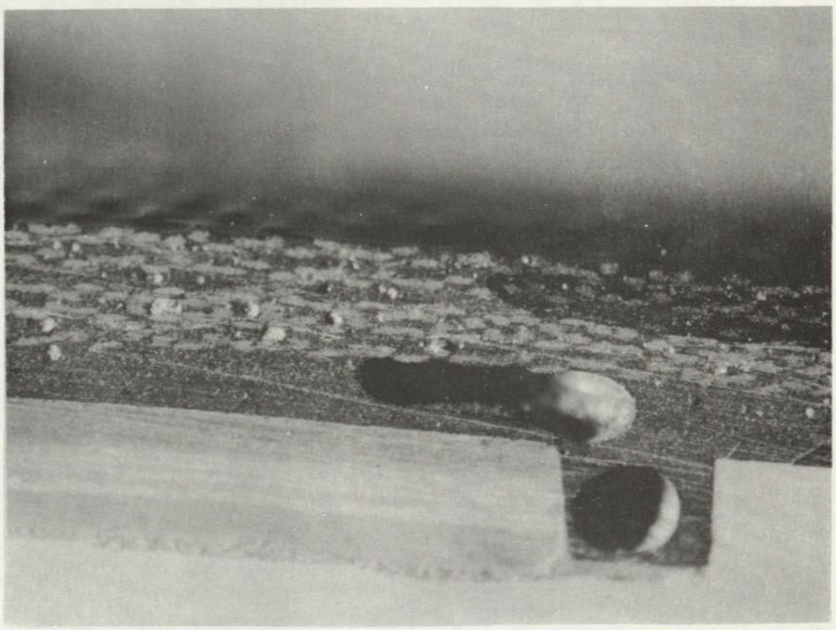

G-2486

Mag. 8X

Figure 38. Voids Near Defect Edge of Bottle No. 6

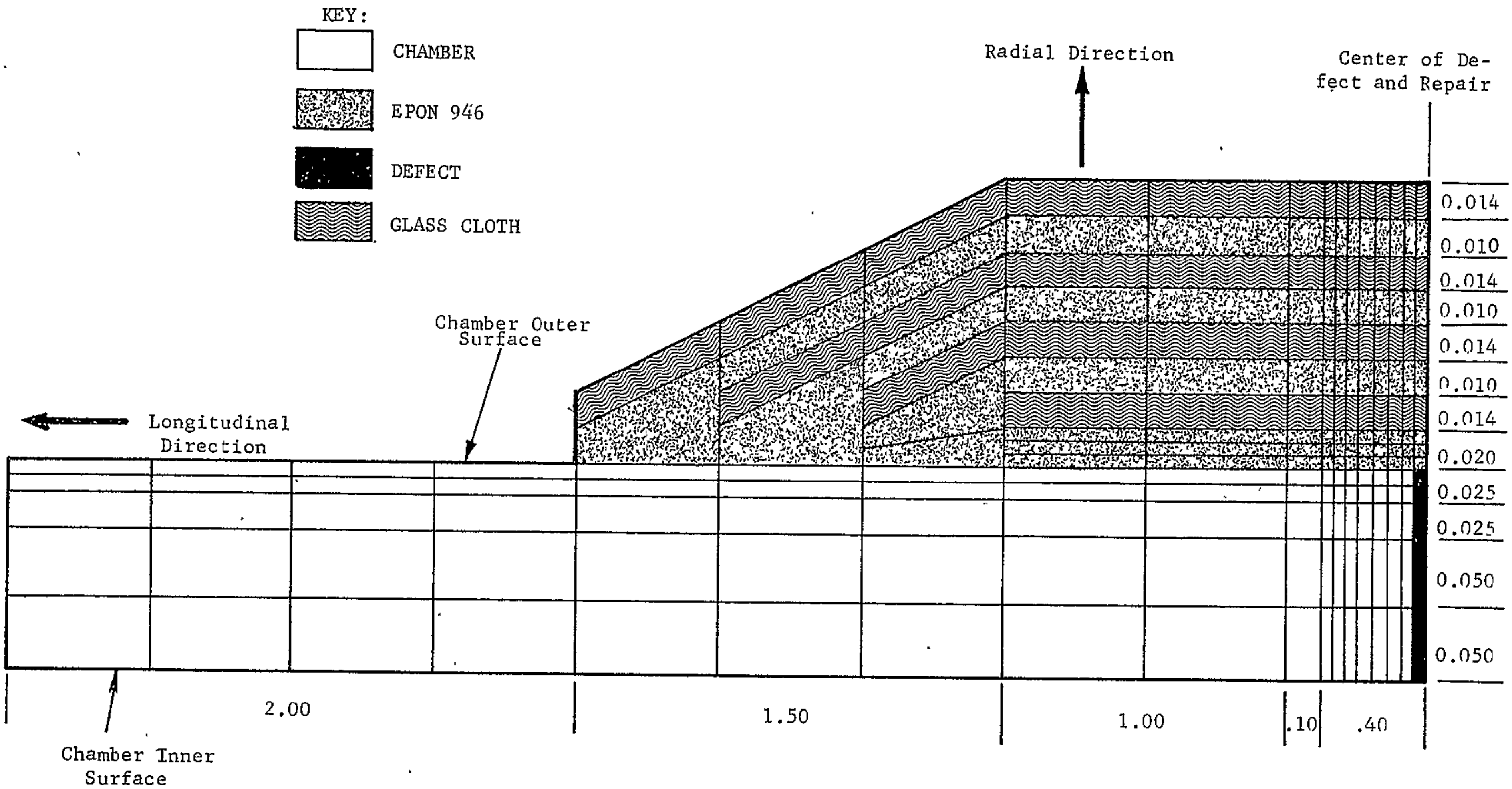

Figure 39. Finite Elements in Cross-Section of Four-Ply Repair

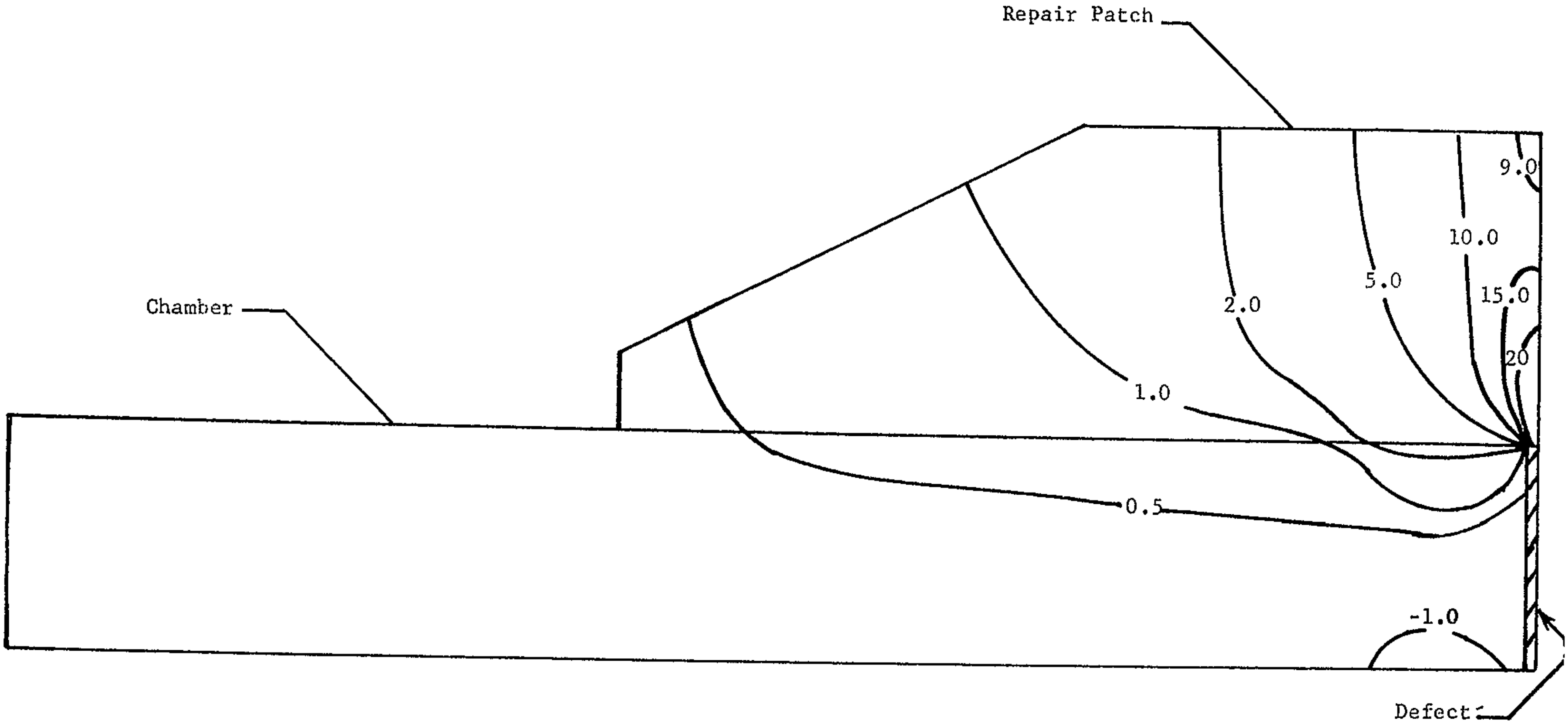

Figure 40. Axial Strain (%) Distribution in a Four-Ply Patch for a 30.0-In.-Diameter Chamber Subjected to 1000 psi Internal Pressure (7500 lb/in. Axial Load)

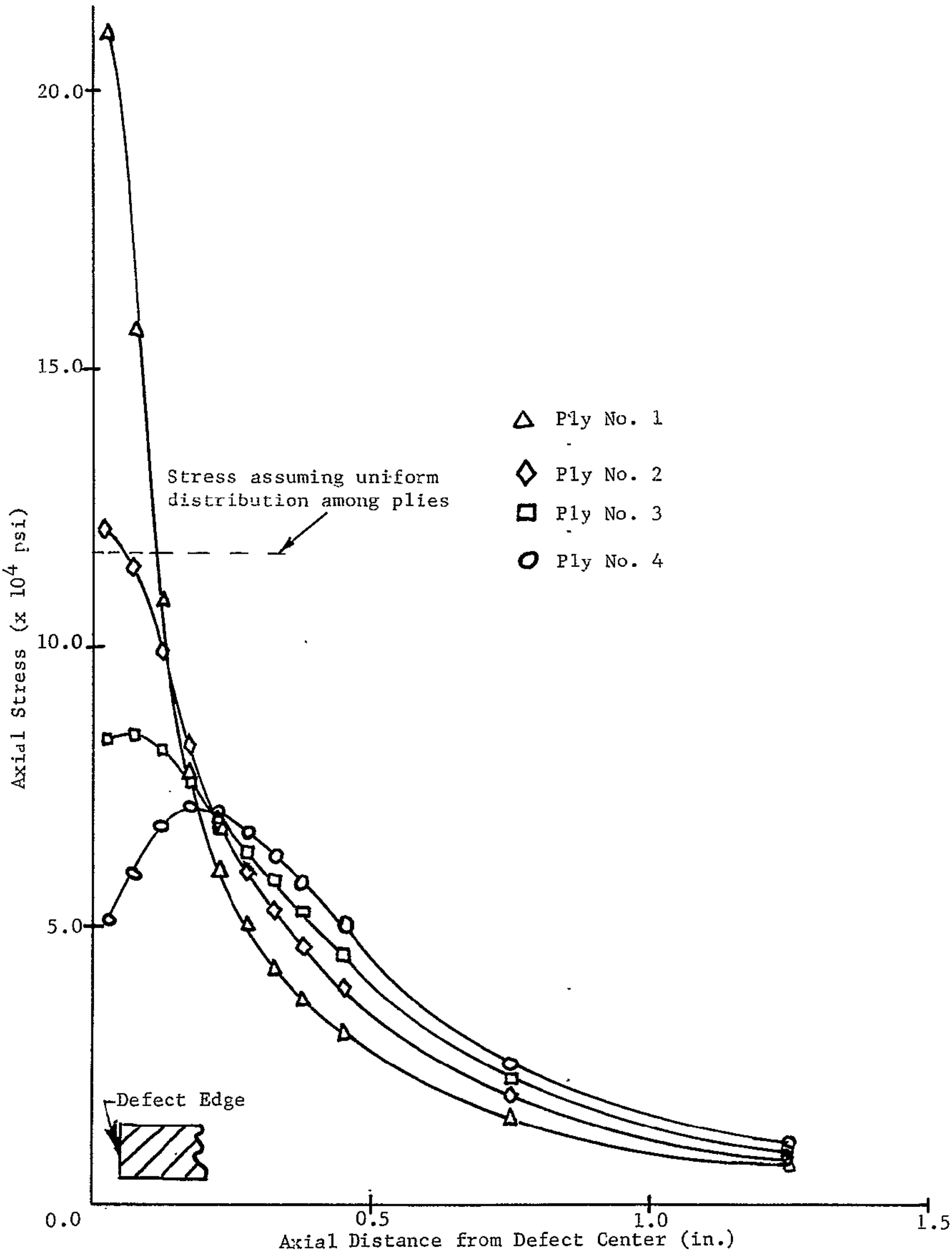

Figure 41. Axial Stress Distribution in a Four-Ply Patch for a 30.0-In.-Diameter Chamber Subjected to 1000 psi Internal Pressure (7500 lb/in. Axial Load)

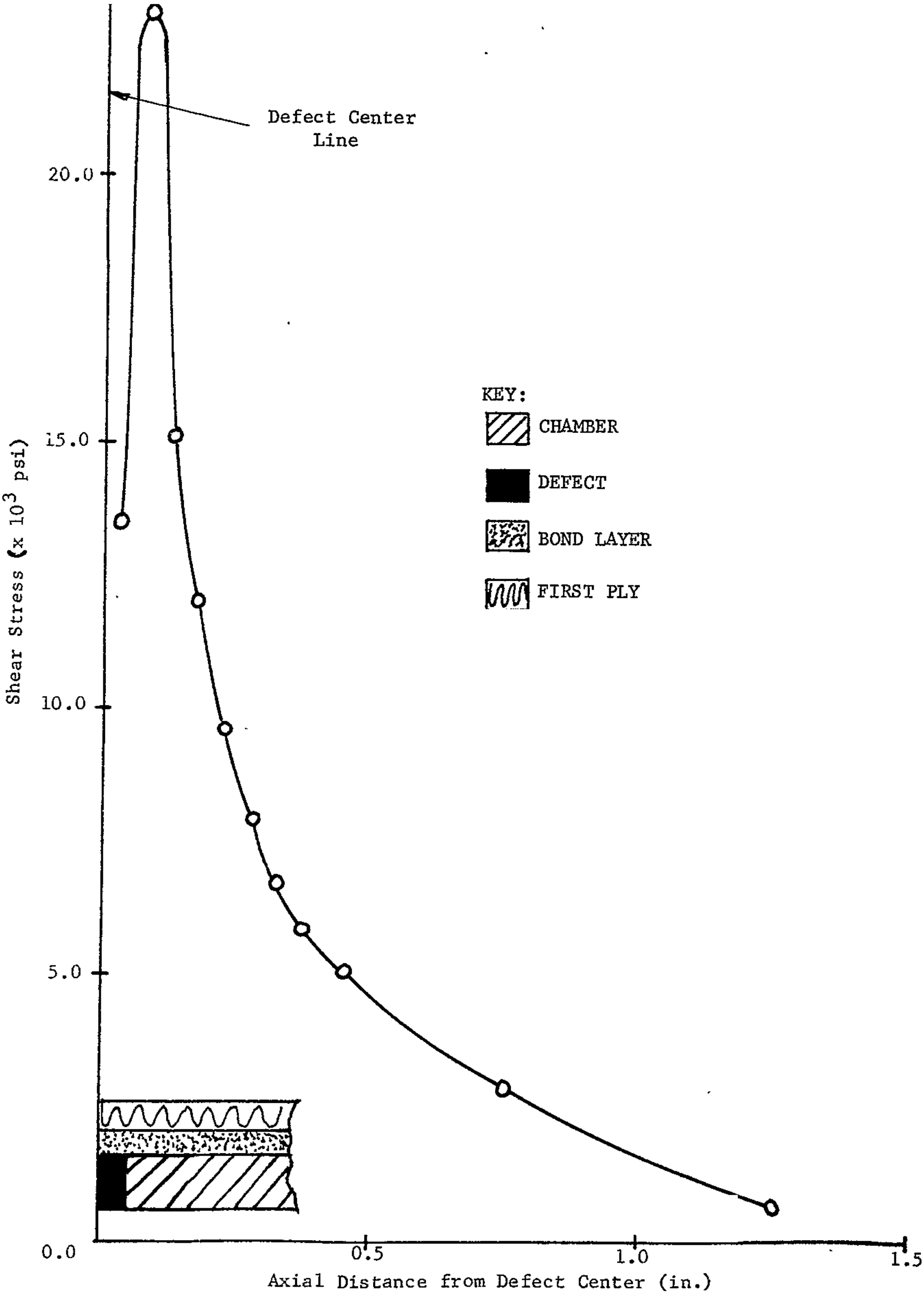

Figure 42. Shear Stress Distribution in Bond Layer Elements Nearest the Chamber Wall of a Four-Ply Patch for a 30.0-In.-Diameter Chamber Subjected to 1000 psi Internal Pressure (7500 lb/in. Axial Load)

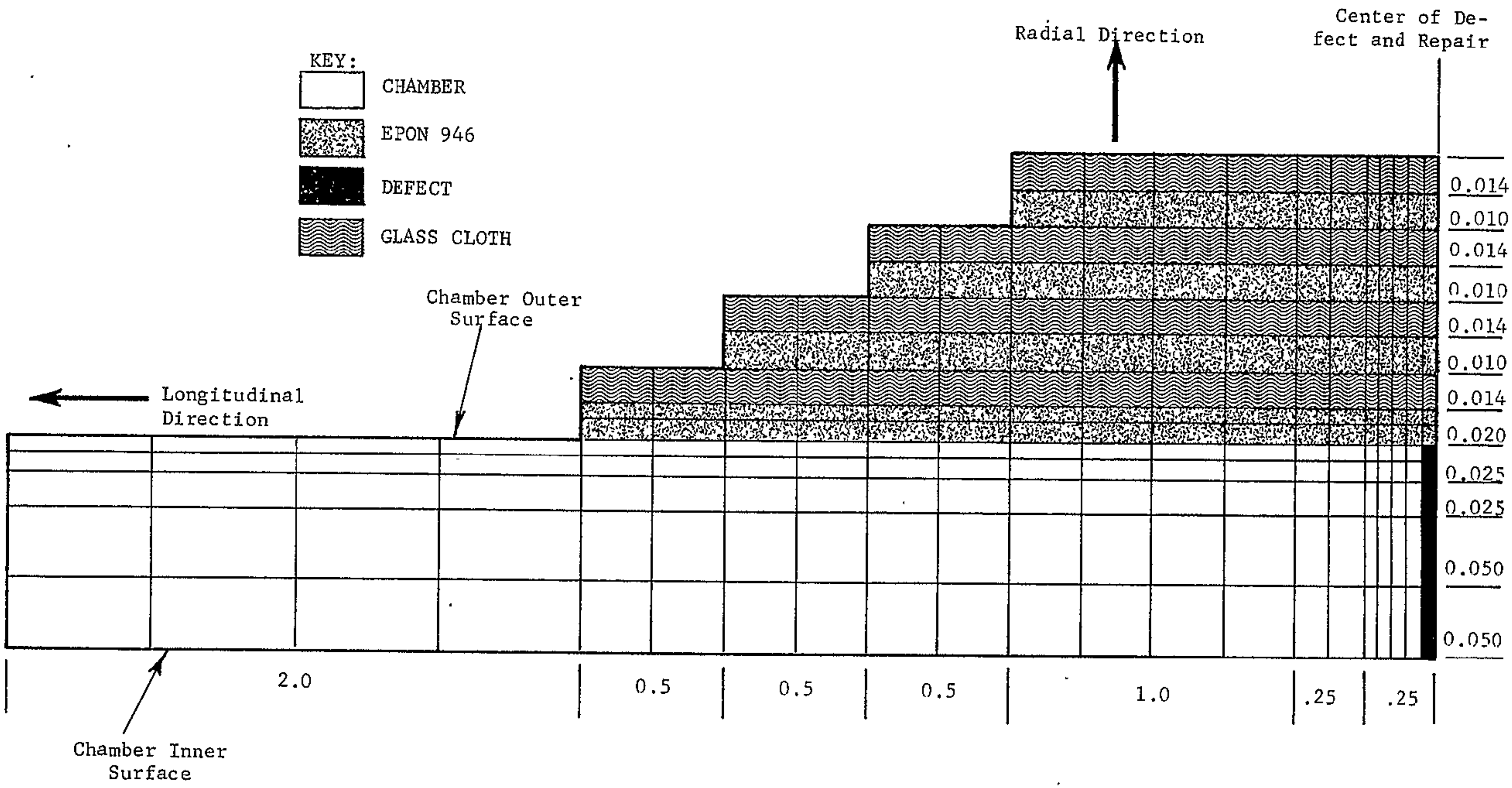

Figure 43. Finite Elements in Cross-Section of Four-Ply Inverted Repair

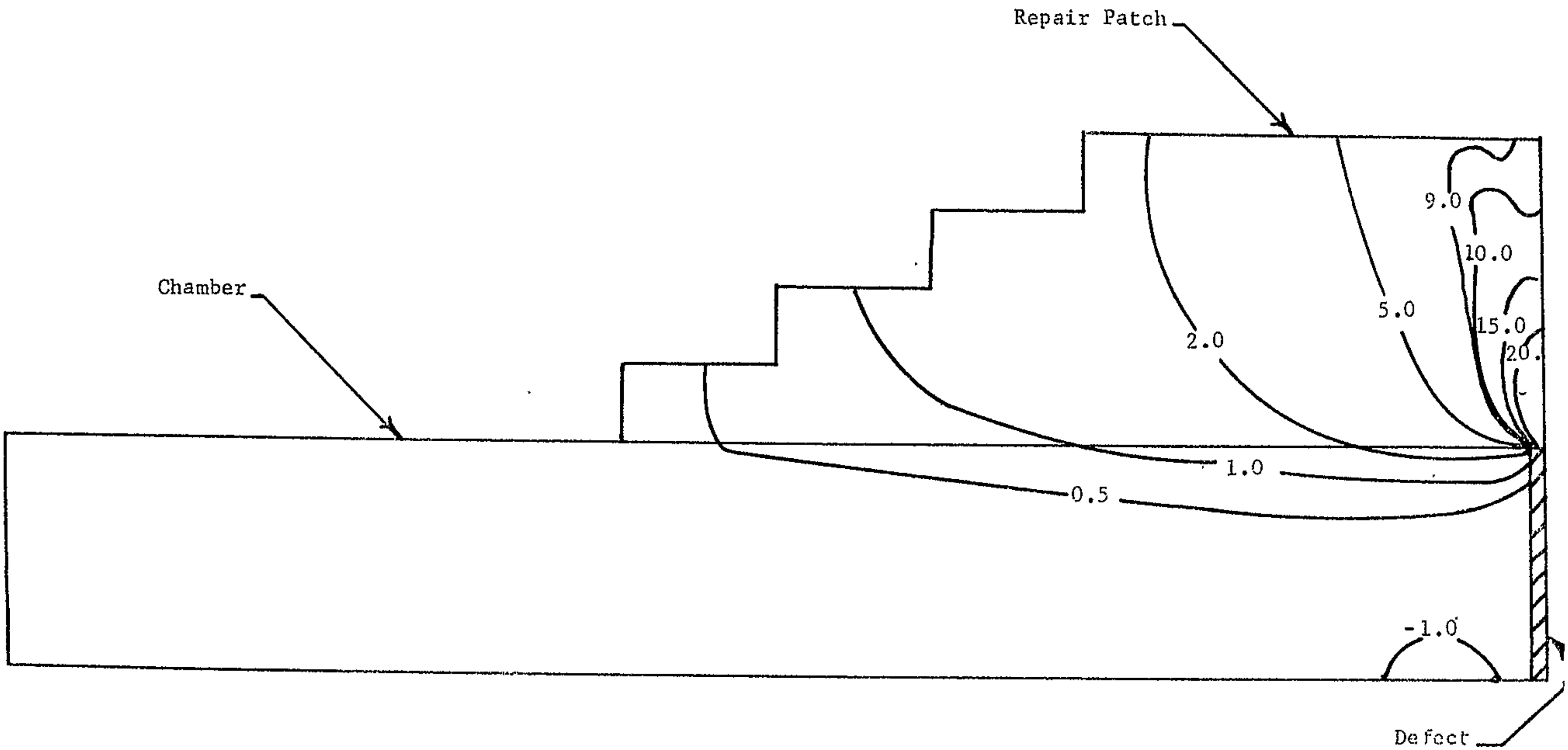

Figure 44. Axial Strain (%) Distribution in a Four-Ply Inverted Patch for a 30.0-In.-Diameter Chamber Subjected to 1000 psi Internal Pressure (7500 lb/in. Axial Load)

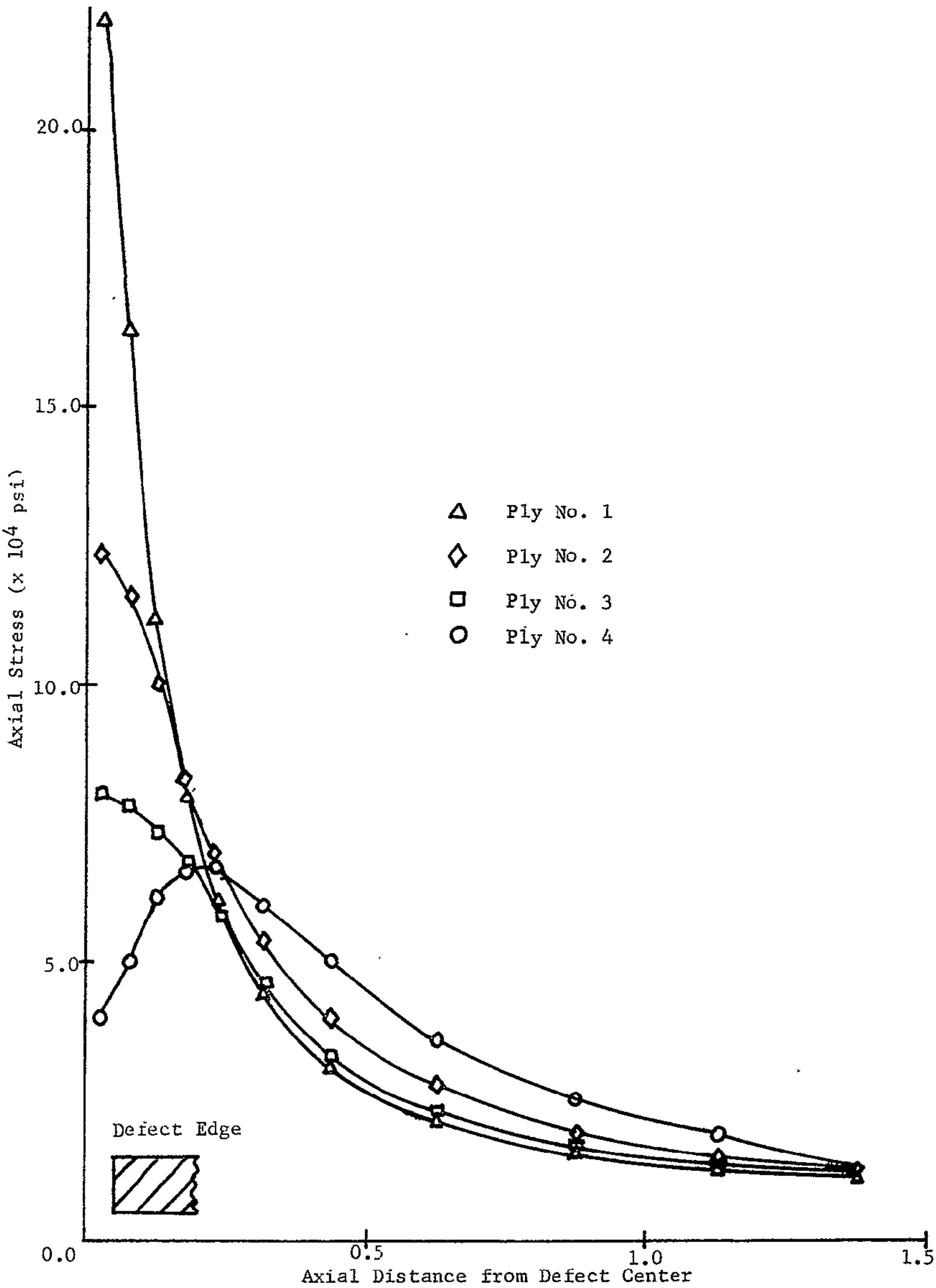

Figure 45. Axial Stress Distribution in a Four-Ply Inverted Patch for a 30.0-In.-Diameter Chamber Subjected to 1000 psi Internal Pressure (7500 lb/in. Axial Load)

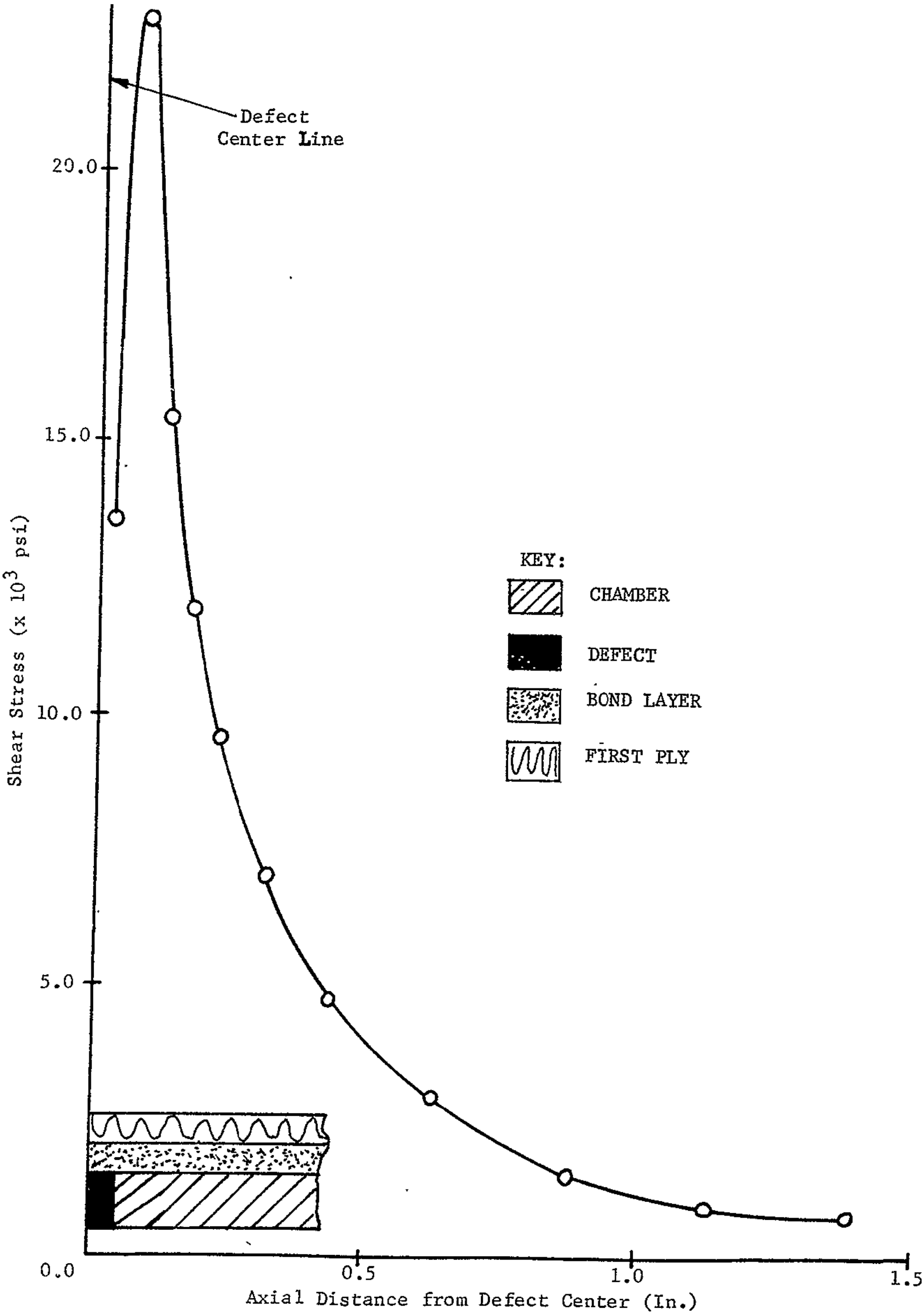

Figure 46. Shear Stress Distribution in Bond Layer Elements Nearest the Chamber Wall of a Four-Ply Inverted Patch for a 30.0-In.-Diameter Chamber Subjected to 1000 psi Internal Pressure (7500 lb/in. Axial Load)

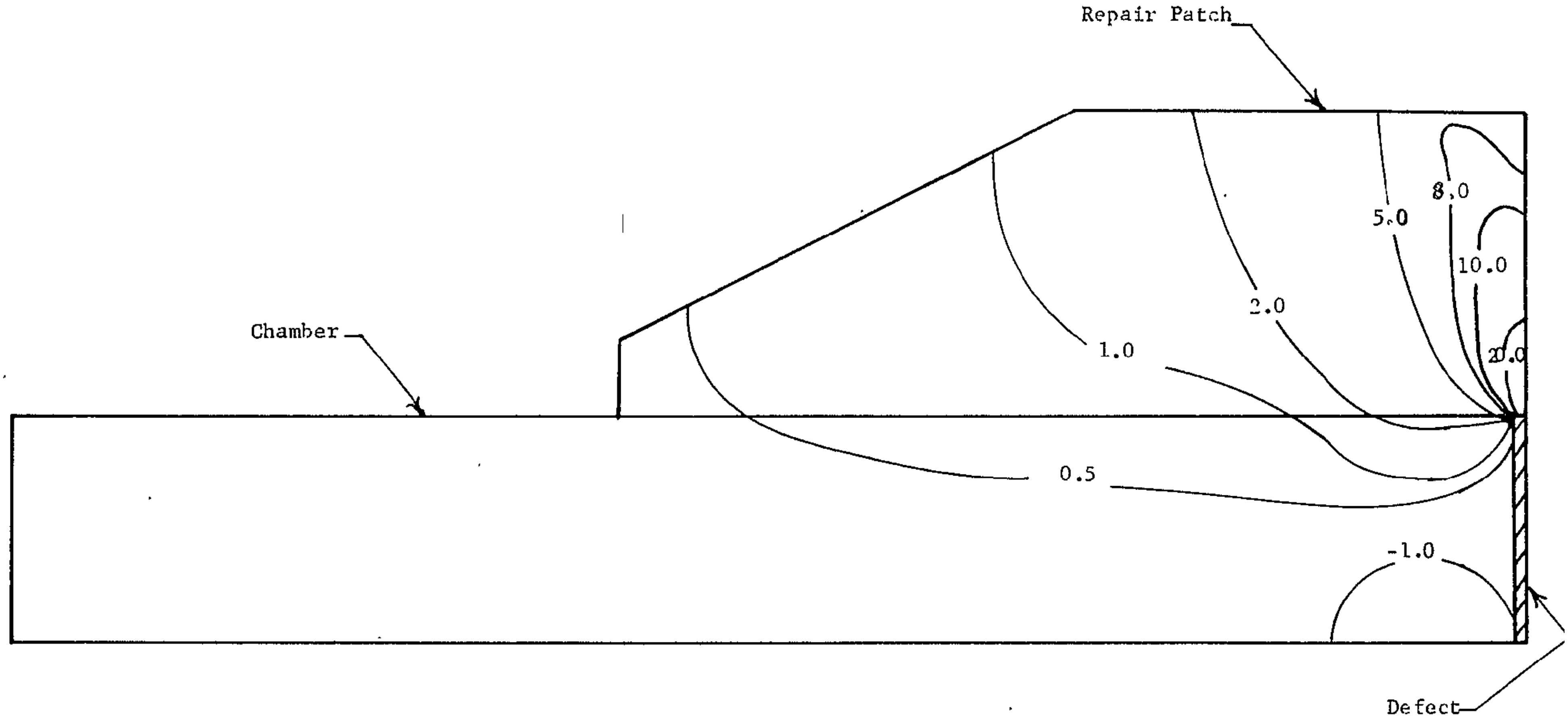

Figure 47. Axial Strain (%) Distribution in a Four-Ply Repair with a Fiberglass Layer in Bond Line for a 30.0-In.-Diameter Chamber Subjected to 1000 psi Internal Pressure (7500 lb/in. Axial Load)

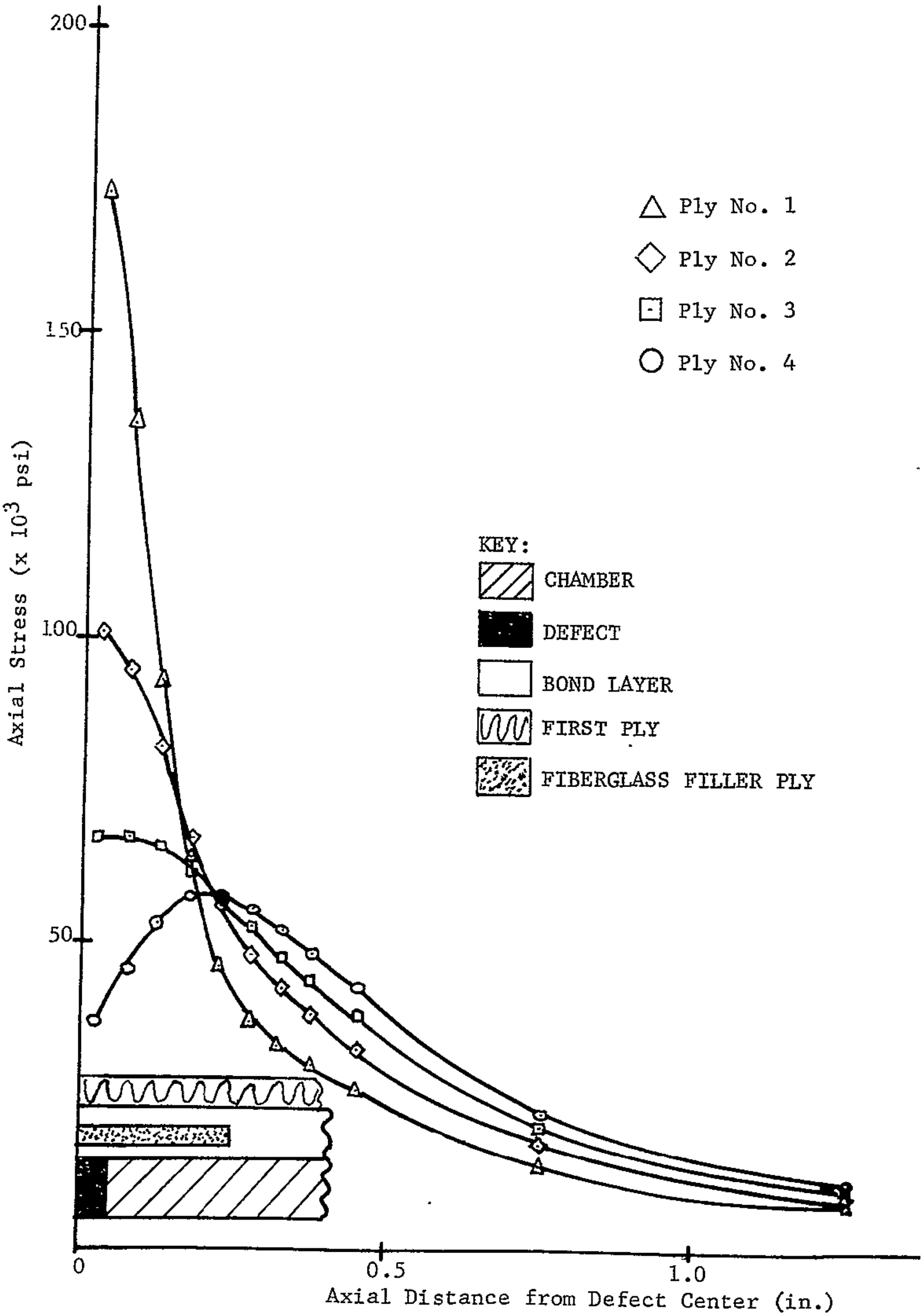

Figure 48. Axial Stress Distribution per Ply for a Four-Ply Repair with a Fiberglass Filler Ply (7500 lb/in. Axial Load)

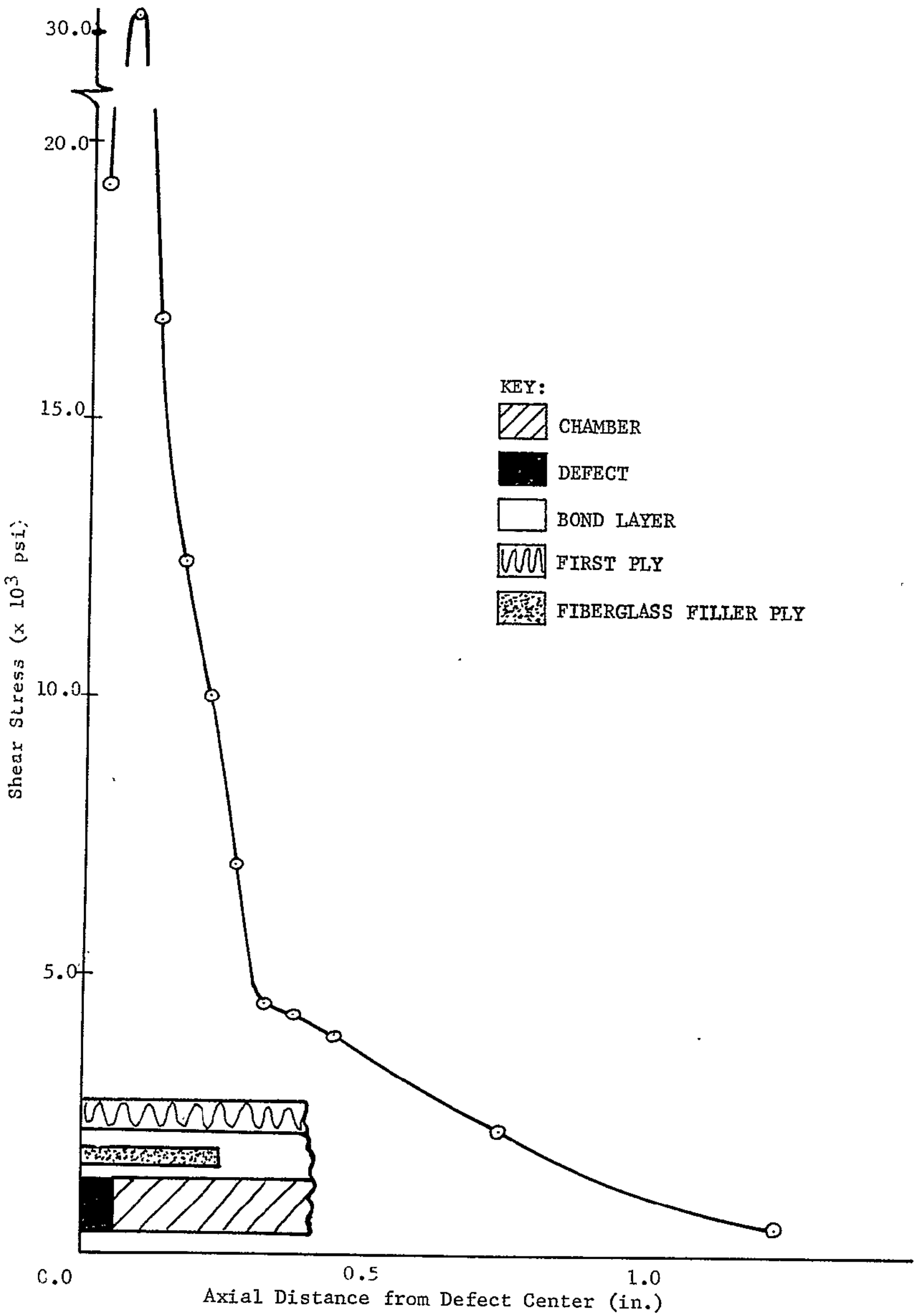

Figure 49. Shear Stress Distribution in Bond Layer Elements Nearest the Chamber Wall with a Fiberglass Filler Ply (7500 lb/in. Axial Load)

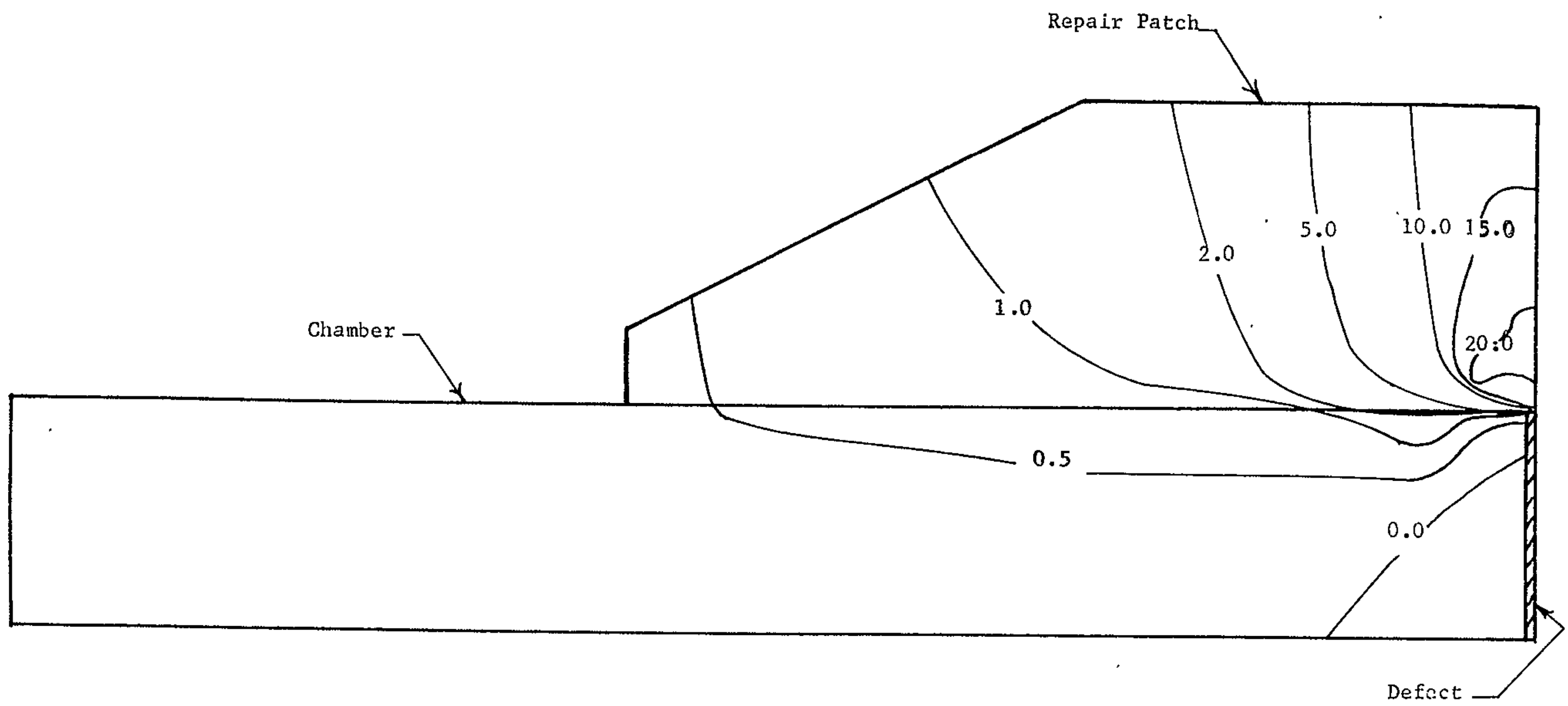

Figure 50. Axial Strain (%) Distribution in a Four-Ply Repair with a Rubber Layer in Bond Line for a 30.0-In.-Diameter Chamber Subjected to 1000 psi Internal Pressure (7500 lb/in. Axial Load)

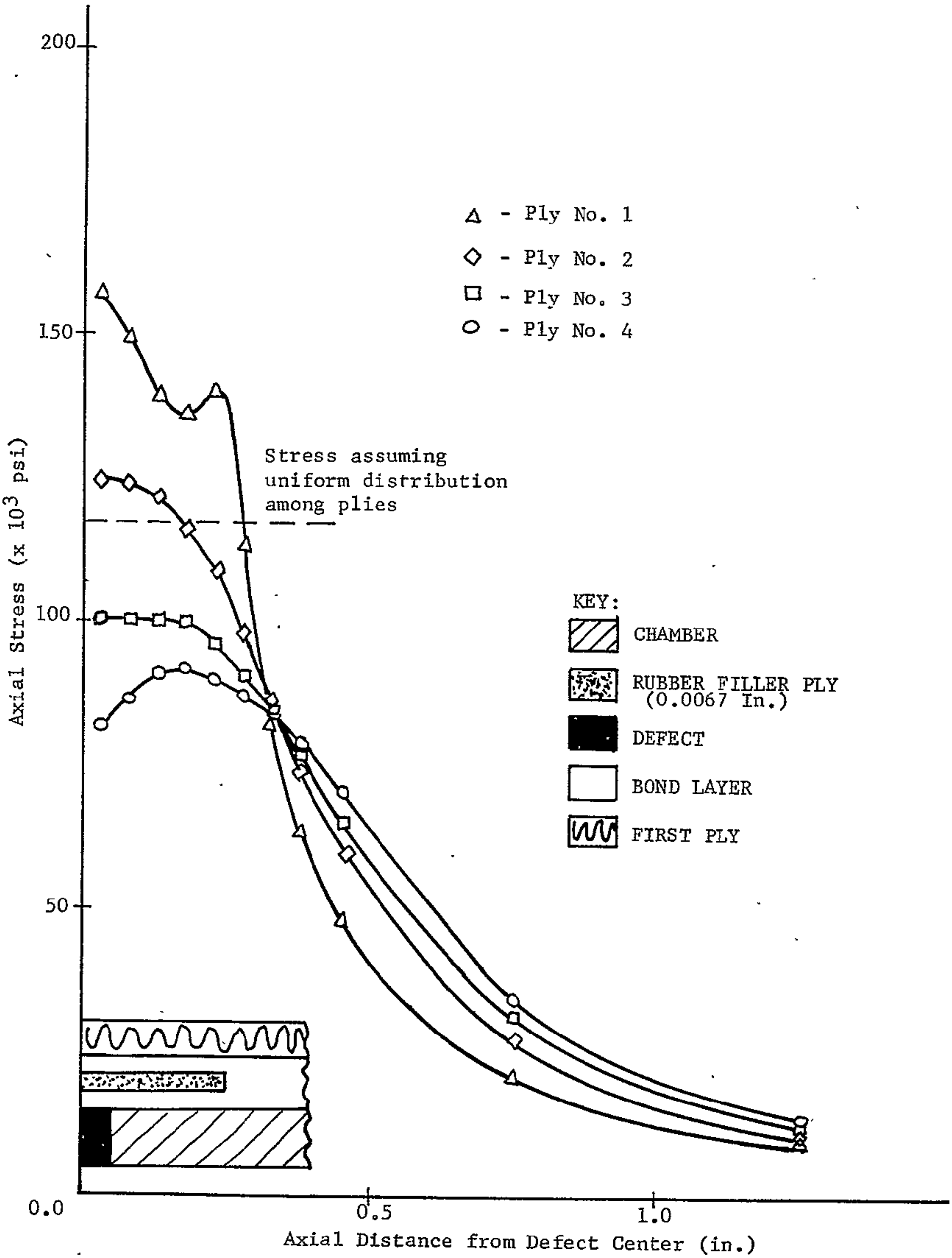

Figure 51. Axial Stress Distribution Per Ply for a Four-Ply Repair with a Rubber Filler Ply (7500 lb/in. Axial Load)

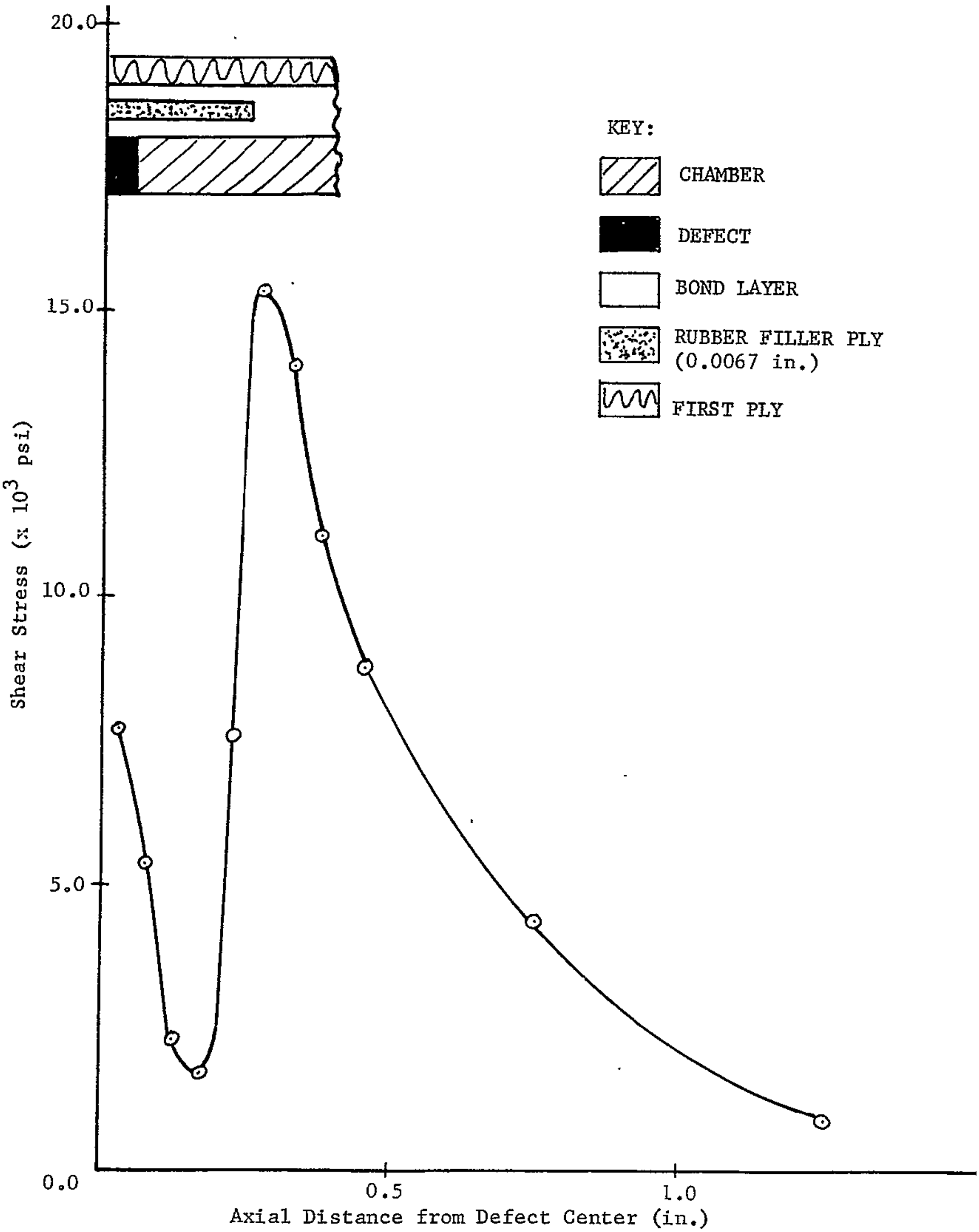

Figure 52. Shear Stress Distribution in Bond Layer Elements Nearest the Chamber Wall with a Rubber Filler Ply (7500 lb/in. Axial Load)

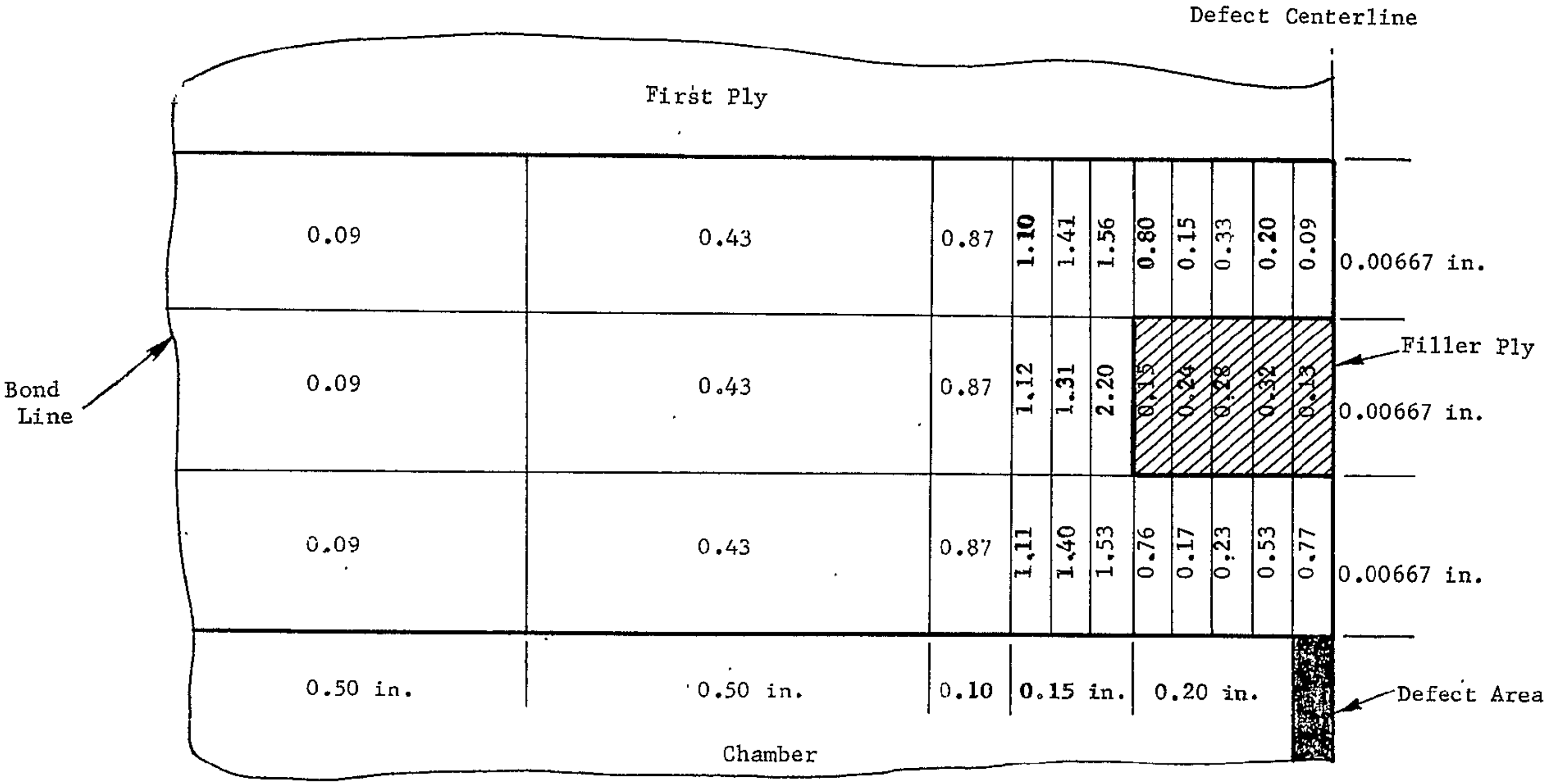

Figure 53. Shear Stress (x 10^4 psi) Distribution for a Bond Line with a 0.00667-In.-Thick Rubber Filler Ply (7500 lb/in. Axial Load)

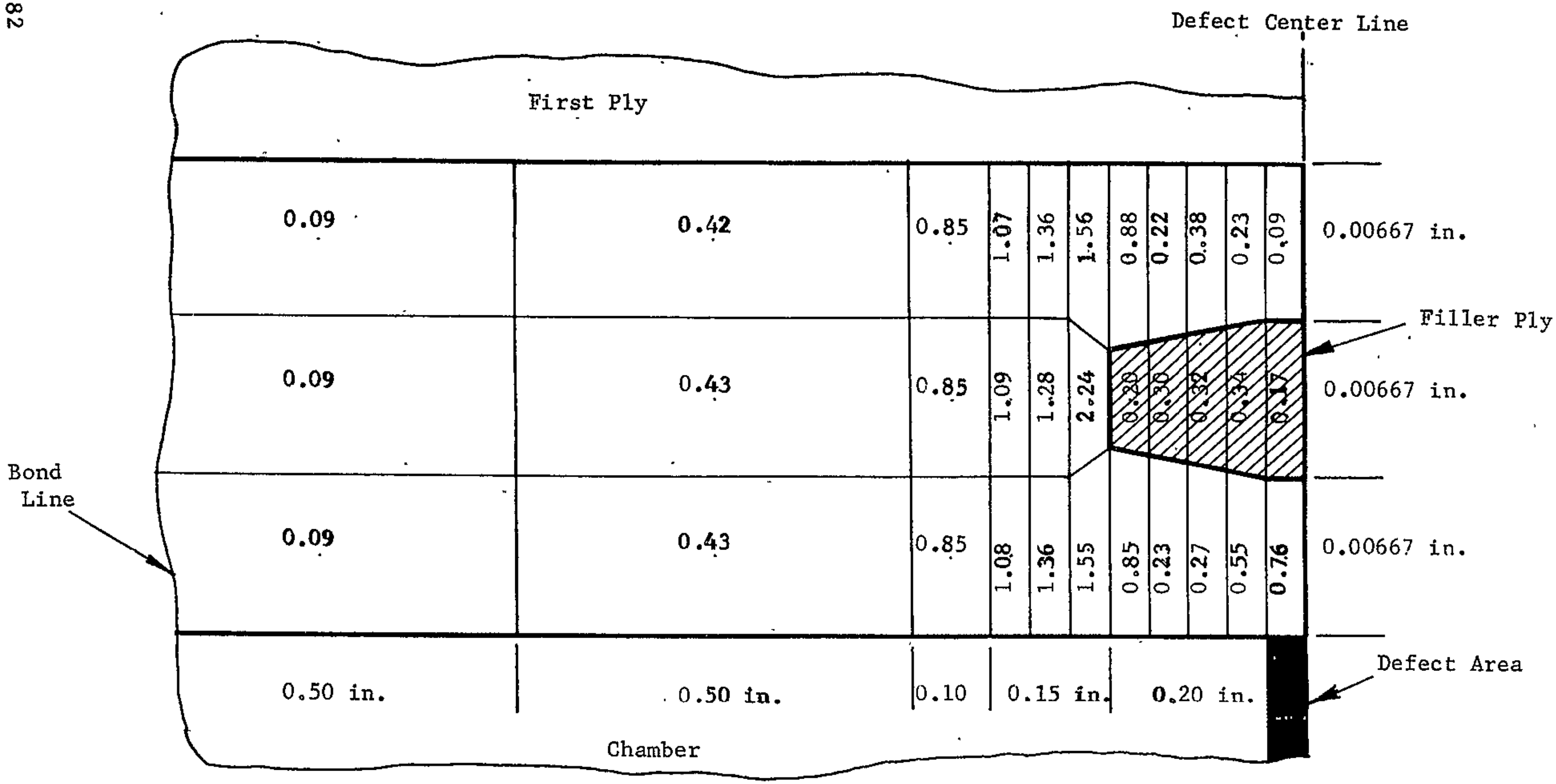

Figure 54. Shear Stress (x 10^4 psi) Distribution for a Bond Line with a Rubber Filler Ply Tapered to 0.004-In.-Thickness (7500 lb/in. Axial Load)

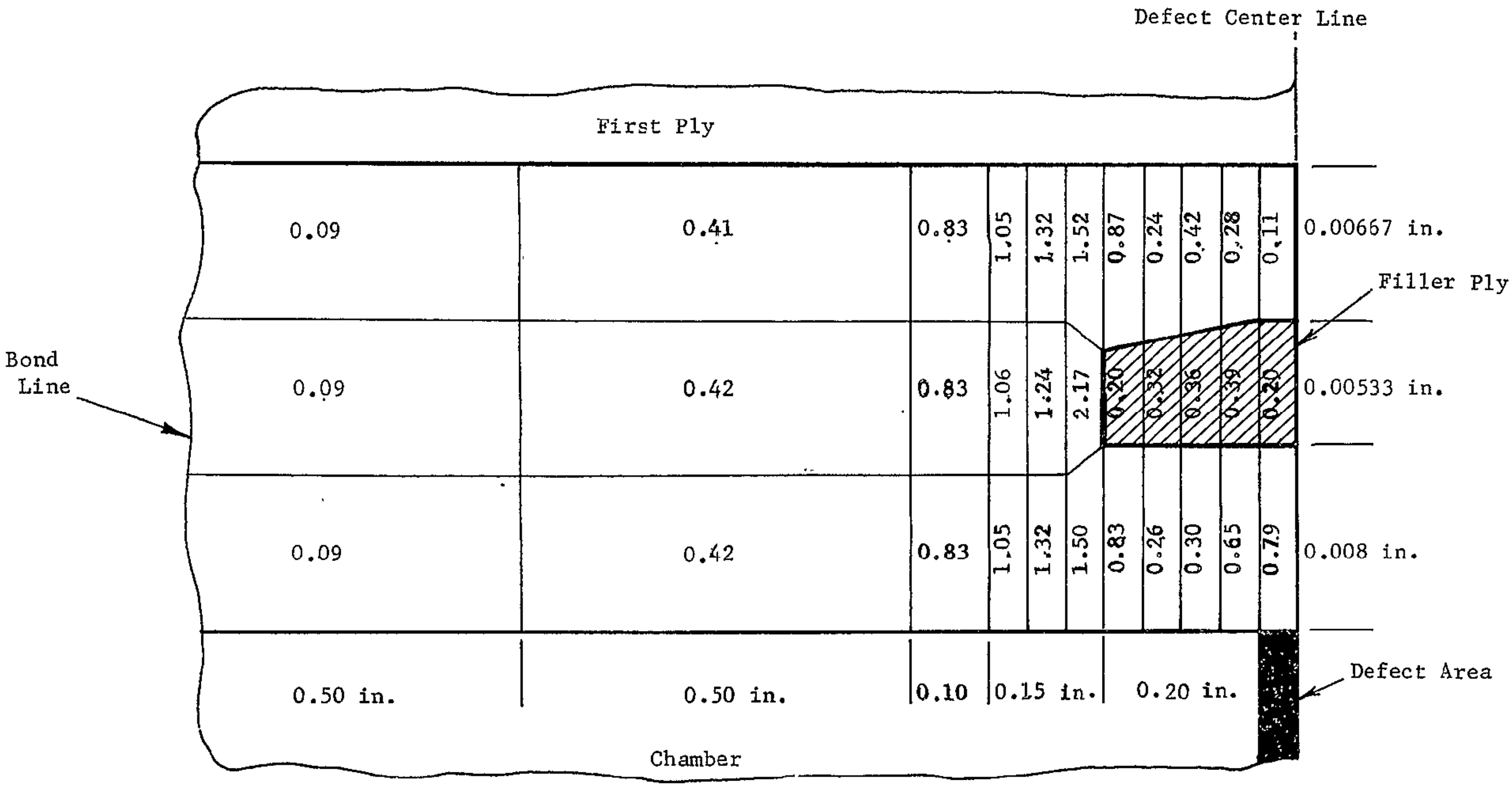

Figure 55. Shear Stress (x 10^4 psi) Distribution for a Bond Line with a Rubber Filler Ply Partially Tapered to 0.004-In. Thickness (7500 lb/in. Axial Load)

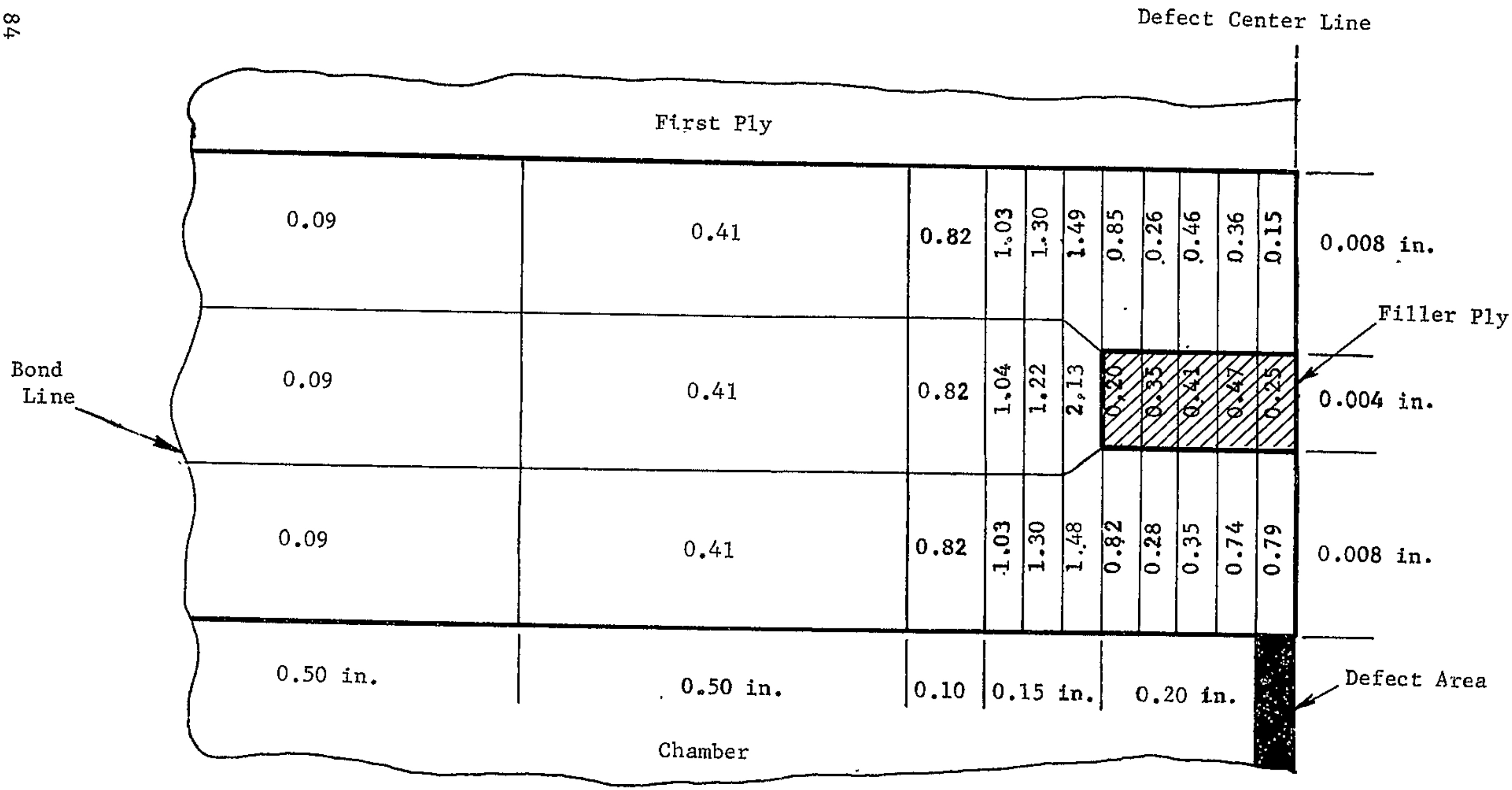

Figure 56. Shear Stress (x 10^4 psi) Distribution for a Bond Line with a Rubber Filler Ply 0.004-In. Thick (7500 lb/in. Axial Load)

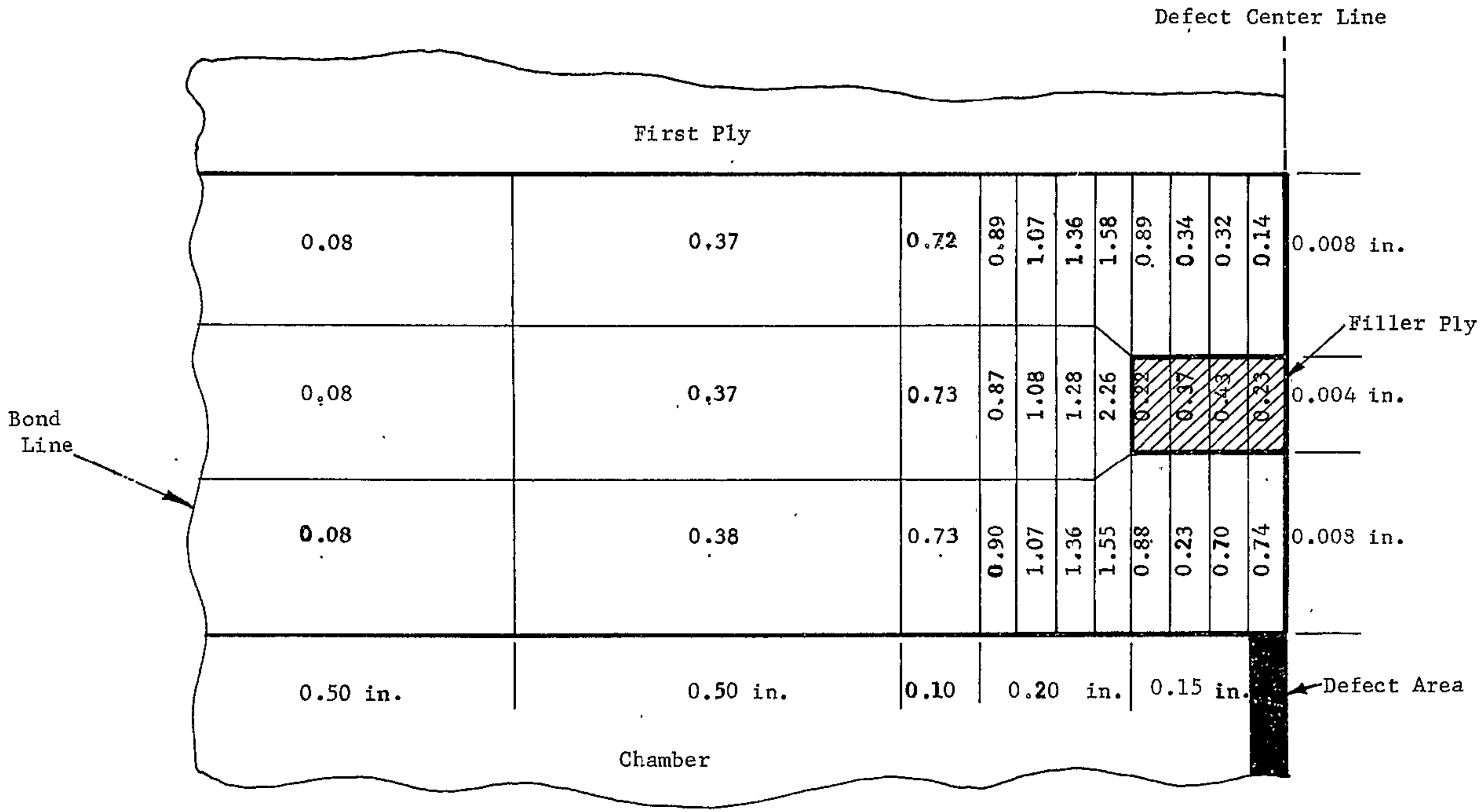

Figure 57. Shear Stress (x 10^4 psi) Distribution for a Bond Line with a Rubber Filler Ply 0.004-In. Thick and 0.20 In. Long (7500 lb/in. Axial Load)

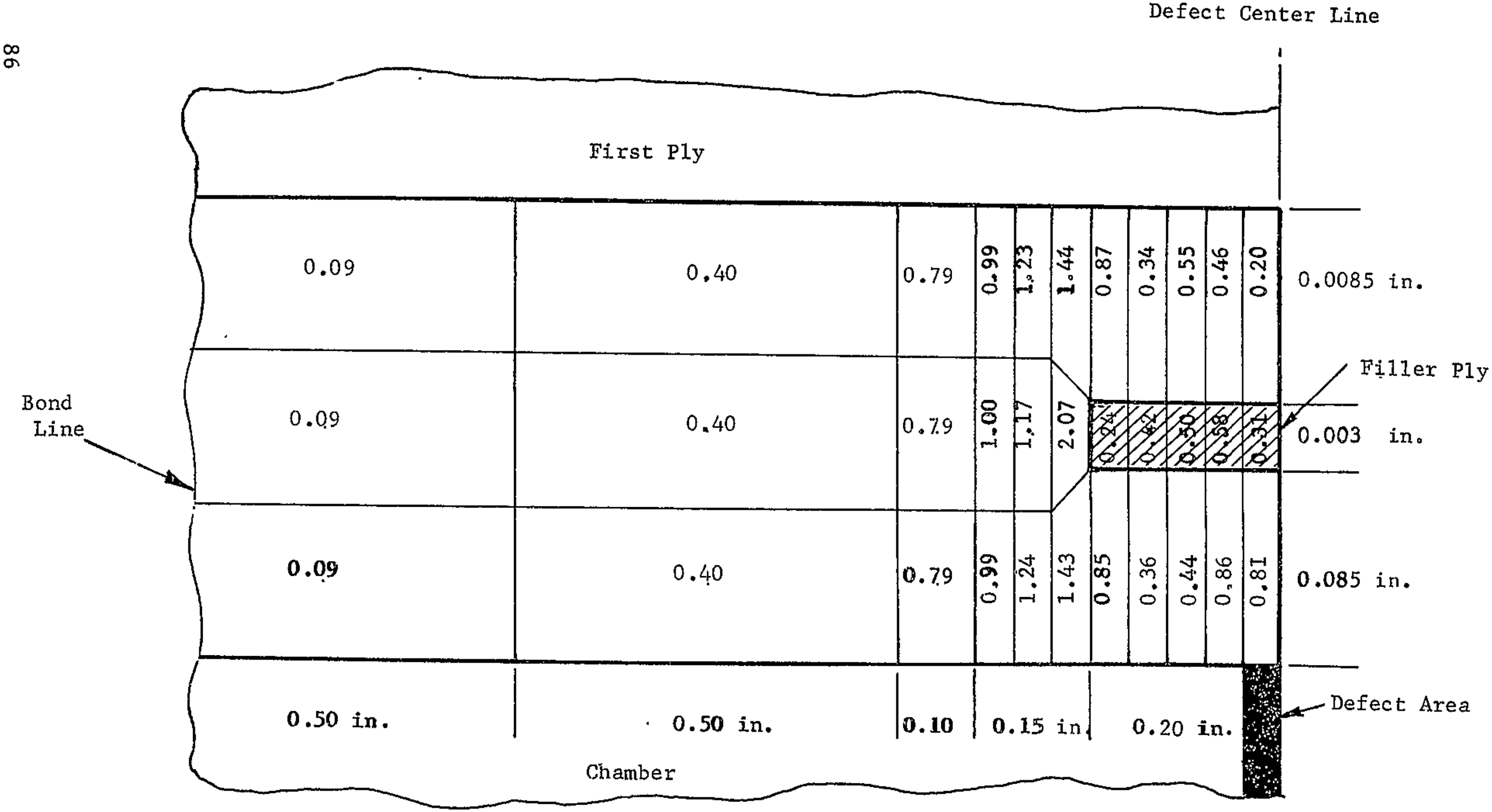

Figure 58. Shear Stress (x 10^4 psi) Distribution for a Bond Line with a 0.003-In.-Thick Rubber Filler Ply (7500 lb/in. Axial Load)

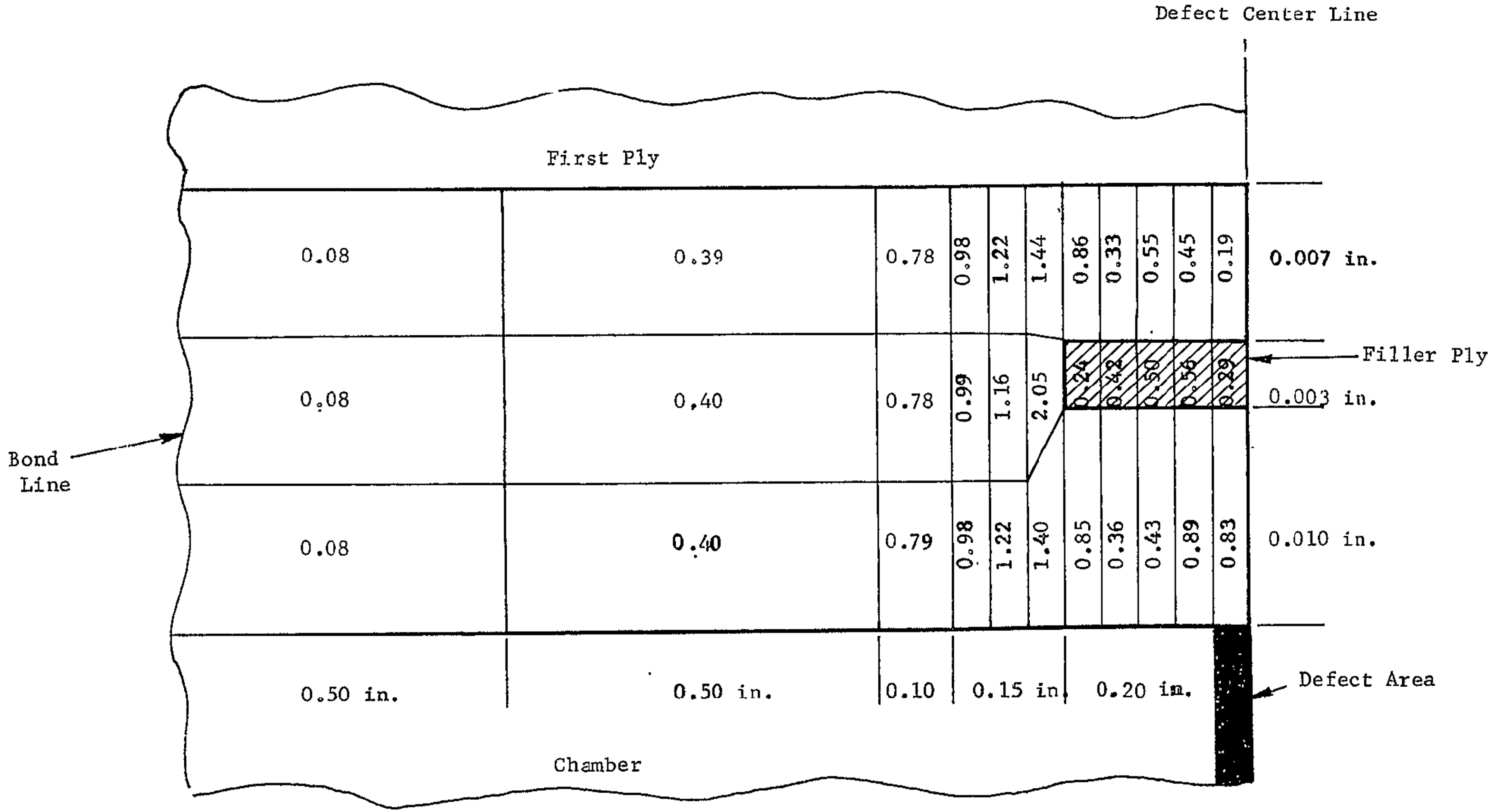

Figure 59. Shear Stress (x 10^4 psi) Distribution for a Bond Line with 0.003-In. Thick Rubber Filler Ply Offset from Center of Bond Line (7500 lb/in. Axial Load)

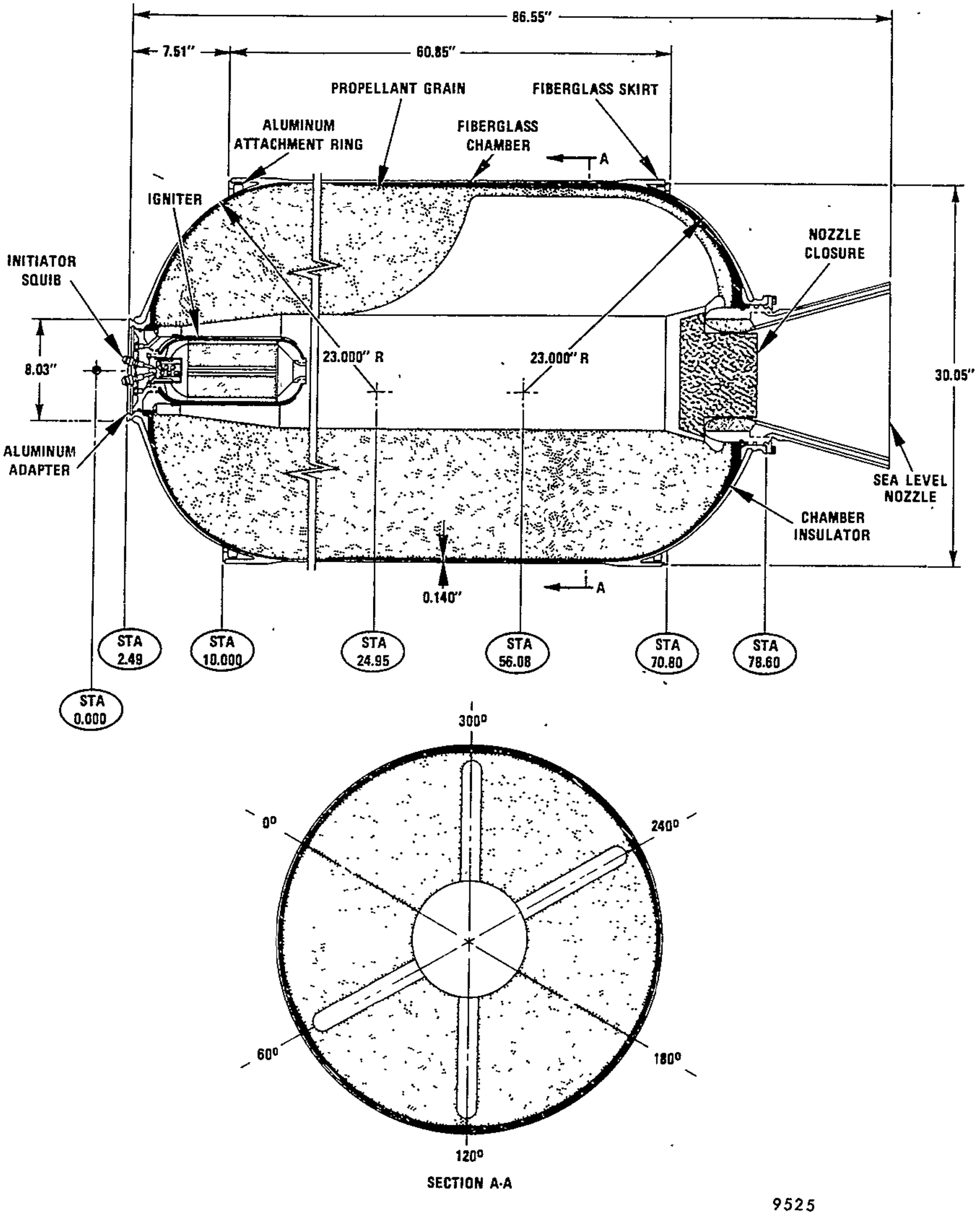

Figure 60. Rocket Motor X259

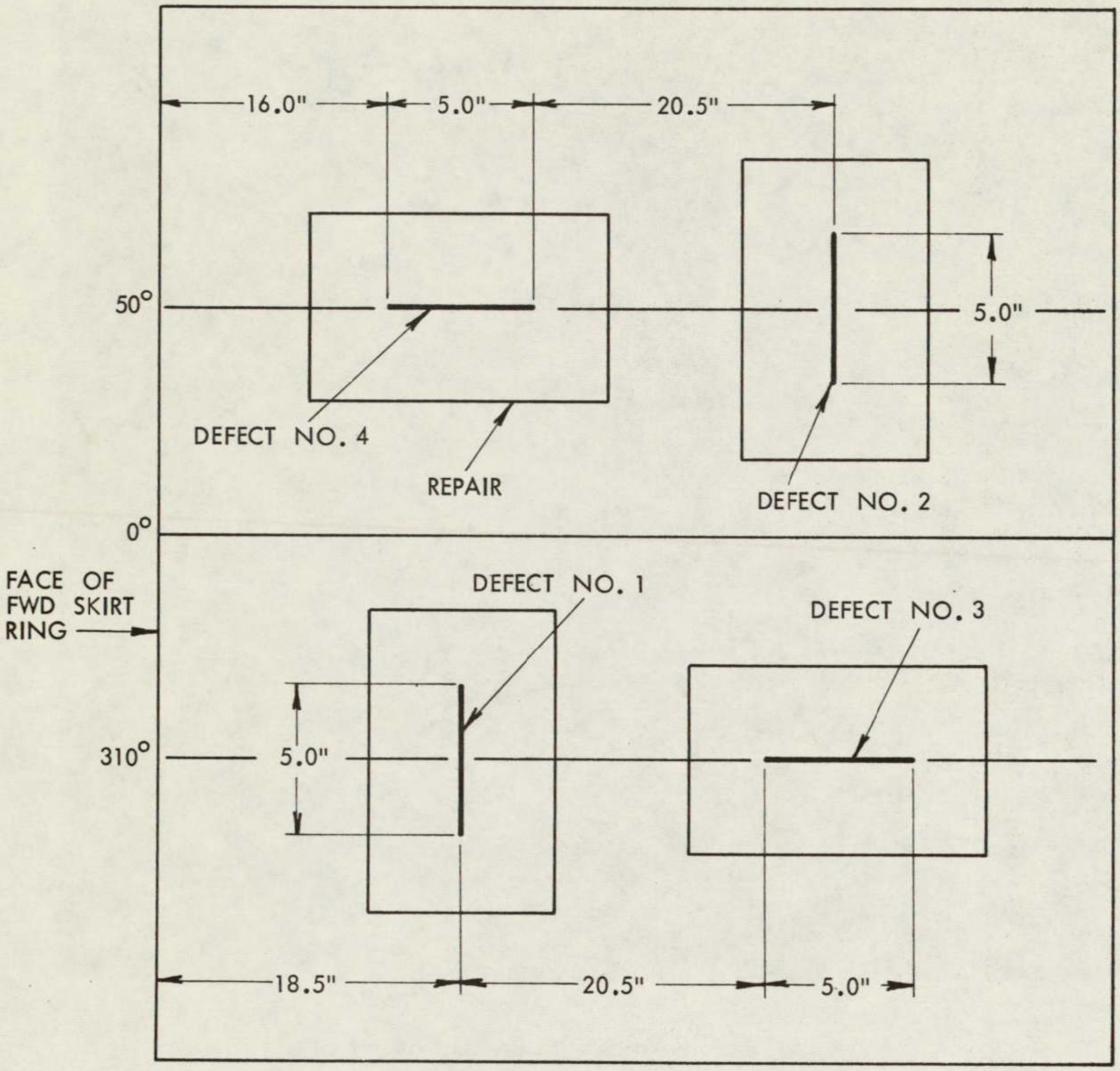

NOTE: Angular orientation - Forward looking Aft - Counterclockwise

9833

Figure 61. Defect Location on X 259 Cylindrical Section

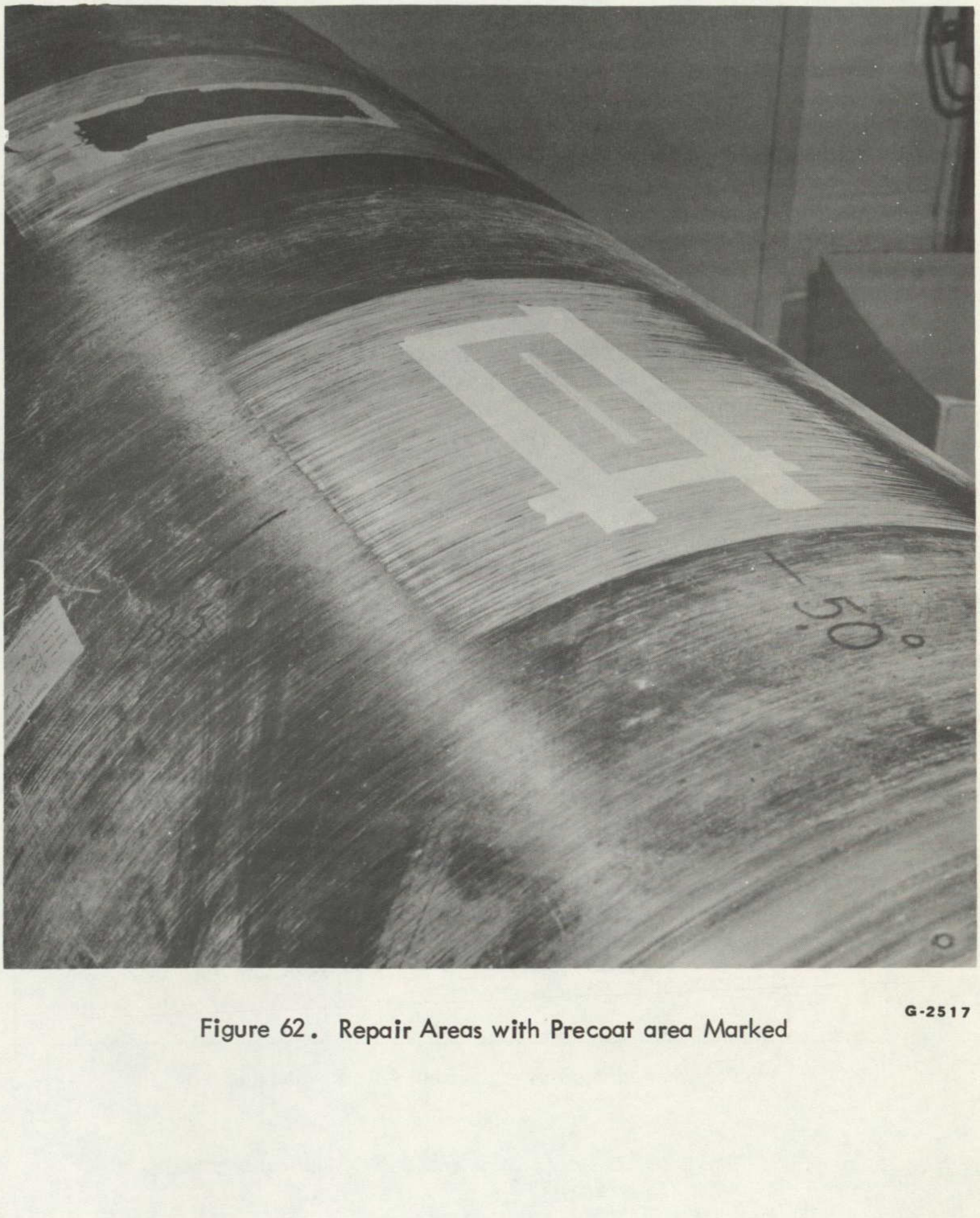

G-2517

Figure 62. Repair Areas with Precoat area Marked

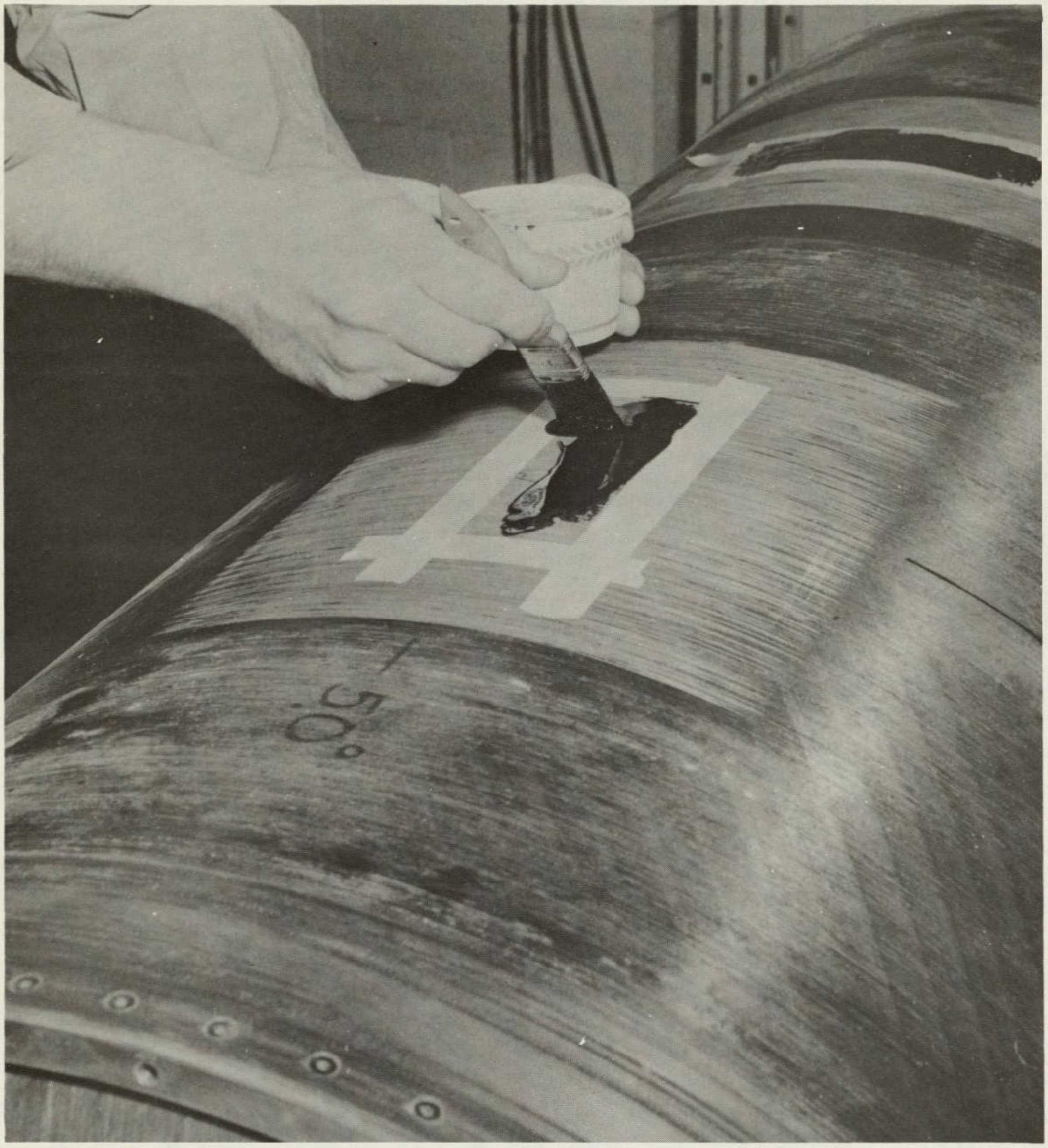

Figure 63. Application of Precoat to Defect Area

G-2521

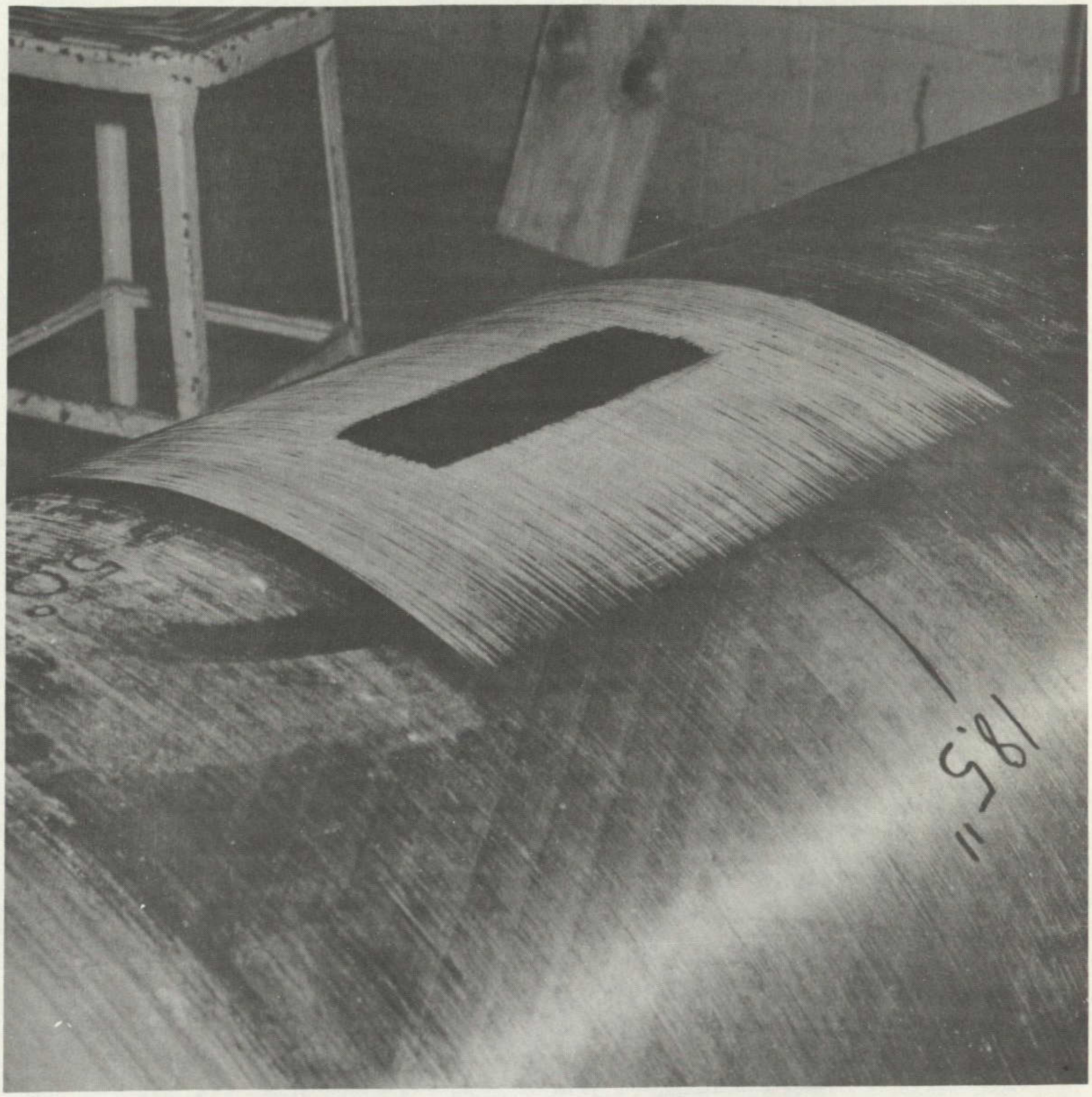

Figure 64. Precoat with Edges Tapered

G-2516

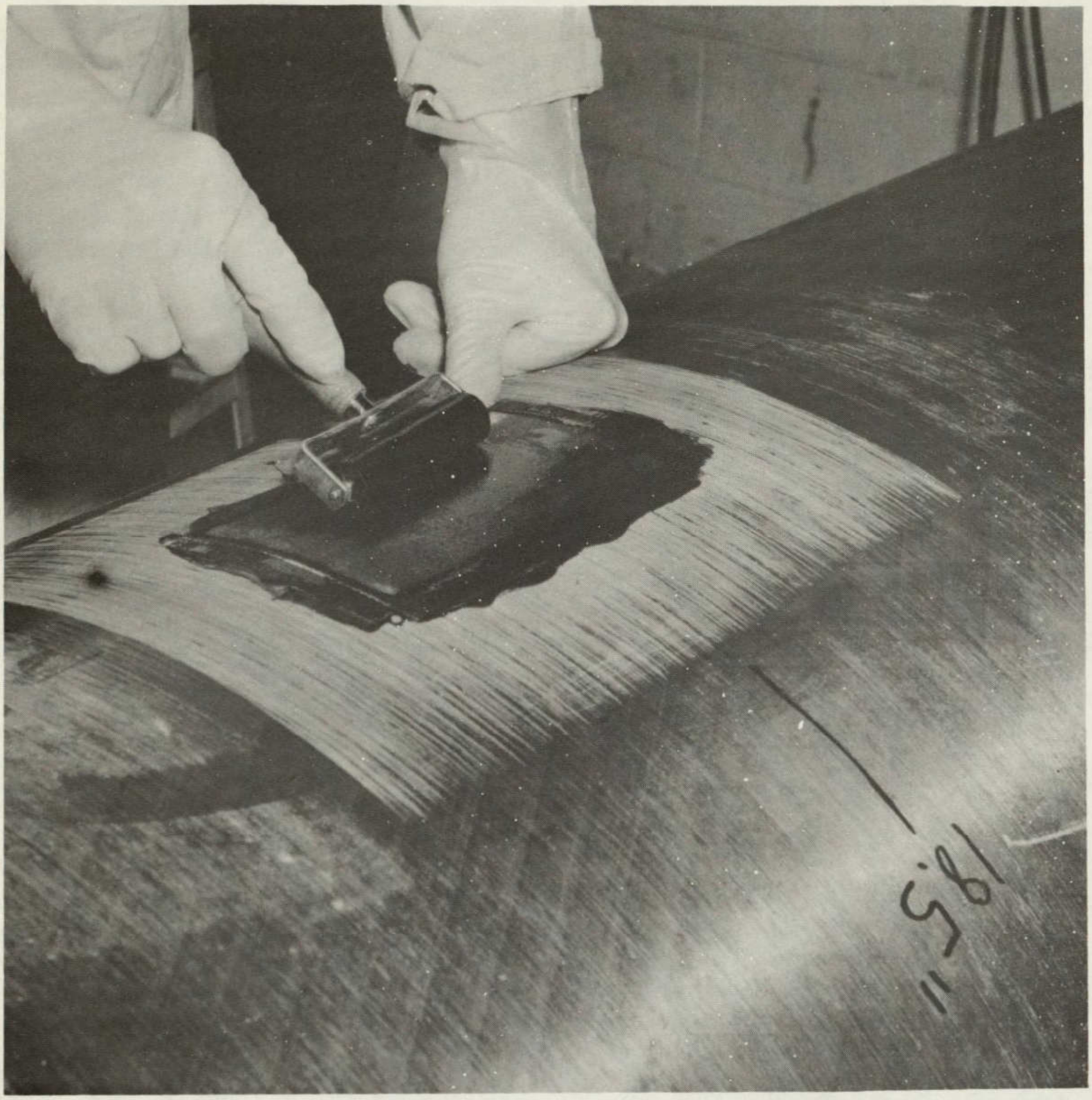

Figure 65. Application of First Ply of Patch

G-2519

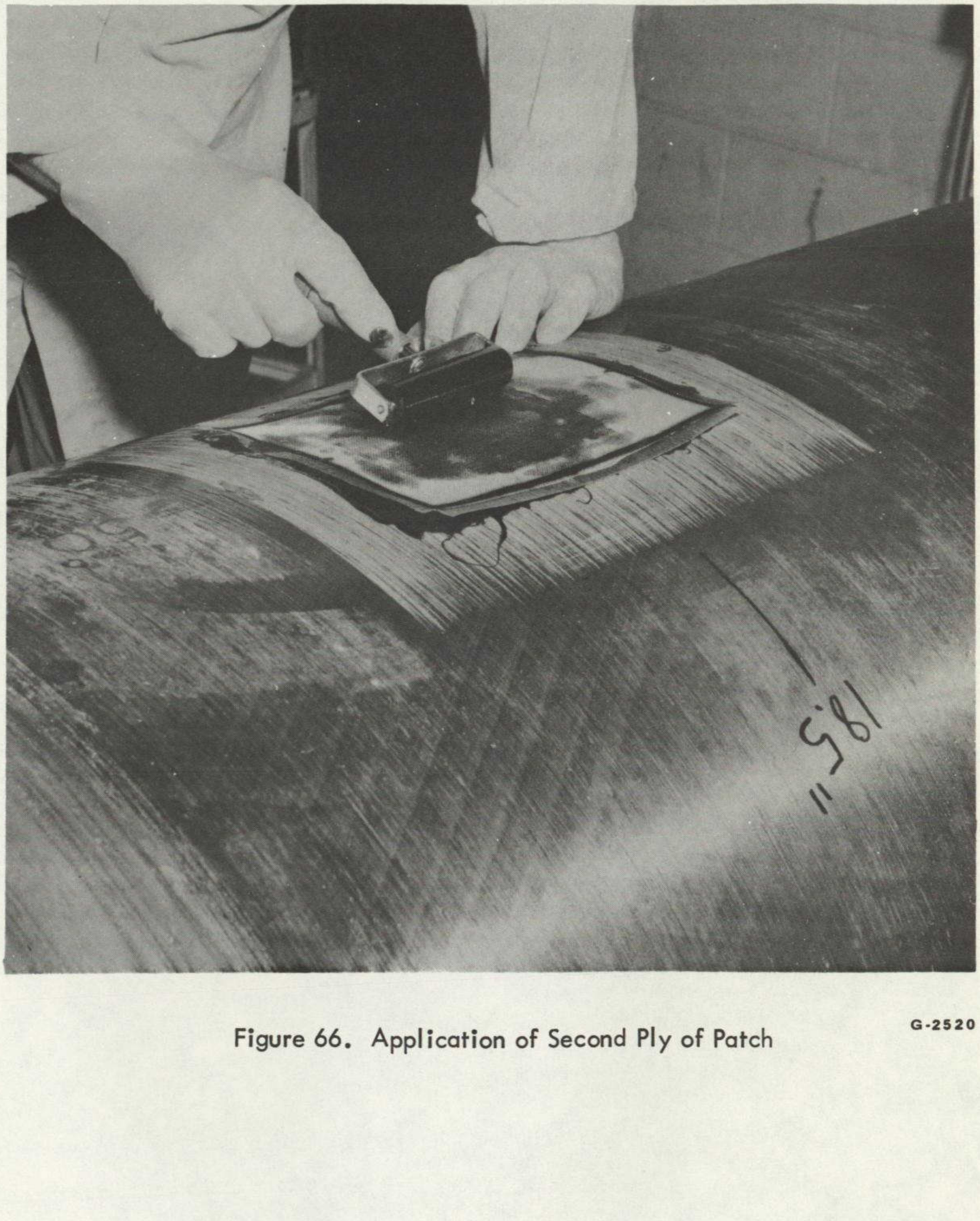

Figure 66. Application of Second Ply of Patch G-2520

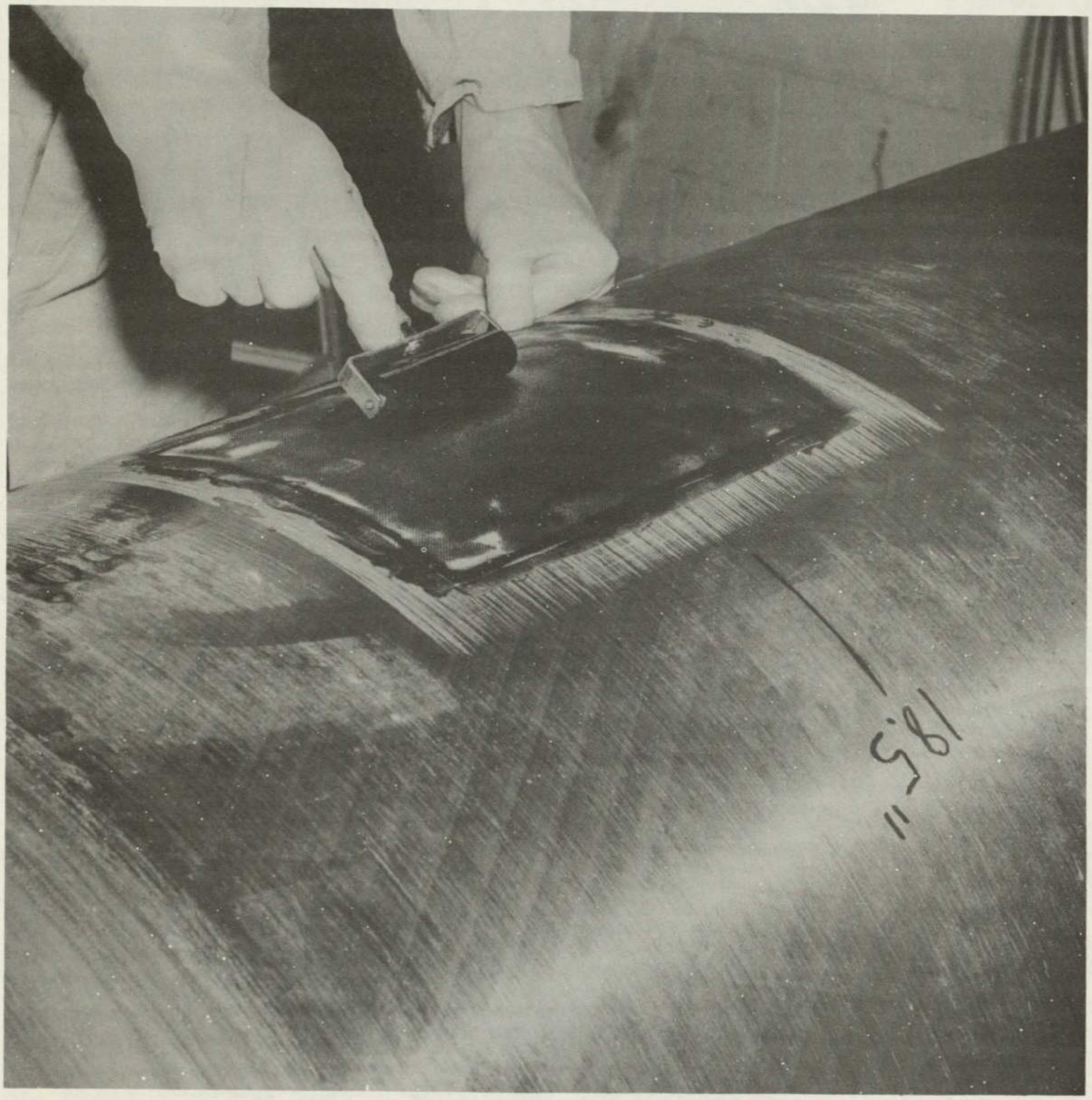

Figure 67. Application of Third Ply of Patch G-2518

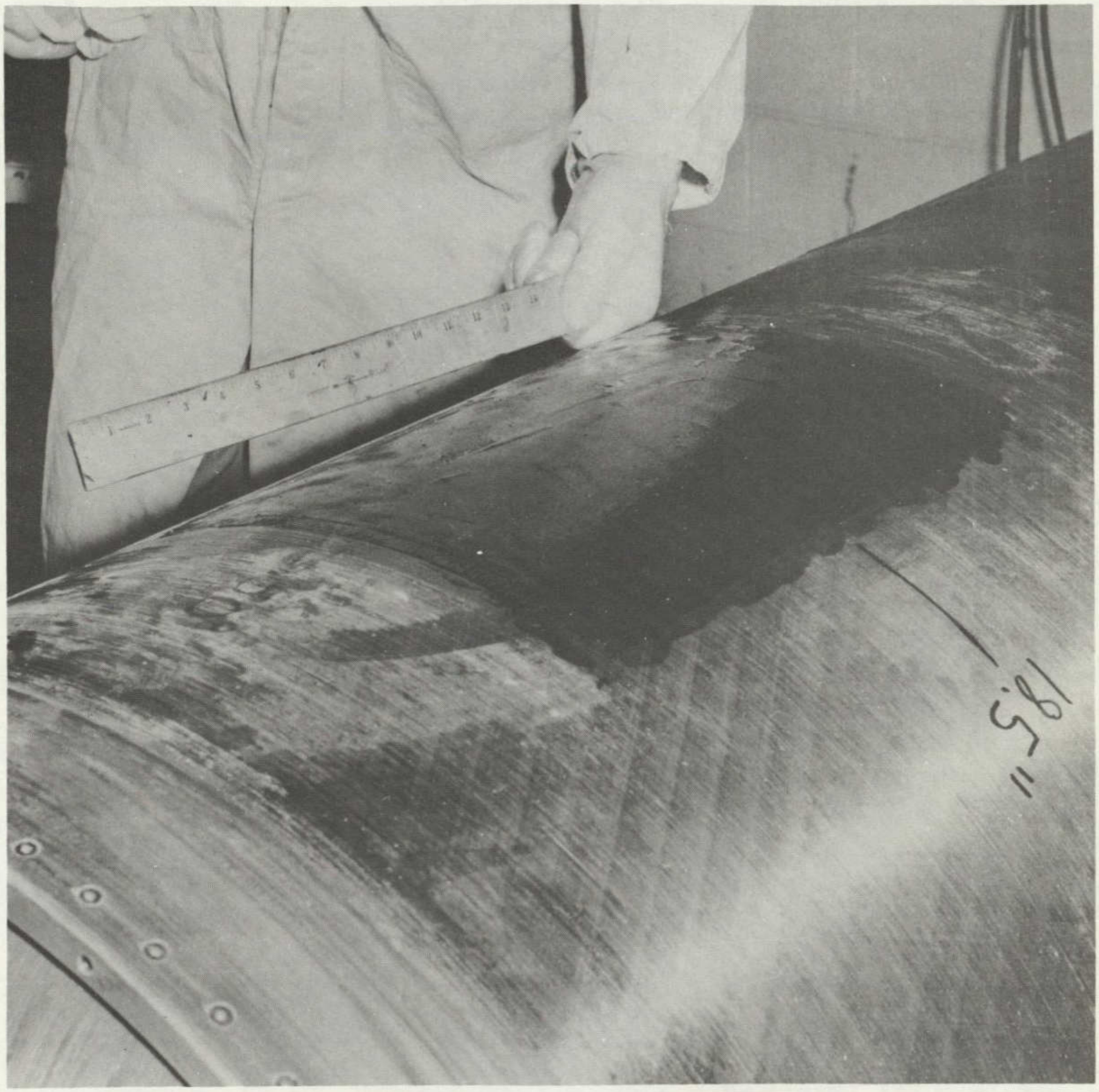

Figure 68. Patch Appearance After Application of Fourth Ply

G-2515

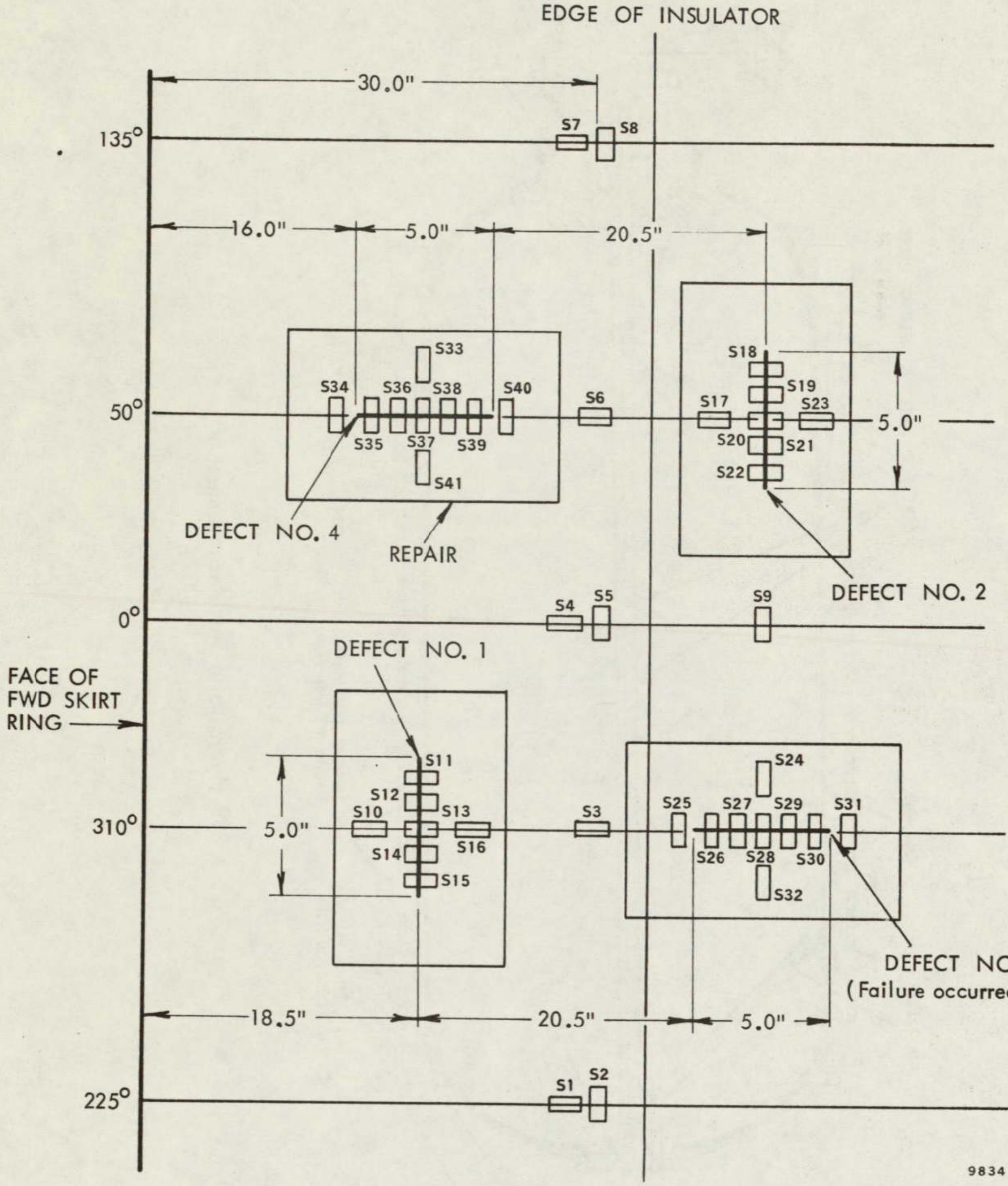

NOTE: Angular Orientation - Forward Looking Aft - Counterclockwise

Figure 69. Case Instrumentation

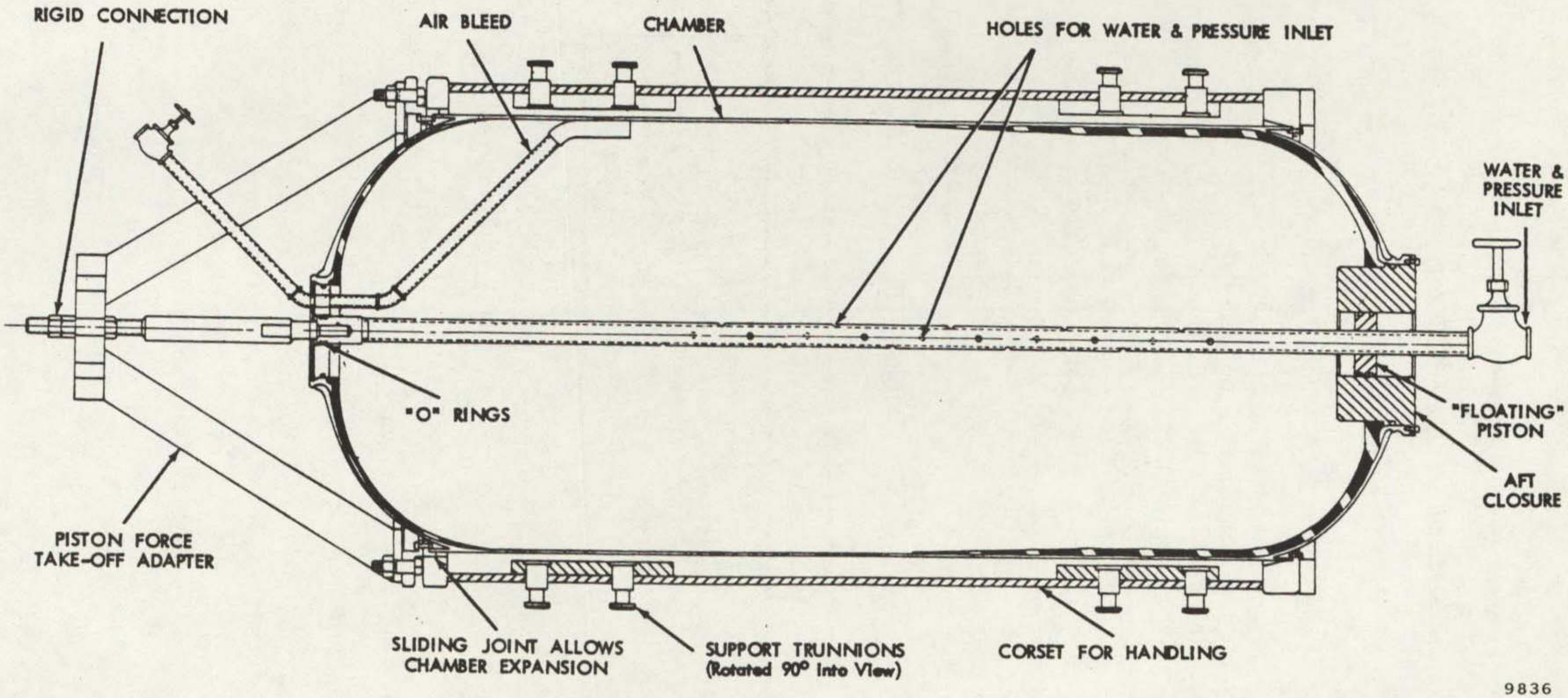

Figure 70. X259 Hydrostatic Test Arrangement

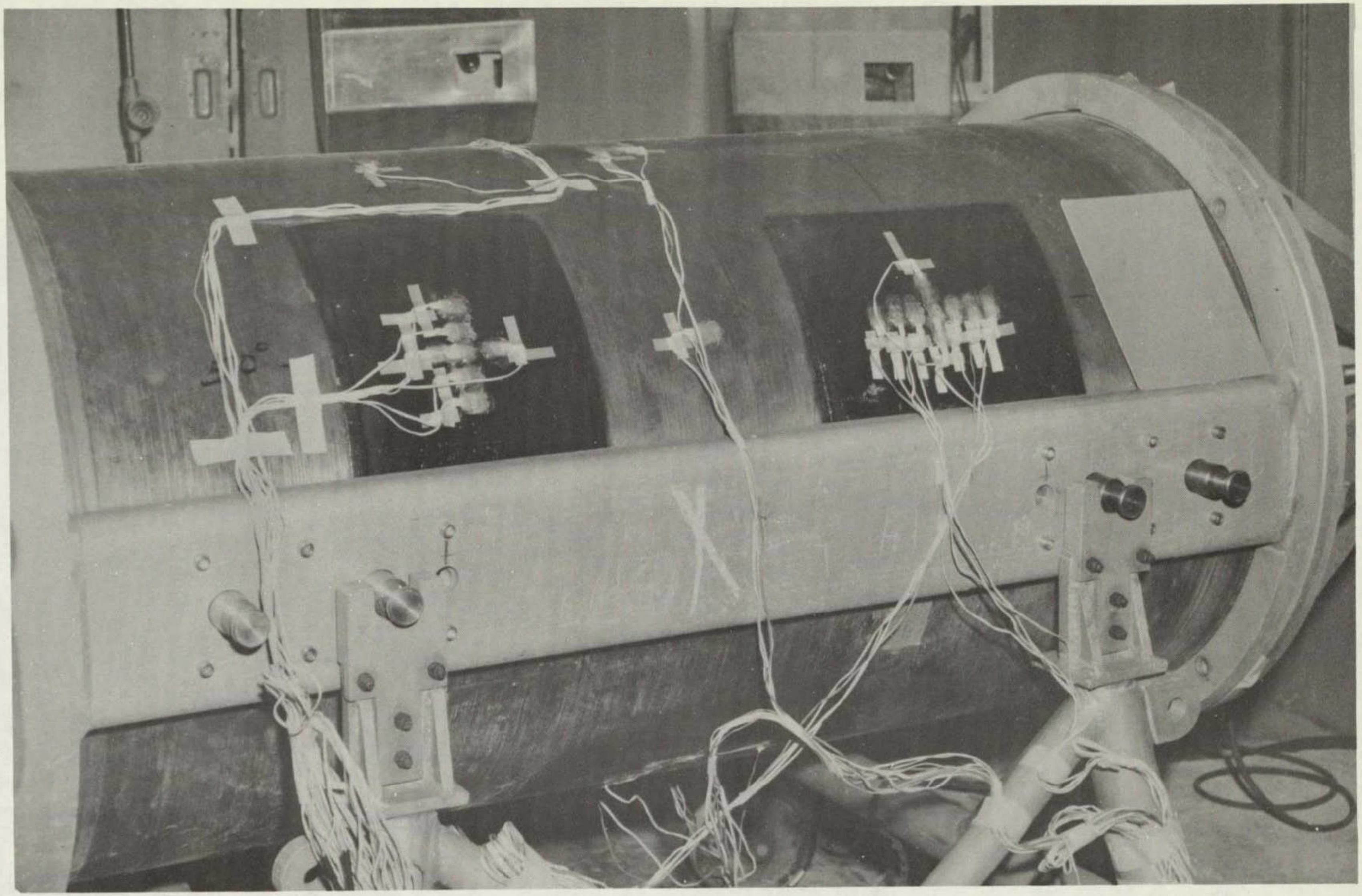

G-2514

Figure 71. X259 Pretest Configuration (50° View)

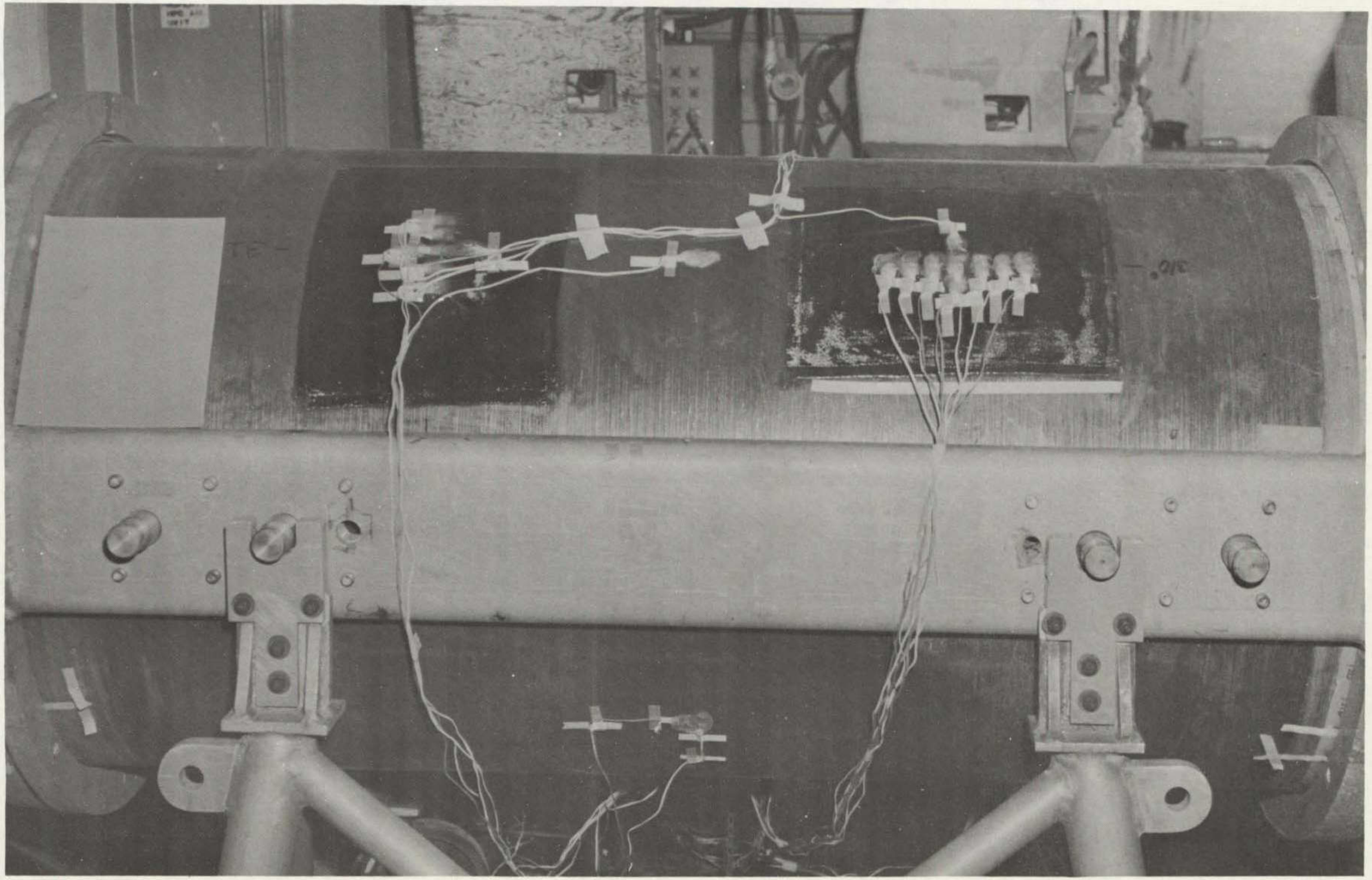

G-2512

Figure 72. X259 Pretest Configuration (310° View)

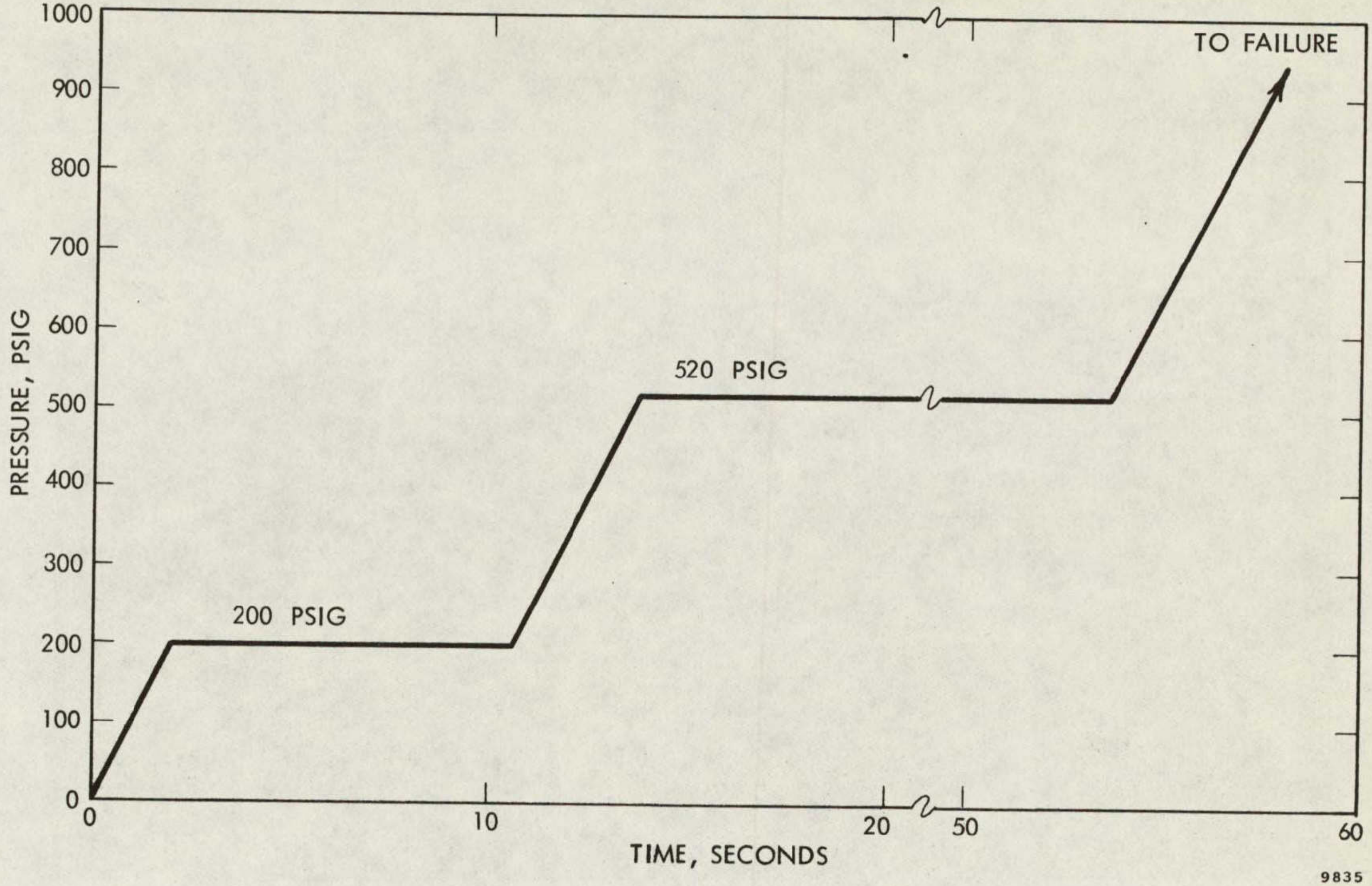

Figure 73. Pressure vs Time Program

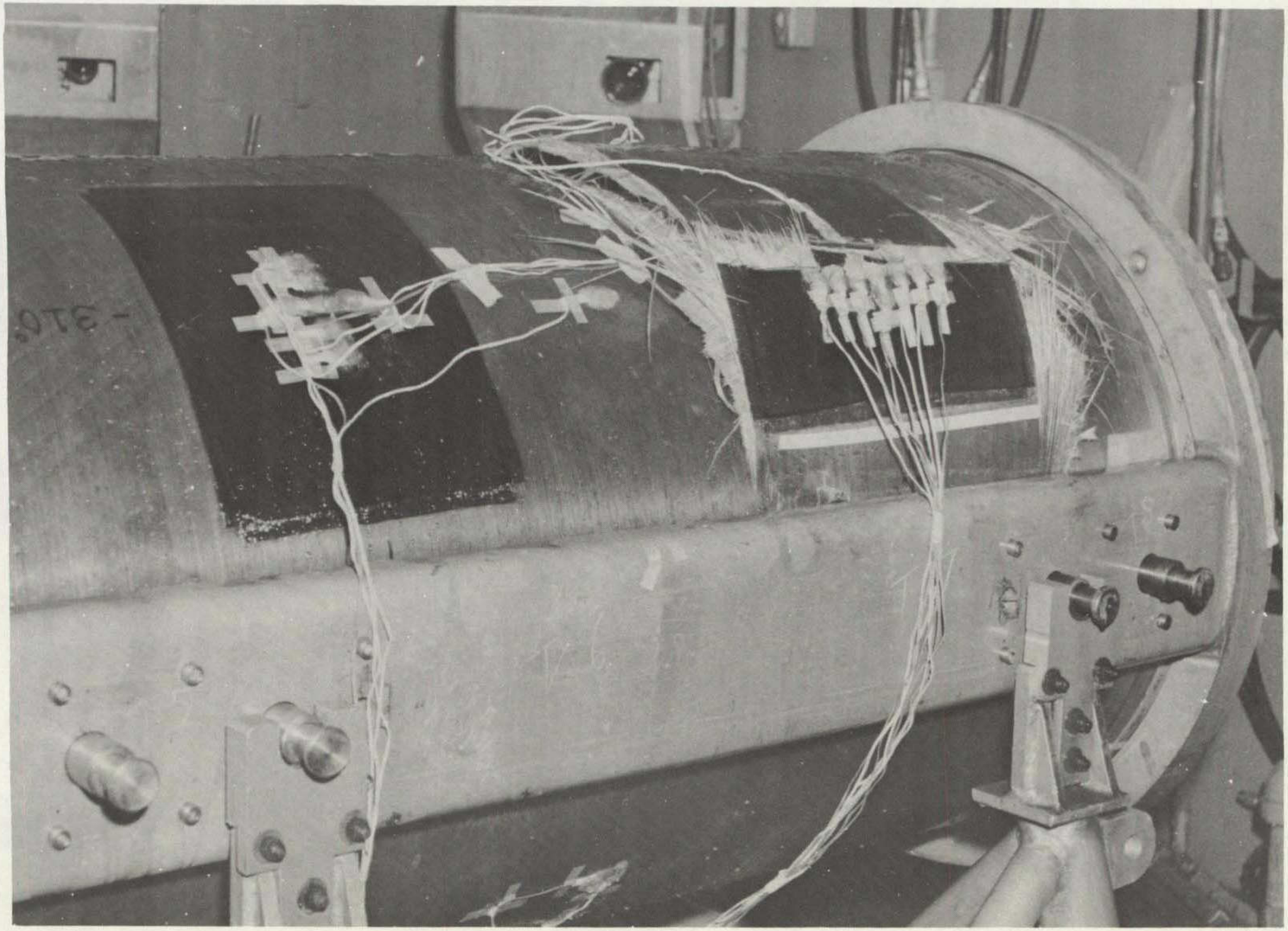

Figure 74. Post-test View of Failure

G-2511

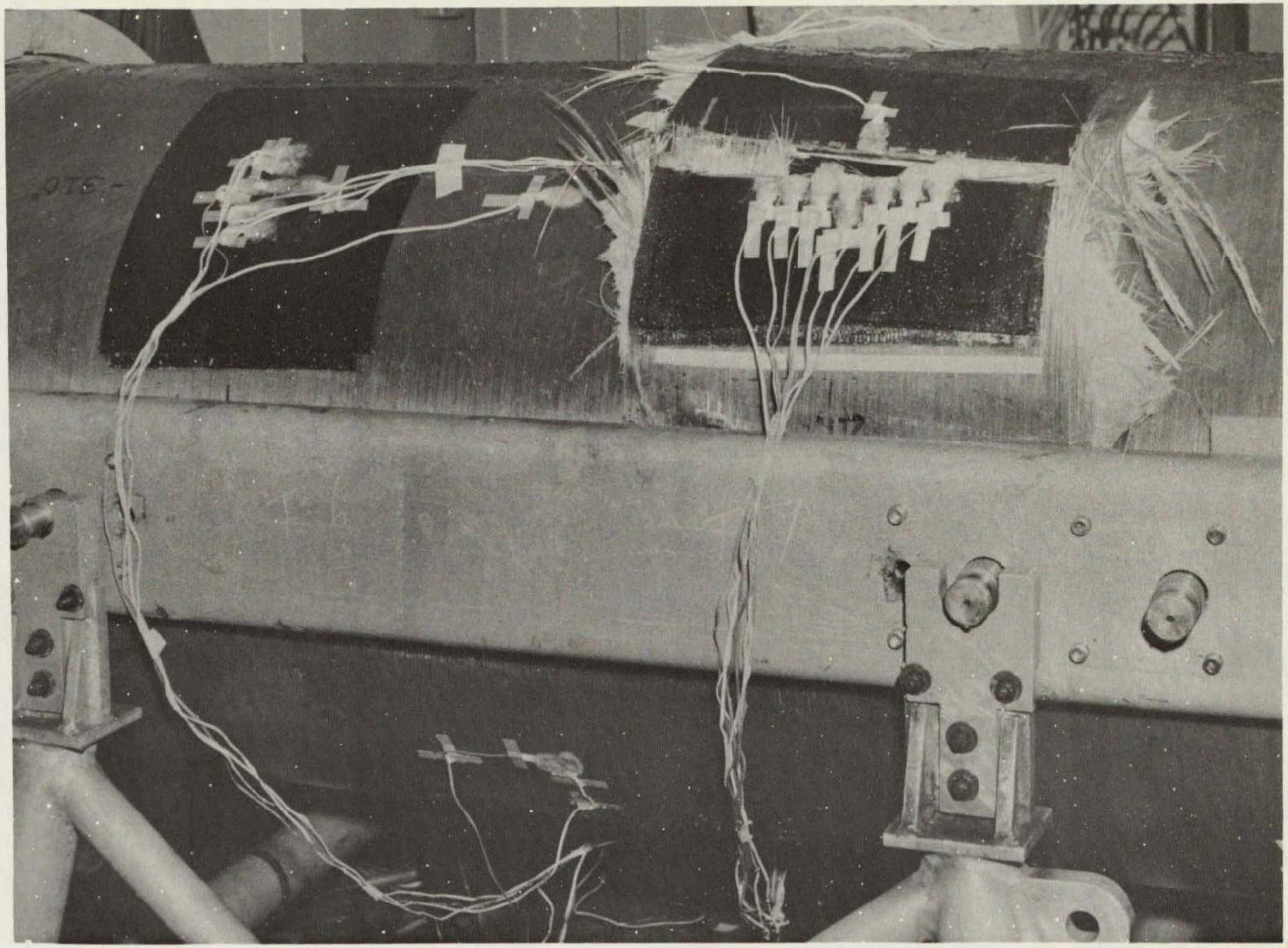

Figure 75. Post-test View of Failure

G-2513

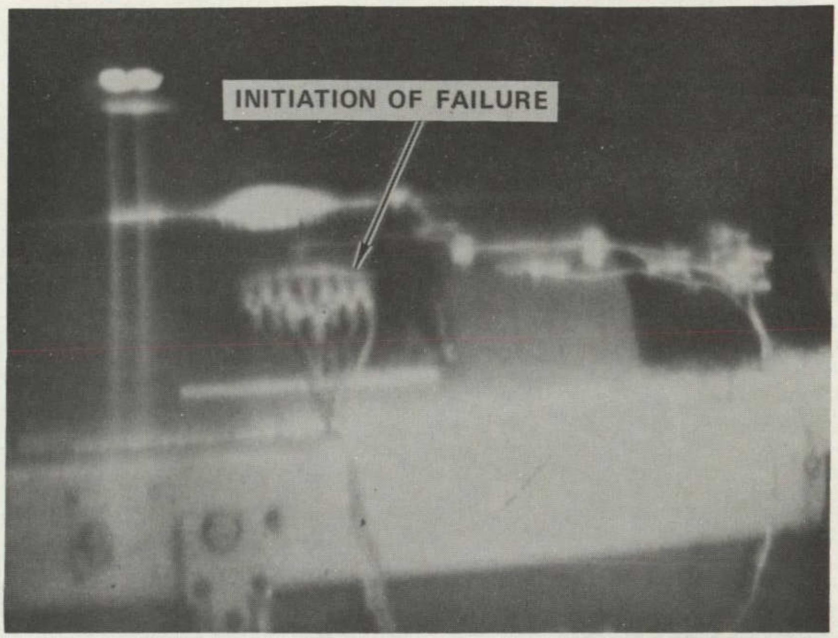

A

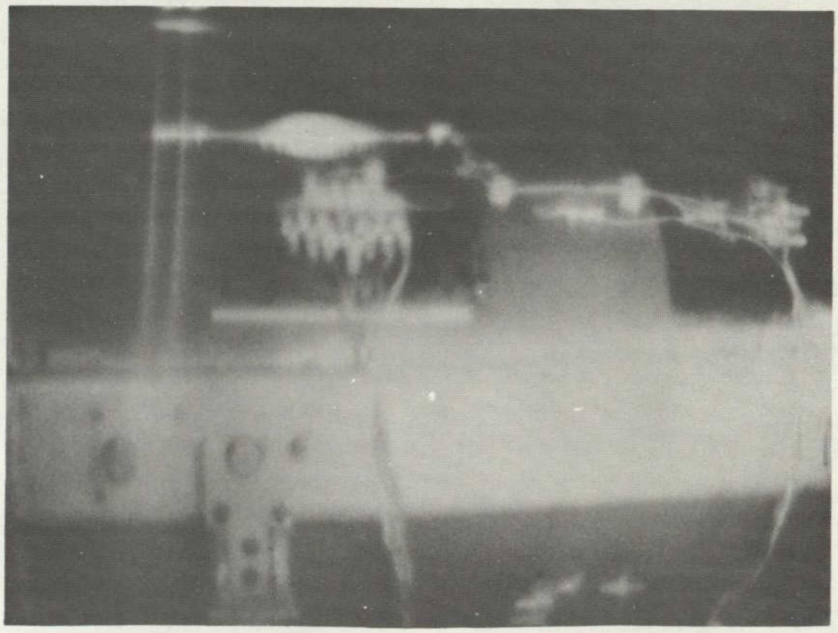

B

G-2522

Figure 76. X259 Hydrotest Failure

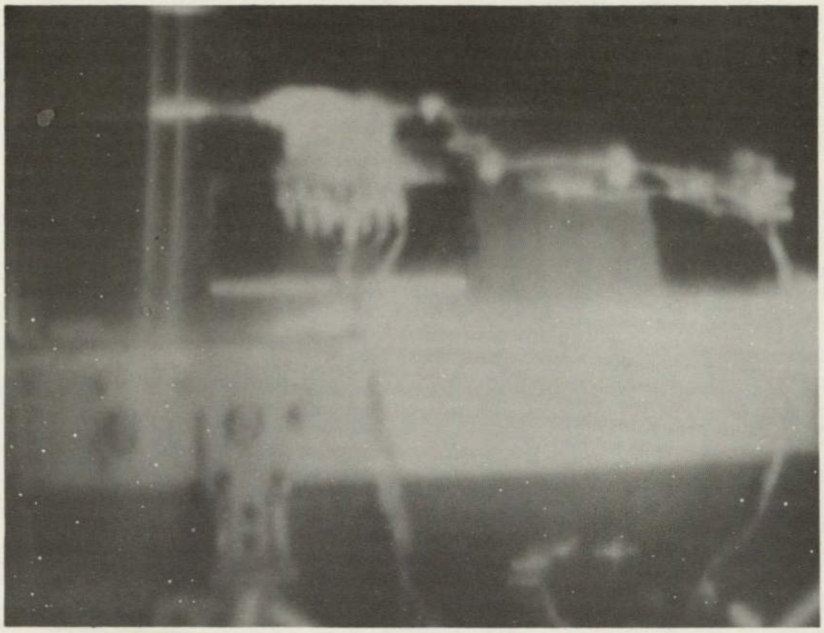

C

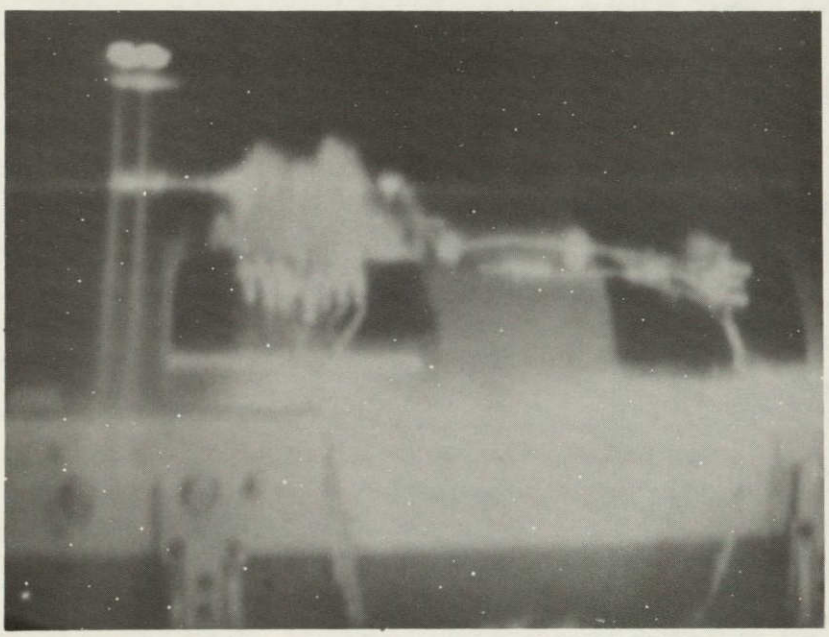

D

G-2523

Figure 76. (Continued)

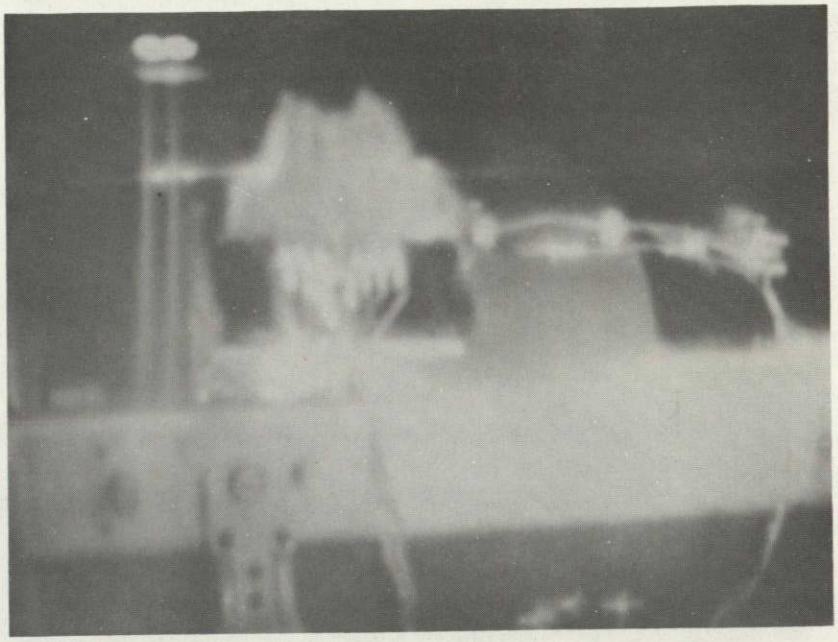

E

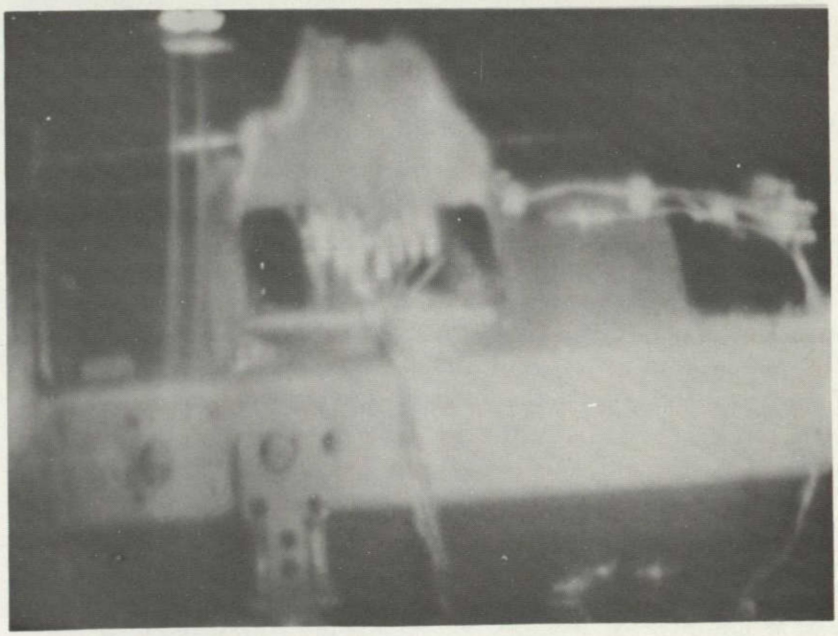

F

G-2524

Figure 76. (Continued)

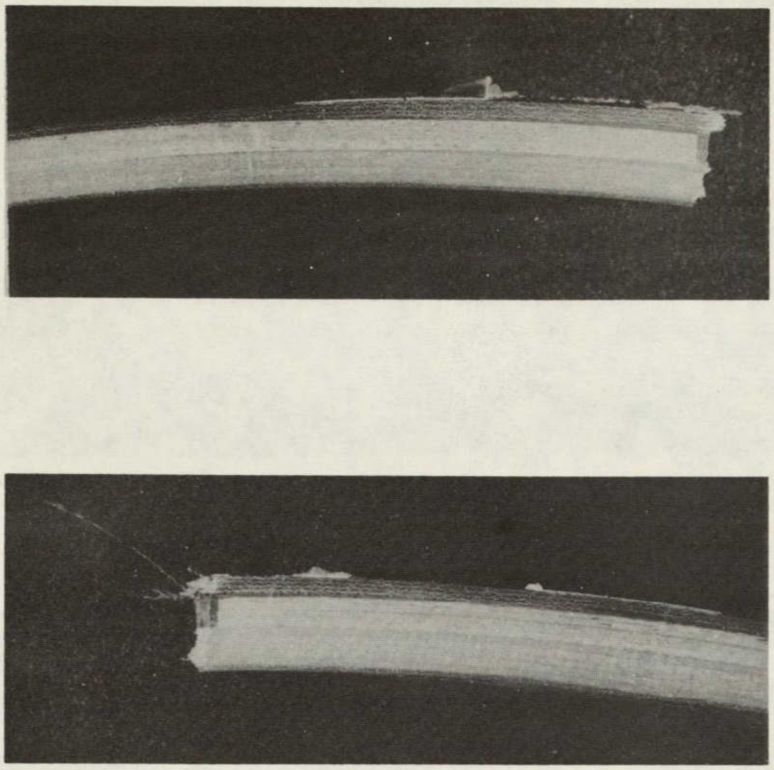

Figure 77. Center Section of Failed Defect (X 1) G-2527

NOTE: Lower Part of Section is the Insulator

3

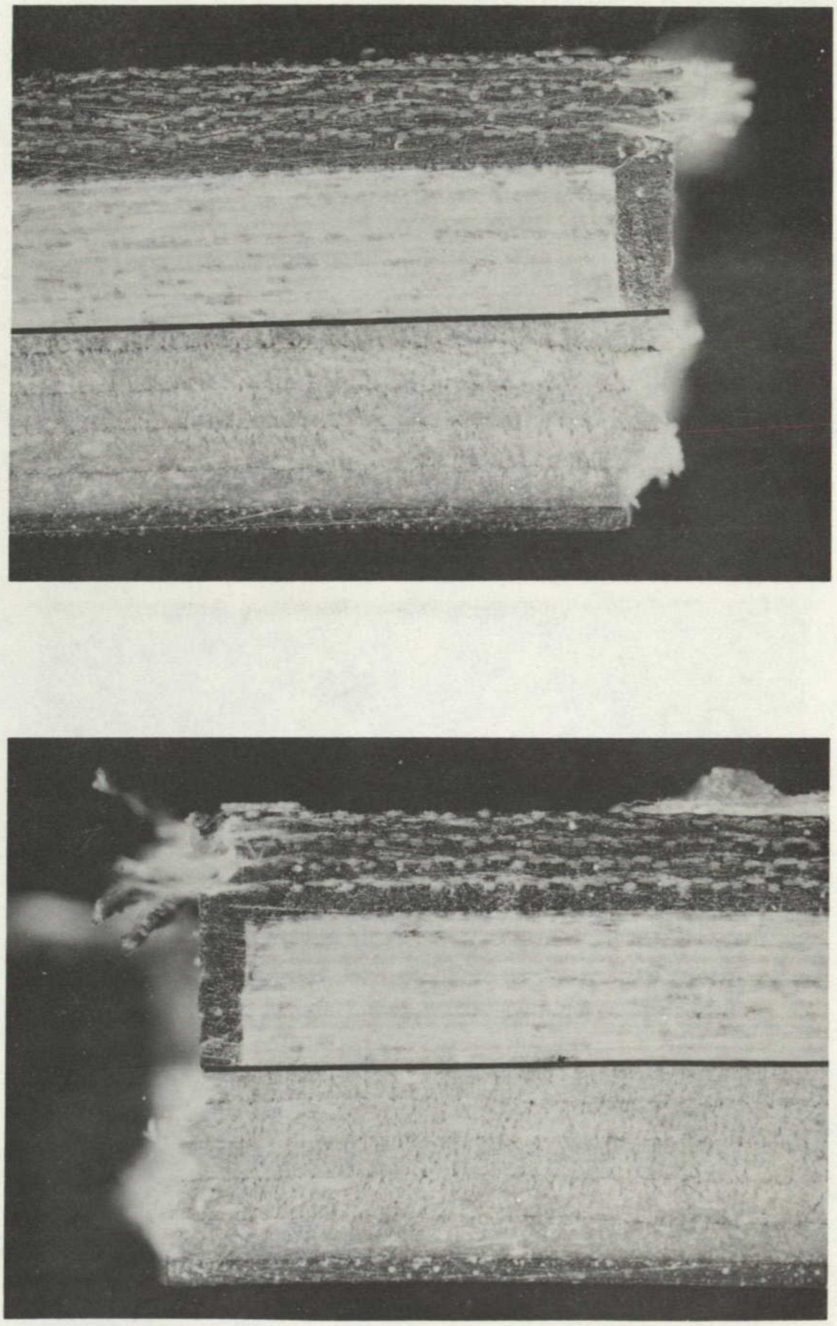

Figure 78. Center Section of Failed Defect (X 5)

G-2528

NOTE: Lower part of section is the insulator and a hand drawn line has been added to show the material boundaries.

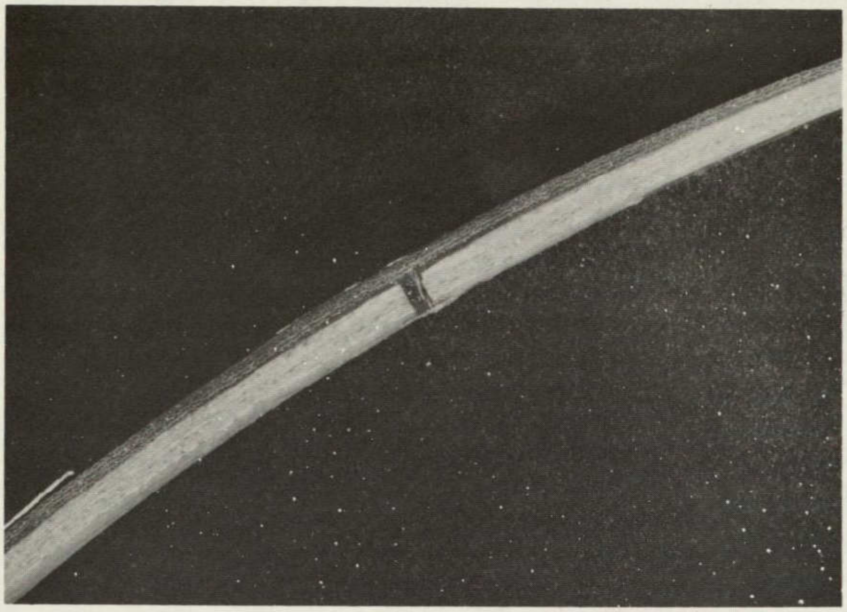

(X 1)

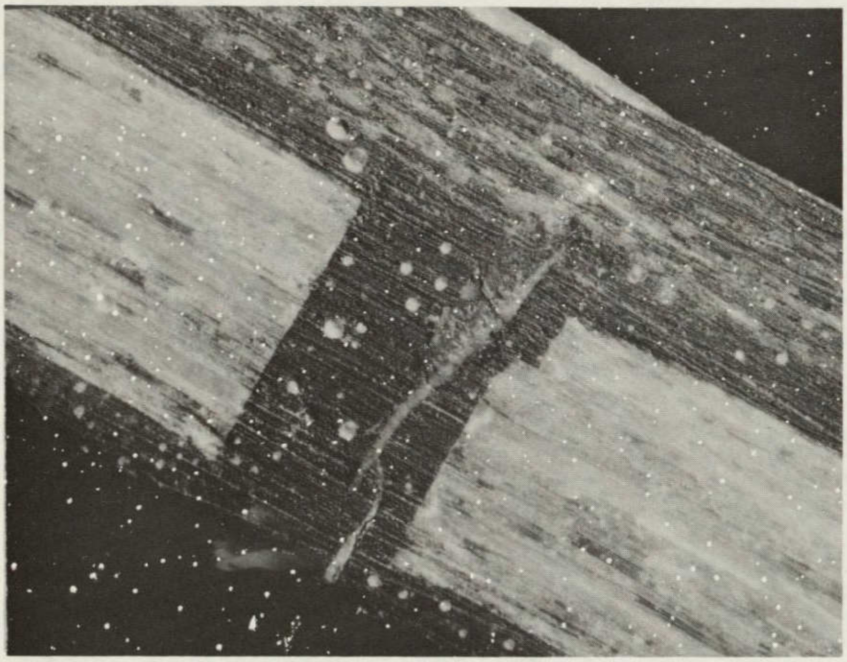

(X 10)

G-2529

Figure 79. Center Section of Nonfailure Defect (Side A)

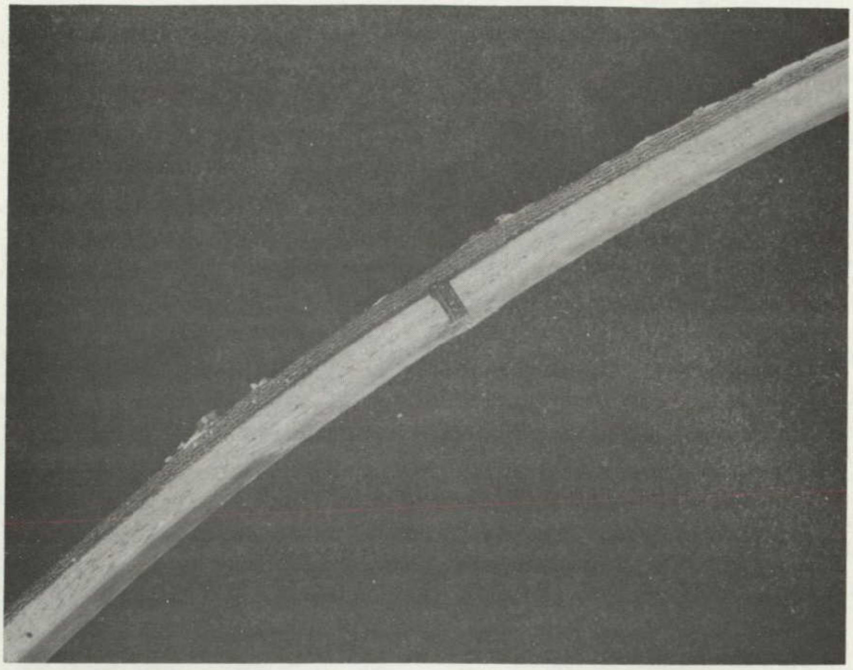

(X 1)

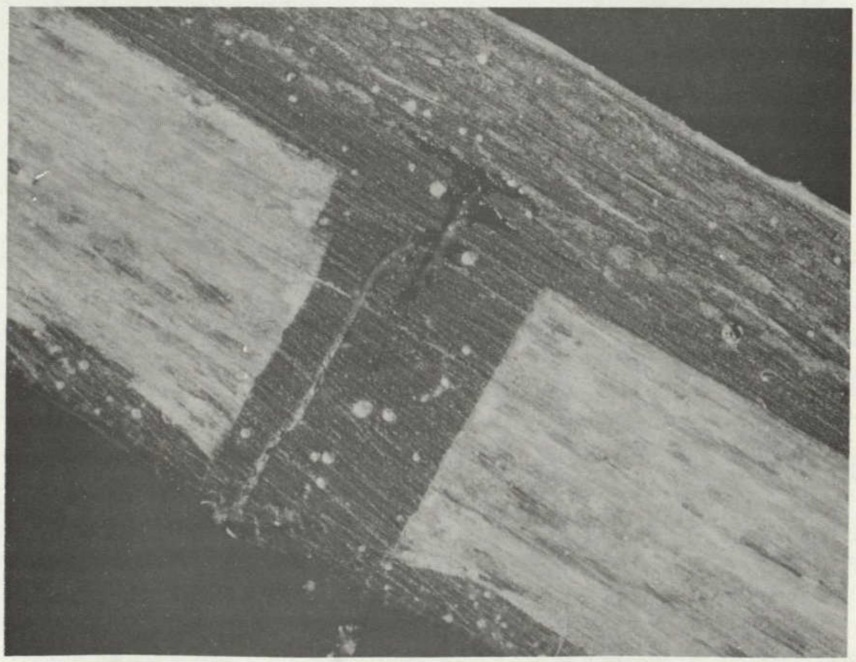

(X 10)

G-2530

Figure 80. Center Section of Nonfailure Defect (Side B)

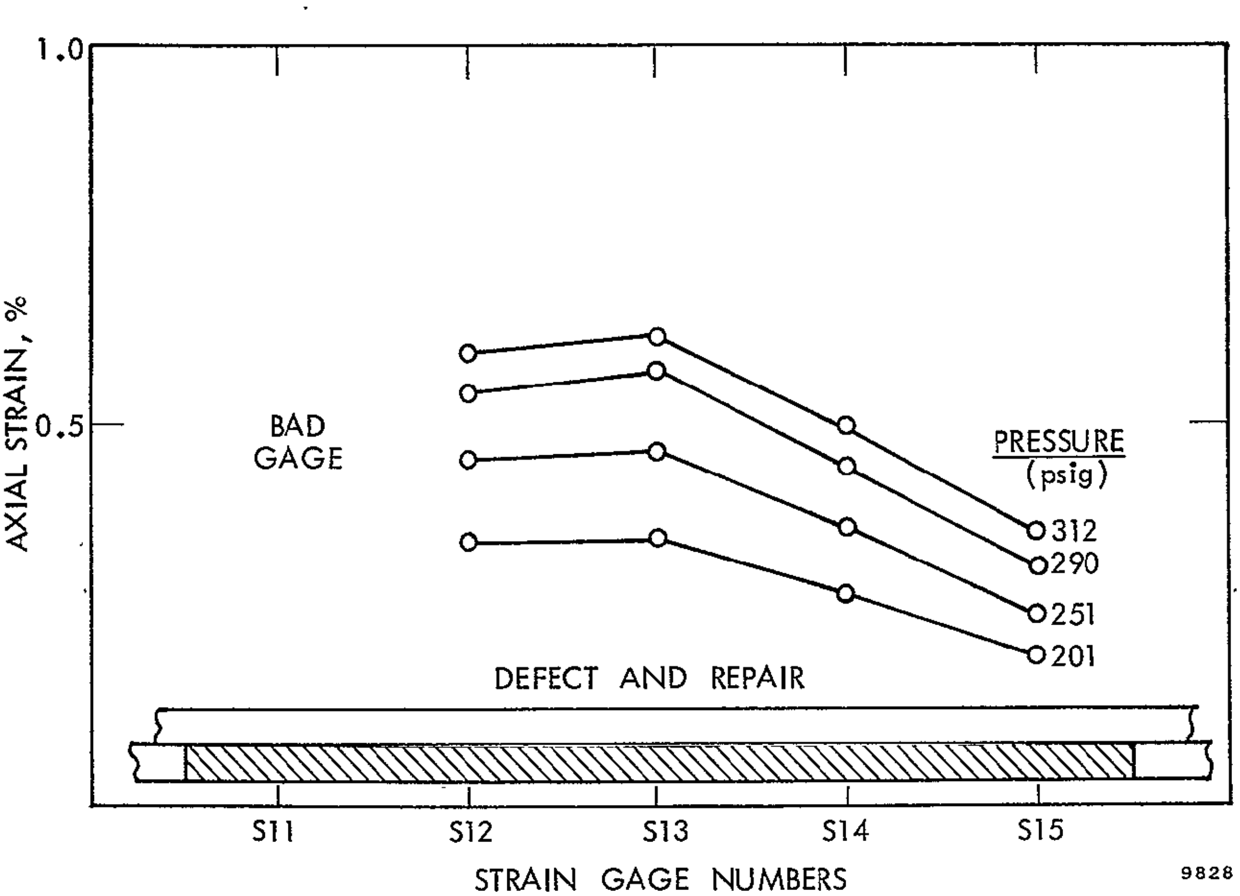

Figure 81. Axial Strain vs Pressure for Defect No. 1

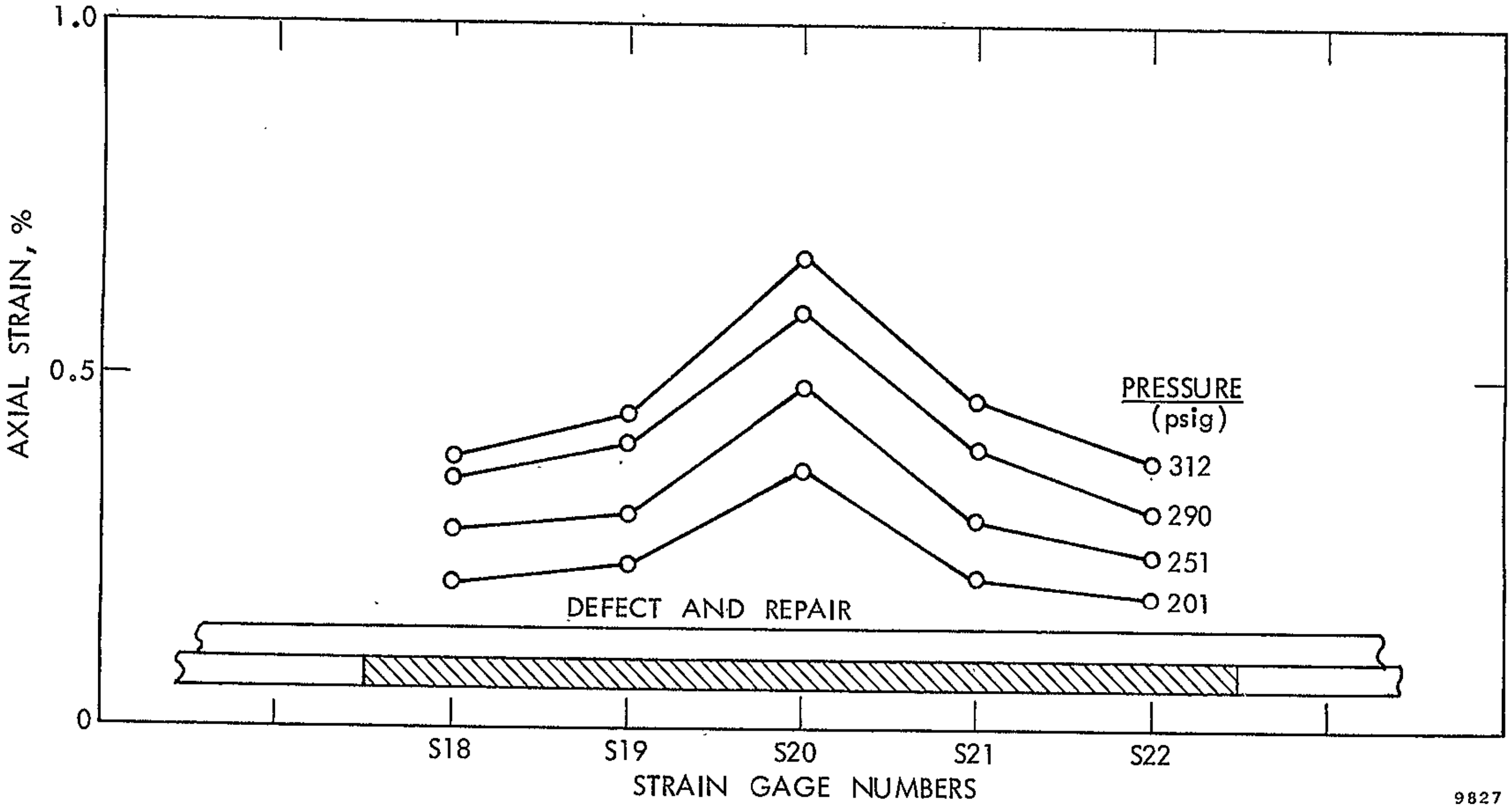

Figure 82. Axial Strain vs Pressure for Defect No. 2

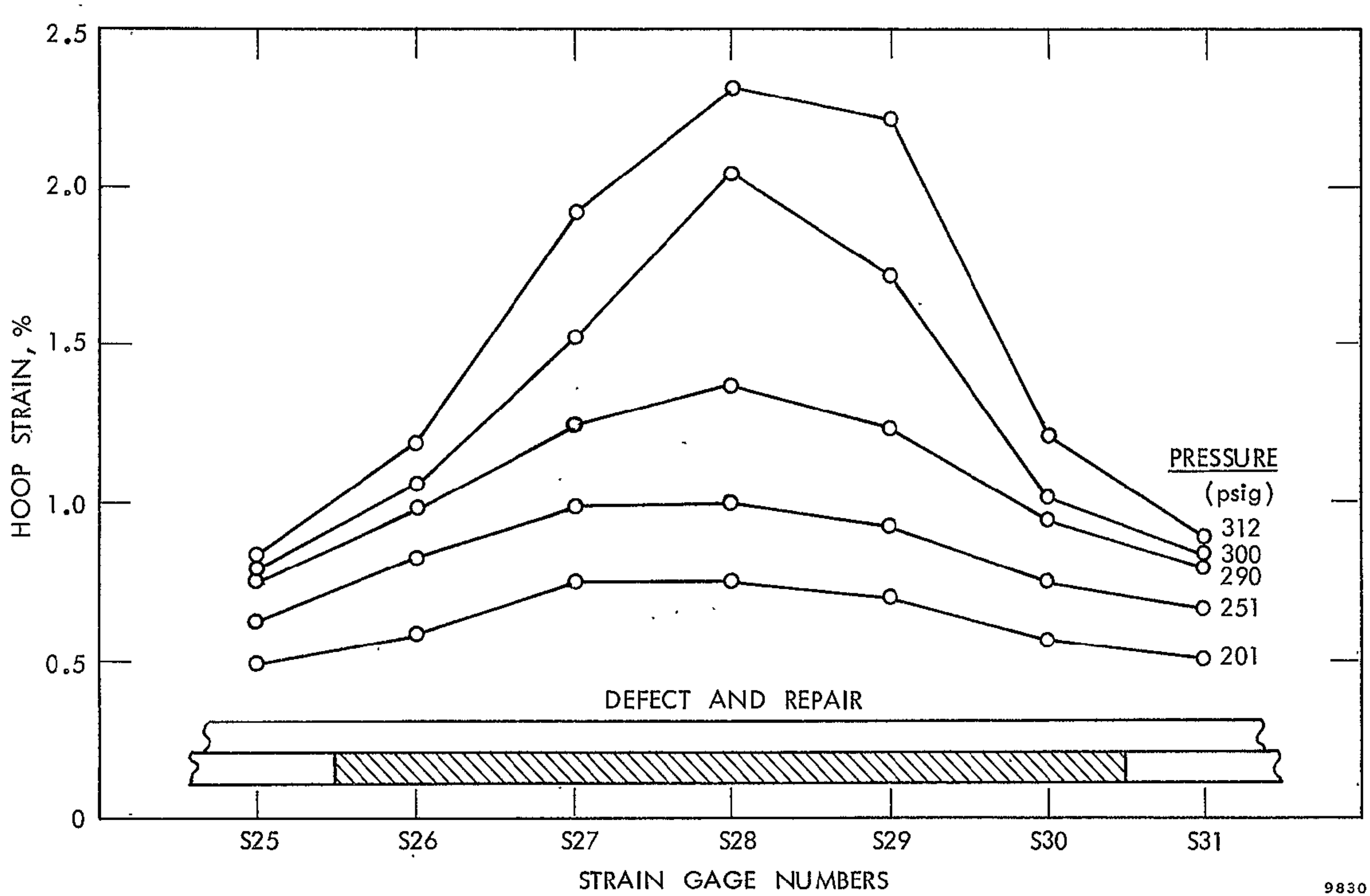

Figure 83. Hoop Strain vs Pressure for Defect No. 3

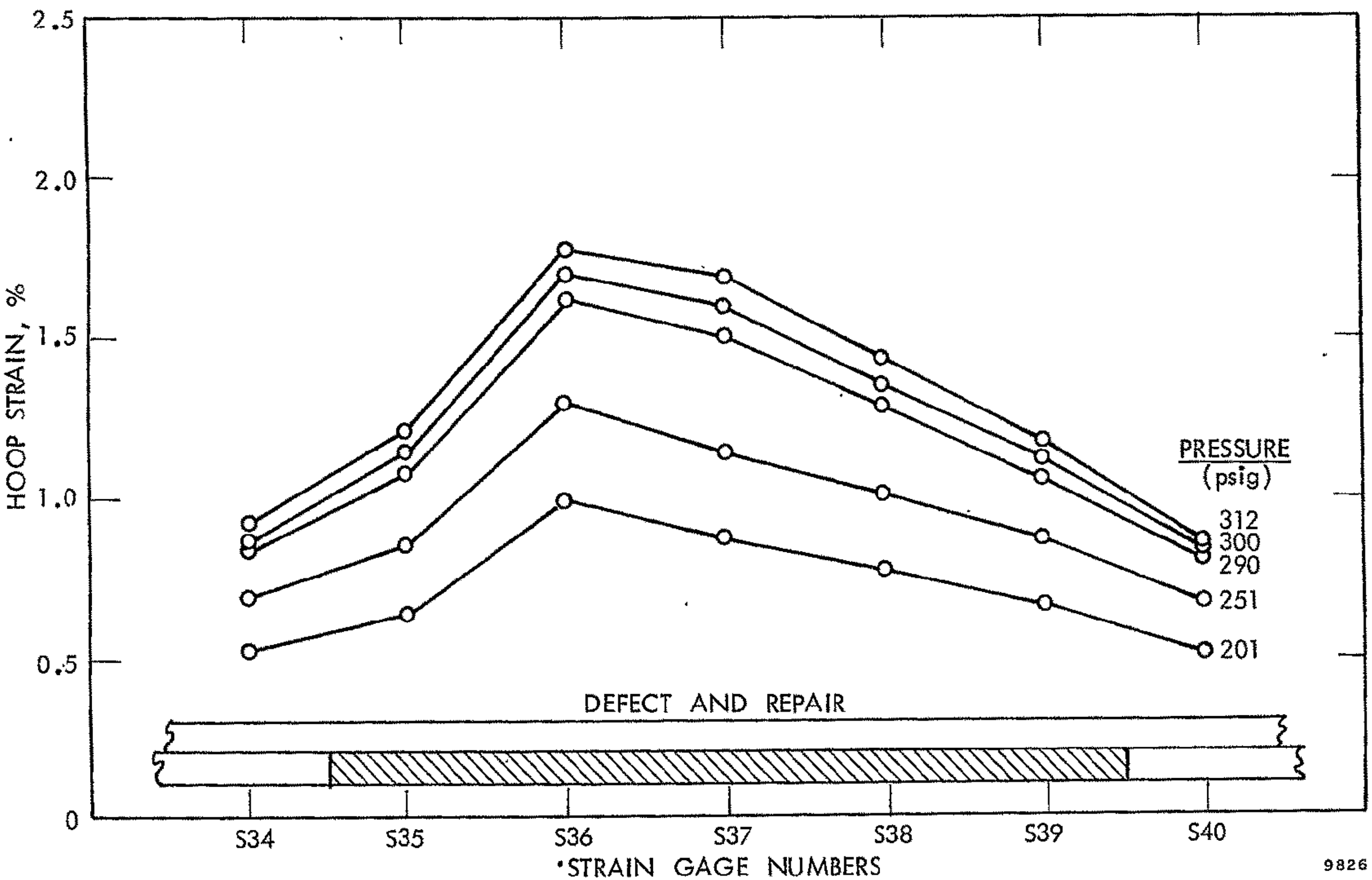

Figure 84, Hoop Strain vs Pressure for Defect No. 4

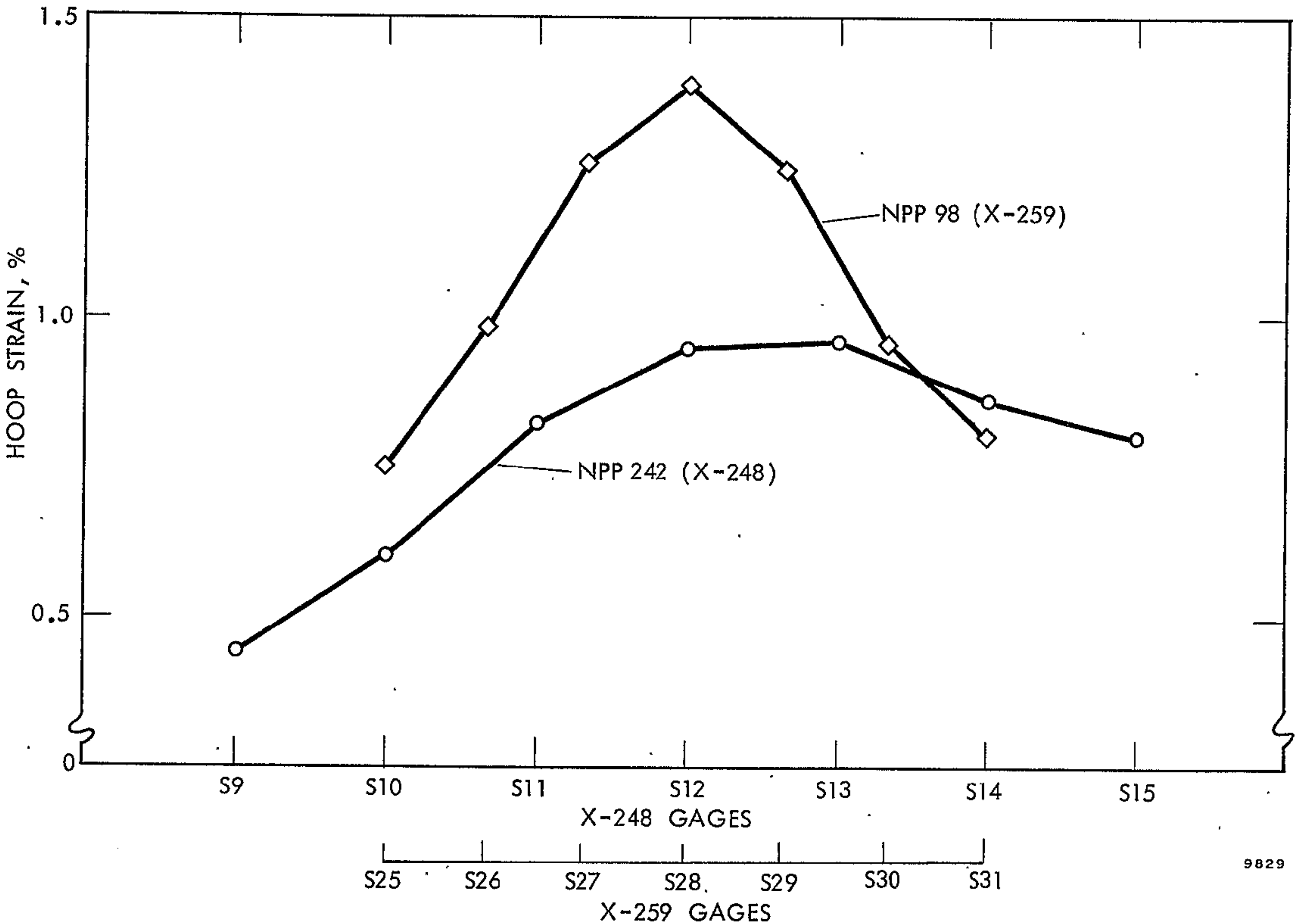

Figure 85. Comparison of Hoop Strain at Equal Pressures (290 Psig) for X248 and X259 Repairs

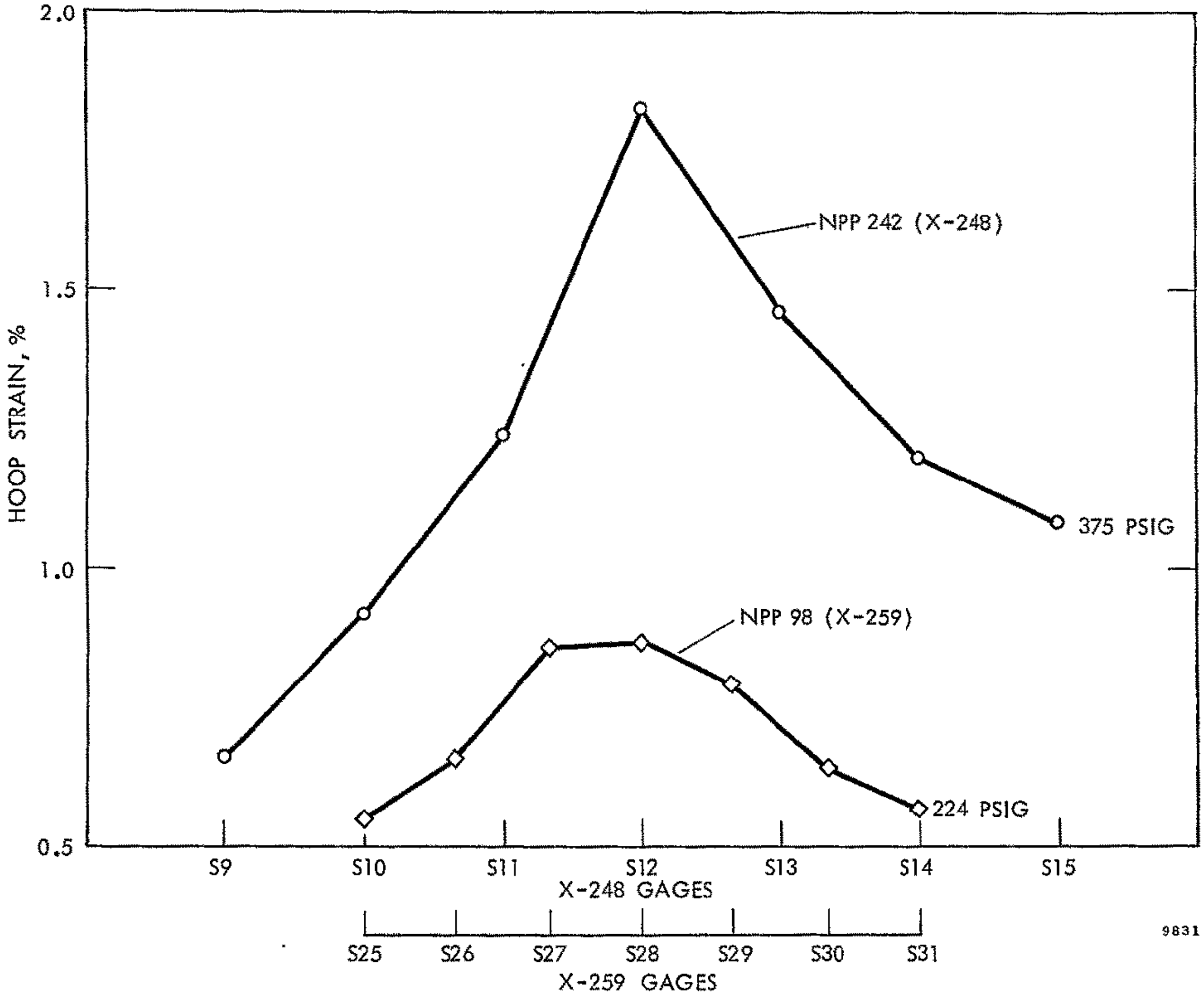

Figure 86. Comparison of Hoop Strain at Equivalent Load Levels for X248 and X259 Repairs

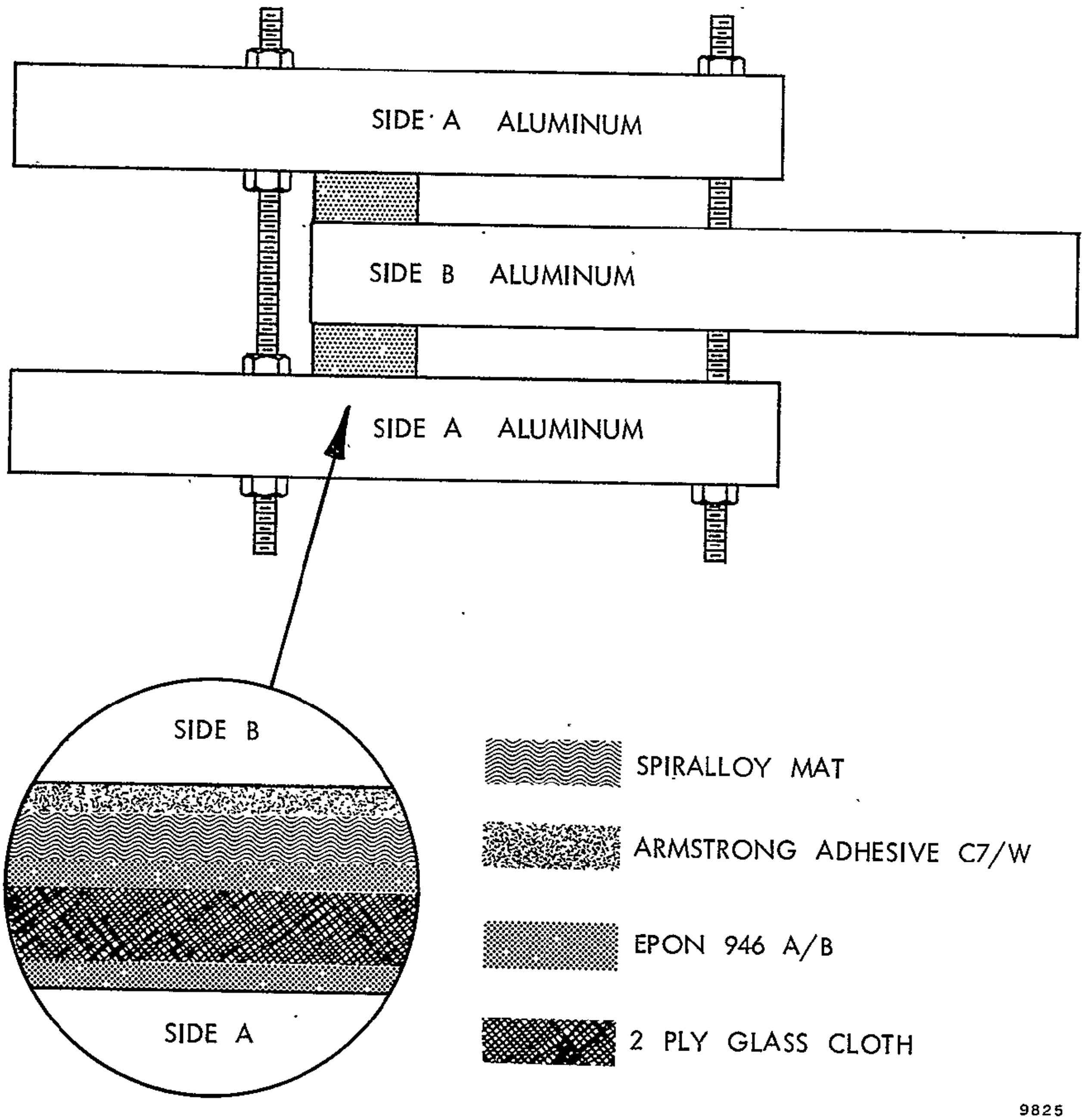

Figure 87. Three-Plate Shear Specimens

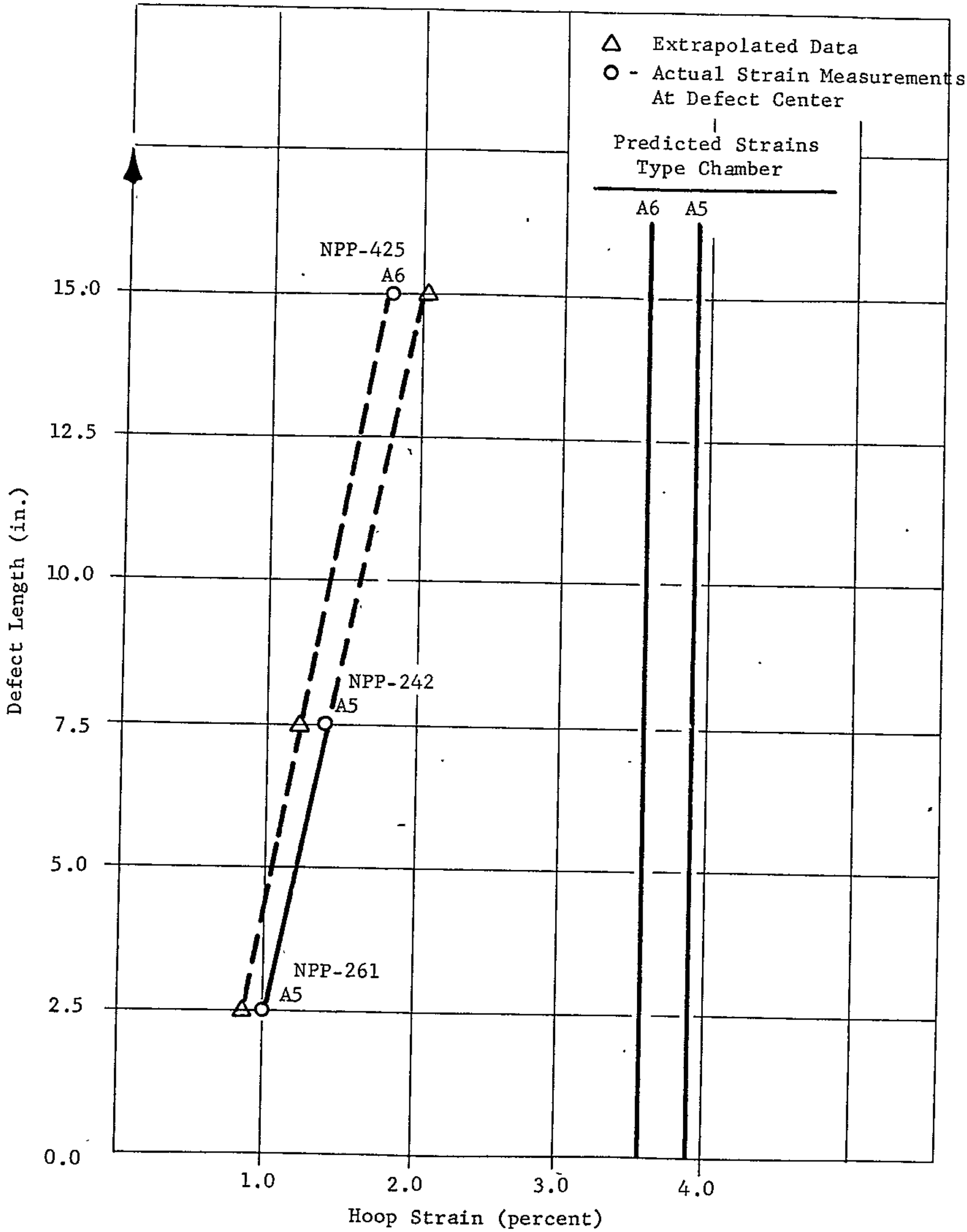

Figure 88. Comparison of Predicted and Actual Strains for a Four Ply Repair of a 0.1-In.-Wide Defect at 350 psia

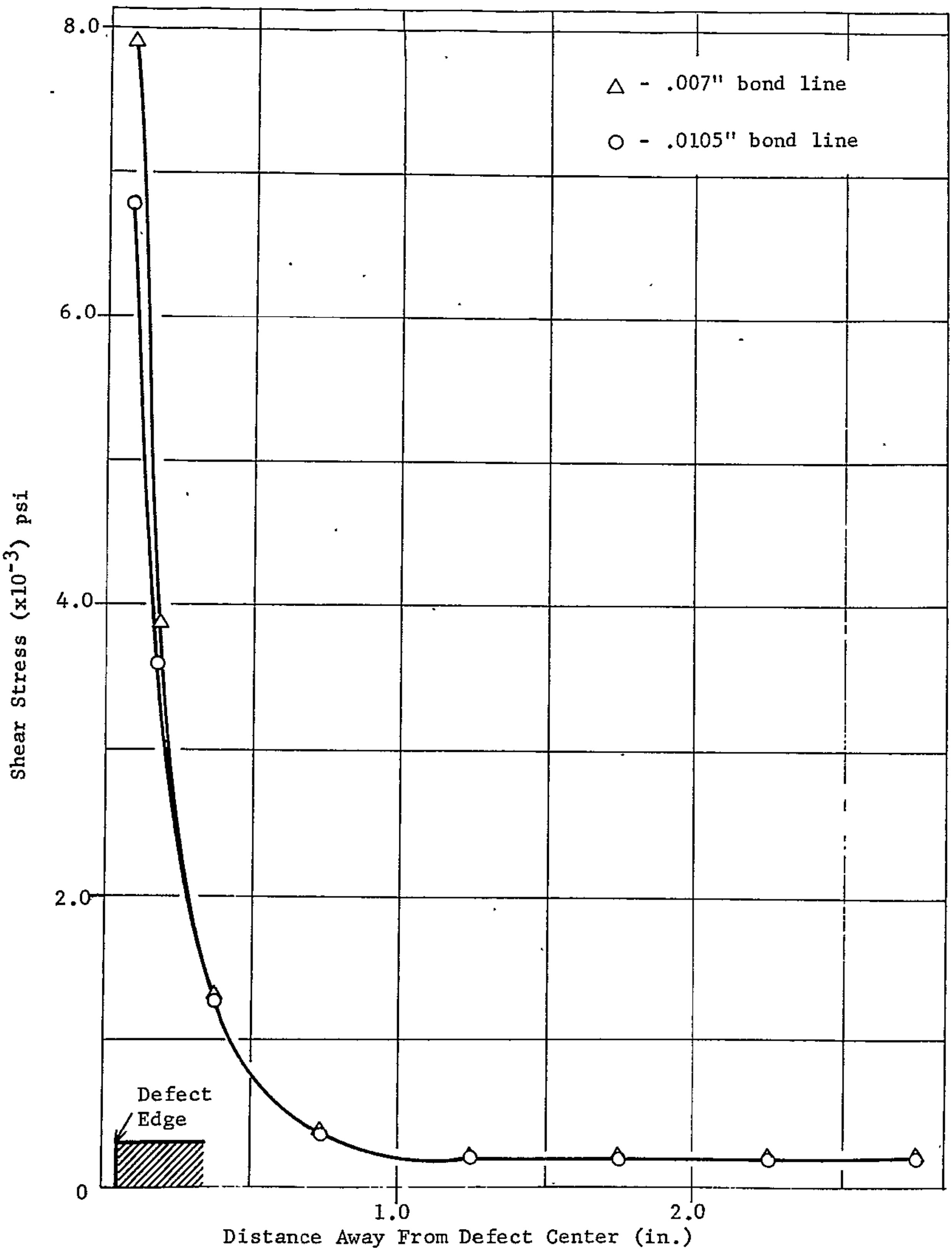

Figure 89. Comparison of Shear Stresses for Two Bond Line Thicknesses

APPENDIX A

X259 HYDROBURST TEST PLAN

HERCULES INCORPORATED
ALLEGANY BALLISTICS LABORATORY
CUMBERLAND, MARYLAND

December 16, 1969

NASA Defects Test Program

X259 Hydroburst
Test Plan

TP-NASAD-1003
Contract: NAS1-9293

X259-NPP-98

CDRC

FOR INFORMATION ONLY
NOT FOR MANUFACTURING USE

Edward S. Kyle 12-18-69
Test Director

Ronald B. Eme 12/19/69
Product Engineering

12/18/69
Testing

12/19/69
Navy/Space Motors Program Office

National Aeronautics and
Space Administration

4. Test Description

4.1 General

The subject chamber will have four 5.0 inch long x 0.1 inch wide (through fiberglass) defects inflicted in the cylindrical section. The defects will then be repaired using present patching technique. Following the repair, the chamber will be subjected to a hydroburst test to determine the failure pressure of the repaired case.

4.2 Repair Procedure

4.2.1 Repair Materials

The materials used for the repair patch will be Owens-Corning S/81-904 finish fiberglass cloth and an Epon 946 resin system.

4.2.2 Repair Configuration

4.2.2.1 Circumferential Defects

The repair patch for the two 5.0 in. circumferential defects will consist of four plies of overlapping cloth. The circumferential and axial dimensions of the four plies, not including a 0.5 in. fringe, will be as follows:

Ply 1 - 7.0 in. cir. x 4.0 in. axial

Ply 2 - 9.0 in. cir. x 6.0 in. axial

Ply 3 - 11.0 in. cir. x 8.0 in. axial

Ply 4 - 13.0 in. cir. x 10.0 in. axial

4.2.2.2 Axial Defects

The repair patch for the two 5.0 in. long axial defects will consist of four plies of overlapping cloth. The

1. Introduction

This document governs the hydroburst test to be conducted on X259 NPP-98 under the NASA Defects Test Program. The test consists of inflicting four cylindrical section defects repairing them with fiberglass cloth patches and then subjecting the case to a hydroburst test to evaluate the repair technique.

2. Test Control

2.1 This test plan defines the specifications, objectives, test arrangement, instrumentation requirements, data recording and reduction requiremenets and photographic coverage for the subject test program.

2.2 Any changes to this test plan which affect the objectives of the test shall be made by a controlled document, "Testing Change Order" (TCO).

2.3 Minor changes affecting instrumentation locations and mode of recording shall require only the written approval of the Test Director. These changes shall be entered on the Operating Area Test Plan, Data Acquisition Sheets, and all necessary work orders. Each change shall be dated and initialed by the Test Director. All changes will be approved by the Product Engineering Test Representative in writing in the Test Director's log prior to initiating the test sequence. These changes shall be documented on a Deviation Sheet which shall form a part of the data package.

3. Test Objectives

3.1 To demonstrate that the present patching technique can be successfully applied to a modern design rocket motor case.

circumferential and axial dimensions of the four plies, not including a 0.5 in. fringe, will be as follows:

Ply 1 - 4.0 in. cir. x 7.0 in. axial
Ply 2 - 6.0 in. cir. x 9.0 in. axial
Ply 3 - 8.0 in. cir. x 11.0 in. axial
Ply 4 - 10.0 in. cir. x 13.0 in. axial

4.2.3 Repair Technique

4.2.3.1 The repair area will be marked off and then sanded until the chamber's gloss has been removed.

4.2.3.2 The sanded area will then be cleaned with Methylene Chloride.

4.2.3.3 A thick layer (minimum of 0.020 in.) of one half hour B-staged Epon 946 resin will be applied to the area within one-inch of the defect.

4.2.3.4 After B-staging for a minimum of 4 hours, the edges of the resin will be tapered to avoid air pockets.

4.2.3.5 A thick layer of one half hour B-staged Epon 946 resin will then be applied to the chamber.

4.2.3.6 The first ply of fiber glass cloth is placed over the defect and the resin is worked up through the ply.

4.2.3.7 Another layer of resin is then added. The next ply is placed over the first ply and the resin is again worked up through the ply. This step is repeated for all the subsequent plies.

4.2.3.8 Upon the completion of patching, the repaired chamber is allowed to cure for a minimum of seven days at room temperature.

4.2.3.9 The two defects at the 50° location will be repaired first. A minimum of 36 hours will elapse before the unit is rotated so that the two defects at 310° can be repaired.

4.2.3.10 Still photographs depicting the defected chamber and each step of the repair procedure will be obtained.

4.3 Preliminary Test Operations

4.3.1 The chamber is to be delivered to the Instrument Shop and instrumented in accordance with Figure 1.

4.3.2 Prepare a pressure versus time data trak program as shown in Figure 2.

4.3.3 The servo control system and Miller Ram Pressurization System will then be set up in accordance with GOP 1-74-04 and GOP 1-74-05, respectively.

4.3.4 Conduct a dry run with the pressurization system "dead headed" to verify the pressure profile program.

4.3.5 Set up the motion picture coverage as shown in Figure 3.

4.3.6 The data system will be programmed as shown in Table 1 - "Instrumentation Requirements"

4.4 Test Operation

4.4.1 The hydrotest closures will be installed as defined in HXD 1-1111.

4.4.2 The instrumented case will then be set up in the test stand in accordance with HXD 1-1112 Revision 3 and Drawing 259-1502.

4.4.3 Fill the chamber with water using the fill pipe procedure in accordance with HXD 1-1112 Revision 3.

4.4.4 All instrumentation is to be connected to bay lines and the data recording system set as defined in HXD 1-441.

4.4.5 Color still photographs are to be taken of the test setup and detailed coverage of both defected-repaired areas are also required.

4.4.6 The chamber will then be pressurized to failure using the Data Trak programmed closed loop servo system controlling the Miller Ram Pressurization System to provide a pressure profile as shown in Figure 2.

4.4.7 Color still photographs will then be taken of the post-test setup with emphasis on detailing the failure area.

5. Data Processing

5.1 Structures Laboratory

5.1.1 All processed oscillograph records and the original copy of the Test Data Acquisition Sheet shall be delivered to the Test Director immediately after the test. The oscillograph shall contain the following additional information.

1. Structures Laboratory Test Number
2. Start of each test (date and time)
3. Visicorder channel identification

5.1.2 All oscillograph records shall show T-0.

5.1.3 The digital tape, along with a copy of the Data Acquisition Sheet shall be delivered to the Computations Department as soon as possible after completion of the test.

5.1.4 The motion picture film will be sent to Washington, D. C., for normal processing unless otherwise specified.

5.2 Computations

5.2.1 The digital tape shall be processed and the data ready for review within five (5) working days after the test. The digital data shall be reviewed by the Test Director prior to plotting the data.

5.2.2 Process the data as follows:

1. Data printouts shall begin at T-1 second and continue for 1 second past failure.

NOTE: Test duration will be specified by the Test Director.

2. Digital printouts of all data shall be as follows:
   0 to 2 seconds prior to failure = 5 samples/second
   2 seconds prior to failure, through 2 seconds after failure = 30 samples/second.

3. Three copies of the data printouts shall be required.

4. A plot of all data versus time shall be required.

5. All graphs shall be plotted beginning at T-1 seconds.

6. The graphs shall be reviewed by Computations and the Test Director prior to release for distribution.

INSTRUMENTATION REQUIREMENTS

NOTE: 1. CW Denotes Clockwise Location
CCW Denotes Counter Clockwise Location

2. Visicorder Speeds:

1 inch per second T-0 to T+50 Seconds

4 inch per second T+50 to failure

INSTRUMENTATION REQUIREMENTS

Table I

Gage Location No.	Location	Max. Expected Value	Calib-ration	Type of Gage	Recording	Figure
P1	Chamber Pressure	660 psig	+4	N/A	D30 Visicorder	N/A
P2	Chamber Pressure	660 psig	+4	N/A	D30 Visicorder	N/A
	Case Cylindrical Section					
S1	30.0" Aft @ 225° - Axial	2%	+1	PA3	D30 Visicorder	1
S2	30.0" Aft @ 225° - Hoop	4%	+1	PA3	D30 Visicorder	1
S3	30.0" Aft @ 310° - Axial	2%	+1	PA3	D30 Visicorder	1
S4	30.0 Aft @ 0° - Axial	2%	+1	PA3	D30 Visicorder	1
S5	30.0" Aft @ 0° - Hoop	4%	+1	PA3	D30 Visicorder	1
S6	30.0" Aft @ 50° - Axial	2%	+1	PA3	D30 Visicorder	1
S7	30.0" Aft @ 135° - Axial	2%	+1	PA3	D30 Visicorder	1
S8	30.0" Aft @ 135° - Hoop	4%	+1	PA3	D30 Visicorder	1
S9	41.5" Aft @ 0° - Hoop	4%	+1	PA3	D30 Visicorder	1
S10	17.5" Aft @ 310° - Axial	5%	+1	PA7	D30 Visicorder	1
S11	18.5" Aft 2" CCW from 310° Axial	5%	+1	PA7	D30 Visicorder	1
S12	18.5" Aft 1.0" CCW from 310° Axial	5%	+1	PA7	D30 Visicorder	1
S13	18.5" Aft @ 310° - Axial	5%	+1	PA7	D30 Visicorder	1
S14	18.5" Aft 1.0" CW from 310° Axial	5%	+1	PA7	D30 Visicorder	1
S15	18.5" Aft 2" CW from 310° Axial	5%	+1	PA7	D30 Visicorder	1
S16	19.5" Aft @ 310° - Axial	5%	+1	RA7	D30 Visicorder	1
S17	40.5" Aft @ 50° - Axial	5%	+1	PA7	D30 Visicorder	1
S18	41.5" Aft 2" CCW from 50° Axial	5%	+1	PA7	D30 Visicorder	1
S19	41.5" Aft 1.0" CCW from 50° Axial	5%	+1	PA7	D30 Visicorder	1

INSTRUMENTATION REQUIREMENTS

Gage Location No.	Location	Max. Expected Value	Calibration	Type of Gage	Recording	Figure
S20	41.5" Aft @ 50° - Axial	5%	+1	PA7	D30 Visicorder	1
S21	41.5" Aft 1.0" CW from 50° Axial	5%	+1	PA7	D30 Visicorder	1
S22	41.5" Aft 2" CW from 50° Axial	5%	+1	PA7	D30 Visicorder	1
S23	42.5" Aft @ 50° - Axial	5%	+1	PA7	D30 Visicorder	1
S24	41.5" Aft 1" CCW from 310° Hoop	5%	+1	PA7	D30 Visicorder	1
S25	38.5" Aft @ 310° - Hoop	5%	+1	PA7	D30 Visicorder	1
S26	39.5" Aft @ 310° - Hoop	5%	+1	PA7	D30 Visicorder	1
S27	40.5" Aft @ 310° - Hoop	5%	+1	PA7	D30 Visicorder	1
S28	41.5" Aft @ 310° - Hoop	5%	+1	PA7	D30 Visicorder	1
S29	42.5" Aft @ 310° - Hoop	5%	+1	PA7	D30 Visicorder	1
S30	43.5" Aft @ 310° - Hoop	5%	+1	PA7	D30 Visicorder	1
S31	44.5" Aft @ 310° - Hoop	5%	+1	PA7	D30 Visicorder	1
S32	41.5" Aft 1" CW from 310° Hoop	5%	+1	PA7	D30 Visicorder	1
S33	18.5" Aft 1" CCW from 50° Hoop	5%	+1	PA7	D30 Visicorder	1
S34	15.5" Aft @ 50° - Hoop	5%	+1	PA7	D30 Visicorder	1
S35	16.5" Aft @ 50° - Hoop	5%	+1	PA7	D30 Visicorder	1
S36	17.5" Aft @ 50° - Hoop	5%	+1	PA7	D30 Visicorder	1
S37	18.5" Aft @ 50° - Hoop	5%	+1	PA7	D30 Visicorder	1
S38	19.5" Aft @ 50° - Hoop	5%	+1	PA7	D30 Visicorder	1
S39	20.5" Aft @ 50° - Hoop	5%	+1	PA7	D30 Visicorder	1
S40	21.5" Aft @ 50° - Hoop	5%	+1	PA7	D30 Visicorder	1
S41	18.5" Aft 1" CW from 50° Hoop	5%	+1	PA7	D30 Visicorder	1

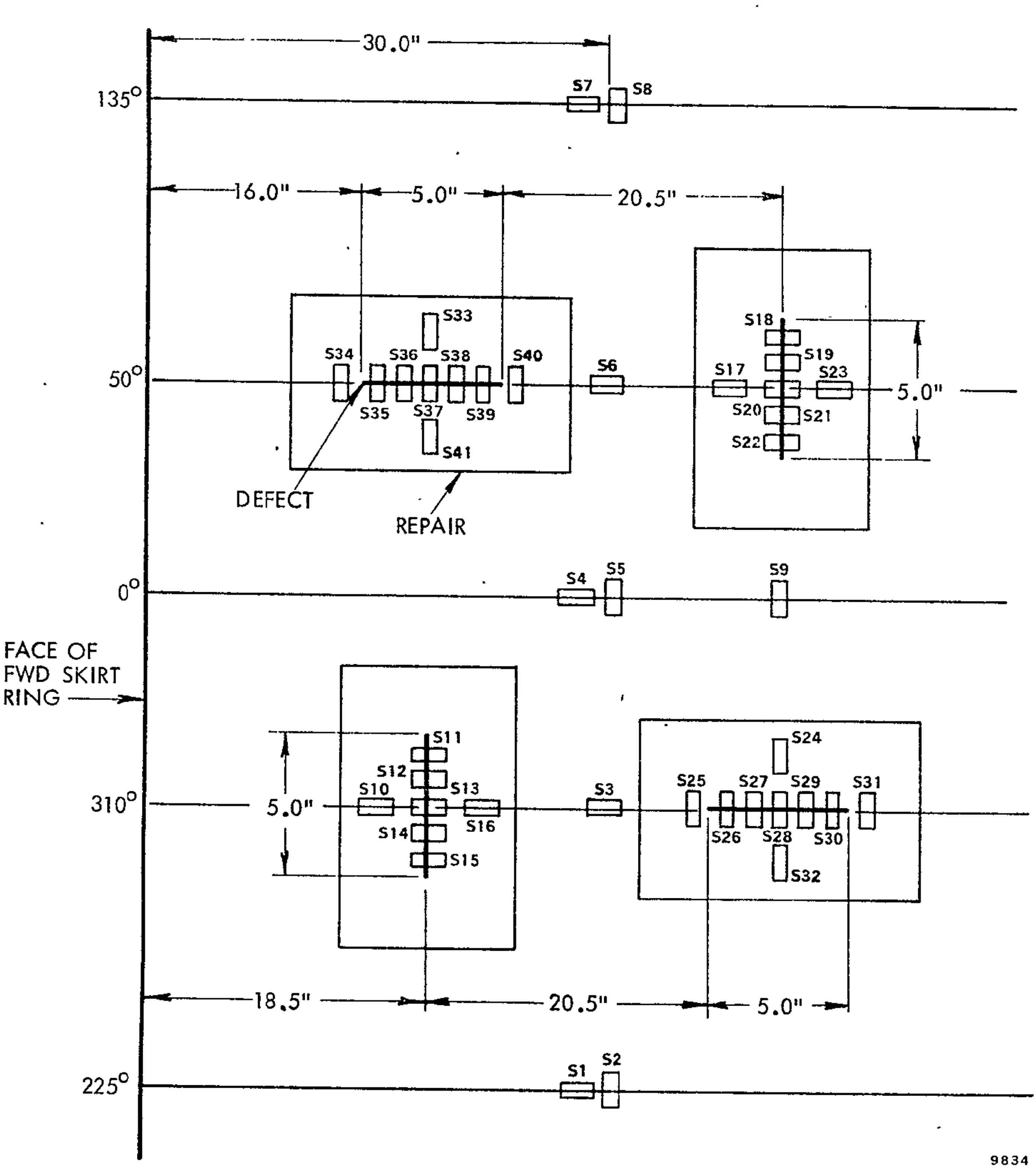

NOTE: Angular Orientation - Forward Looking Aft - Counterclockwise

Figure 1. Case Instrumentation

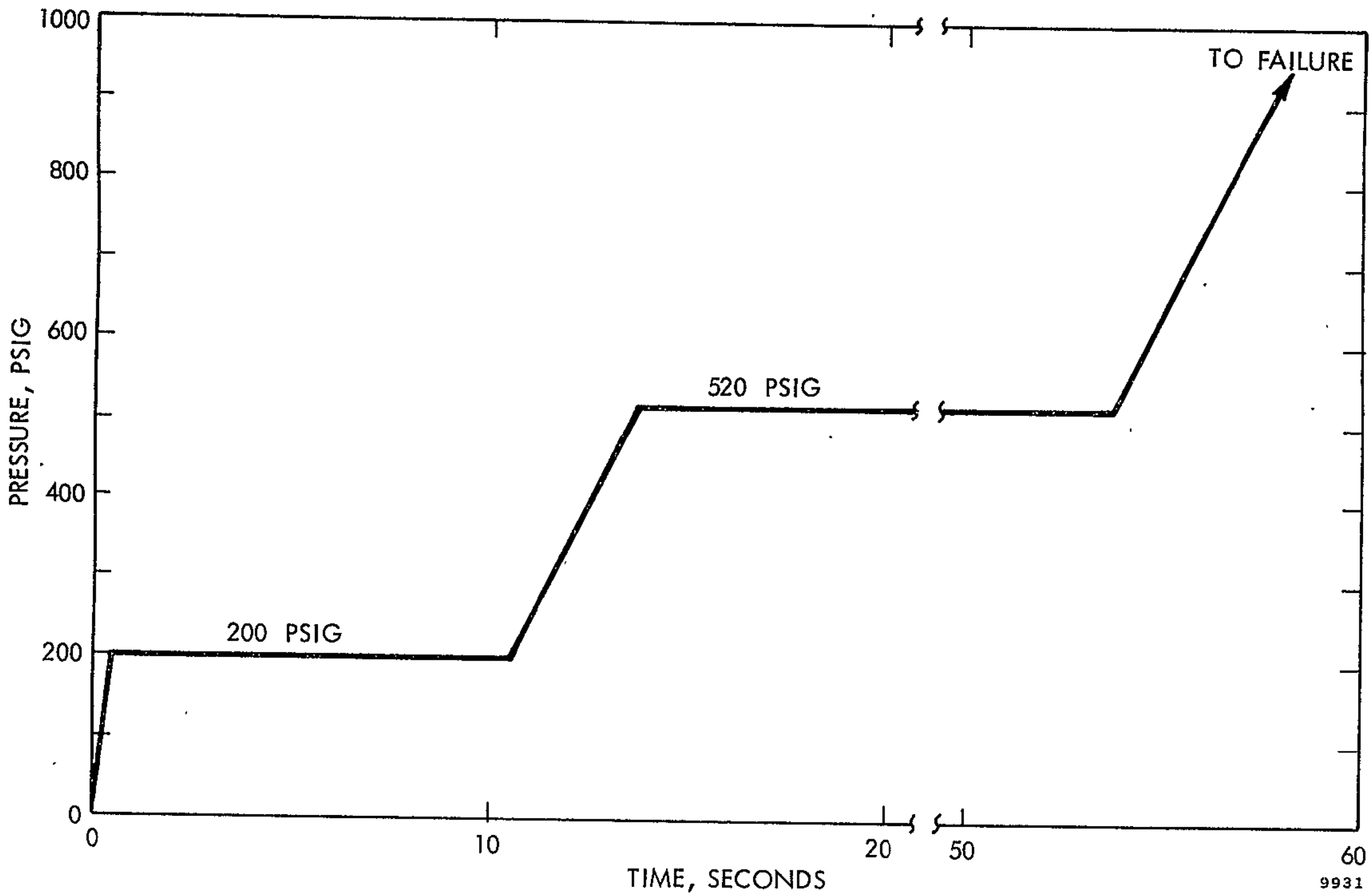

FIGURE 2
Pressure vs Time Program

X259 Hydroburst Motion Picture Coverage

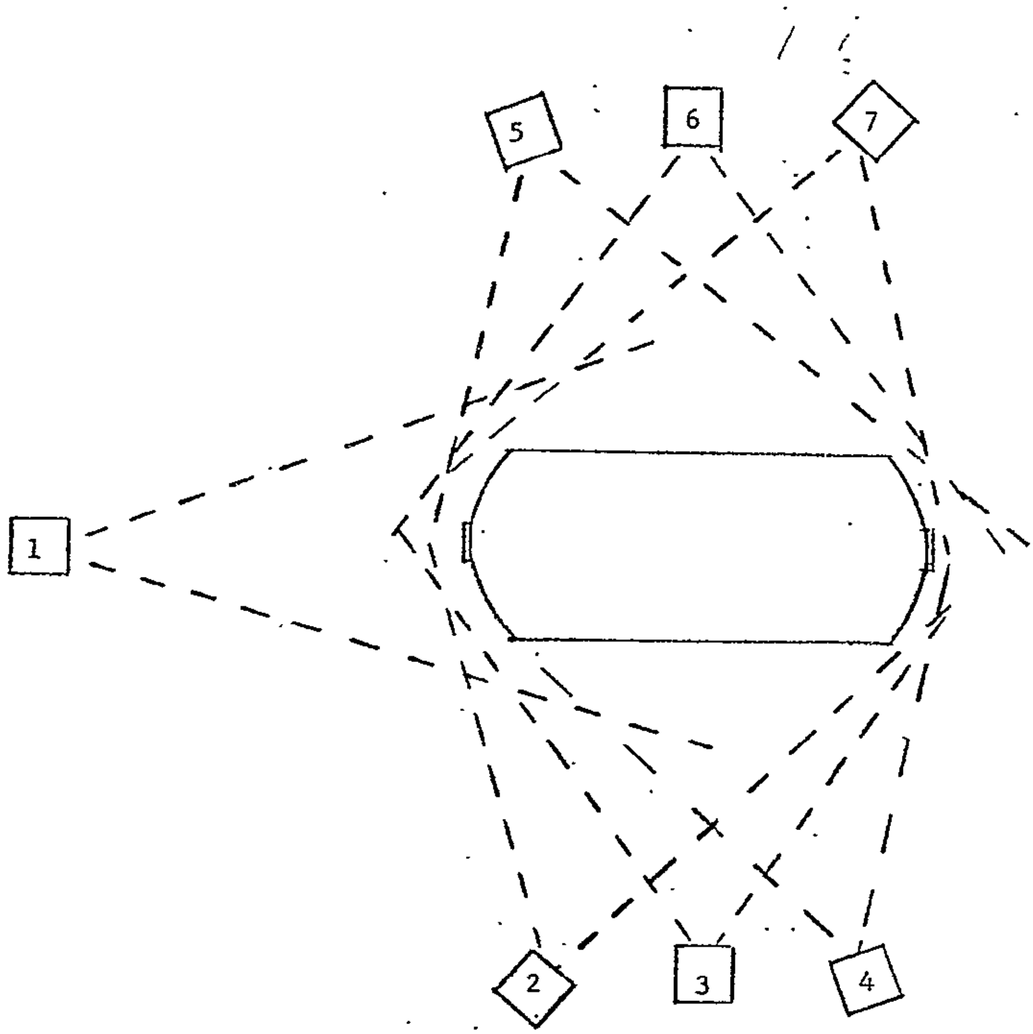

Position	Make	Speed	Film	Coverage
1	Fastax	250 fps	Color	T-2 to T+100
2	Fastax	1000 fps	Color	T+10 to T+25
3	Fastax	750 fps	Color	T+24.5 to T+44.5
4	Fastax	1000 fps	Color	T+44 to T+59
5	Fastax	1000 fps	Color	T+10 to T+25
6	Fastax	750 fps	Color	T+24.5 to T+44.5
7	Fastax	1000 fps	Color	T+44 to T+59

NOTE: 1. Cameras are to show defected-repair areas.

2. Use light bars if necessary.

Figure 3

APPENDIX B

REPAIR PROCEDURE FOR FIBERGLASS DEFECTS IN THE CYLINDRICAL SECTION OF ROCKET MOTORS

UOP 1-1738

REVISION 3

HERCULES INCORPORATED

ALLEGANY BALLISTICS LABORATORY
CUMBERLAND, MARYLAND

CONTROLLED

COPY NO. ___________

DIST. BY CDRC ______

UNIT OPERATING PROCEDURE

UNIT SPIRALLOY

OPERATION REPAIR OF SPIRALLOY MOTOR CASE GOUGES (CYLINDRICAL SECTION ONLY)

EFFECTIVE DATE 7-9-70

THIS DOCUMENT SUPERSEDES UOP 1-1738, Revision 2.

PREPARED BY Paul K. Amtower DATE 6-10-70

APPROVED FOR USE BY HERCULES INCORPORATED

R. J. Wilson	6/29/70	R. B. Ennis	7/6/70
[signature]	7/6/70	R. R. Hillen	7/7/70
W. B. Bauserman	7/6/70	[signature]	7/7/70

APPROVED FOR DISTRIBUTION

Paul K. Amtower 7-9-70

BY DIRECTION OF MANAGER OF OPERATIONS DIVISION DATE

This document consists of a cover page and pages 1 to 6 inclusive.

141-142

1. SCOPE

1.1 This document describes the materials, equipment, and procedure necessary to repair a Spiralloy Motor Case.

2. REQUIREMENTS

2.1 The procedures indicated herein are those used by Hercules Incorporated, Allegany Ballistics Laboratory. The use of equivalent procedures or equipment other than that indicated in this document shall have written approval from Allegany Ballistics Laboratory.

2.2 Operations shall be performed in the sequence listed unless otherwise specified in this document.

2.3 All items which form a part of the end product of these operations shall be Quality Control accepted.

2.4 Required inspection and processing data shall be recorded on the Manufacturing and Inspection Record (M & IR) unless otherwise specified.

2.5 All measuring devices that require calibration shall be inspected prior to an operation to verify that calibration intervals have not been exceeded.

3. APPLICABLE DOCUMENTS

3.1 The latest issue of the following documents form a part of this document to the extent specified herein unless otherwise specified by Allegany Ballistics Laboratory.

Specifications

MIL-D-6998	Dichloromethane, Technical
HS-CP-259	Cloth, Glass, S/81-904, Unfinished
HXS 1-153	Adhesive, Epoxy Resin Base with Amine Curing Agent

Publications

GOP 1-00-28	Storage, Mixing, and Disposal of Incompatible Adhesive Ingredients

4. MATERIALS AND EQUIPMENT

Material	Description*
Masking tape	
Glass cloth	HS-CP-259
Cloth	Clean, lint-free
Aloxite cloth	Number (No.) 80
Epon 946, Parts A and B	HXS 1-153
Methylene chloride	MIL-D-6998
Squeegee cards	

Equipment	Description*
Scissors	
Paint brush	Nylon bristle, 1½ inches wide
Roller	Small, hard rubber

*(Unless otherwise indicated, source is commercial.)

5. SAFETY

5.1 All safety precautions and practices established in the General Operating Procedures for the area in which this operation is performed shall be observed.

5.2 The compatibility of materials used in these operations, which may come in contact with propellant, shall be known.

NOTE: IF AT ANY TIME DURING THIS OPERATION, THERE SHOULD BE AN UNUSUAL OCCURRENCE OF A NATURE WHICH WOULD AFFECT THE SAFETY OF THE OPERATION OR THE QUALITY OR COST OF THE PRODUCT, THEN THIS OPERATION SHALL BE BROUGHT TO A SAFE AND ORDERLY STOP AND OPERATIONS SUPERVISION NOTIFIED.

6. CASE SURFACE PREPARATION

6.1 Move the applicable unit to a building specified by supervision.

6.2 Set the unit in the horizontal position with the area to be repaired up.

6.3 Locate area to be repaired, in cylindrical section, parallel to motor. Exact location of defect will be called out on work order.

6.4 Take the defect length and number of plys from the work order and determine the size of the top (i.e., last) ply using chart in Figure 1. Add 1½ inches to the basic length and width to determine the size of the area to be sanded. Using these dimensions, outline the area to be sanded with masking tape. Ensure that the defect is in the center of the area to be sanded.

6.5 Remove cured resin from the areas bounded by the tape. Hand sand using #80 Aloxite cloth until resin has been removed close to glass fibers. Removal has been accomplished when No Gloss is visible.

6.6 Wipe away the resin dust with a clean, soft, lint-free cloth.

6.7 Saturate a clean, soft, lint-free cloth with methylene chloride and clean sanded areas to remove grit, dirt, and finger oils. Air dry 15 minutes.

6.8 Thoroughly mix 100 parts by weight of Epon 946, Part A with 15 $\pm$ 0.3 parts by weight of Epon 946 Part B, in a wax-free, paper cup at ambient temperature thoroughly. Prepare batch sizes of 230 grams each, and use within 1/2 hour after resin is mixed. Prepare as many batches as required to patch the motor.

NOTE: "B-Stage" resin for 15 minutes prior to applying to case.

7. PATCHING CASE

7.1 Outline an area one inch outboard of the defect with masking tape.

7.2 Using a clean nylon brush, apply a thick layer (minimum of 0.020 inch) of resin to the enclosed area. Make certain that defect is filled with resin. Let this layer B-Stage for four hours.

7.3 Remove the masking tape and taper the edge of the resin layer to help avoid air pockets, with a clean nylon brush.

7.4 Apply a thick coat (minimum of 0.020 inch) of resin to the entire sanded area with a clean nylon brush.

7.5 Place first ply (smallest previously cut and furnished) over defect with length-side oriented over length of gouge, one inch on each end (see Figure 1). Roll the ply down, gently working from the defect toward the edges, being careful to eliminate air pockets.

7.6 After resin has been worked up through glass cloth, apply a thick coat (minimum of 0.020 inch) of resin to the first patch ply.

7.7 Repeat 7.5 and 7.6 for each subsequent ply. On final ply, do not apply a coat of resin to the entire patched area.

7.8 Four to six hours after finishing patch, remove the masking tape.

±10° 75°

7.9 Allow patched area to cure at 75°F. ± 10° for a minimum of 48 hours prior to moving the unit. Allow patched area to cure a minimum total of seven days at 75°F. ± 10° before static firing or hydrotesting.

NOTE: When unit contains defects on opposite sides to be patched and patched area will contact saddle after rotating, cure patched areas at 75°F. ± 10° for a minimum of 70 hours before turning unit.

FRINGE
1/4 to 1/2 Typ.

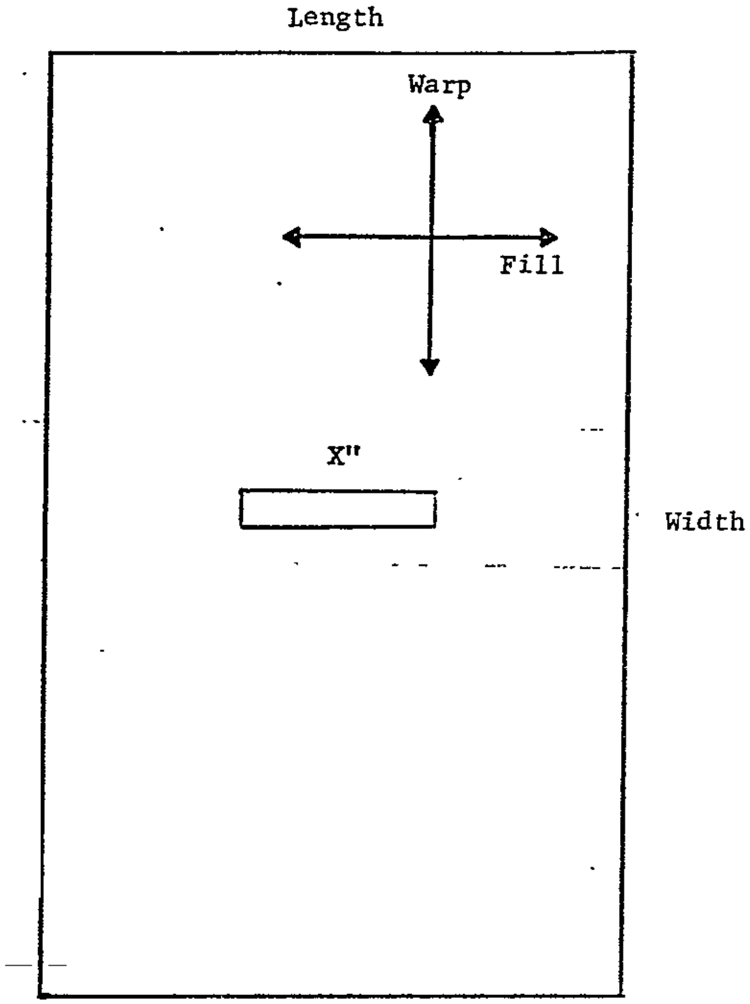

Basic Dimensions Exclusive of Fringe:

PLY.	Length	Width
First	X + 2 inches	4
Second	X + 4 inches	6
Third	X + 6 inches	8
Fourth	X + 8 inches	10
Fifth	X + 10 inches	12

Figure 1

APPENDIX C

HYDROTEST DATA FOR

X259 ROCKET MOTOR DEFECTS INVESTIGATION

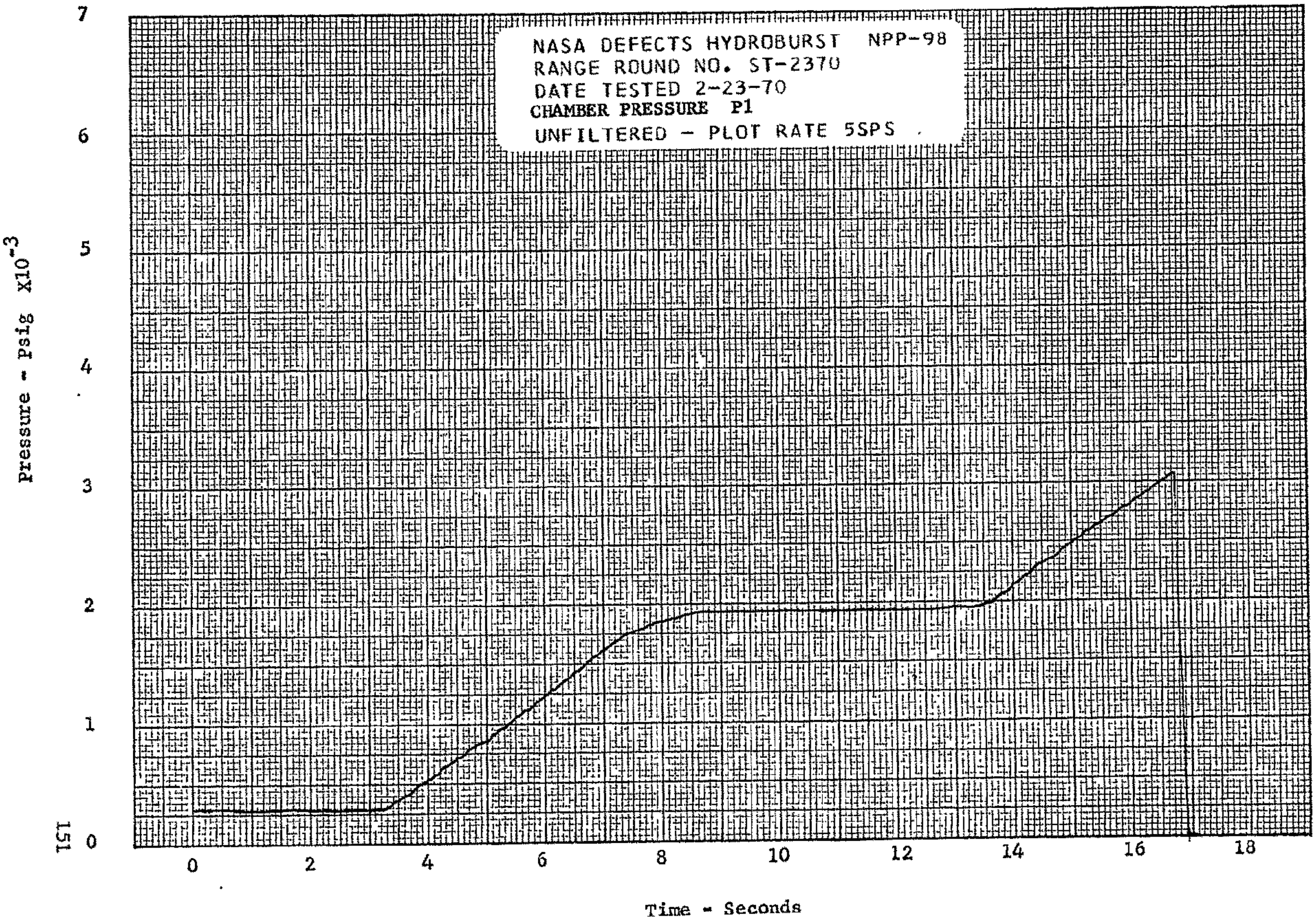
NASA DEFECTS HYDROBURST NPP-98
RANGE ROUND NO. ST-2370
DATE TESTED 2-23-70
CHAMBER PRESSURE P1
UNFILTERED - PLOT RATE 5SPS
Pressure - Psig X10^-3
0
1
2
3
4
5
6
7
0
2
4
6
8
10
12
14
16
18
Time - Seconds

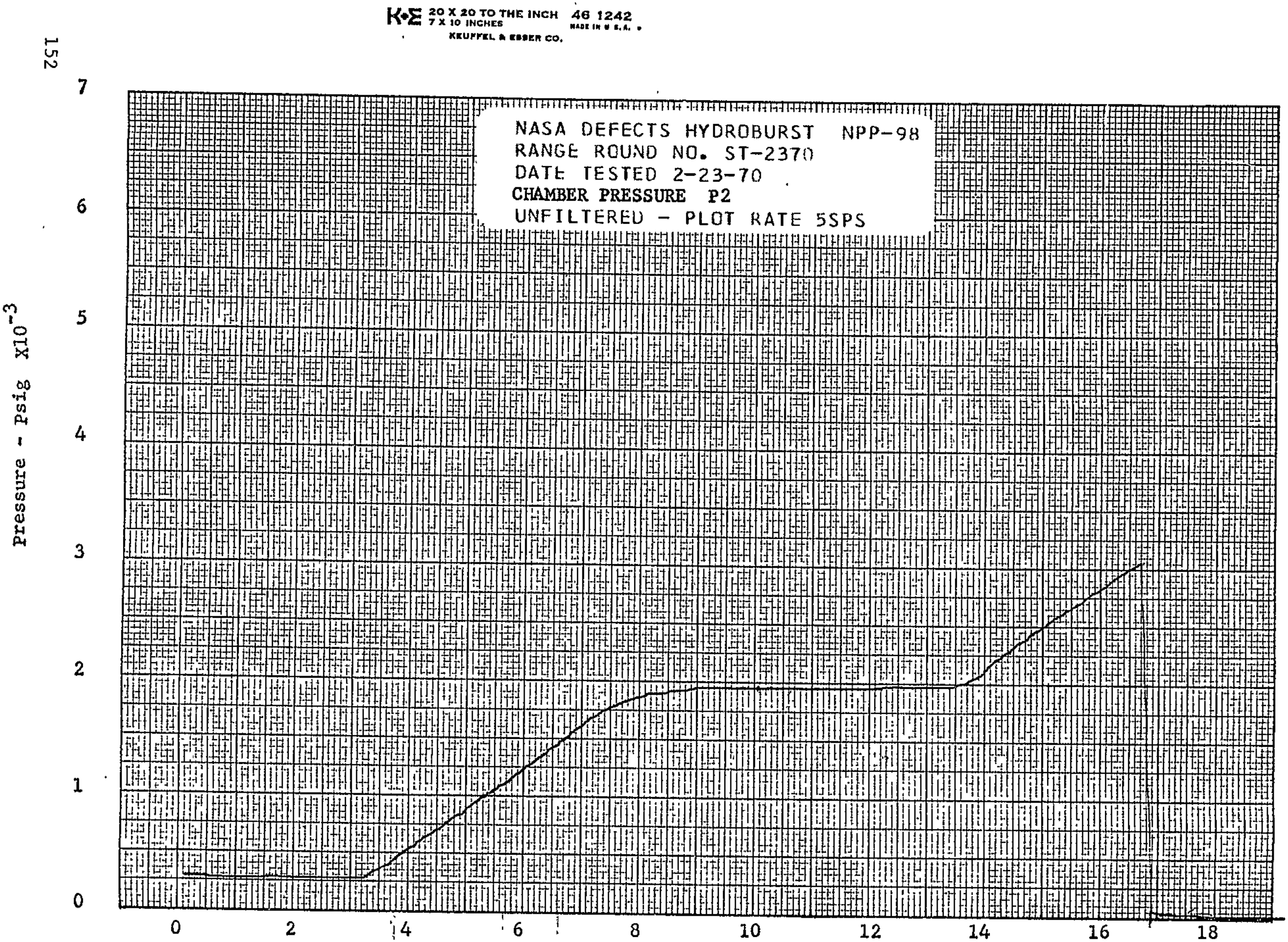
K•E 20 X 20 TO THE INCH 7 X 10 INCHES
46 1242
KEUFFEL & ESSER CO.
NASA DEFECTS HYDROBURST NPP-98
RANGE ROUND NO. ST-2370
DATE TESTED 2-23-70
CHAMBER PRESSURE P2
UNFILTERED - PLOT RATE 5SPS
Pressure - Psig X10^{-3}
0
1
2
3
4
5
6
7
0
2
4
6
8
10
12
14
16
18

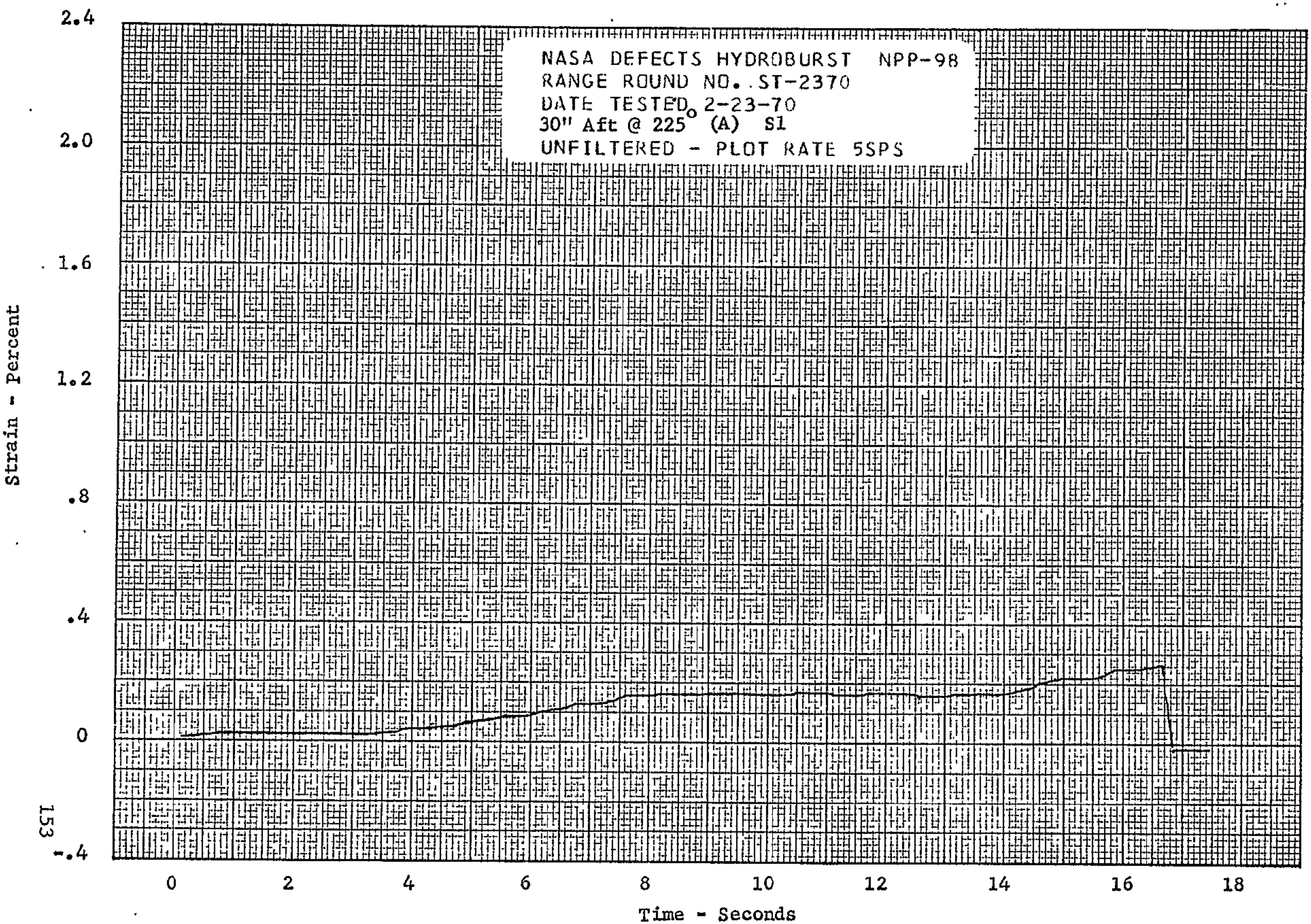
NASA DEFECTS HYDROBURST NPP-98
RANGE ROUND NO. ST-2370
DATE TESTED 2-23-70
30" Aft @ 225° (A) S1
UNFILTERED - PLOT RATE 5SPS
Strain - Percent
2.4
2.0
1.6
1.2
.8
.4
0
-.4
0
2
4
6
8
10
12
14
16
18
Time - Seconds

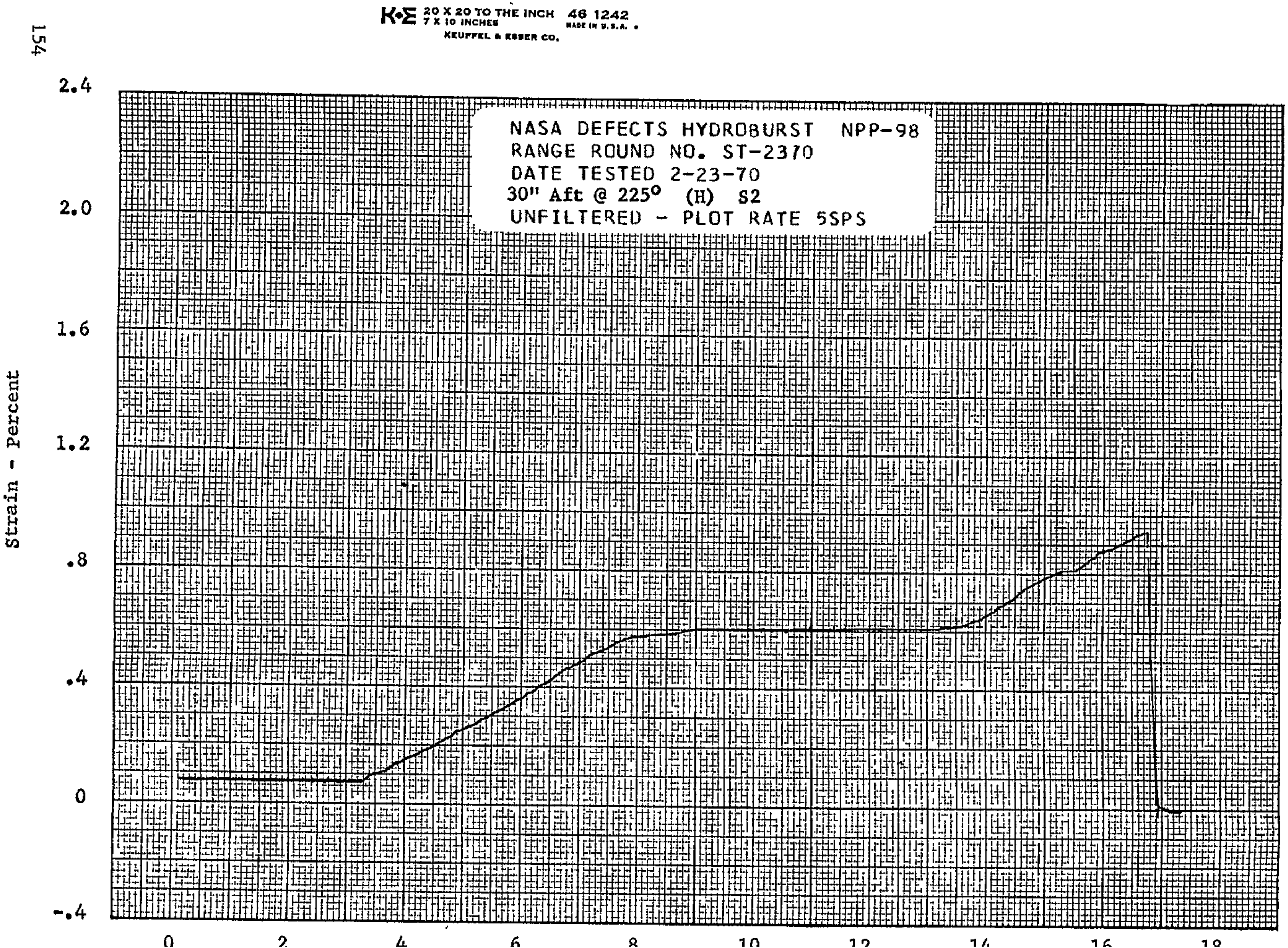
K•E 20 X 20 TO THE INCH 7 X 10 INCHES 46 1242
KEUFFEL & ESSER CO. MADE IN U.S.A.
NASA DEFECTS HYDROBURST NPP-98
RANGE ROUND NO. ST-2370
DATE TESTED 2-23-70
30" Aft @ 225° (H) S2
UNFILTERED - PLOT RATE 5SPS
Strain - Percent
2.4
2.0
1.6
1.2
.8
.4
0
-.4
0
2
4
6
8
10
12
14
16
18

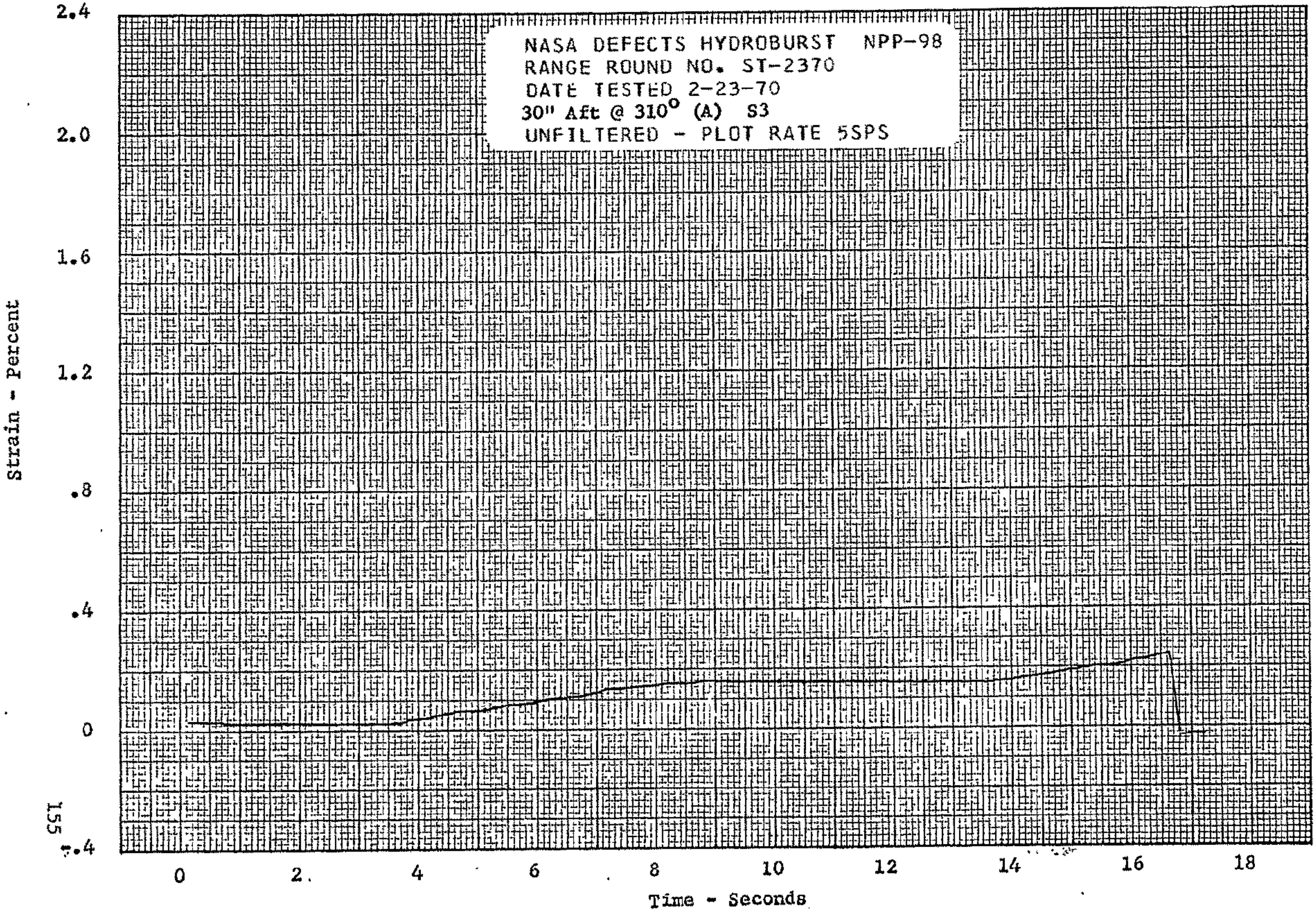
NASA DEFECTS HYDROBURST NPP-98
RANGE ROUND NO. ST-2370
DATE TESTED 2-23-70
30" Aft @ 310° (A) S3
UNFILTERED - PLOT RATE 5SPS
Strain - Percent
2.4
2.0
1.6
1.2
.8
.4
0
-.4
0
2
4
6
8
10
12
14
16
18
Time - Seconds

K+E 20 X 20 TO THE INCH 7 X 10 INCHES 46 1242 KEUFFEL & ESSER CO.

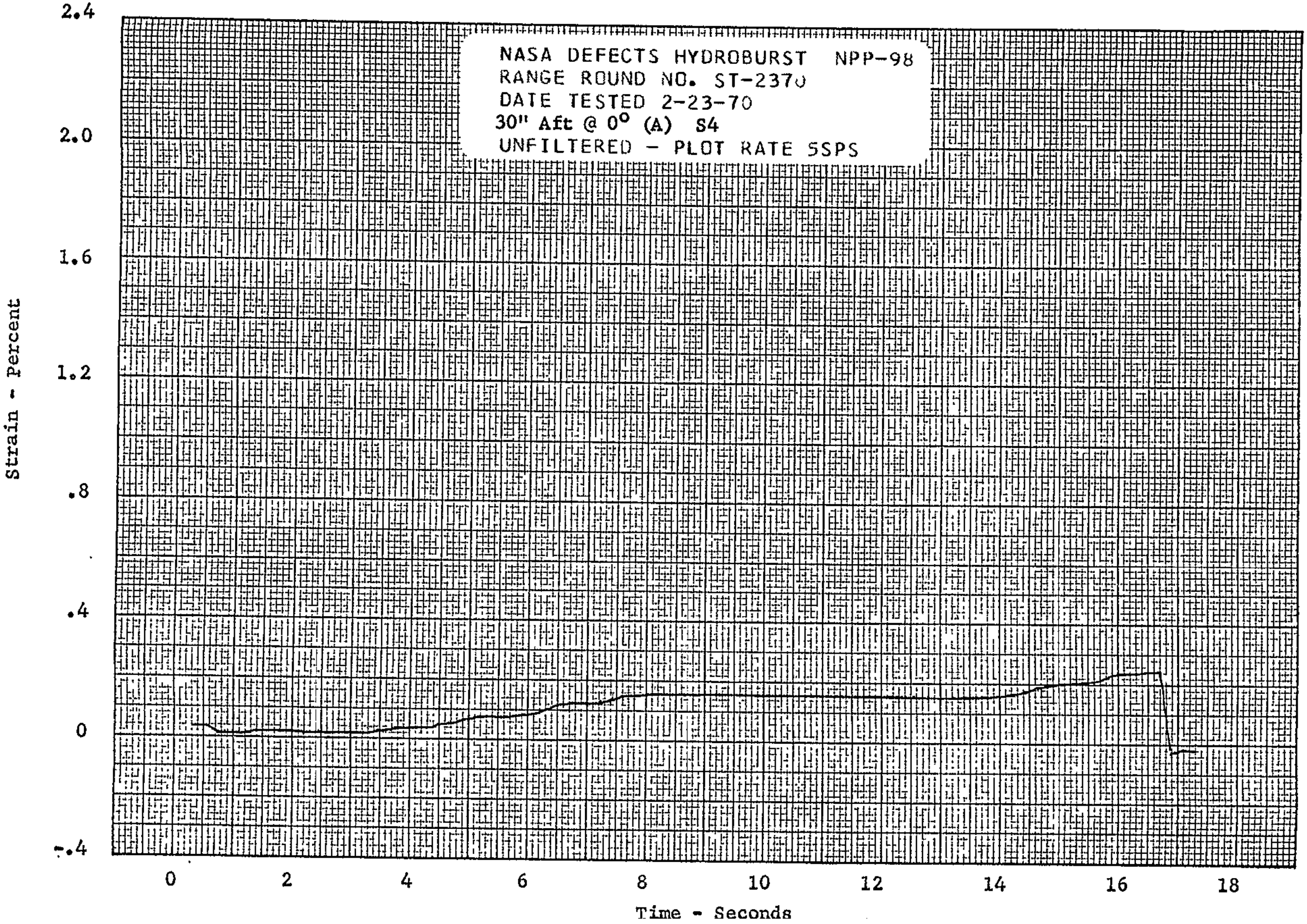

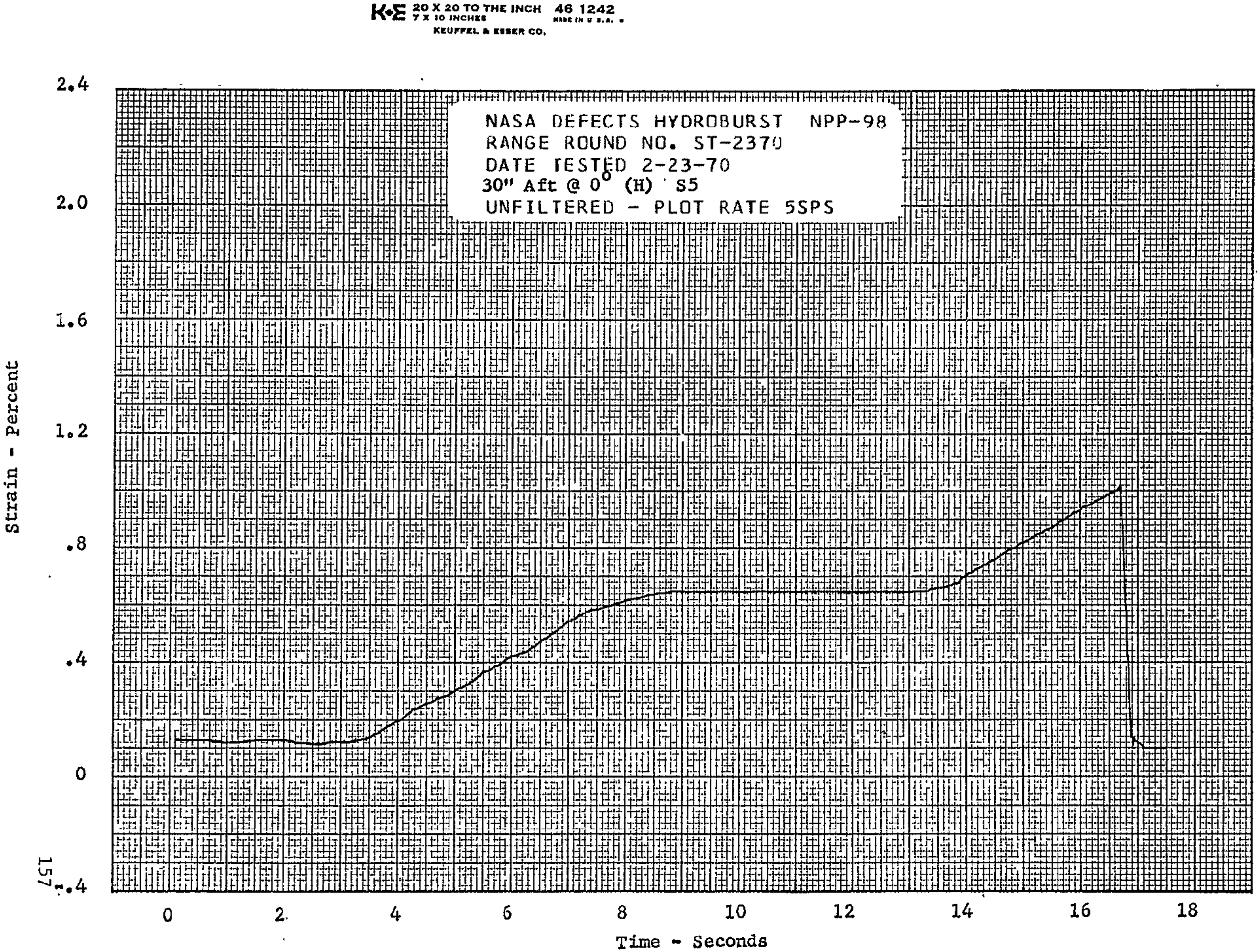

K+E 20 X 20 TO THE INCH 46 1242
7 X 10 INCHES
KEUFFEL & ESSER CO.
NASA DEFECTS HYDROBURST NPP-98
RANGE ROUND NO. ST-2370
DATE TESTED 2-23-70
30" Aft @ 0° (H) S5
UNFILTERED - PLOT RATE 5SPS
2.4
2.0
1.6
1.2
.8
.4
0
-.4
Strain - Percent
0
2
4
6
8
10
12
14
16
18
Time - Seconds

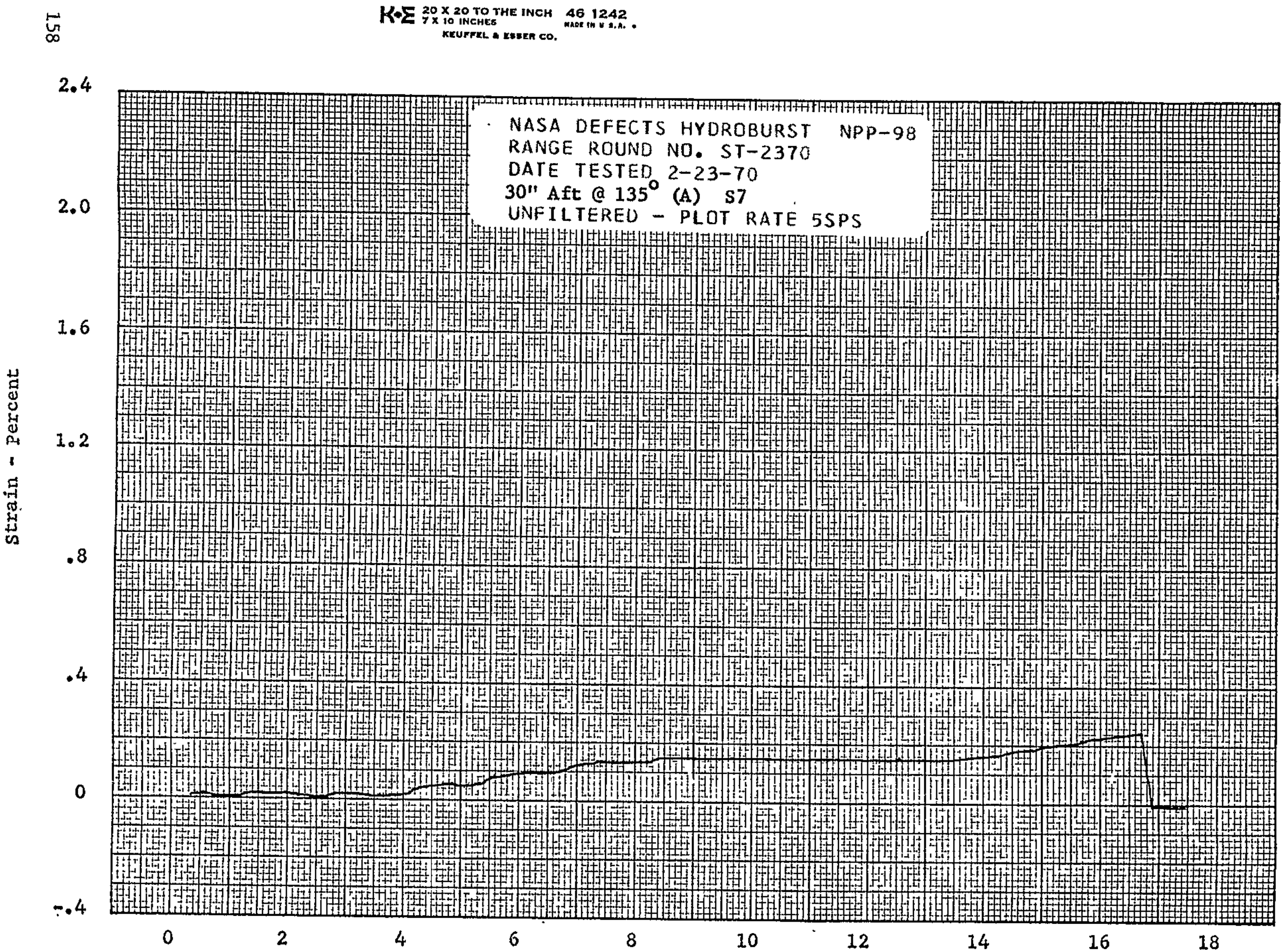
K•Σ 20 X 20 TO THE INCH 7 X 10 INCHES KEUFFEL & ESSER CO. 46 1242 MADE IN U.S.A.
NASA DEFECTS HYDROBURST NPP-98
RANGE ROUND NO. ST-2370
DATE TESTED 2-23-70
30" Aft @ 135° (A) S7
UNFILTERED - PLOT RATE 5SPS
Strain - Percent
2.4
2.0
1.6
1.2
.8
.4
0
-.4
0
2
4
6
8
10
12
14
16
18

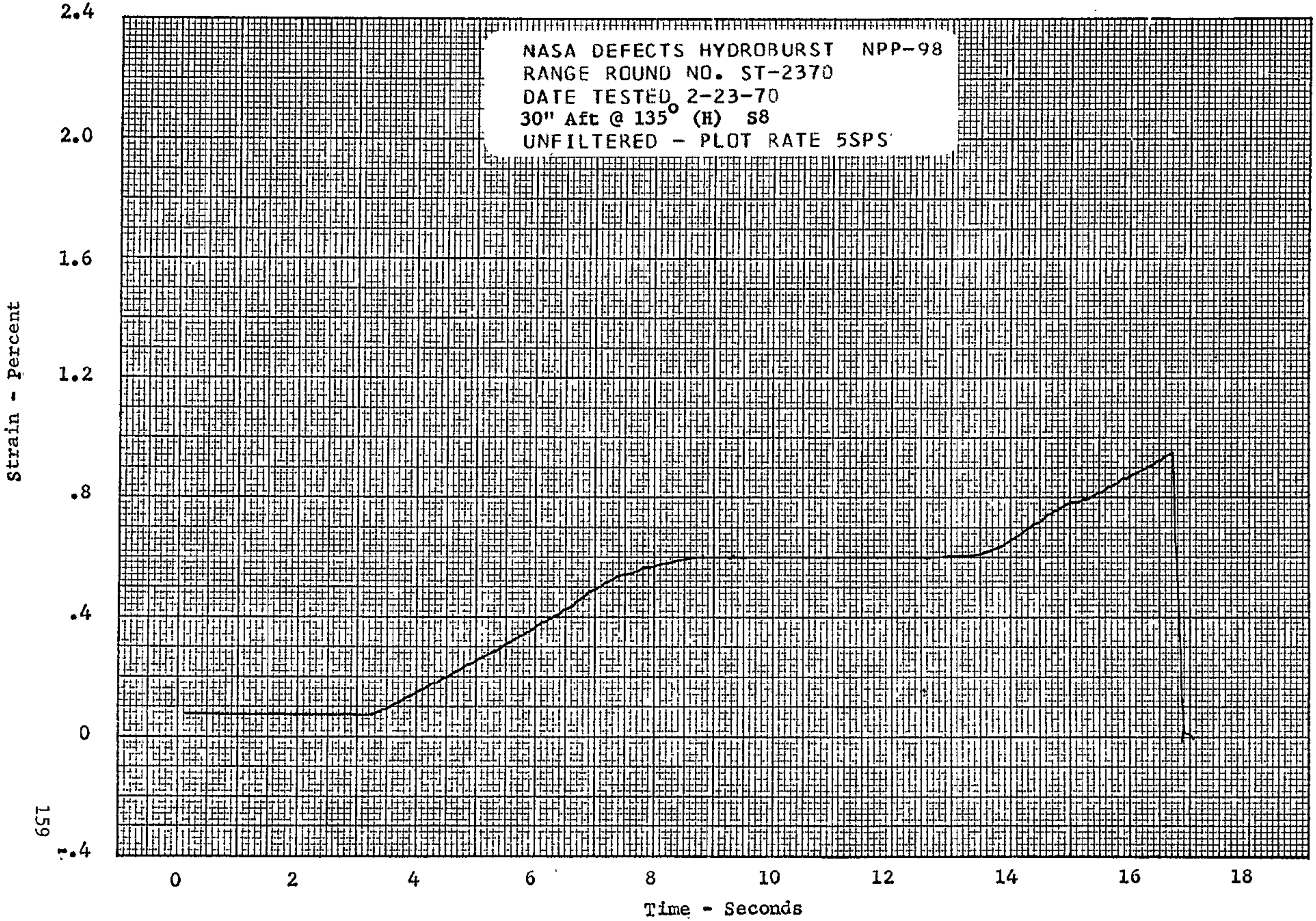
NASA DEFECTS HYDROBURST NPP-98
RANGE ROUND NO. ST-2370
DATE TESTED 2-23-70
30" Aft @ 135° (H) S8
UNFILTERED - PLOT RATE 5SPS
Strain - Percent
2.4
2.0
1.6
1.2
.8
.4
0
-.4
0
2
4
6
8
10
12
14
16
18
Time - Seconds

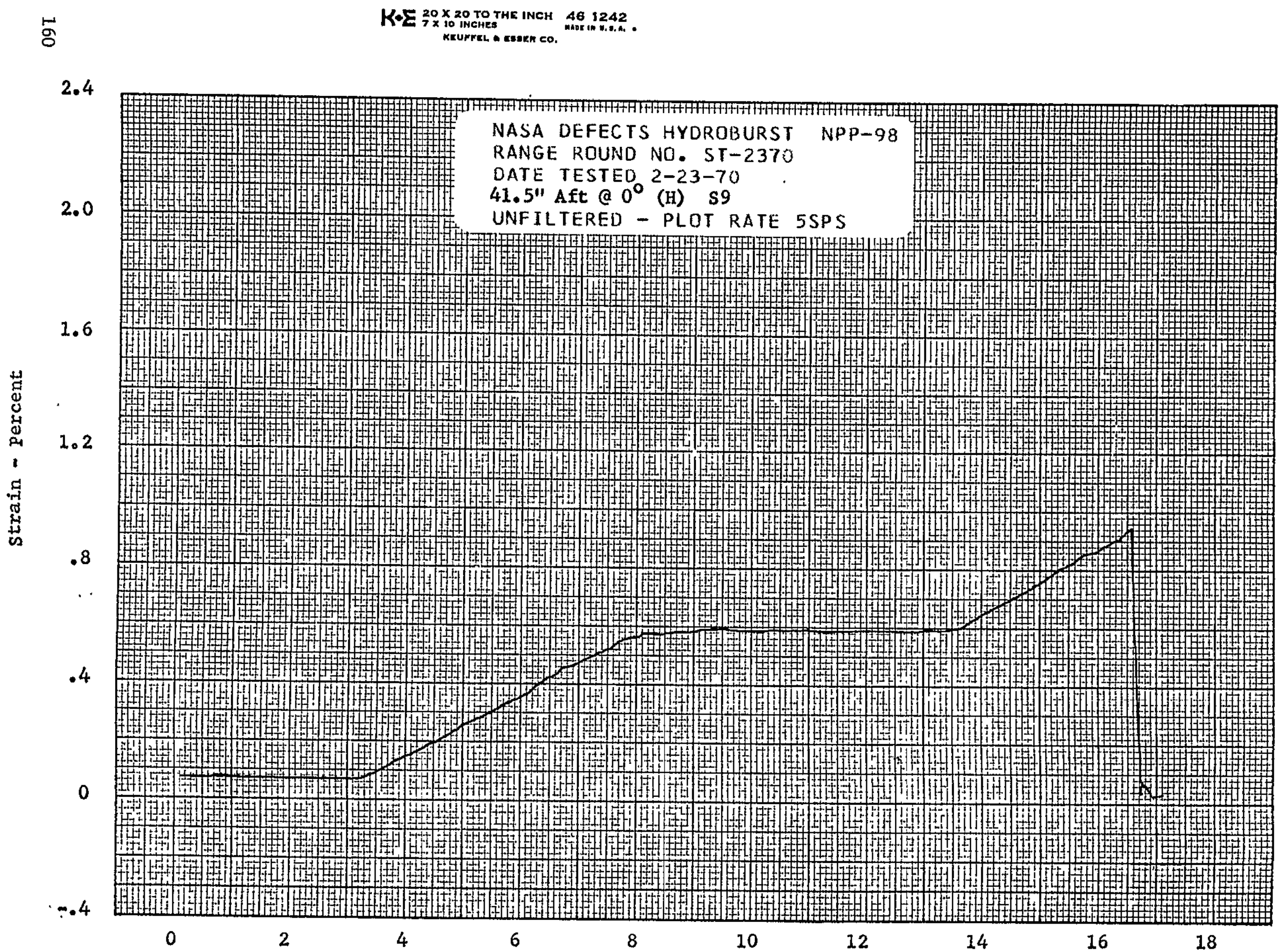
K+E 20 X 20 TO THE INCH 46 1242
7 X 10 INCHES
KEUFFEL & ESSER CO.
NASA DEFECTS HYDROBURST NPP-98
RANGE ROUND NO. ST-2370
DATE TESTED 2-23-70
41.5" Aft @ 0° (H) S9
UNFILTERED - PLOT RATE 5SPS
Strain - Percent
2.4
2.0
1.6
1.2
.8
.4
0
-.4
0
2
4
6
8
10
12
14
16
18

K+E 20 X 20 TO THE INCH 7 X 10 INCHES 46 1242 MADE IN U.S.A. KEUFFEL & ESSER CO.

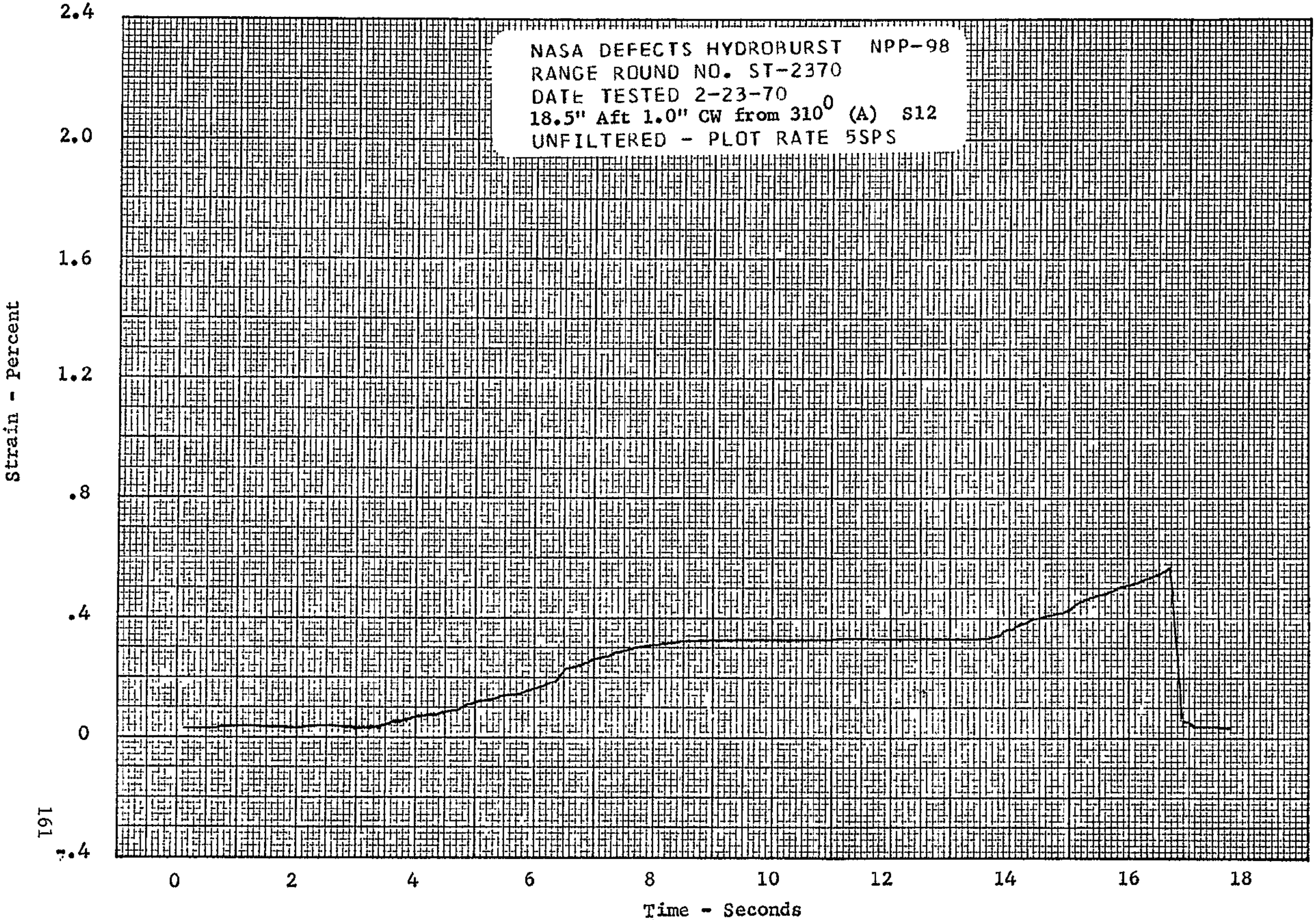

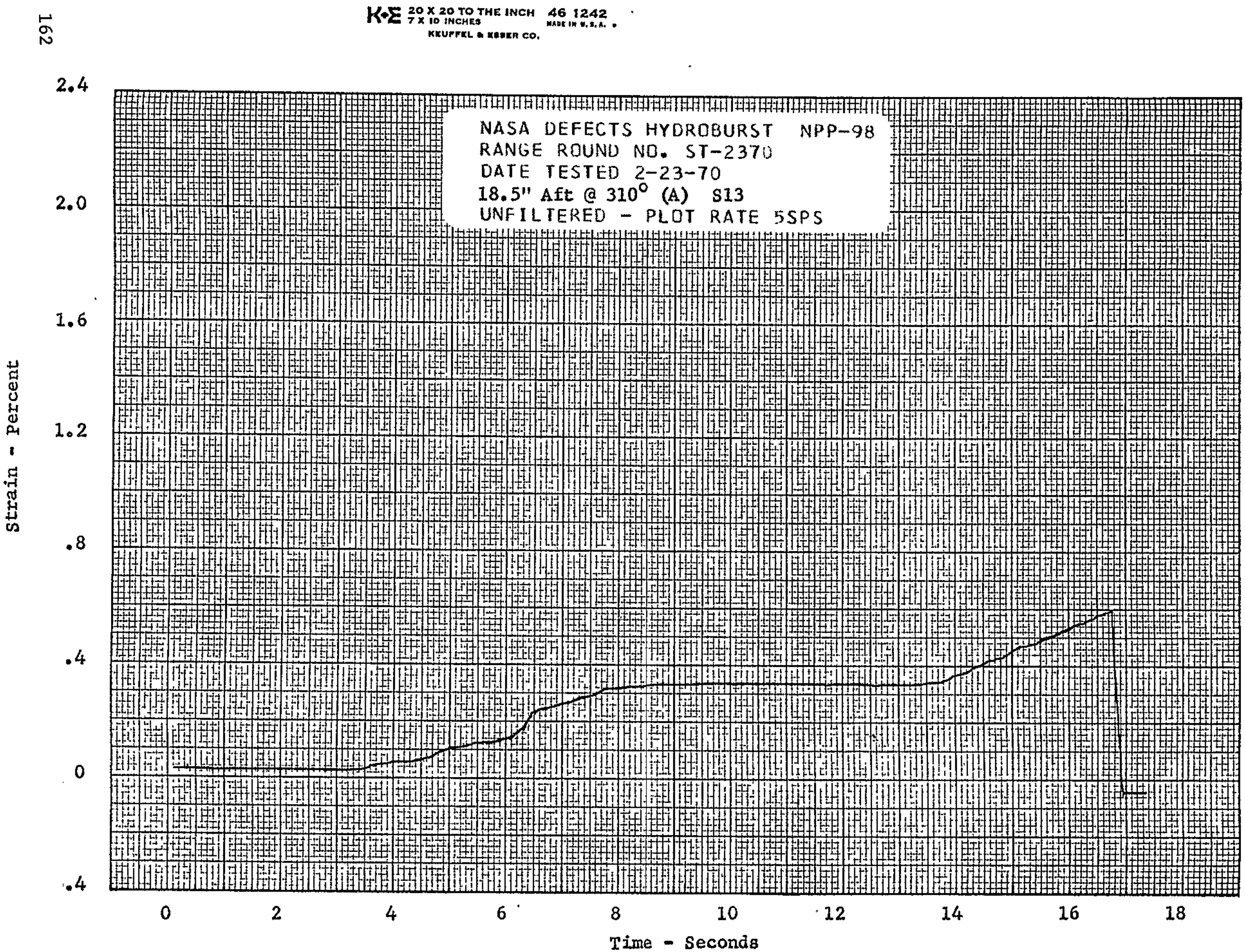
K+E 20 X 20 TO THE INCH 7 X 10 INCHES KEUFFEL & ESSER CO. 46 1242
NASA DEFECTS HYDROBURST NPP-98
RANGE ROUND NO. ST-2370
DATE TESTED 2-23-70
18.5" Aft @ 310° (A) S13
UNFILTERED - PLOT RATE 5SPS
Strain - Percent
2.4
2.0
1.6
1.2
.8
.4
0
-.4
0
2
4
6
8
10
12
14
16
18
Time - Seconds

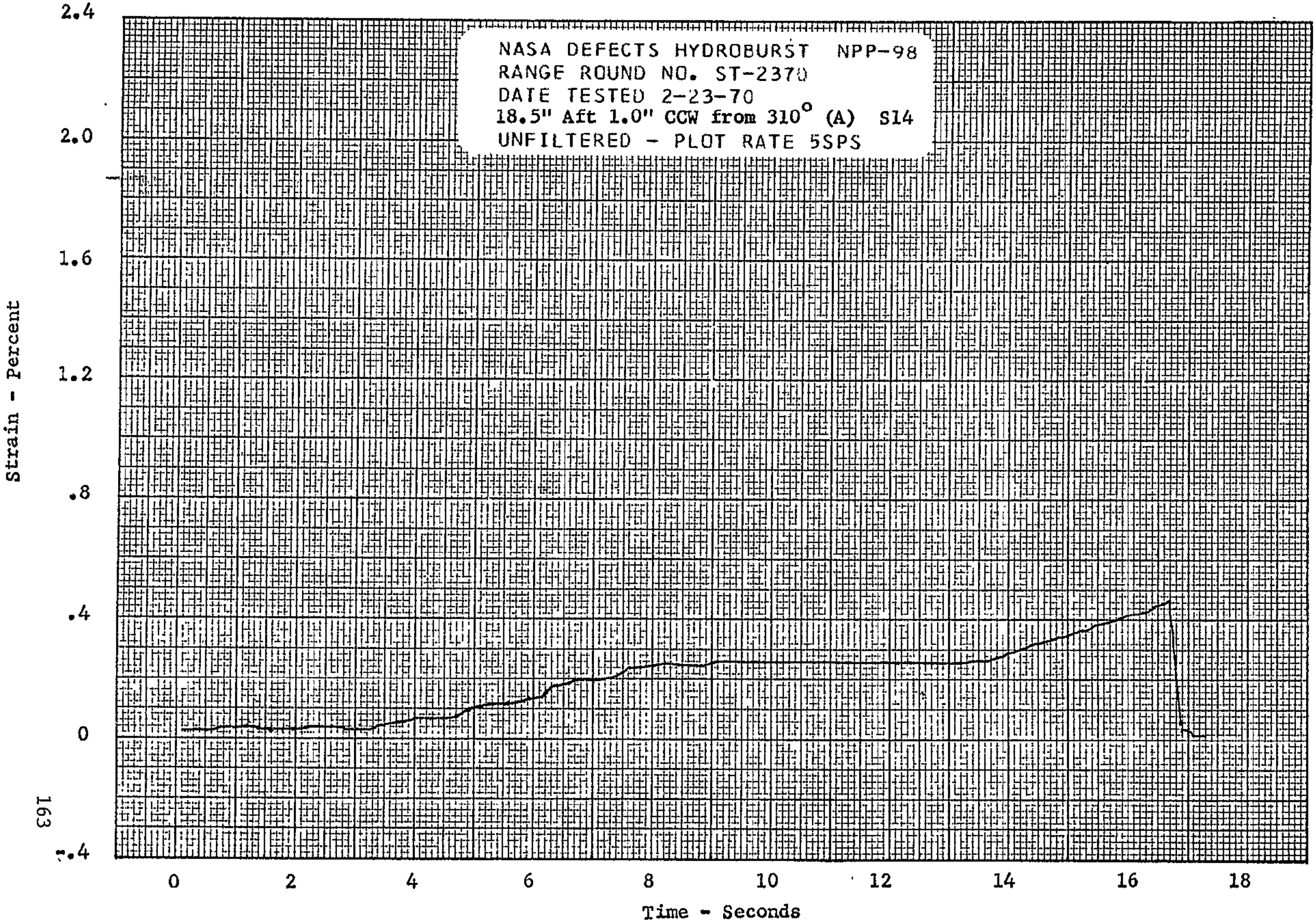
NASA DEFECTS HYDROBURST NPP-98
RANGE ROUND NO. ST-2370
DATE TESTED 2-23-70
18.5" Aft 1.0" CCW from 310° (A) S14
UNFILTERED - PLOT RATE 5SPS
Strain - Percent
2.4
2.0
1.6
1.2
.8
.4
0
-.4
0
2
4
6
8
10
12
14
16
18
Time - Seconds

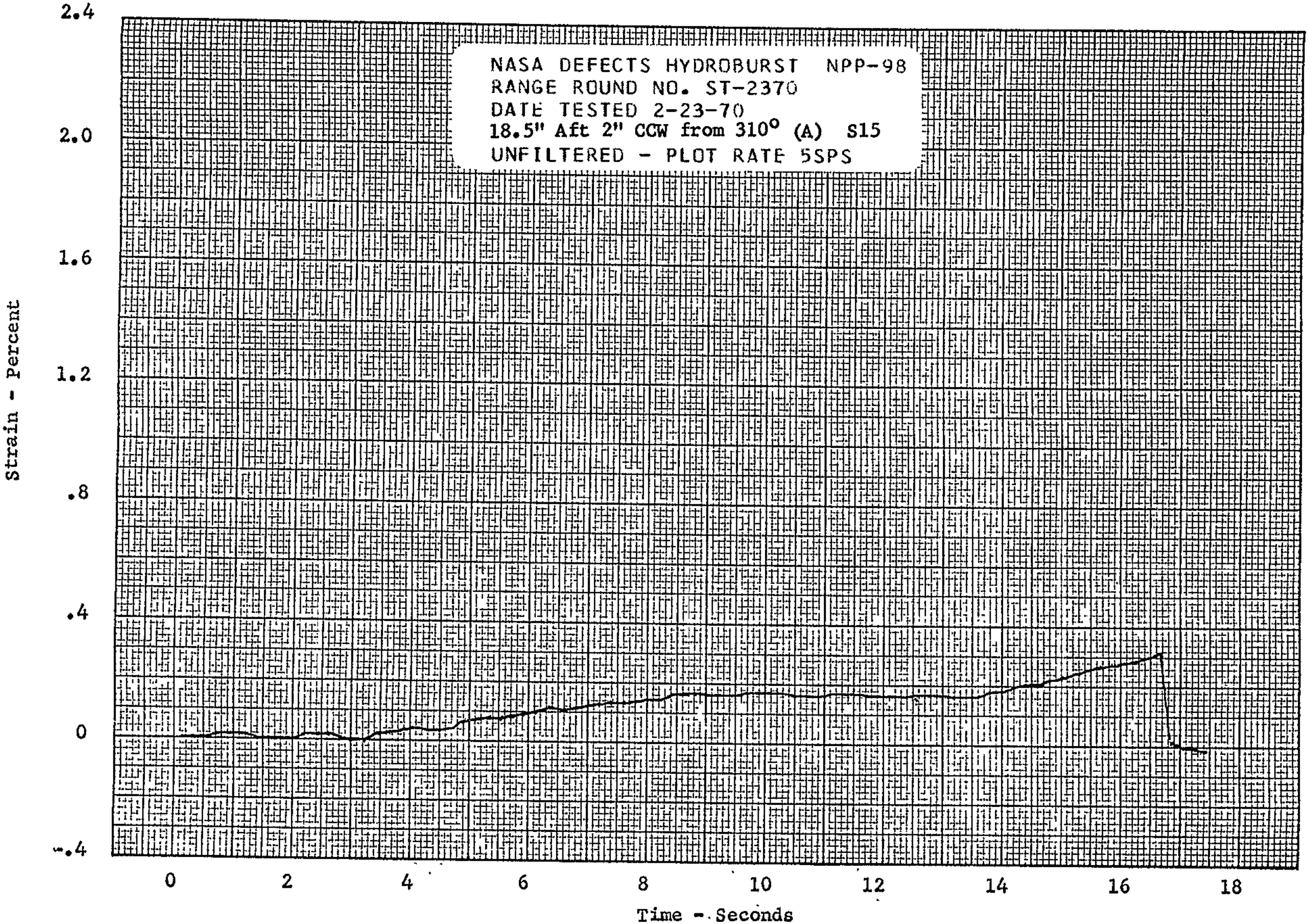
NASA DEFECTS HYDROBURST NPP-98
RANGE ROUND NO. ST-2370
DATE TESTED 2-23-70
18.5" Aft 2" CCW from 310° (A) S15
UNFILTERED - PLOT RATE 5SPS
Strain - Percent
2.4
2.0
1.6
1.2
.8
.4
0
-.4
0
2
4
6
8
10
12
14
16
18
Time - Seconds

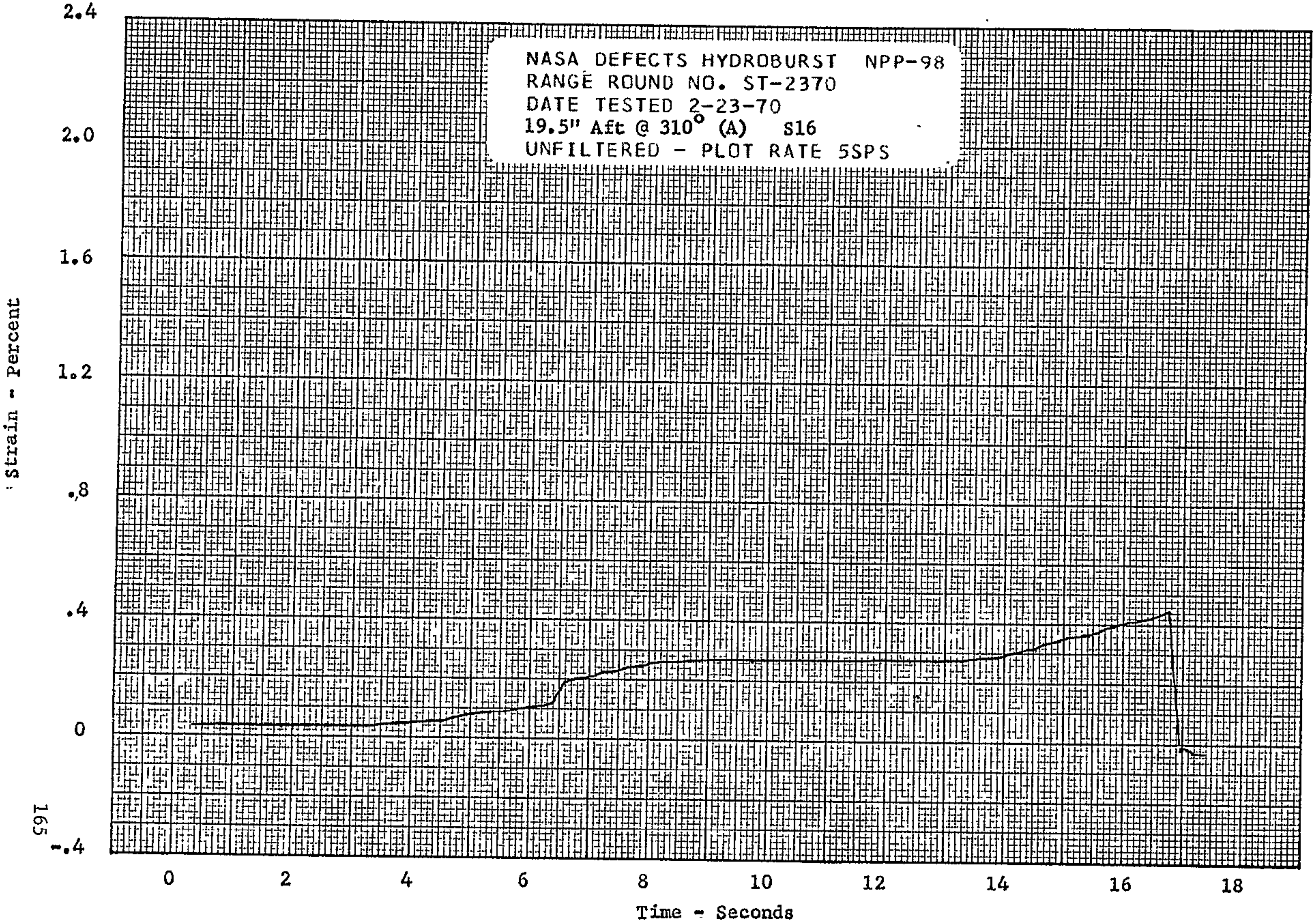

NASA DEFECTS HYDROBURST NPP-98
RANGE ROUND NO. ST-2370
DATE TESTED 2-23-70
19.5" Aft @ 310° (A) S16
UNFILTERED - PLOT RATE 5SPS
Strain - Percent
2.4
2.0
1.6
1.2
.8
.4
0
-.4
0
2
4
6
8
10
12
14
16
18
Time - Seconds

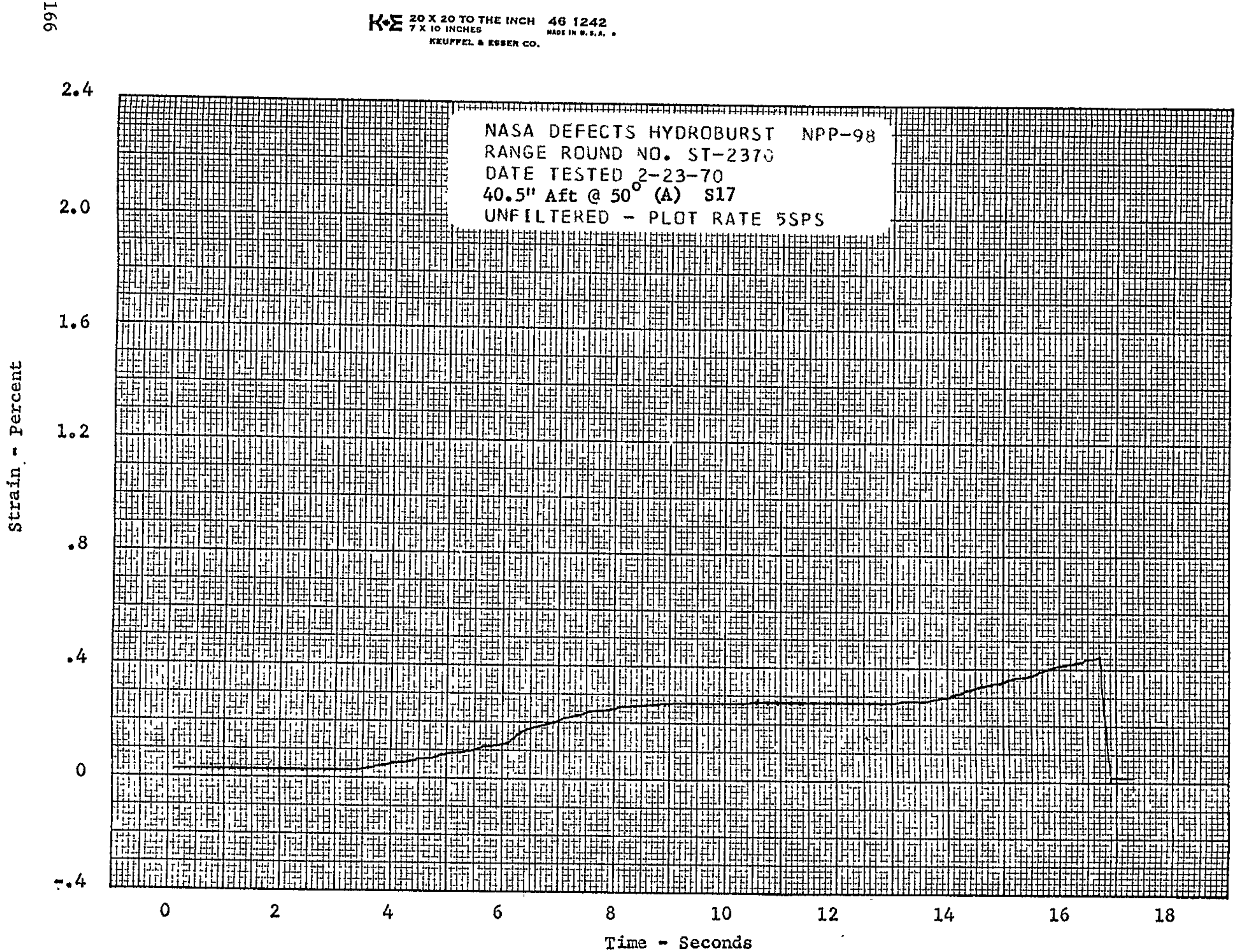
K+E 20 X 20 TO THE INCH 46 1242
7 X 10 INCHES
MADE IN U.S.A.
KEUFFEL & ESSER CO.
NASA DEFECTS HYDROBURST NPP-98
RANGE ROUND NO. ST-2370
DATE TESTED 2-23-70
40.5" Aft @ 50° (A) S17
UNFILTERED - PLOT RATE 5SPS
2.4
2.0
1.6
1.2
.8
.4
0
-.4
Strain - Percent
0
2
4
6
8
10
12
14
16
18
Time - Seconds

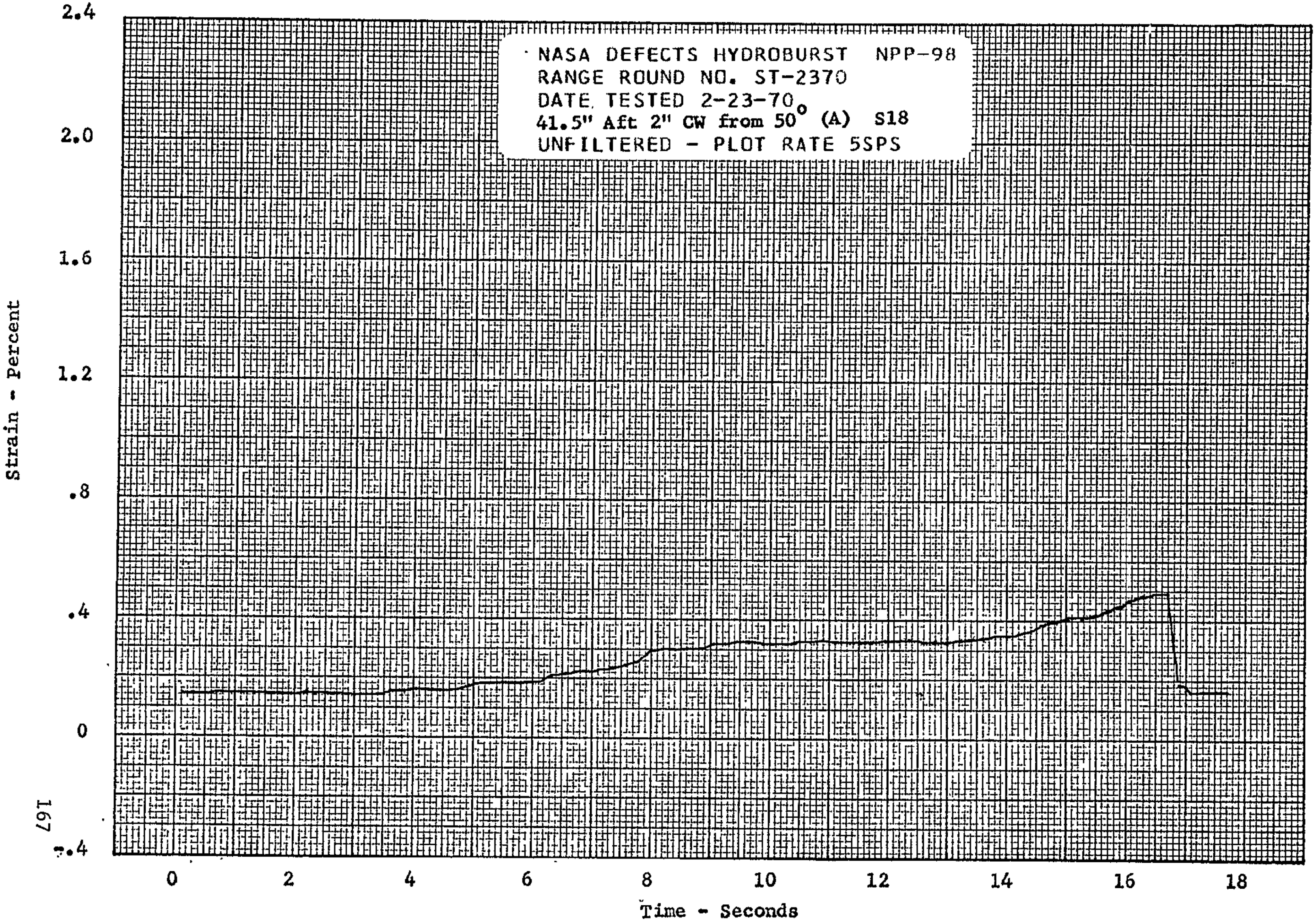
NASA DEFECTS HYDROBURST NPP-98
RANGE ROUND NO. ST-2370
DATE TESTED 2-23-70
41.5" Aft 2" CW from 50° (A) S18
UNFILTERED - PLOT RATE 5SPS
Strain - Percent
2.4
2.0
1.6
1.2
.8
.4
0
-.4
0
2
4
6
8
10
12
14
16
18
Time - Seconds

K+E 20 X 20 TO THE INCH 46 1242
7 X 10 INCHES
KEUFFEL & ESSER CO.
MADE IN U.S.A.

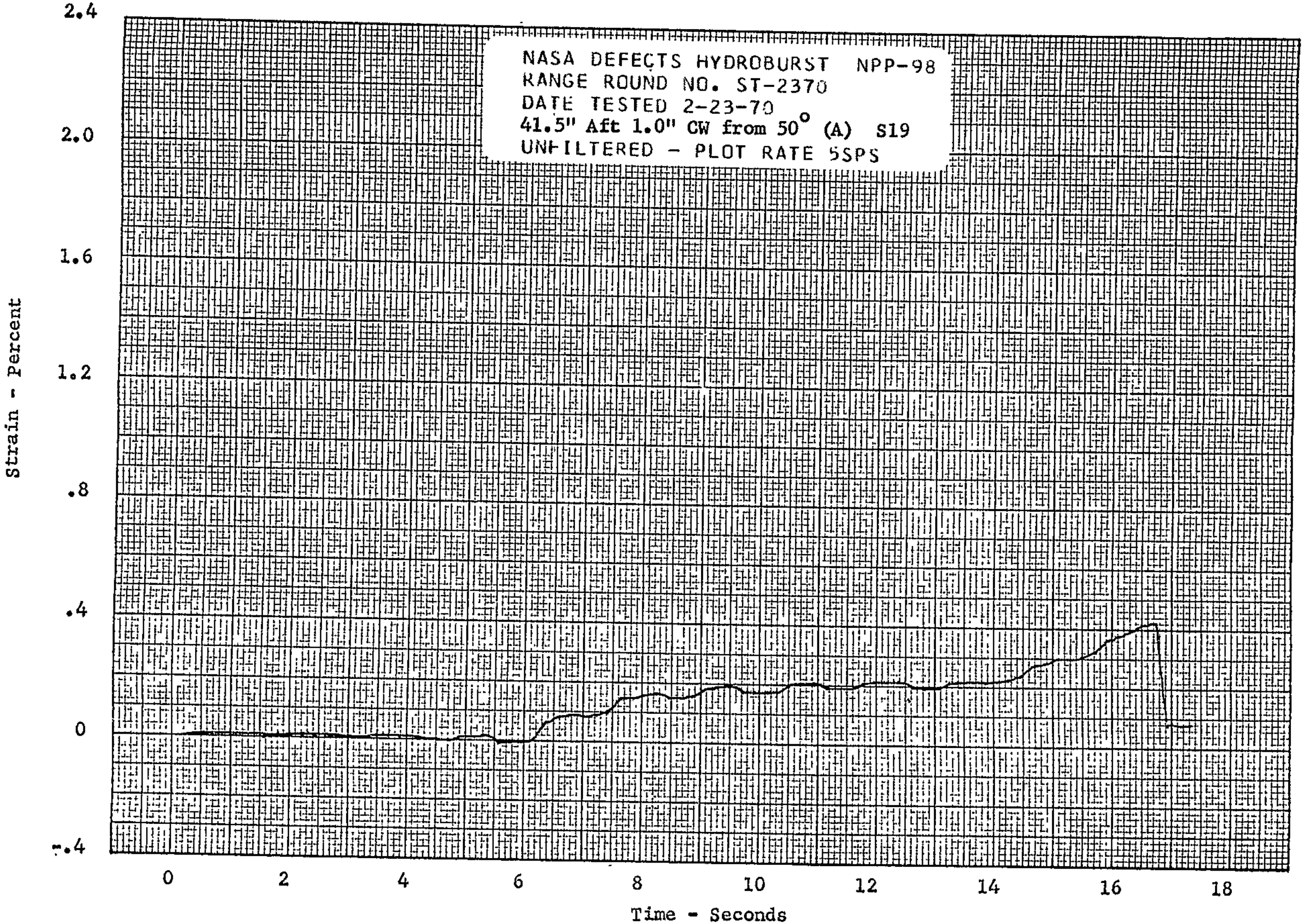

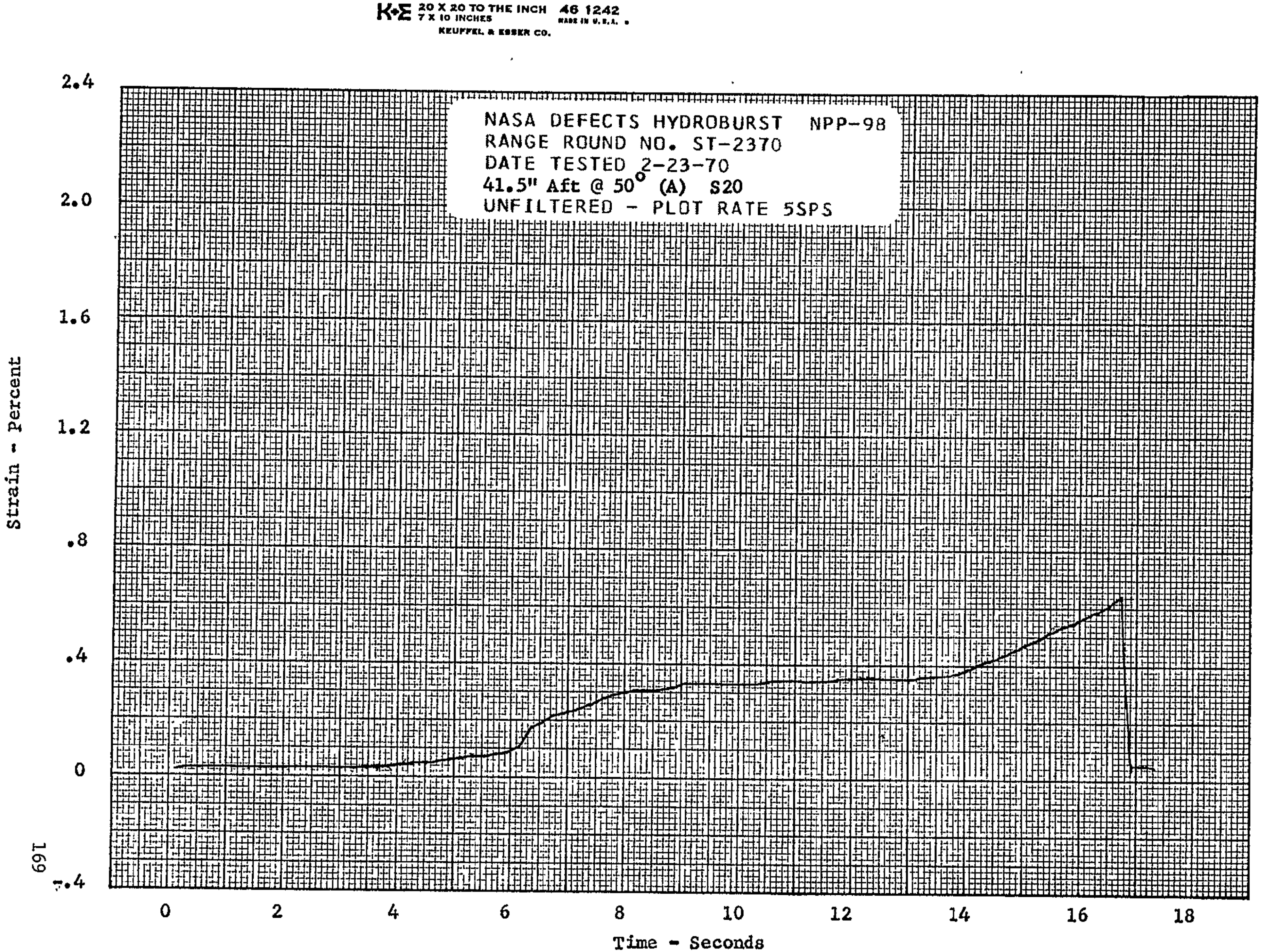
K+E 20 X 20 TO THE INCH 46 1242
7 X 10 INCHES
KEUFFEL & ESSER CO.
NASA DEFECTS HYDROBURST NPP-98
RANGE ROUND NO. ST-2370
DATE TESTED 2-23-70
41.5" Aft @ 50° (A) S20
UNFILTERED - PLOT RATE 5SPS
Strain - Percent
2.4
2.0
1.6
1.2
.8
.4
0
-.4
0
2
4
6
8
10
12
14
16
18
Time - Seconds

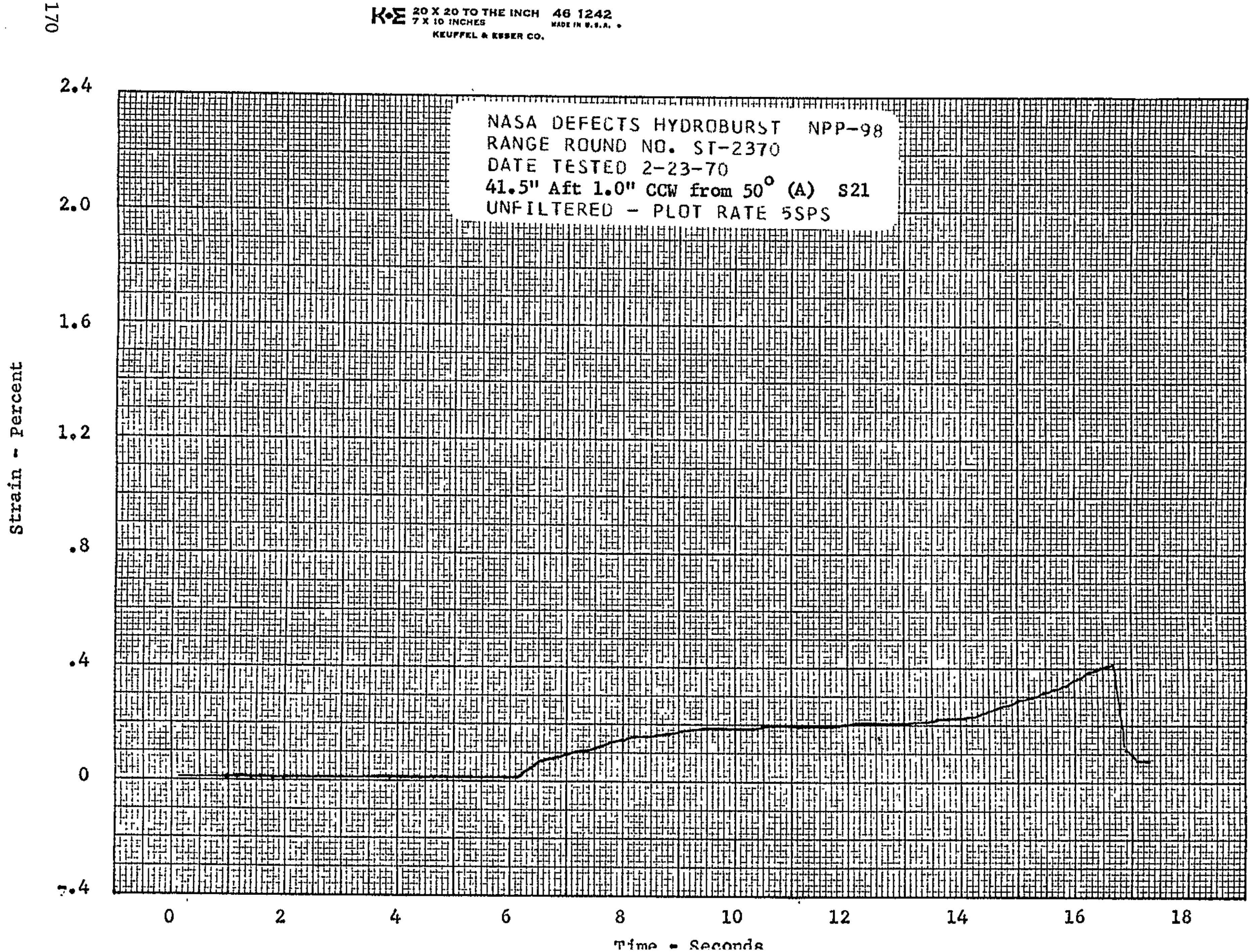
K•E 20 X 20 TO THE INCH 7 X 10 INCHES 46 1242
KEUFFEL & ESSER CO.
NASA DEFECTS HYDROBURST NPP-98
RANGE ROUND NO. ST-2370
DATE TESTED 2-23-70
41.5" Aft 1.0" CCW from 50° (A) S21
UNFILTERED - PLOT RATE 5SPS
Strain - Percent
2.4
2.0
1.6
1.2
.8
.4
0
-.4
0
2
4
6
8
10
12
14
16
18
Time - Seconds

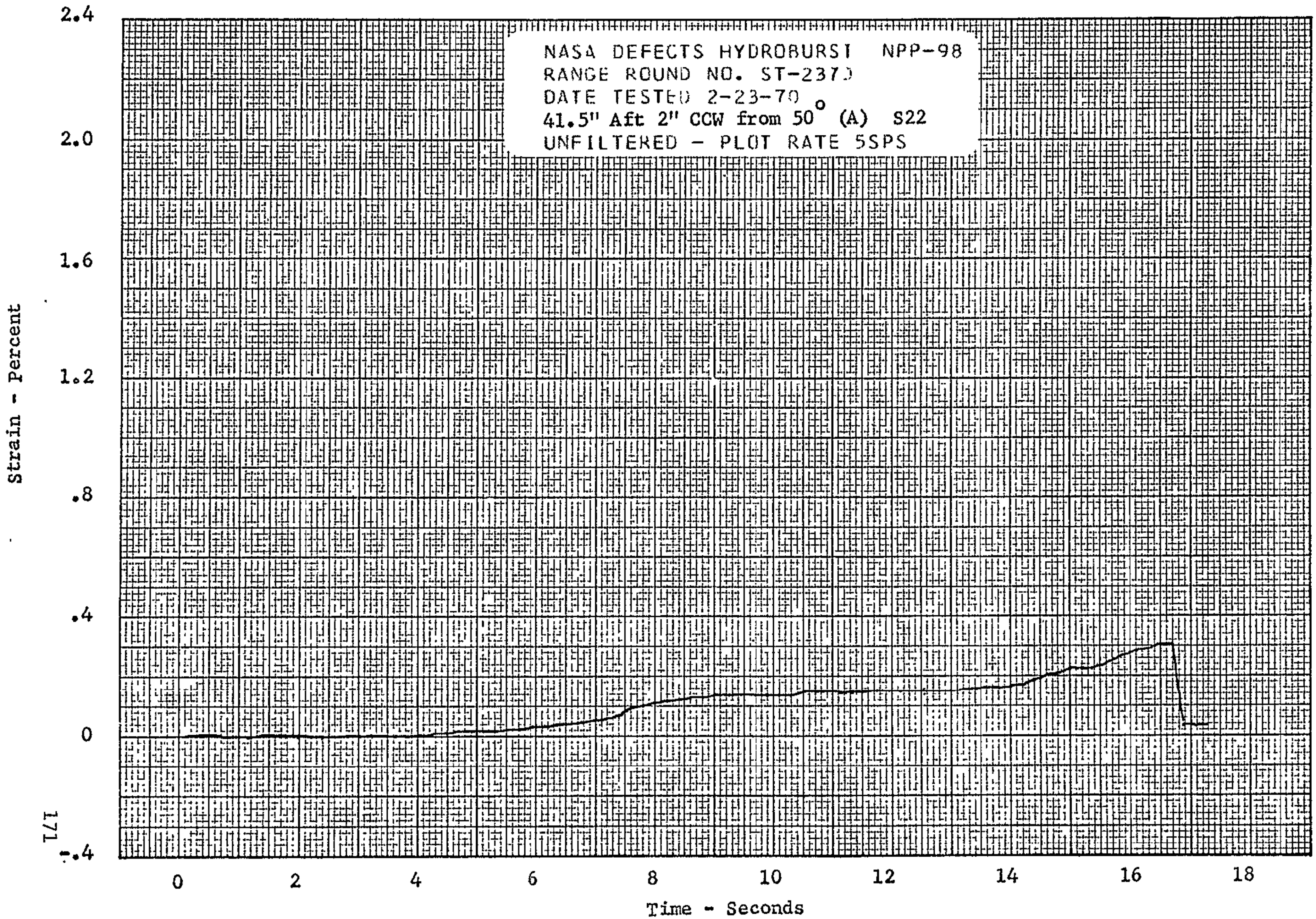
NASA DEFECTS HYDROBURST NPP-98
RANGE ROUND NO. ST-2373
DATE TESTED 2-23-70
41.5" Aft 2" CCW from 50° (A) S22
UNFILTERED - PLOT RATE 5SPS
Strain - Percent
2.4
2.0
1.6
1.2
.8
.4
0
-.4
0
2
4
6
8
10
12
14
16
18
Time - Seconds

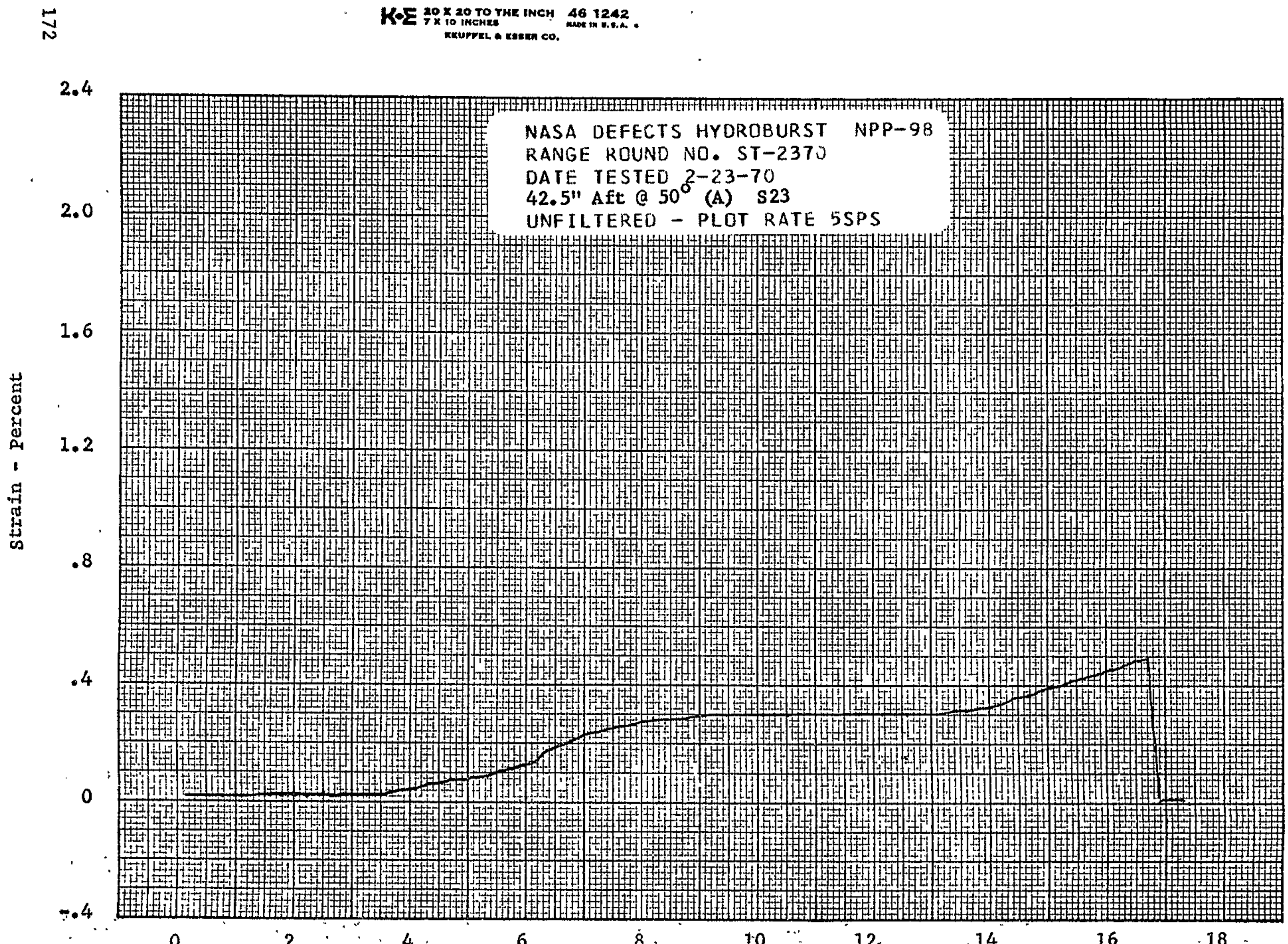
K+E 20 X 20 TO THE INCH 46 1242
7 X 10 INCHES
KEUFFEL & ESSER CO.
NASA DEFECTS HYDROBURST NPP-98
RANGE ROUND NO. ST-2370
DATE TESTED 2-23-70
42.5" Aft @ 50° (A) S23
UNFILTERED - PLOT RATE 5SPS
Strain - Percent
2.4
2.0
1.6
1.2
.8
.4
0
-.4
0
2
4
6
8
10
12
14
16
18

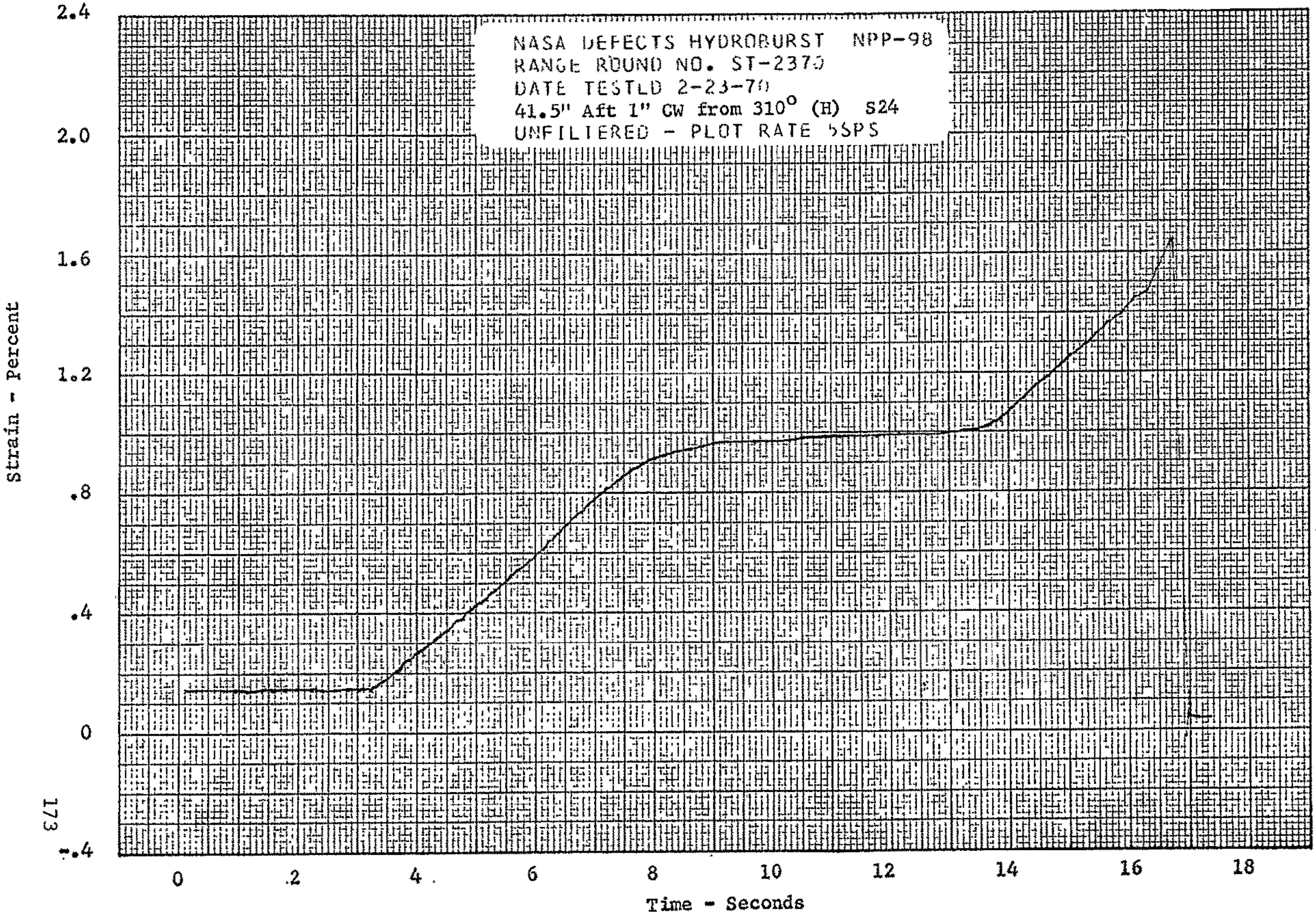

NASA DEFECTS HYDROBURST NPP-98
RANGE ROUND NO. ST-2370
DATE TESTED 2-23-70
41.5" Aft 1" CW from 310° (H) S24
UNFILTERED - PLOT RATE 5SPS
2.4
2.0
1.6
1.2
.8
.4
0
-.4
Strain - Percent
0
2
4
6
8
10
12
14
16
18
Time - Seconds

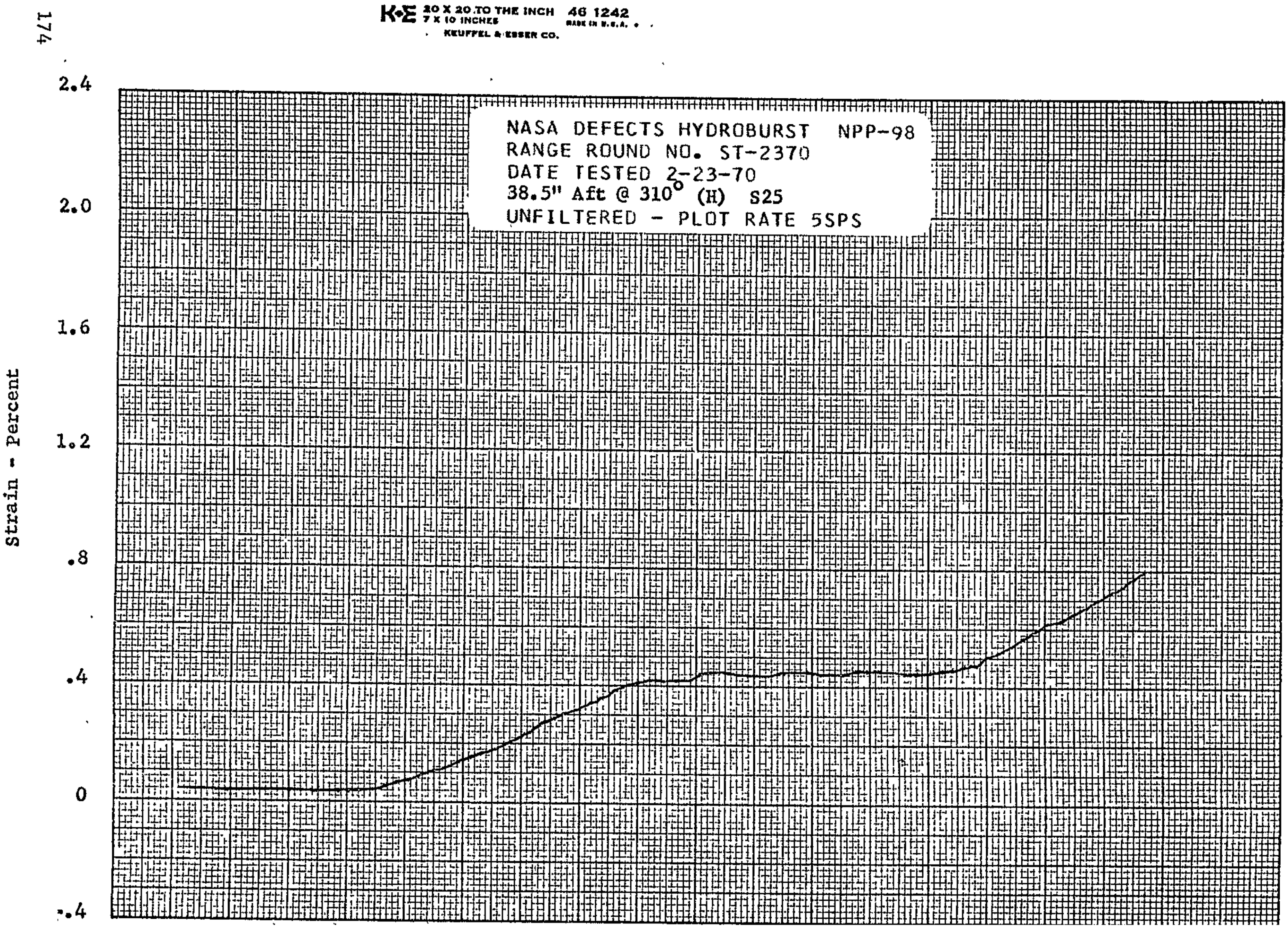
K+E 20 X 20 TO THE INCH 7 X 10 INCHES
46 1242
KEUFFEL & ESSER CO.
NASA DEFECTS HYDROBURST NPP-98
RANGE ROUND NO. ST-2370
DATE TESTED 2-23-70
38.5" Aft @ 310° (H) S25
UNFILTERED - PLOT RATE 5SPS
Strain - Percent
2.4
2.0
1.6
1.2
.8
.4
0
-.4

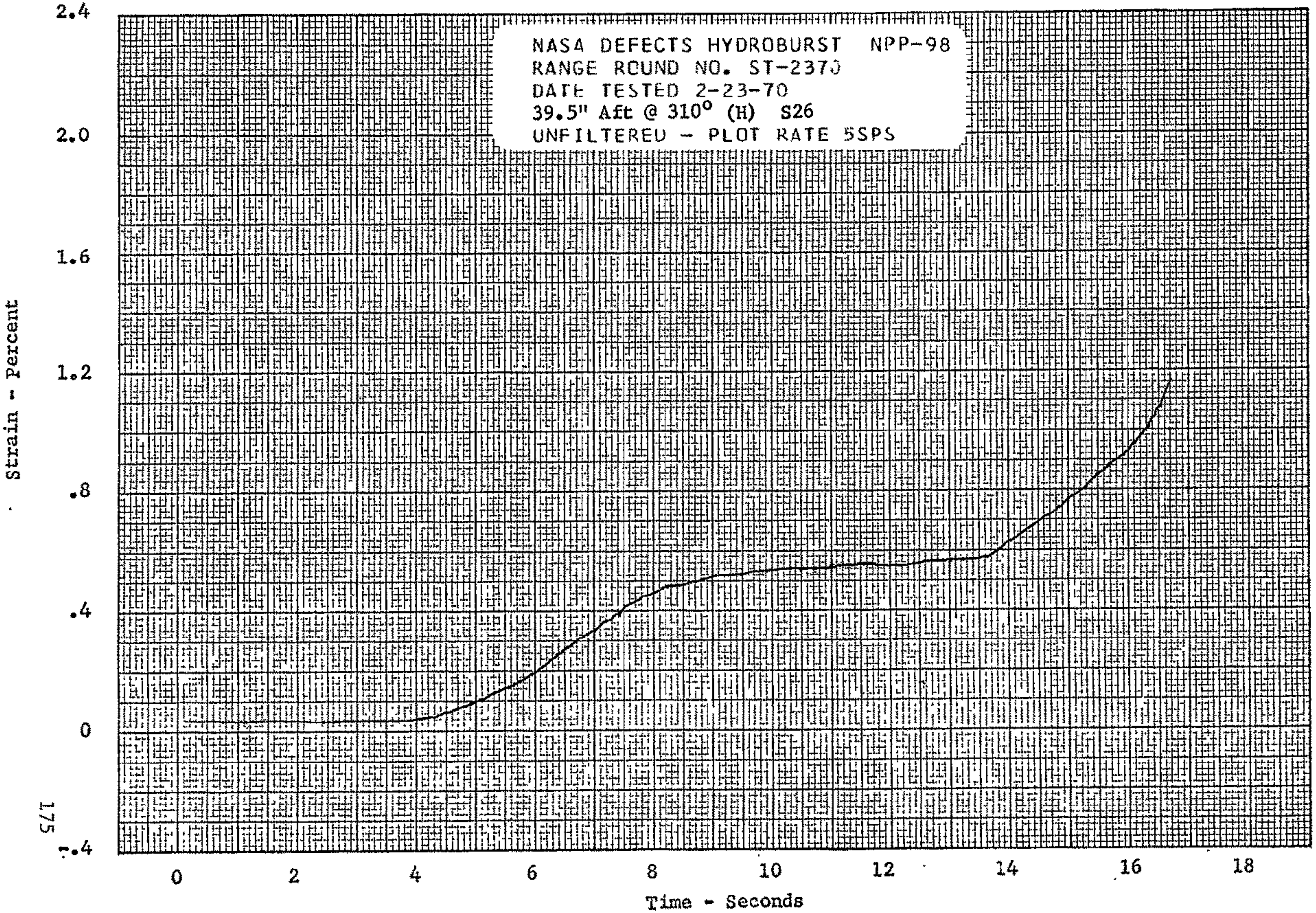
NASA DEFECTS HYDROBURST NPP-98
RANGE ROUND NO. ST-2370
DATE TESTED 2-23-70
39.5" Aft @ 310° (H) S26
UNFILTERED - PLOT RATE 5SPS
Strain - Percent
2.4
2.0
1.6
1.2
.8
.4
0
-.4
0
2
4
6
8
10
12
14
16
18
Time - Seconds

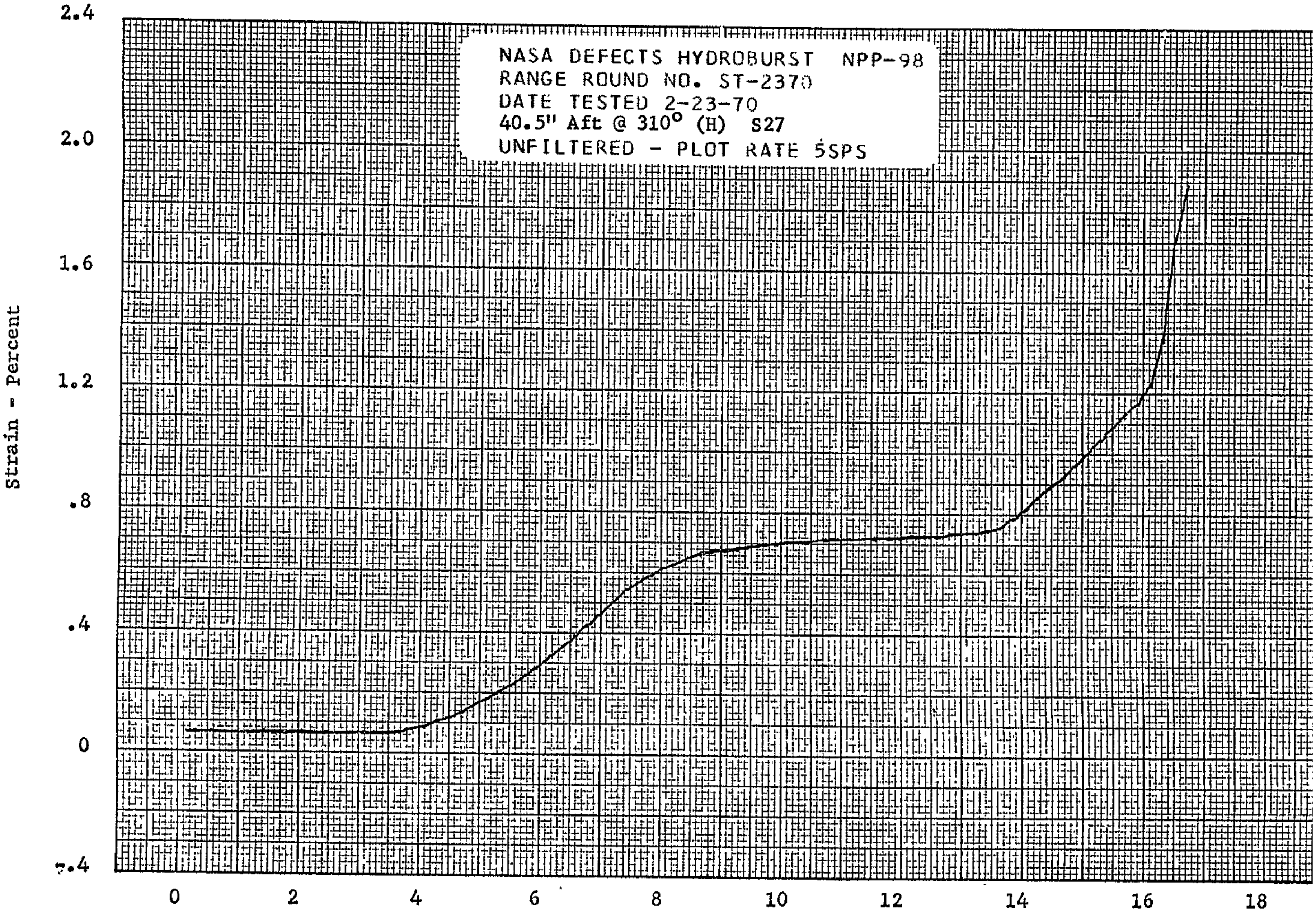
NASA DEFECTS HYDROBURST NPP-98
RANGE ROUND NO. ST-2370
DATE TESTED 2-23-70
40.5" Aft @ 310° (H) S27
UNFILTERED - PLOT RATE 5SPS
Strain - Percent
2.4
2.0
1.6
1.2
.8
.4
0
-.4
0
2
4
6
8
10
12
14
16
18

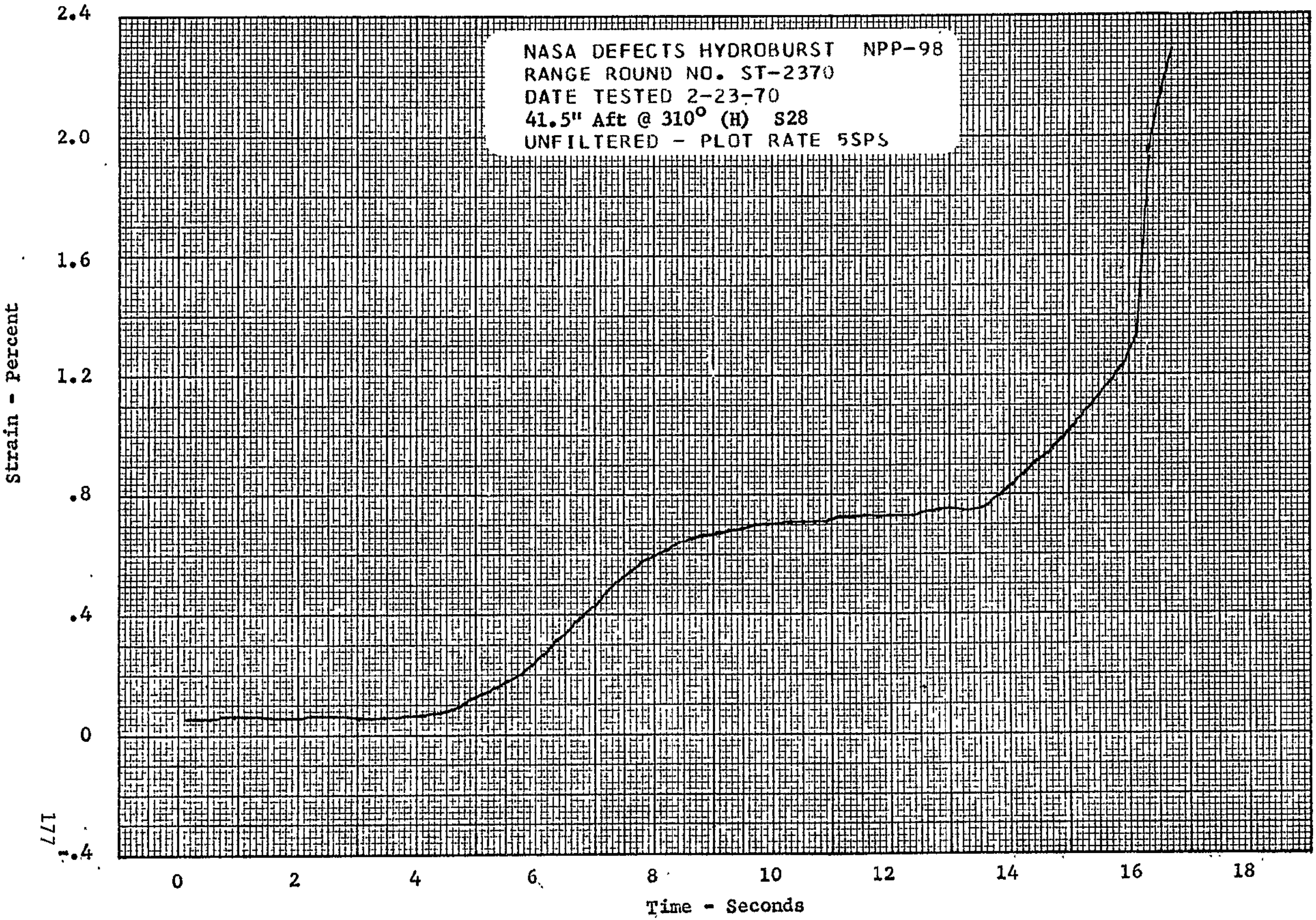
NASA DEFECTS HYDROBURST NPP-98
RANGE ROUND NO. ST-2370
DATE TESTED 2-23-70
41.5" Aft @ 310° (H) S28
UNFILTERED - PLOT RATE 5SPS
Strain - Percent
2.4
2.0
1.6
1.2
.8
.4
0
-.4
0
2
4
6
8
10
12
14
16
18
Time - Seconds

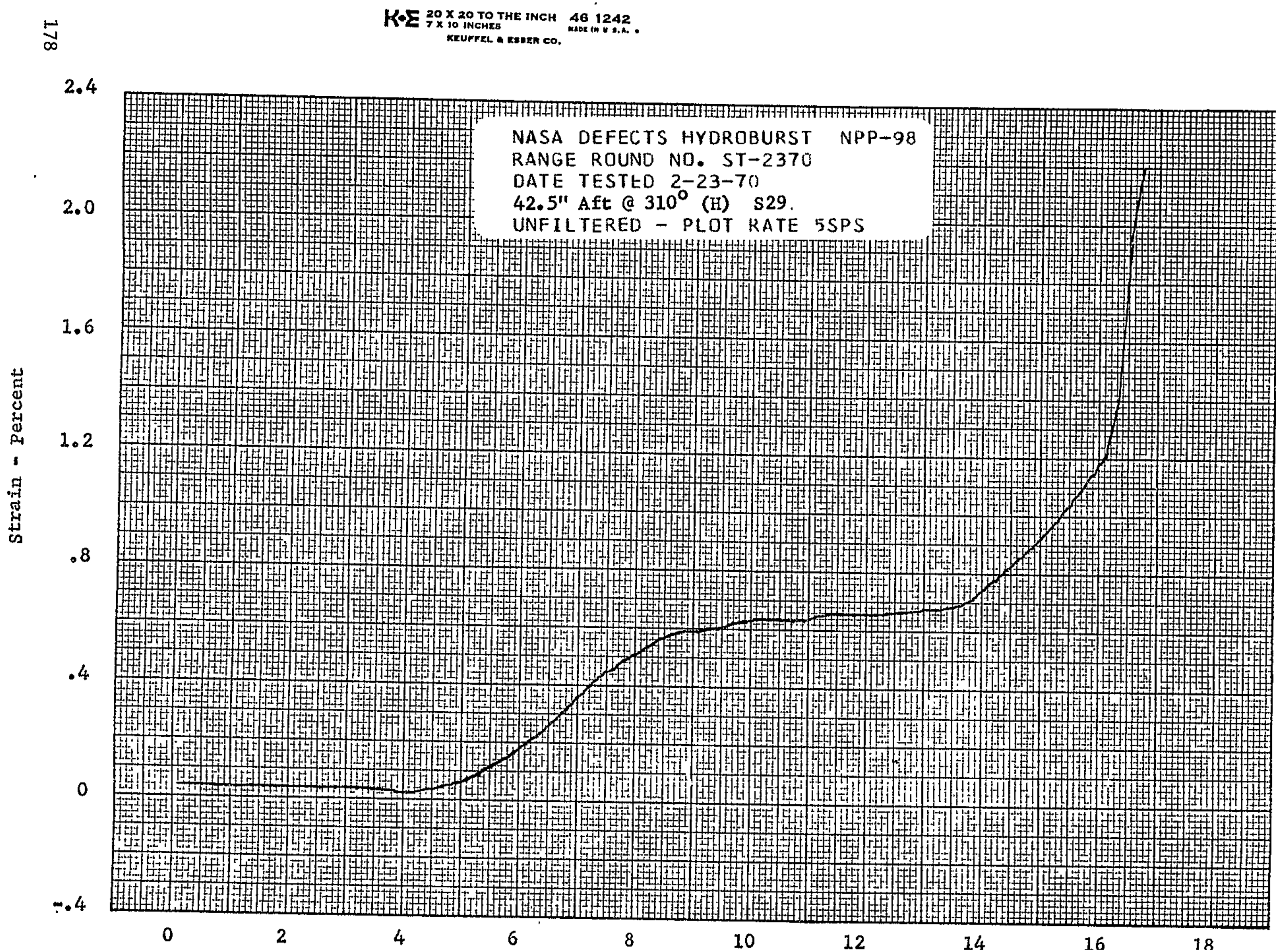
K•E 20 X 20 TO THE INCH 46 1242
7 X 10 INCHES
KEUFFEL & ESSER CO.
NASA DEFECTS HYDROBURST NPP-98
RANGE ROUND NO. ST-2370
DATE TESTED 2-23-70
42.5" Aft @ 310° (H) S29
UNFILTERED - PLOT RATE 5SPS
Strain - Percent
2.4
2.0
1.6
1.2
.8
.4
0
-.4
0
2
4
6
8
10
12
14
16
18

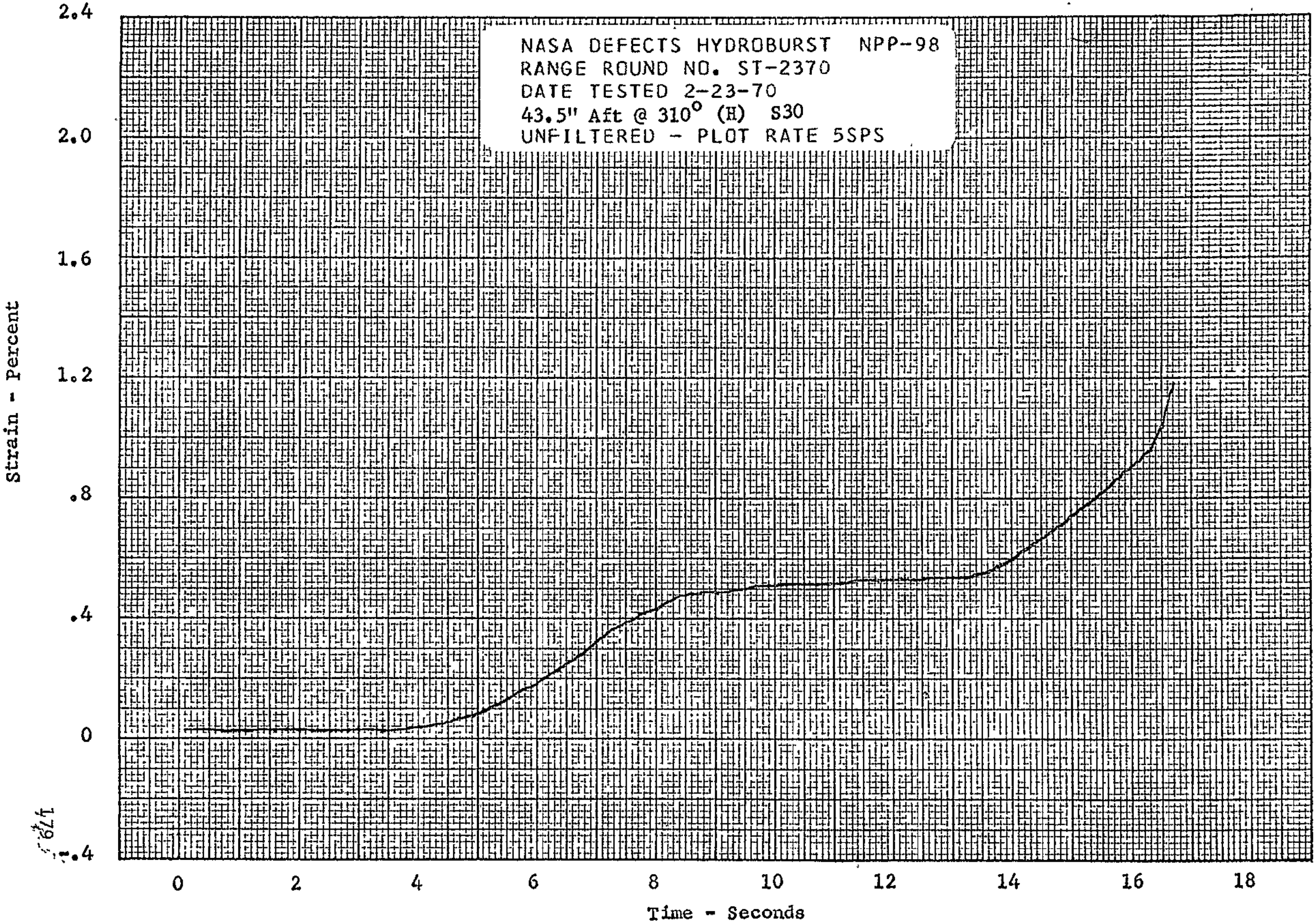
NASA DEFECTS HYDROBURST NPP-98
RANGE ROUND NO. ST-2370
DATE TESTED 2-23-70
43.5" Aft @ 310° (H) S30
UNFILTERED - PLOT RATE 5SPS
Strain - Percent
2.4
2.0
1.6
1.2
.8
.4
0
-.4
0
2
4
6
8
10
12
14
16
18
Time - Seconds

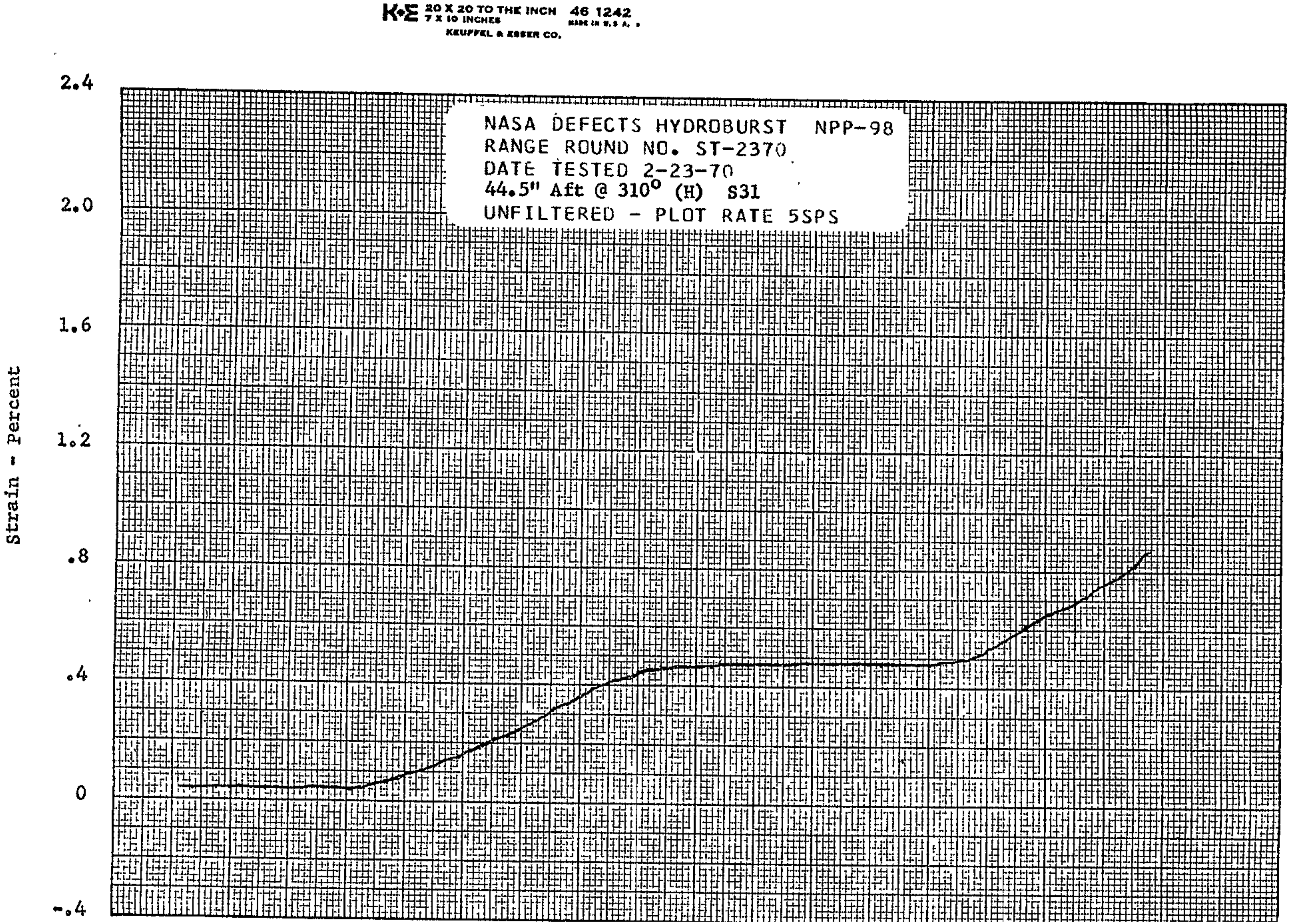
K+E 20 X 20 TO THE INCH 7 X 10 INCHES 46 1242
KEUFFEL & ESSER CO.
NASA DEFECTS HYDROBURST NPP-98
RANGE ROUND NO. ST-2370
DATE TESTED 2-23-70
44.5" Aft @ 310° (H) S31
UNFILTERED - PLOT RATE 5SPS
Strain - Percent
2.4
2.0
1.6
1.2
.8
.4
0
-.4

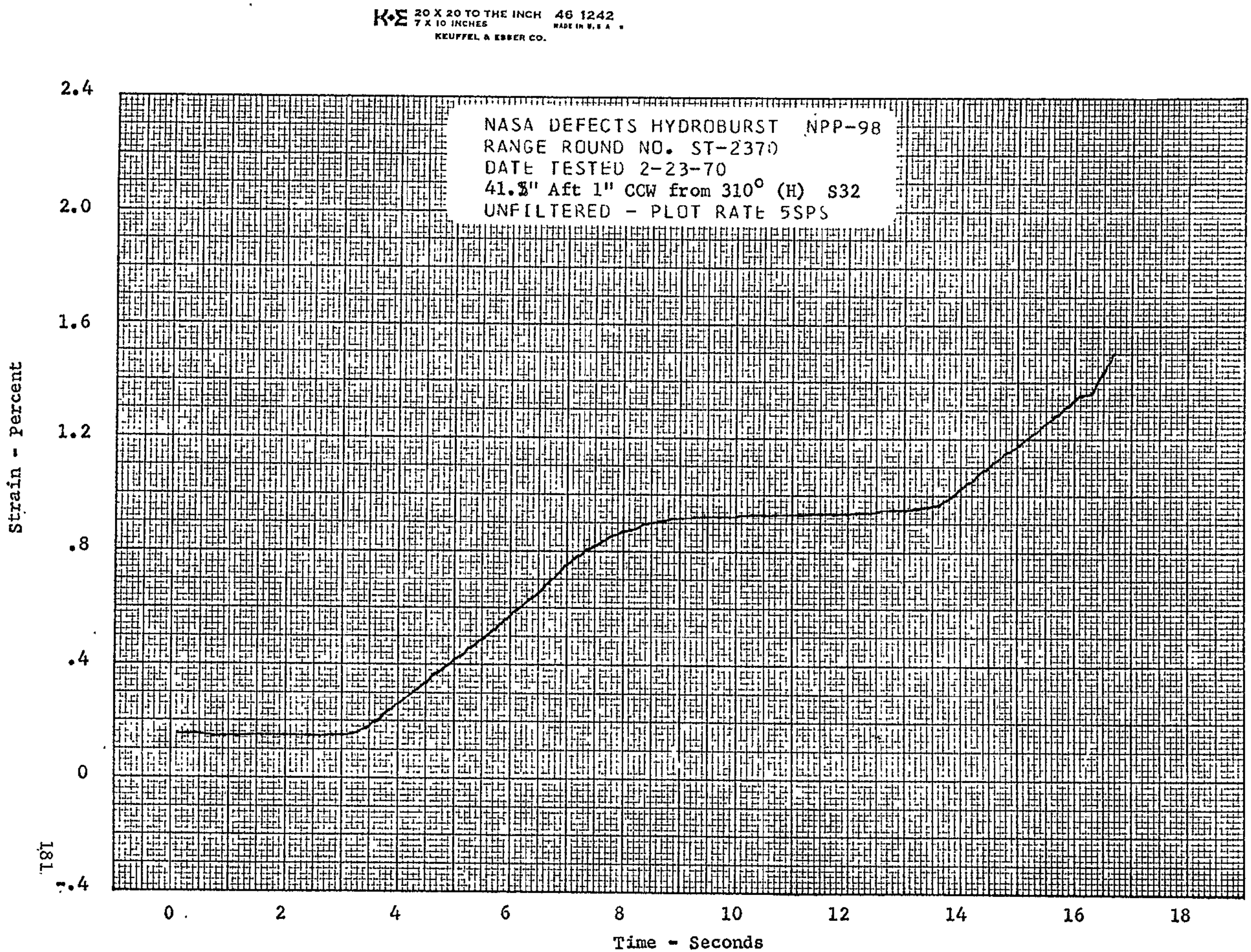
K+E 20 X 20 TO THE INCH 46 1242
7 X 10 INCHES MADE IN U.S.A.
KEUFFEL & ESSER CO.
NASA DEFECTS HYDROBURST NPP-98
RANGE ROUND NO. ST-2370
DATE TESTED 2-23-70
41.5" Aft 1" CCW from 310° (H) S32
UNFILTERED - PLOT RATE 5SPS
Strain - Percent
2.4
2.0
1.6
1.2
.8
.4
0
-.4
0
2
4
6
8
10
12
14
16
18
Time - Seconds

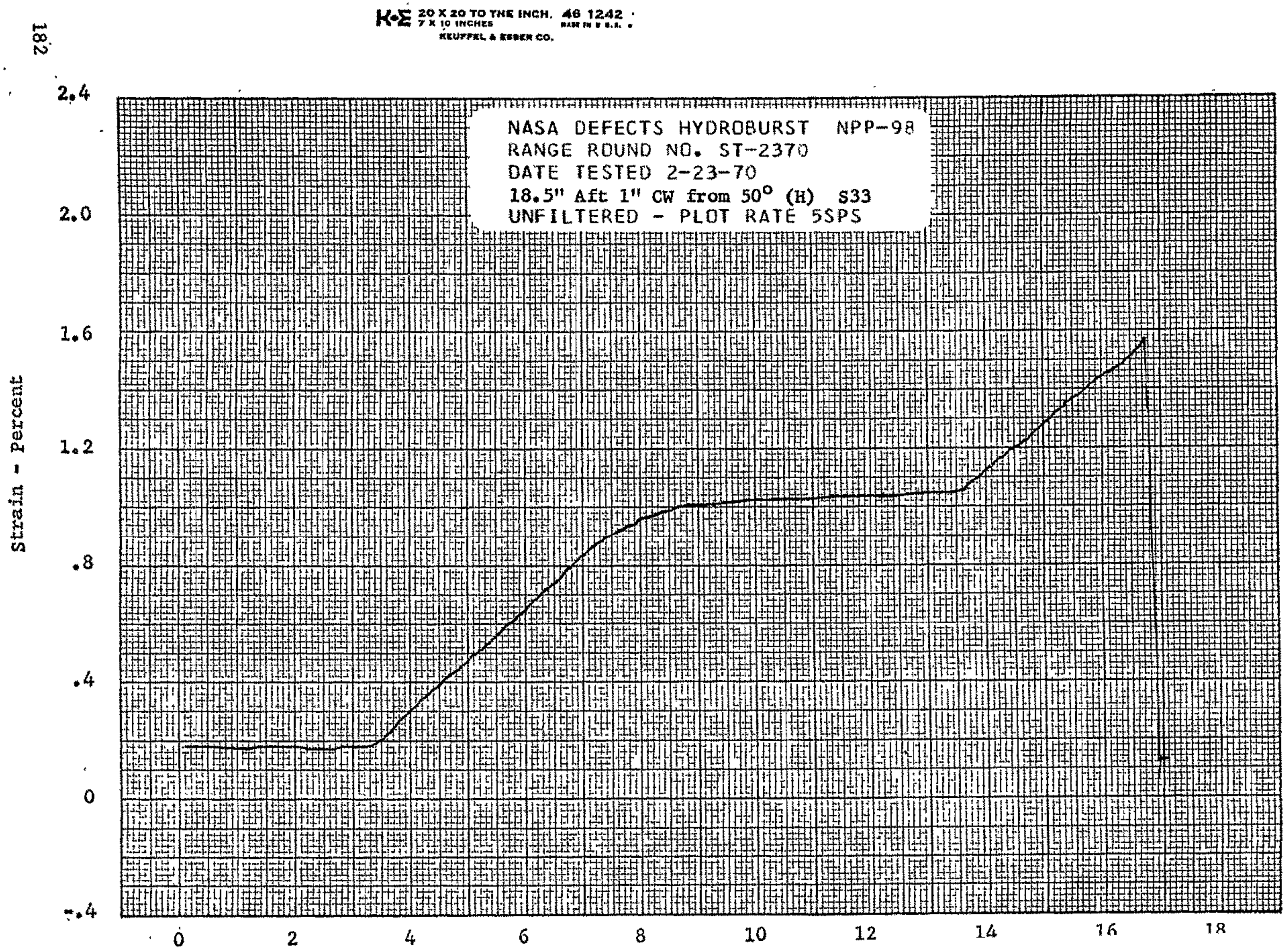
K+E 20 X 20 TO THE INCH. 46 1242
7 X 10 INCHES
KEUFFEL & ESSER CO.
NASA DEFECTS HYDROBURST NPP-98
RANGE ROUND NO. ST-2370
DATE TESTED 2-23-70
18.5" Aft 1" CW from 50° (H) S33
UNFILTERED - PLOT RATE 5SPS
Strain - Percent
2.4
2.0
1.6
1.2
.8
.4
0
-.4
0
2
4
6
8
10
12
14
16
18

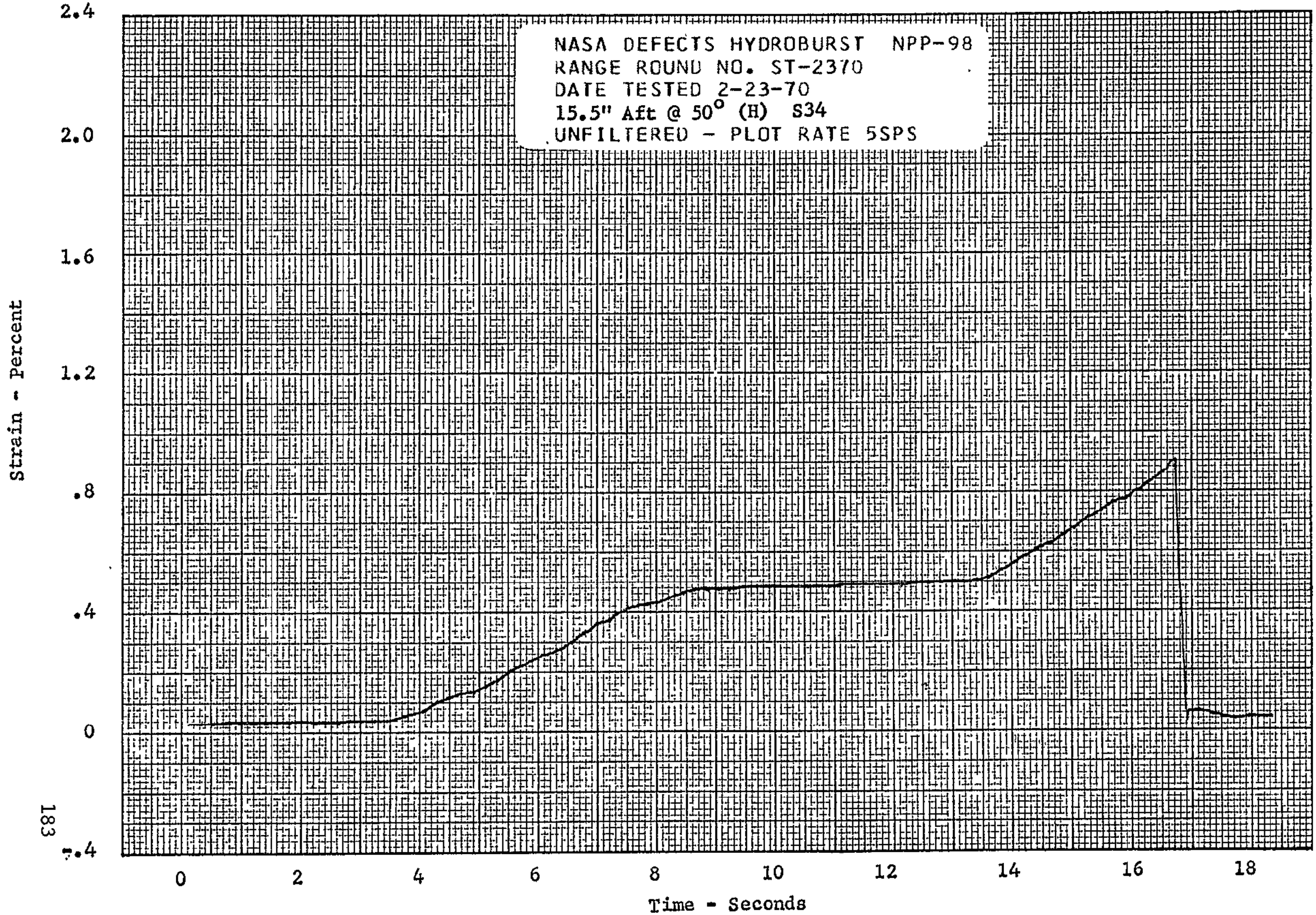
NASA DEFECTS HYDROBURST NPP-98
RANGE ROUND NO. ST-2370
DATE TESTED 2-23-70
15.5" Aft @ 50° (H) S34
UNFILTERED - PLOT RATE 5SPS
Strain - Percent
2.4
2.0
1.6
1.2
.8
.4
0
-.4
0
2
4
6
8
10
12
14
16
18
Time - Seconds

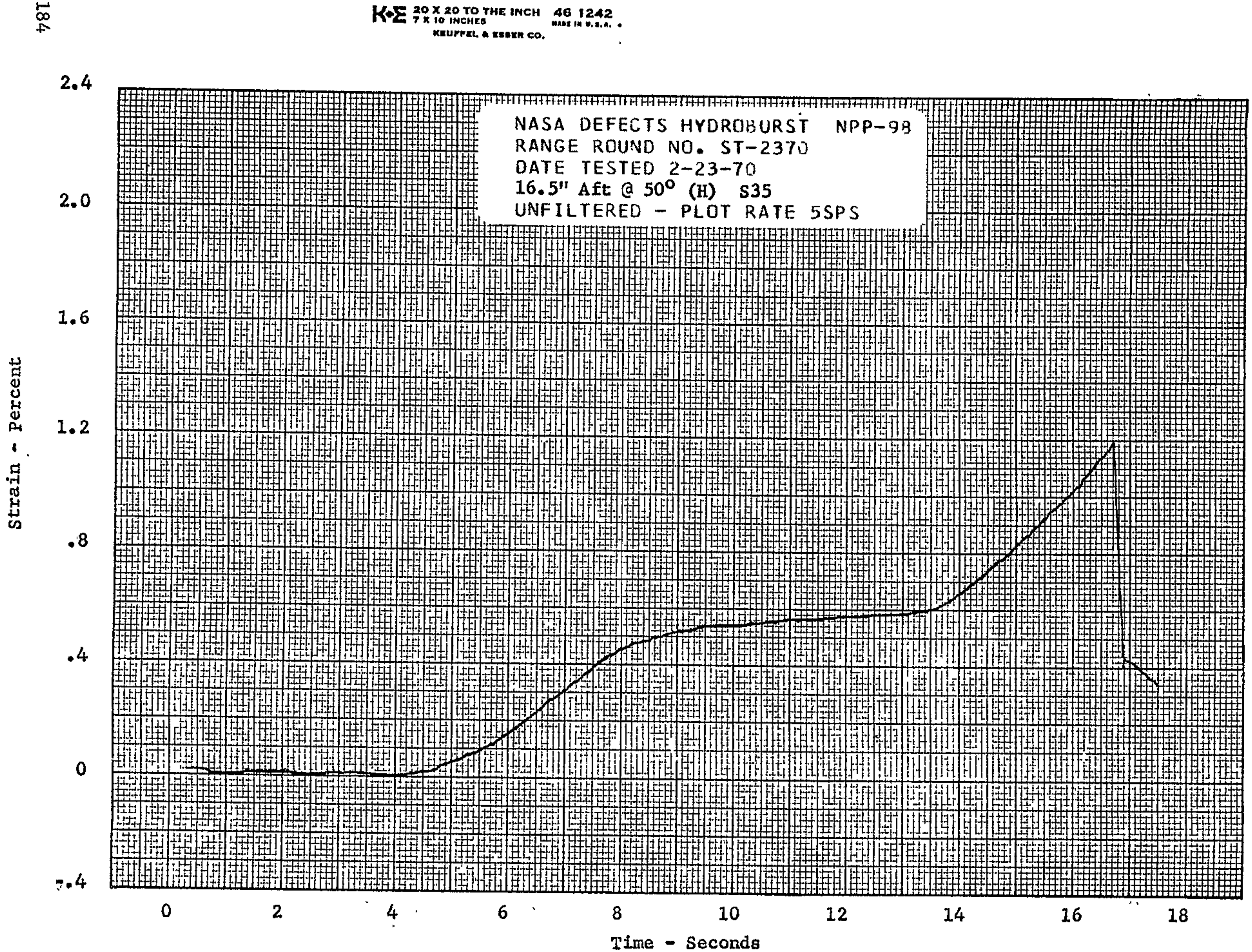
K•E 20 X 20 TO THE INCH 46 1242
7 X 10 INCHES MADE IN U.S.A.
KEUFFEL & ESSER CO.
NASA DEFECTS HYDROBURST NPP-98
RANGE ROUND NO. ST-2370
DATE TESTED 2-23-70
16.5" Aft @ 50° (H) S35
UNFILTERED - PLOT RATE 5SPS
Strain - Percent
2.4
2.0
1.6
1.2
.8
.4
0
-.4
0
2
4
6
8
10
12
14
16
18
Time - Seconds

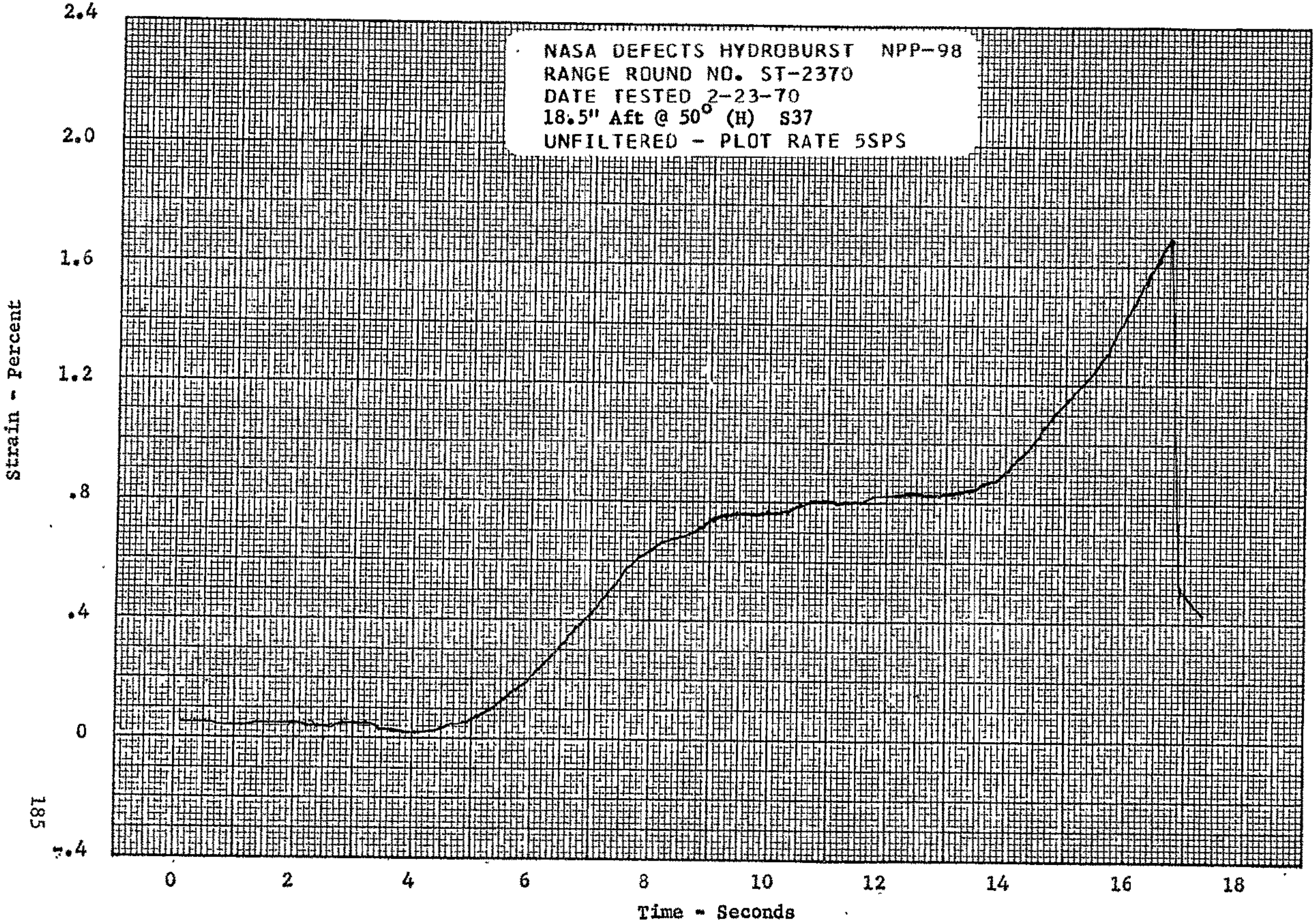
NASA DEFECTS HYDROBURST NPP-98
RANGE ROUND NO. ST-2370
DATE TESTED 2-23-70
18.5" Aft @ 50° (H) S37
UNFILTERED - PLOT RATE 5SPS
Strain - Percent
2.4
2.0
1.6
1.2
.8
.4
0
-.4
0
2
4
6
8
10
12
14
16
18
Time - Seconds

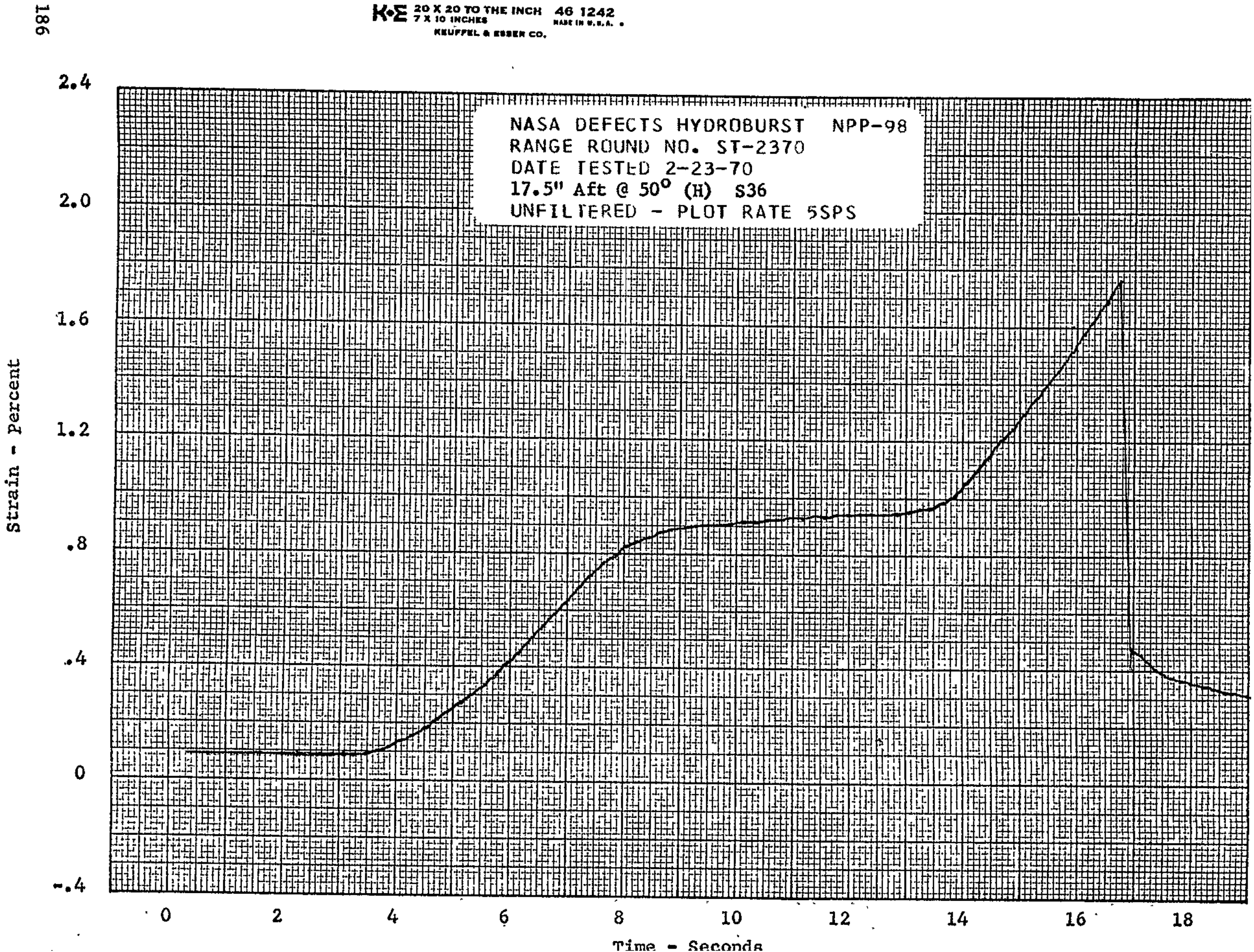
K•E 20 X 20 TO THE INCH 7 X 10 INCHES
46 1242
KEUFFEL & ESSER CO.
NASA DEFECTS HYDROBURST NPP-98
RANGE ROUND NO. ST-2370
DATE TESTED 2-23-70
17.5" Aft @ 50° (H) S36
UNFILTERED - PLOT RATE 5SPS
Strain - Percent
2.4
2.0
1.6
1.2
.8
.4
0
-.4
0
2
4
6
8
10
12
14
16
18
Time - Seconds

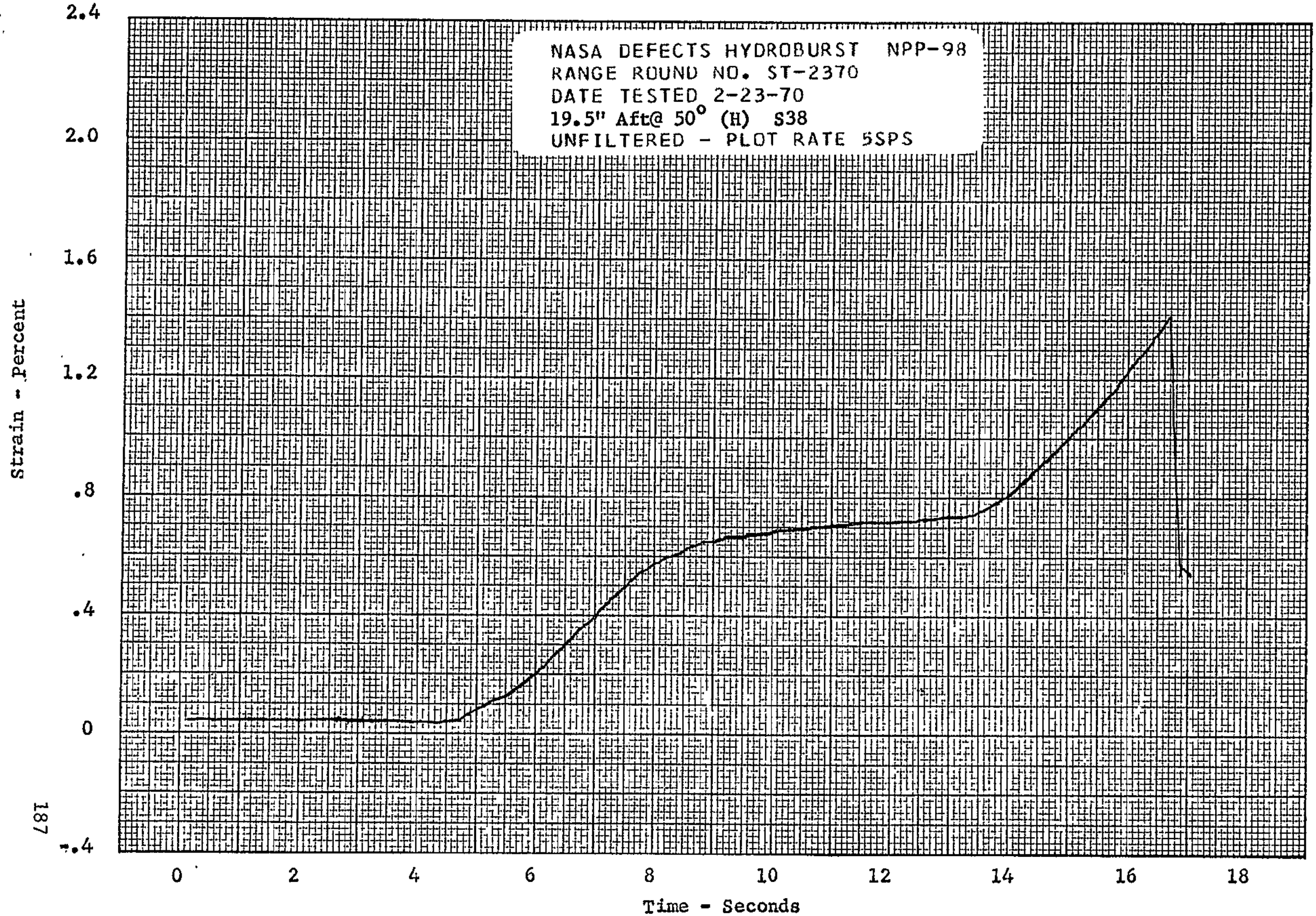
NASA DEFECTS HYDROBURST NPP-98
RANGE ROUND NO. ST-2370
DATE TESTED 2-23-70
19.5" Aft@ 50° (H) S38
UNFILTERED - PLOT RATE 5SPS
Strain - Percent
2.4
2.0
1.6
1.2
.8
.4
0
-.4
0
2
4
6
8
10
12
14
16
18
Time - Seconds

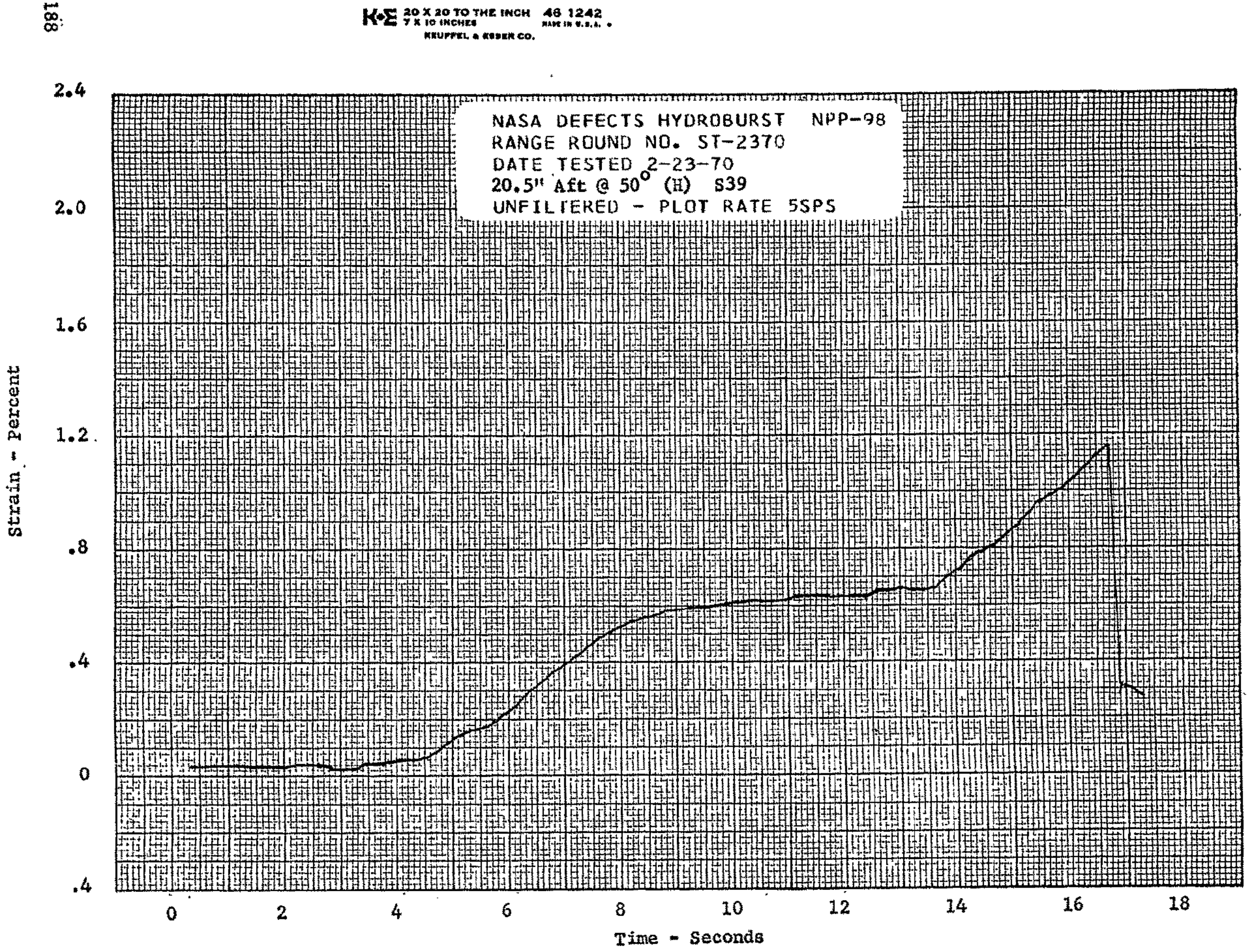
K+E 20 X 20 TO THE INCH 46 1242
7 X 10 INCHES
KEUFFEL & ESSER CO.
NASA DEFECTS HYDROBURST NPP-98
RANGE ROUND NO. ST-2370
DATE TESTED 2-23-70
20.5" Aft @ 50° (H) S39
UNFILTERED - PLOT RATE 5SPS
Strain - Percent
2.4
2.0
1.6
1.2
.8
.4
0
.4
0
2
4
6
8
10
12
14
16
18
Time - Seconds

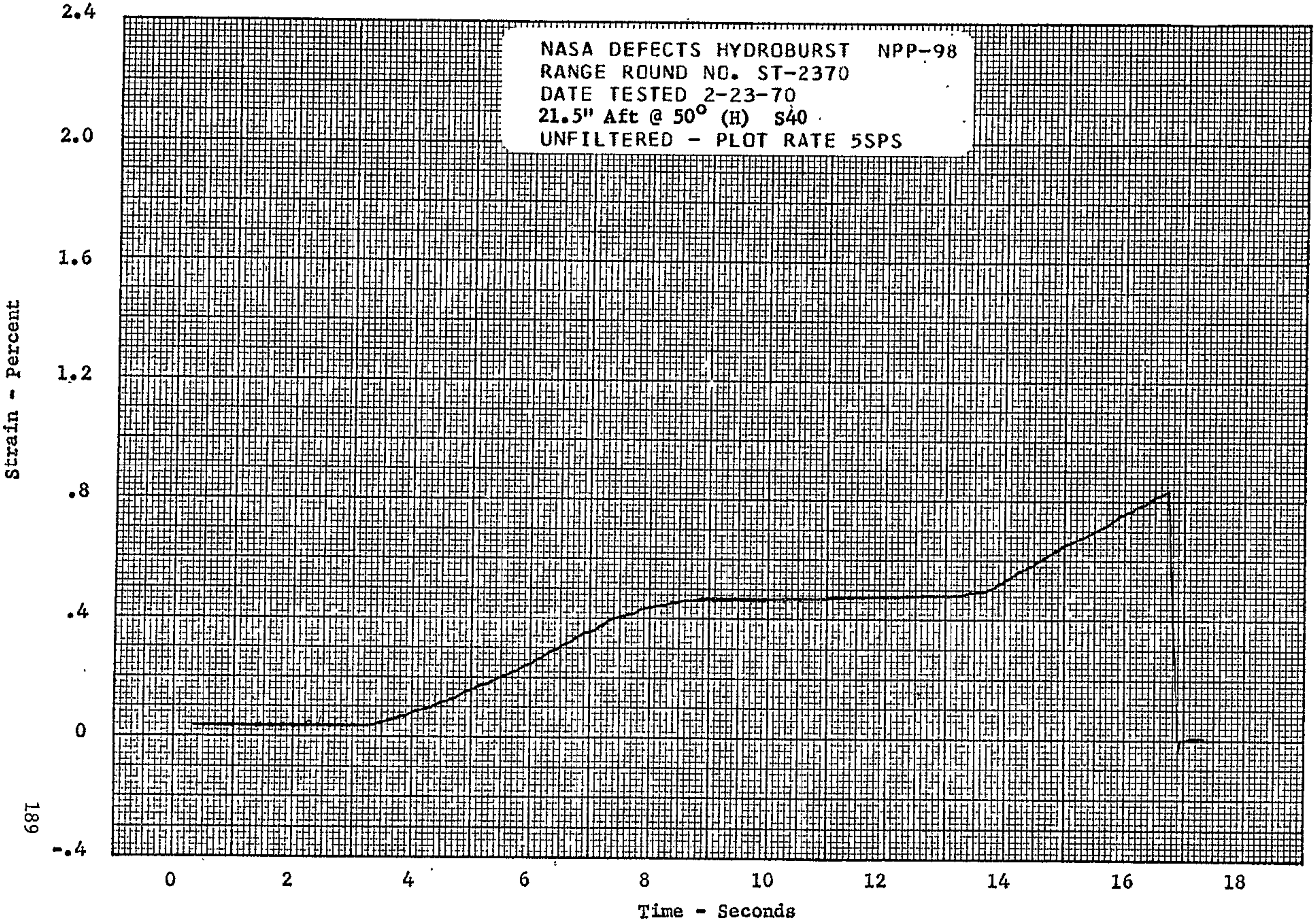
NASA DEFECTS HYDROBURST NPP-98
RANGE ROUND NO. ST-2370
DATE TESTED 2-23-70
21.5" Aft @ 50° (H) S40
UNFILTERED - PLOT RATE 5SPS
Strain - Percent
2.4
2.0
1.6
1.2
.8
.4
0
-.4
0
2
4
6
8
10
12
14
16
18
Time - Seconds

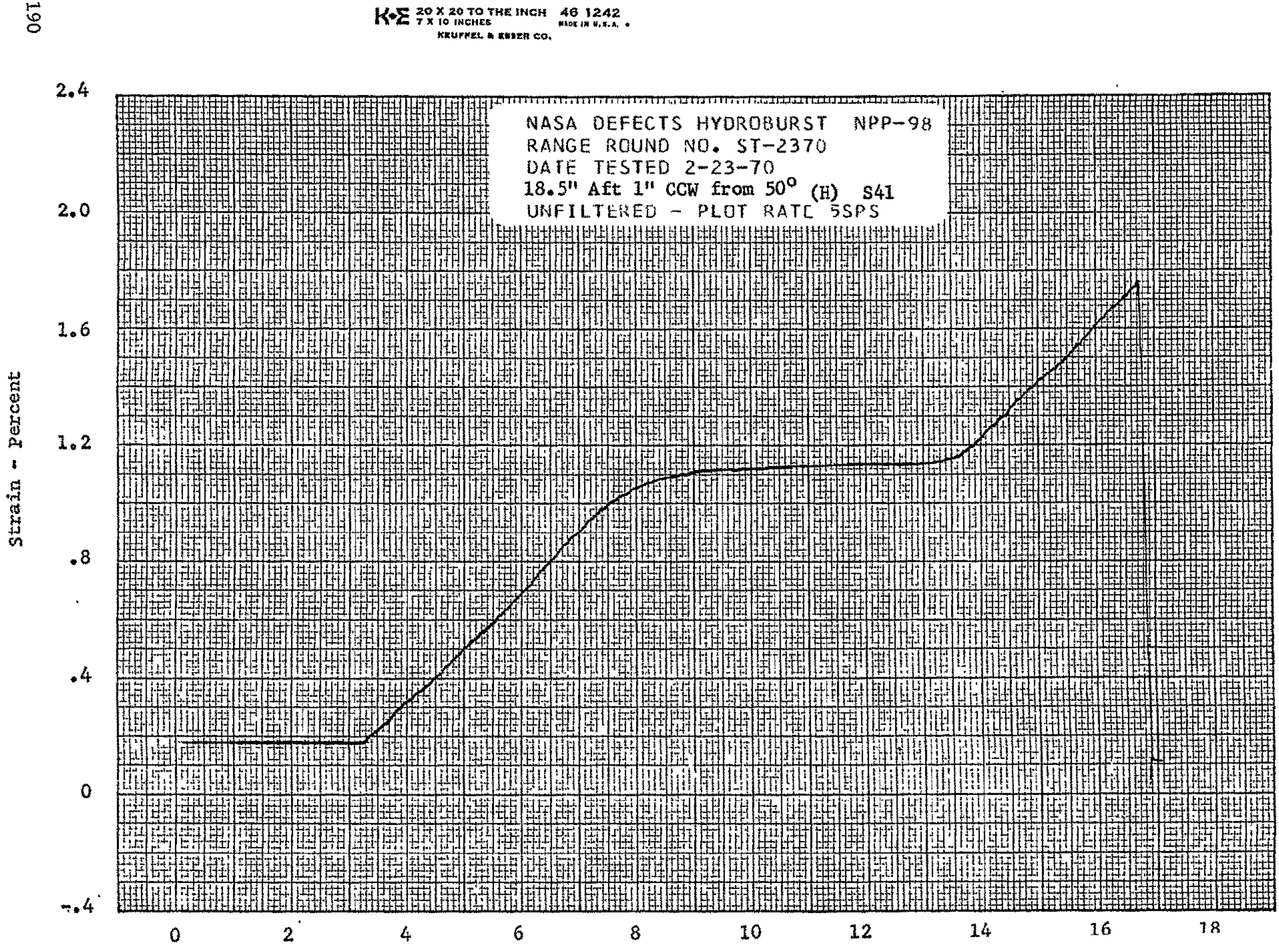
K&E 20 X 20 TO THE INCH 46 1242
7 X 10 INCHES MADE IN U.S.A.
KEUFFEL & ESSER CO.
NASA DEFECTS HYDROBURST NPP-98
RANGE ROUND NO. ST-2370
DATE TESTED 2-23-70
18.5" Aft 1" CCW from 50° (H) S41
UNFILTERED - PLOT RATE 5SPS
Strain - Percent
2.4
2.0
1.6
1.2
.8
.4
0
-.4
0
2
4
6
8
10
12
14
16
18

NASA CR-66946

DISTRIBUTION LIST

NAS1-9293

	No. Copies
NASA Langley Research Hampton, Virginia 23365	
Attention: Research Program Records Unit, Mail Stop 122	1
Raymond L. Zavasky, Mail Stop 117	1
John Cleary, Mail Stop 143	1
Richard F. Mulliken, Mail Stop 498	5
Robert L. Swain, Mail Stop 498-B	1
R. M. Boykin, Jr., Mail Stop 315	1
Harvey G. McComb, Jr., Mail Stop 188-C	1
V. D. Crowder, Mail Stop 358	1
Robert Bowers, LTV, Mail Stop 358	1
Charles B. King, Mail Stop 205	1
NASA Ames Research Center Moffett Field, California 94035	
Attention: Library, Mail Stop 202-3	1
NASA Flight Research Center P. O. Box 273 Edwards, California 93523	
Attention: Library	1
Jet Propulsion Laboratory 4800 Oak Grove Drive Pasadena, California 91103	
Attention: Library, Mail 111-113	1
Winston Gin, Mail 125-159	1
R. A. Happe, Mail Stop 81-2	1
NASA Manned Spacecraft Center 2101 Webster Seabrook Road Houston, Texas 77058	
Attention: J. G. Thibodeaux, Code EP	1
Library, Code BM6	1
NASA Marshall Space Flight Center Huntsville, Alabama 35812	
Attention: Library	1
John Q. Miller, S&E-ASTN-PJ	1
NASA Wallops Station Wallops Island, Virginia 23337	
Attention: Library	1
Eldred H. Helton, FTD-VILB	1

DISTRIBUTION LIST

NAS1-9293

	No. Copies
NASA Lewis Research Center 21000 Brookpart Road Celveland, Ohio 44135	
Attention: Library, Mail Stop 60-3	1
Carl C. Ciepluch, Mail Stop 500-205	1
William J. Brown, Mail Stop 500-203	1
NASA John F. Kennedy Space Center Kennedy Space Center, Florida 32899 Attention: Library, Code IS-CAS-42B	
National Aeronautics and Space Administration Washington, D. C. 20546	
Attention: Library, Code USS-10	1
William Cohen, Code RPM	1
Robert W. Ziem, Code RPS	1
Norman J. Mayer, Code RV-2	1
Michael Gruber, Code MCL	1
Dr. Robert L. Levine, Code RPL	1
Joseph E. McGolrick, Code SV	1
Ward W. Wilcox, Code RPX	1
David L. Winterhalter, Code MAT	1
Richard J. Wisniewski, Code RMD	1
NASA Goddard Space Flight Center Greenbelt, Maryland 20771	
Attention: Library	1
Air Force Rocket Propulsion Laboratory Edwards Air Force Base Edwards, California 93523	
Attention: Code SREP	1
Code RPM	1
Lt. S. W. Beckwith, Code RPMCB	1
Dr. F. N. Kelley, Code RPMCP	1
Air Force Systems Command Andrews Air Force Base Washington, D. C. 20331 Attention: Code SCTR	
Army Ammunition and Supply Agency Joliet, Illinois 60431	
Attention: RDL Quality Assurance, Technical Library	1
Aerojet General Corporation P. O. Box 15847 Sacramento, California 95813	
Attention: Dr. K. W. Bills	1

NASA CR-66946

DISTRIBUTION LIST

NAS1-9293

	No. Copies
Naval Weapons Center China Lake, California 93557 Attention: K. H. Bischel	1
Technical Library, Code 793	1
Rohm & Haas Company Huntsville, Alabama 35808 Attention: J. J. Brisbane	
Ballistic Research Laboratories Surveillance & Reliability Laboratories Aberdeen Proving Ground, Maryland 21005 Attention: O. P. Bruno	1
Code AMXBR-1	1
Office of Naval Research Department of the Navy Washington, D. C. 20360 Attention: J. M. Crowley	1
Picatinny Arsenal Dover, New Jersey 07801 Attention: B. D. Lehman	1
Daniel J. Malloy, Technical Information Section	1
Library, SMUPA-VA6	1
Redstone Scientific Information Center U. S. Missile Command Redstone Arsenal, Alabama 35809 Attention: Document Section	1
Army Research Office Box CM, Duke Station Durham, North Carolina 27706 Attention: Code CRD-AA-IP	1
Chemical Propulsion Information Agency Applied Physica Laboratory Johns Hopkins University 8621 Georgia Avenue Silver Spring, Maryland 20910 Attention: Library	1
R. D. Brown	1
Naval Missile Center Point Mugu, California 93041 Attention: Technical Library, Code 5632.2	1

DISTRIBUTION LIST

NAS1-9293

	No. Copies
Naval Ordnance Station Indian Head, Maryland 20640 Attention: Morris Altshuler, Building 863, Trailer 1394, Code DDB 10	1
Naval Ordnance Systems Command Washington, D. C. 20360 Attention: Technical Library, ORD-9132	1
White Sands Missile Range White Sands Missile Range, New Mexico 88002 Attention: Technical Library	1
United Technology Center P. O. Box 358 Sunnyvale, California 94088 Attention: Technical Library	1
R. A. Jankowski	1
Naval Weapons Center China Lake, California 93557 Attention: A. Adicoff, Code 5056	1
University of Texas Defense Research Laboratory P. O. Box 8029 Austin, Texas 78712 Attention: E. B. Becker	1
IIT Research Institute 10 W 35th Street Chicago, Illinois 60616 Attention: Document Library	1
Midwest Research Institute 425 Volker Boulevard Kansas City, Missouri 64110 Attention: Library	1
Oline Mathieson Chemical Corporation P. O. Box Drawer G Marion, Illinois 62959 Attention: Research Library	1
University of Illinois Aeronautical Engineering Department Urbana, Illinois 61801 Attention: Dr. H. H. Hilton	1

NASA CR-66946

DISTRIBUTION LIST

NAS1-9293

	No. Copies
McDonnell Douglas Corporation Missile and Space Systems Division 3000 Ocean Park Boulevard Santa Monica, California 90406 Attention: R. V. Mellette, Dept. A2-260	1
Atlantic Research Corporation Shirley Highway at Edsall Road Alexandria, Virginia 22314 Attention: C. N. Robinson	1
U. S. Army Missile Command Propulsion Laboratory Redstone Arsenal, Alabama 35809 Atttention: R. E. Sikon, AMSMI-RKP	1
Emerson Electric Company 31000 Florissant Avenue St. Louis, Missouri 63136 Attention: T. F. Hoekel	1
Lockheed Propulsion Company P. O. Box 111 Redlands, California 92374 Attention: A. Vonder Esch, Chief Engineer	1
Rocketdyne Solid Rocket Division P. O. Box 548 McGregor, Texas 76657 Attention: Dr. J. S. Noel	1
Bell Aerosystems Box 1 Buffalo, New York 14240 Attention: Technical Library	1
Shell Chemical Corporation 50 W. 50th Street New York City, New York 10020 Attention: Technical Library	1
Corning Glass Works 80 Houghton Park Corning, New York 14820 Attention: Technical Library	1

NASA CR-66946

DISTRIBUTION LIST

NAS1-9293

	No. Copies
Goodyear Aerospace Corporation 1220 Massilon Road Akron, Ohio 44315 Attention: Technical Library	1
Narmco Manufacturing Company Materials Division Victoria and Placentia Streets Costa Mesa, California 92627 Attention: Technical Library	1
CREK AFCRL L. G. Hanscom Field Bedford, Massachusetts, 01730 Attention: William P. Lynch	1
Wright-Patterson Air Force Base Dayton, Ohio 45433 Attention: Technical Library	1
Air Force Office of Scientific Research 1400 Wilson Boulevard Arlington, Virginia 22209 Attention: Code SREP	1
Defense Documentation Code OSR-1 Cameron Station, Building 5 Alexandria, Virginia 23314	1
Aerojet General Corporation P. O. Box 15847 Sacramento, California 95813 Attention: Technical Library, 2432-2015A	1
Battelle Memorial Institute 505 King Avenue Columbus, Ohio 43201 Attention: Reports Library	1
Lockheed Propulsion Company P. O. Box 111 Redlands, California 92374 Attention: Library, Dept. 2100, Building 123	1

NASA CR-66946

DISTRIBUTION LIST

NAS1-9293

	No. Copies
North American Rockwell Corporation Rocketdyne Division 6633 Canoga Avenue Canoga Park, California 91304 Attention: Library, Dept. 086-306	1
Dr. E. L. Alexander, D/991-37S SS-11	1
Stanford Research Institute 333 Ravenswood Avenue Menlo Park, California 94025 Attention: Document Center for Propulsion Sciences	1
Thiokol Chemical Corporation Huntsville Division Huntsville, Alabama 35807 Attention: Technical Library	1
Thiokol Chemical Corporation Wasatch Division Brigham City, Utah 94302 Attention: Richard Reinhart	1
TRW Inc. One Space Park Redland Beach, California 90278 Attention: Technical Information Center	1
U. S. Naval Research Laboratory Washington, D. C. 20390 Attention: Stephen D. Hart	1
Robert Arret	1
Naval Weapons Station Concord, California 94520 Attention: Howard Heffan	1
NASA Scientific and Technical Information Facility P. O. Box 33 College Park, Maryland 20740	1 plus reproducible

cc: W. J. Rue/J. E. Midgarden/Central File
J. K. Mann
D. J. Sine
R. P. Carter
J. C. Leslie
R. E. Randolph
R. R. Rizzo
A. A. Vicario
J. G. Poesch
T. C. White
R. J. Dale
E. D. Casseday
V. L. Grapes
R. A. Miesmer
J. A. McCoy
C. R. Hitt
E. J. Locasio
Library (3)
Contract File
PBO File

Radford - W. B. Helbert

Bacchus - R. F. H. Woodberry
H. L. Holt
W. Mathews
Library (2)

Research Center - Wilmington
Library (2)

John Hinchman
Mail Stop 287
Thiokol Chemical Corp.
Brigham City, Utah 84302